

Copyright
by
Yuchul Kim
2011

The Dissertation Committee for Yuchul Kim
certifies that this is the approved version of the following dissertation:

**Spatial Spectrum Reuse in Wireless Networks
Design and Performance**

Committee:

Gustavo de Veciana, Supervisor

Jeffrey G. Andrews

Lili Qiu

Sanjay Shakkottai

Sujay Sanghavi

**Spatial Spectrum Reuse in Wireless Networks
Design and Performance**

by

Yuchul Kim, B.E.; M.S.

Dissertation

Presented to the Faculty of the Graduate School of

The University of Texas at Austin

in Partial Fulfillment

of the Requirements

for the Degree of

Doctor of Philosophy

The University of Texas at Austin

May. 2011

Dedicated to my wife Jeongeon

Acknowledgments

I would like to give my special thanks to my supervisor Professor Gustavo de Veciana for his continuous support, encouragement, guidance, and understanding. He has demonstrated how an excellent researcher thinks, speaks, writes, works, and plans. His enthusiasm for quality research, teaching and careful guidance made my work more enjoyable and my every effort fruitful. They eventually led me to finish my Ph.D. successfully.

I want to thank to Professor Jeffrey G. Andrews, Professor Lili Qiu, Professor Sanjay Shakkottai, and Professor Sujay Sanghavi for being my Ph.D. committee members and for their helps. I also would thank to Professor Francois Baccelli for helpful discussions and comments on my research. I would thank to Zhanfeng Jia, Qingjiang Tian, Linhai He, and David Julian for their helpful support during my internship at Qualcomm.

My many thanks go to my (former) lab mates Ayis, Balaji, Bilal, Hongseok, Vinay, Virag, and Zheng for their helps and insightful advices. I also would thank to my Korean friends Heejung, Jung, Minchan, Sanghyun, Sungho, and Taehyun who started their graduate studies in UT with me, and to Cheolhee, Goochul, Insoo, Kitaek, Larkkwon, Wonsoo, Youngchun, and Youngsang who made my life more enjoyable while living in the same complex.

I would thank to my parents, my sister, my wife's parents, and wife's brother who always have been there with encouragement and continuous support. I also thank to my daughter Jay who gave me the joy of being a father. Last but not least, I cannot thank anyone more than my wife Jeongeon for her devotion, support and sacrifice. I am indebted to her in every aspect of my life.

Spatial Spectrum Reuse in Wireless Networks

Design and Performance

Yuchul Kim, Ph.D.

The University of Texas at Austin, 2011

Supervisor: Gustavo de Veciana

This dissertation considers the design, evaluation and optimization of algorithms/ techniques/ system parameters for distributed wireless networks specifically ad-hoc and cognitive wireless networks.

In the first part of the dissertation, we consider ad-hoc networks using *opportunistic carrier sense multiple access (CSMA) protocols*. The key challenge in optimizing the performance of such systems is to find a good compromise among three interdependent quantities: the density and channel quality of the scheduled transmitters, and the resulting interference seen at receivers. We propose two new channel-aware slotted CSMA protocols and study the tradeoffs they achieve amongst these quantities. In particular, we show that when properly optimized these protocols offer substantial improvements relative to regular CSMA – particularly when the density of nodes is moderate to high. Moreover, we show that a simple quantile based opportunistic CSMA protocol can achieve robust performance gains without requiring careful parameter optimization.

In the second part of the dissertation, we study a cognitive wireless network where licensed (primary) users and unlicensed ‘cognitive’ (secondary) users coexist on shared

spectrum. In this context, many *system design parameters* affect the joint performance, e.g., outage and capacity, seen by the two user types. We explore the performance dependencies between primary and secondary users from a spatial reuse perspective, in particular, in terms of the outage probability, node density and joint network capacity. From the design perspective the key system parameters determining the joint transmission capacity, and tradeoffs, are the detection radius (detection signal to interference and noise power ratio (SINR) threshold) and decoding SINR threshold. We show how the joint network capacity region can be optimized by varying these parameters.

In the third part of the dissertation, we consider a cognitive network in a *heterogeneous* environment, including indoor and outdoor transmissions. We characterize the joint network capacity region under three different spectrum (white space) detection techniques which have different degrees of radio frequency (RF) - environment awareness. We show that cognitive devices relying only on the classical signal energy detection method perform poorly due to limitations on detecting primary transmitters in environments with indoor shadowing. This can be circumvented through direct use (e.g., database access) of location information on primary transmitters, or better yet, on that of primary receivers. We also show that if cognitive devices have positioning information, then the secondary network's capacity increases monotonically with increased indoor shadowing in the environment.

This dissertation extends the recent efforts in using stochastic geometric models to capture large scale performance characteristics of wireless systems. It demonstrates the usefulness of these models towards understanding the impact of physical /medium access (MAC) layer parameters and how they might be optimized.

Contents

Acknowledgments	v
Abstract	vi
List of Tables	x
List of Figures	xi
Chapter 1. Introduction	1
Chapter 2. Spatial Reuse and Fairness of Mobile Ad-Hoc Networks with Channel-Aware CSMA Protocols	5
2.1 Introduction	5
2.2 System Model	13
2.3 Performance Metrics	17
2.4 Transmission Performance Analysis	21
2.5 Spatial Reuse	28
2.6 Spatial Fairness	42
2.7 System implementation	48
2.8 Conclusion	52
2.9 Appendix : Derivation of $u'(n, t_0, \tau, \lambda)$	53
2.10 Appendix : Convergence of $I_{\Phi_M}^\gamma$	60
Chapter 3. Understanding the Design Space of Cognitive Networks	67
3.1 Introduction	67
3.2 System Model	71
3.3 Performance of Primary Network	75
3.4 Performance of Secondary Network	80

3.5	Capacity and Joint Network Capacity Region	87
3.6	Impact of System Parameters	90
3.7	Concluding Remarks	98
3.8	Appendix : Proof of Lemma 1	99
Chapter 4. Heterogeneous Environments and RF-Environment Awareness		101
4.1	Introduction	101
4.2	System Model	104
4.3	Computing joint Network capacity Region Roadmap and Overview of Results	115
4.4	Performance of Signal Energy Detection Technique	118
4.5	Performance of Positioning-assisted Technique	125
4.6	Performance of Receiver Location-Aware Technique	127
4.7	Maximum Contention Density for Secondary Nodes given ϵ -outage constraint	131
4.8	Joint Network Capacity Region	132
4.9	Conclusion	139
4.10	Appendix : Proof of Theorem 7	143
4.11	Appendix : Proof of Theorem 9	144
4.12	Appendix : Proof of Theorem 10	145
4.13	Appendix : Proof of Theorem 11	146
4.14	Appendix : Numerically computed quantities	148
4.15	Appendix : Computing Outage Probability of L-oSRx	149
Chapter 5. Conclusion and Future Work		156
5.1	Conclusion	156
5.2	Future Work	157
Bibliography		159
Vita		173

List of Tables

2.1	Summary of notations	18
4.1	Summary of Parameters	114

List of Figures

2.1	A realization of modified Matérn hardcore process : Blue points are the realization of marked Poisson point process where each point has an independent identically distributed mark denoting its timer value in $[0, 1]$. If a point has the smallest timer value in its neighborhood (neighborhood is not shown here but formally defined later in (2.3)), then, it is selected as a CSMA transmitter. Selected CSMA transmitters were drawn inside boxes.	7
2.2	The density of active transmitters for O/QT-CSMA increases and saturates as λ increases due to the carrier sensing in CSMA protocol. Increasing the qualification threshold γ reduces the density of qualified transmitters without affecting the asymptotic density of active transmitters $\lambda_{dens}(\nu)$; so the effect is a shift of the curves to the right hand side. Increasing carrier sensing threshold ν increases $\lambda_{dens}(\nu)$ since it makes the mean size of a typical transmitter's neighborhood smaller.	30
2.3	The success probability versus the density of transmitters for various ν and γ	32
2.4	The density of successful transmissions in a network with intermediate density	36
2.5	The asymptotic density of successful transmissions for O/QT-CSMA exhibits a phase transition phenomenon depending on the value of the scaling speed constant c when qualification threshold γ is selected as the logarithm function of node density λ : $\gamma = c \log(\lambda/\lambda_q)$ with $c > 0$ and $a > 0$. The quantities in the square bracket denote the associated density of qualified nodes $\lim_{\lambda \rightarrow \infty} \lambda p_{\gamma(\lambda)}$ which are always larger than their associated asymptotic density of successful transmissions.	39
2.6	Fairness index of access frequency versus the mean number of contenders $\bar{N}_{s,0}^\gamma(\nu)$ under the Assumption 1.	45
2.7	Comparison of the dominated sets of O-CSMA, QT-CSMA and QT ₀ -CSMA.	49
2.8	Slot structure for CDMA case.	50
2.9	$h(\cdot)$ is a function computed in (2.14). $u'(\cdot)$ is a function we computed above for $N_0 = n \geq 0$ and $t_0 \in [0, 1)$	61
2.10	Constructing $\Psi^{(n+1)}$ from $\Psi^{(n)}$ and $\hat{\Psi}^{(n)}$	64
3.1	A primary transmitter and an associated receiver	76

3.2	The impact from harmful interference from STxs and PTxs when r_d is set to d_p are shown. In $S1$ (upper figure), PRx around the edge of coverage experience increased $P_{o,1}$ due to interference from STxs. In $S2$ (down figure), not only STxs but also other PTxs give interference to PRxs. So $P_{o,1}$ starts to increase even when PRx is very close to its nearest PTx.	78
3.3	Conditioned on that there is no PTxs in $b(Z_i, r_d) \cup b(W, r_{ps})$, the outage of a SRx W can be caused by potential STxs in the hatched region $b(W, r_{ss})$. Whether a potential STxs, e.g., at location $z \in b(W, r_{ss})$, can give harmful interference to W depends on the potential PTxs in $b(z, r_d) \setminus (b(Z_i, r_d) \cup b(W, r_{ps}))$	82
3.4	$P_{o,2}(\lambda_p, \lambda_s)$ were shown for $S1$ and $S2$. If any hidden PTx exists ($ b(W, r_{ps}) \setminus b(Z_i, r_d) > 0$), then $P_{o,2}(\lambda_p, \lambda_s)$ can not be lowered than its outage wall $P_{o,2}^w(\lambda_p, d_s)$ even if $\lambda_s \rightarrow 0$. In legends, UB and LB mean upper and lower bound respectively.	84
3.5	Transmission density of secondary network T_s is maximized at λ_s^* and exponentially decreases as λ_p increases.	85
3.6	Optimal contention density λ_s^* is not sensitive to λ_p in the regime of interest	86
3.7	Contention density of secondary node under ϵ -constraint(Left: $S1$ with $k_2 = 0$, Right: $S2$ with $k_2 > 0$) were shown. In $S2$ as λ_p increases, the number of hidden PTxs increases, which eventually suppresses λ_s^ϵ . . .	89
3.8	Joint network capacity region as a function of r_d	91
3.9	Joint network capacity region as a function of β_s	92
3.10	Two realizations of primary network with the same coverage but different coverage radii were shown. Coverage and guard region were shown as bright and dark gray region respectively. Note that the thickness of guard band is the same, i.e., $\kappa r_{sp}(d_{p1}) = \kappa r_{sp}(d_{p1})$	95
3.11	Impact of burstness of coverage and STx's transmit power on C_2 . . .	96
4.1	The joint network capacity region of primary (C_1) and secondary capacity (C_2) was shown under 10dB of penetration loss for three different white space detection techniques. 50% of STxs are indoor and remaining 50% are outdoor. λ_r denotes the density of primary receivers. When the density of primary transmitter is $\lambda_p = 2 \times 10^{-10}$, the gain of positioning-assisted technique to signal energy detection technique is 76%, and that of receiver location-aware technique is 177%.	103
4.2	A typical realization of primary and secondary networks under three white space detection methods is shown. Shaded region denotes the coverage of PTxs with radius d_p	117
4.3	Impact of STxs' interference to outage probability of PRx at distance d to its nearest PTx	121

4.4	Conditioned that there are no PTxs in $b(Z_o, r_d^E) (\supset b(W_o, r_{ps}))$, an E-oSRx W_o can be interfered by potential E-oSTxs in $b(W_o, r_{ss}^{oo})$ or potential E-iSTxs in $b(W_o, r_{ss}^{io})$. Their activities are determined by surrounding PTxs in $b(z, r_d^E)$ for E-oSTxs and $b(z, r_d^{Ei})$ for E-iSTxs.	124
4.5	The outage probability of a typical E-oSTx and E-iSTx are shown. The gap between outage probability of E-oSTx and that of E-iSTx comes from the attenuated interference from outside to E-iSTxs.	126
4.6	Joint network capacity regions of signal energy detection method (left) and positioning-assisted method (right) under various indoor shadowing level ψ with fixed $a_o = 0.5$. The numbers above/below markers in graphs denote the density of PTxs λ_p at the collection of markers with the similar C_1 values.	140
4.7	Joint network capacity regions under receiver location-aware technique. The numbers above markers in graphs denotes the density of PTxs λ_p at the collection of markers with the similar C_1 values.	141
4.8	Joint network capacity region under various a_o with $\psi = -10$ dB. Case $a_o = 0.5$ is shown in Fig.4.1.	142
4.9	PTx X and PRx Y were shown with E-STxs using signal energy detection method. Left figure corresponds to the case with detection radius considering only outdoor devices in Section 4.4.1 and right figure corresponds to the case with conservative detection radius in Section 4.4.2.	152
4.10	Conditioned that there are no PTxs in $b(Z_o, r_d) (\supset b(W_o, r_{ps}))$, a G-oSRx W_o can be interfered by potential G-oSTx in $b(W_o, r_{ss}^{oo})$ or G-iSTxs in $b(W_o, r_{ss}^{io})$. Their activities are determined by surrounding PTxs in $b(z, r_d)$ for both G-oSTxs and G-iSTxs.	153
4.11	Conditioned that there are no PTxs in $b(W_o, s_o) (\supset b(Z_o, r_d^L))$, a L-oSRx W_o can be interfered by potential L-oSTx in $b(W_o, r_{ss}^{oo})$ or L-iSTxs in $b(W_o, r_{ss}^{io})$. Their activities are determined by surrounding PTxs, e.g., PTxs in $b(z, r_d^L)$ for a L-oSTx at z and PTxs in $b(z, r_d^{Li})$ for a L-iSTx at z . But, no PRxs outside of coverage and $r_{ss}^{oo} + r_d^L < s_o$ in our scenario guarantee that all harmful L-STxs are active.	154
4.12	A PTx X is located at $(-20000, 0)$ and L-oSTx Z_o is located in the the origin. The PIA of the L-oSTx Z_o is drawn as shaded region. The inner and outer discs given as $\mathcal{I}_{Z_o}^{ol} = b(O, r_{sp}(\ X - a\))$ and $\mathcal{I}_{Z_o}^{ou} = b(O, r_{sp}(\ X - b\))$ respectively can be used to compute an approximated area of the PIA. The leftmost and rightmost point of the PIA are denoted as a and b in the figure.	154

4.13 The PTx coverage $b(X, d_p)$ is partially shown as an dotted arc and hatched circle $b(W_o, r_{ss}^{oo})$ denotes a region where potentially harmful L-oSTxs to L-oSRx W_o can be located. For a L-oSTx $z \in b(W_o, r_{ss}^{oo})$, a PIA \mathcal{I}_z^o is drawn with solid thick line. Shaded region denotes a region where $\lambda_r(x) > 0$. In a non-shaded region inside \mathcal{I}_z , we have $\lambda_r(x) = 0$. There are four cases to consider depending the value of d . Case 3 can be merged with Case 4 by assuming $\lambda_r(z) = 0$ in Case 3. Figures were drawn for a L-oSRx only. For a L-iSRx r_{ps} , r_{sp} , r_{ss}^{oo} , and s_o should be replaced with r_{ps}^i , r_{sp}^i , r_{ss}^{oi} and s_i . respectively. 155

Chapter 1

Introduction

Evolving wireless communication and networking technologies have enabled various types of distributed wireless networks such as ad-hoc, mesh, sensor, and peer-to-peer networks. Supporting a large number of concurrent users with high data rate while meeting fairness objectives in such networks involves devising resource sharing mechanisms that can effectively utilize limited resources such as spectrum, time, code, or space.

In this dissertation, we are particularly interested in the achievable spatial reuse for wireless networks sharing a common *spectrum* resource. In wireless settings with radio signal transmitters and receivers, unlike other resources, space is not divisible into discrete units due to the continuity of signal/interference propagation. Thus, spectrum sharing is highly impacted by the achievable spatial reuse for wireless devices, and it is crucial towards achieving high performance especially in a network where nodes are distributed across large areas. A network with a high spatial reuse capability allows a large number of users to transmit concurrently, which consequently provides high throughput to individual nodes.

Spatial reuse is affected by numerous factors, some of which are controllable. Controllable factors are usually given as tunable system parameters or design choices: for example, medium access control (MAC) protocols, transmit power, decoding SINR threshold, carrier sensing threshold, etc. While un-controllable factors are usually external factors from environment such as channel fading and shadowing, existence of interfering heterogenous devices, random placement of nodes, etc; which are usually treated as *uncertainties* under which devices must operate.

Considering the above factors, a key challenge is to design such networks to achieve high performance and robustness while keeping cost/design complexity low. In this dissertation, we study the impact of such factors on system design and performance, in particular from a spatial reuse perspective in the context of ad-hoc and cognitive networks. Below, we briefly summarize the content of this dissertation.

In Chapter 2, we examine the potential benefits of taking advantage of dynamic channel variations between transmitter and receiver pairs. It is known that opportunistic transmissions, i.e., exploiting channel that are good, can achieve significant performance gains due to multi-user diversity [17, 25, 59, 90–92, 107]. We apply and extend this general idea to ad-hoc networks and study how channel variations can be exploited to improve spatial reuse. Specifically, we consider nodes randomly distributed in space who contend to transmit with neighboring nodes using CSMA protocols. We consider two opportunistic CSMA protocols using different strategies to exploit channel variations. Both protocols require status feedback from each receiver to its associated transmitter, and thus incur a certain amount of overhead. However, it turns out that the gain realized by our opportunistic protocols, in terms of both spatial reuse and spatial fairness, is significant relative to non-opportunistic protocols, and thus we argue that opportunistic MAC protocols offer an attractive choice to improve spatial reuse performance even with the increased design complexity/overheads they would require.

In Chapter 3, we consider spectrum/space sharing among two different types of nodes with different access priorities and study how system parameter optimization affects the spatial reuse performance in the context of cognitive networks. In such networks, devices called cognitive radios share the spectrum with licensed devices. However, in doing so, cognitive radios must protect licensed devices from their potentially harmful transmissions/interference [8, 35, 44, 83, 123]. To that end, the cognitive radios transmit only if they detect the absence of licensed nodes in their neighborhoods. In such a scenario, it turns out that the system parameters have a

huge impact on both detection/sensing and spatial reuse performance of cognitive networks. Transmit power, detection threshold, and decoding threshold are the key system parameters which we optimize to maximize the spatial reuse performance of cognitive networks while satisfying the protection requirement. We show that the spectrum/space sharing capability can be significantly improved by adjusting the system parameters.

In Chapter 4, we further explore cognitive networks and study the impact of additional information on the spatial reuse performance of cognitive networks. Specifically, we consider nodes randomly located either indoor or outdoor. The randomness of nodes' locations requires cognitive devices to be more conservative in their detection/transmission operations for protecting licensed nodes, and accordingly in such an environment cognitive networks exhibit poor performance.

In this dissertation we show that various additional information can remove environmental uncertainties and improve the spatial reuse performance of cognitive networks. Specifically, we consider three white space/spectrum detection techniques with different degrees of knowledge of the radio frequency environment:

- signal energy detection;
- positioning-assisted detection;
- and, receiver location-aware detection techniques.

As expected that the more information is available to the cognitive nodes, the higher the spatial reuse performance they can achieve. More specifically, we *quantify* the relative gains of these methods measured in terms of the joint network capacity region of the licensed and the cognitive networks. This exhibits the fundamental tradeoff between the spatial reuse performance of two coexisting networks.

In summary, we study the spatial reuse performance of wireless networks with a large number of nodes randomly distributed in space, specifically focusing on the impact of MAC protocols, optimal parameter selection, and side information regarding the environment.

Chapter 2

Spatial Reuse and Fairness of Mobile Ad-Hoc Networks with Channel-Aware CSMA Protocols

2.1 Introduction

Evaluating and optimizing the capacity of wireless ad-hoc networks has been one of the goals of the networking and information theory research communities for a last decade. Due to the inherent randomness in such networks, e.g., locations of nodes, wireless channels, and node interactions governed by protocols, researchers have developed stochastic models that can parsimoniously capture the uncertainty of such environments while still giving insight on system performance and optimization. Work based on stochastic geometric models have perhaps been the most successful in terms of providing reasonably realistic, yet mathematically tractable, results, see e.g., [13, 51, 113]. This chapter leverages this line of work to study the performance of networks operated under two channel-aware slotted CSMA type protocols.

One of the important factors determining the capacity of a wireless network is the *degree of spatial reuse*; this is mainly determined by the associated medium access control protocol. The following basic protocols: ALOHA, Opportunistic ALOHA (O-ALOHA), and CSMA have been studied in detail in literature. We discuss these briefly below.

ALOHA is a basic MAC protocol in which spatially distributed nodes simply transmit with some probability p . A mathematical model for a spatial version of an ALOHA based wireless ad-hoc network is detailed in [13]; various extensions capturing the impact of modulation techniques on the transmission capacity have been

studied, see e.g., [113]. Because transmitters contend independently, the transmission probability p should be properly chosen as a function of node density so as to achieve a high spatial reuse. This involves finding a compromise between a high density of transmitters and associated excessive interference which deteriorates the quality of transmissions and accordingly leads to low spatial reuse.

In [10, 112], the performance of an opportunistic version of spatial ALOHA (O-ALOHA)¹ was evaluated. In their models, only *qualified* transmitters, namely nodes whose channel quality to their associated receivers exceeds a threshold γ , can transmit with probability p . The resulting spatial reuse is thus affected by both parameters. When properly tuned, this simple channel-aware MAC can increase spatial reuse by roughly 40% relative to simple ALOHA.

Although O-ALOHA can dramatically increase spatial reuse, by qualifying nodes seeing good channels, it still suffers from collisions which limits its performance. Unlike (O-)ALOHA, carrier sense based medium access (CSMA) protocols achieve high spatial reuse by coordinating transmissions. In [11, 87], a modified Matérn hardcore process model for a spatial slotted CSMA protocol was introduced. Each node contends with its ‘neighbors’ via a uniformly distributed contention timer. The node with the earliest timeout wins. As a result the transmitters end up being nicely separated, see e.g., Fig. 2.1. Based on this model, CSMA is shown to increase spatial reuse by roughly 25% over basic ALOHA.

In this chapter, we extend the CSMA ad-hoc network model introduced in [11] to study two simple channel-aware MAC protocols. In the first scheme, named opportunistic CSMA (O-CSMA), we use a channel quality threshold γ , as introduced in [10, 112], to qualify nodes to participate in the CSMA contention process. Optimizing performance of such networks requires selecting γ as a function of node density and

¹The ALOHA considering channel state information (a.k.a opportunistic ALOHA) in single hop network was introduced and studied in [7, 94].

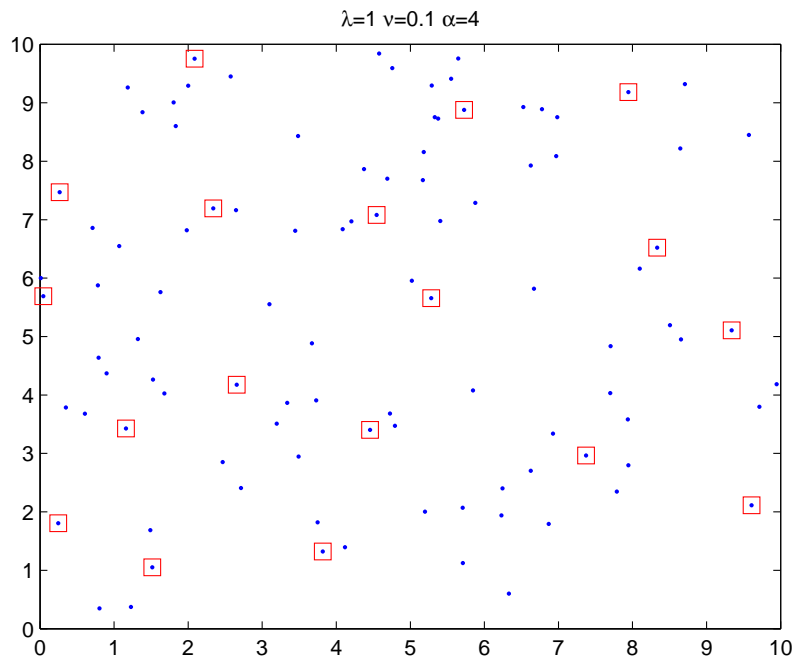


Figure 2.1: A realization of modified Matérn hardcore process : Blue points are the realization of marked Poisson point process where each point has an independent identically distributed mark denoting its timer value in $[0, 1]$. If a point has the smallest timer value in its neighborhood (neighborhood is not shown here but formally defined later in (2.3)), then, it is selected as a CSMA transmitter. Selected CSMA transmitters were drawn inside boxes.

channel variation distributions. In the second scheme called quantile-based CSMA (QT-CSMA), nodes contend based on the quantile of the channel quality to their associated receivers. Doing so allows nodes to transmit when their channel is the ‘best’ in their neighborhood. This also ensures that each node gets a fair share of access opportunities among the nodes in its neighborhood, and circumvents the problem of choosing a density dependent qualification threshold. This is particularly desirable if channel statistics seen across nodes are heterogeneous. Quantile-based scheduling approaches for downlinks in cellular networks were introduced and studied in [17, 90–92] and in the wireless LAN setting in [25, 59].

The performance metrics considered in this chapter are *spatial* averages of network performance, which means the performance metric captures an average over possible realizations of nodes’ locations. This is particularly meaningful, since in real world scenarios nodes are irregularly placed and/or motion might make a performance metric which is a function of nodes’ location is less informative. To that end, we characterize the performance as seen by a *typical* node using tools from stochastic geometry together with analytical/numerical computation methods.

Contributions This chapter makes the following four contributions.

First, to our knowledge, this is the first attempt to evaluate CSMA-based opportunistic MAC protocols, namely O-CSMA and QT-CSMA, in a stochastic geometric framework. Our approach captures the delicate interactions between the channel gains and interference statistics underlying the performance of opportunistically scheduled nodes in ad-hoc networks.

Second, we evaluate the sensitivity of spatial reuse to various protocol parameters, showing a clear advantage of QT-CSMA over O-CSMA which in turn have substantially better performance than simple ALOHA based schemes. To that end, we characterize the interplay between the density of active transmitters and the quality of transmissions as the function of qualification threshold γ and carrier sensing

threshold ν . In addition, we explore the maximum achievable spatial reuse under O/QT-CSMA in asymptotically dense networks by scaling γ as the function of node density. We show that both O/QT-CSMA exhibit a ‘phase transition’ phenomenon for spatial reuse depending on the scaling of γ .

Third, this work is the first to evaluate the spatial fairness realized by these protocols and to find that QT-CSMA can achieve better fairness than CSMA. Specifically we introduce and quantify a spatial fairness index among sets of nodes sharing the same number of neighbors, and which captures the impact of from random node placement.

Finally, we study tradeoffs between spatial fairness and spatial reuse, and compare the Pareto-frontier of O-CSMA and that of QT-CSMA. In this framework, we also evaluate the performance of O-ALOHA, (pure) ALOHA and (pure) CSMA as special cases. In particular, we show that quantile-based CSMA without a qualification step (Q_0 -CSMA) achieves a performance comparable to that of O/QT-CSMA in terms of both fairness and the density of successful transmissions, which is then a robust and attractive choice from an engineering perspective. We present some initial discussion of implementation consideration for such a protocol.

Related Work The two-hop wireless network studied in [46] is perhaps the first analytical model for a multi-hop wireless network. A similar model was used in [104, 105] to study the performance of slotted ALOHA and CSMA protocols respectively. Subsequently [106] and [18] have considered general multi-hop wireless networks.

The Markovian model for a multi-hop CSMA wireless network introduced in [18] has been the basis of much subsequent work. The network is modeled as a graph, where each node denotes a transmitter and if a pair of transmitters can interfere with each other’s receivers they are connected by an edge. Thus viable sets of transmitters correspond to independent sets. A MAC protocol can be modeled as a Markov chain

over independent sets, whose stationary distribution captures the long run performance seen by nodes, but is hard to evaluate.

This idealized model was later extended and widely used to show various insights on system behavior and performance [111] [33] [32] [109] [108] [34]. In [111], various throughput approximations for CSMA/CA based networks are developed, and various fairness driven scheduling methods are proposed and evaluated. The authors show that on a simple linear network with three nodes, CSMA/CA can be very unfair when nodes are aggressively accessing the medium. This problem arises due to location dependent contention in the multi-hop network setting, and can be serious since it can lead to node starvation [82] [42]. Based on the Markov chain model in [18] and [111], [33] studies the impact of asymmetry or so-called border effects and carrier sensing ranges on fairness in a linear topology. The authors confirm that unfairness is due to asymmetry in the network topology, which implies that unfairness can be removed, to a large extent, by either increasing the size of 1D networks or making carrier sense range larger than the receive range. However, it turns out that, in 2D grid networks, a phase-transition like phenomenon occurs whereby unfairness in a large network arises sharply if the intensity of nodes' access is sufficiently high [32]. The emergence of this phenomenon is a result of the regular structure of the grid-network and it vanishes as the network becomes irregular. Still CSMA-based networks exhibit various degrees of unfairness. To explore how to make the CSMA network fair, [109] [108], introduce a Markov chain model, with node-specific access intensities which equalize the per-node throughput. This approach was also used in [86], which introduced a framework translating various fairness objectives to corresponding contention resolution algorithms. The above described Markovian model is simple enough and somewhat tractable, so widely accepted. However, the Markovian model is too idealized to incorporate various PHY/MAC parameters and random factors such as node locations, fading channels² and aggregate interference

²Note that random fading is crucial for studying opportunistic scheduling.

at receivers, all of which have a substantial impact on the performance of individual nodes and the overall network.

With the introduction of the IEEE 802.11 protocol, several researchers have attempted to analyze multi-hop wireless networks using the IEEE 802.11. [24] was one of the early efforts which provided an analytical model for a given fixed network and computed the lower bound on the sum throughput of transmitter-receiver pairs for a given network. However, the model's simplified physical layer, so-called protocol model, does not take into account the impact of aggregate interference. Later, [21] provided a more sophisticated model which takes into account various PHY and MAC layer parameters. The authors linearly approximated the access probability of individual nodes as a function of its success probability and found a linear system like relationship between success probabilities and transmission probabilities of nodes in a given network. This gives a reasonable approximation of the per-node throughput, however, the work does not reveal how the system is affected by various system parameter selections or the inherent randomness in wireless environment. Furthermore performance is evaluated for a *given* fixed network, which is less informative considering mobile nature of wireless nodes.

The above limitations - i.e., not taking into account random fading channel, random node locations, impact of aggregate interference, and capture effect³ - are naturally addressed in research based on stochastic geometric models, see e.g., [13, 51, 102, 113], on which our work is based. In this line of work, the performance metrics of interest is an average over random environments (including fading, node locations, protocols, etc), which can be more informative in terms of representing typical behavior. Specifically the CSMA related work of [11] and [87] used a spatial point process to model spatially distributed wireless nodes using a CSMA-like MAC protocol. These works successfully approximated the statistics of the aggregate interference resulting from

³If two transmitters happen to send their packets to the same receiver, the one with a higher signal strength can be received with non-zero probability. This is called as a capture effect.

CSMA-like MAC nodes by those of a non-homogeneous Poisson point process interferers. The approximation was validated via simulation and was shown to match well. However, characterizing the exact interference statistics is still very hard and has remained an open problem. As a response to this, subsequent work in [41, 45] suggested an alternative approximation for the performance of CSMA nodes which is accurate for asymptotically sparse networks. The carrier sense mechanism models have also been successfully used to study cognitive radio networking scenarios in [65, 68, 88].

Our work is different from the above work in the following aspects. First, we build upon the CSMA model in [11] incorporating *opportunistic scheduling* schemes. We consider the dependency between the channel gain of a scheduled node and the activity of the surrounding nodes (or accordingly the statistics of interference), which has to our knowledge not been explored before. Second, we consider the fairness for *slotted* (or synchronized) CSMA networks. In particular, we study how system parameters and opportunistic CSMA protocols can change the fairness characteristics of the slotted CSMA network.

2.1.1 Organization

In Section 4.2, we describe our system model, including details for our two proposed opportunistic MAC protocols. Two spatial performance metrics of interest (spatial reuse and fairness) are introduced in Section 2.3. In Section 2.4, the transmission and success probability of a typical node under the two MAC protocols are derived. These will be used later to compute the two performance metrics. In Section 2.5, we compare the numerical results for the spatial reuse of O-CSMA and QT-CSMA networks under three node density regimes, and in Section 2.6, the fairness of such networks is evaluated and tradeoffs between spatial reuse and fairness are considered under various parameter values. 4.9 concludes the chapter.

2.2 System Model

2.2.1 Node Distribution and Channel Model

We model an ad-hoc wireless network as a set of transmitters and their corresponding receivers. Transmitters are distributed in \mathbb{R}^2 as an independently marked homogeneous Poisson Point Process (PPP) $\Psi = \{X_i, E_i, T_i, \mathbf{F}_i, \mathbf{F}'_i\}$, where $\Phi \equiv \{X_i\}_{i \geq 1}$ is the PPP with density λ denoting the set of transmitters or their locations in \mathbb{R}^2 and E_i is an indicator function which is equal to 1 if a node X_i transmits and 0 otherwise. The value of E_i is governed by the medium access protocol used and the activity of other nodes $\{X_j\}_{j \neq i}$. We assume that the receiver of each transmitter is located r meters away from the transmitter. The direction from a transmitter to its receiver is randomly distributed, i.e., uniformly on $[0, 2\pi]$. Throughout this chapter, we only consider the performance as seen by a typical receiver.

Let $\mathbf{F}_i = (F_{ij} : j)$ be a vector of random variables F_{ij} denoting the fast fading channel gains between the i th *transmitter* and the j th *receiver* associated with j th transmitter. In particular, F_{ii} denotes the channel gain from i th transmitter to its associated receiver. We assume that F_{ij} are symmetric, i.e., $F_{ij} = F_{ji}$ and independent and identically distributed (i.i.d.) with mean μ^{-1} , i.e., $F_{ij} \sim F$ (For two random variables A and B having the same distribution, we write $A \sim B$.), with cumulative distribution function (cdf) $G(x) = P(F \leq x)$. Let $\mathbf{F}'_i = (F'_{ij} : j)$ be the vector with coordinates F'_{ij} , where F'_{ij} is the random variable denoting fading gain between the i th *transmitter* and the j th *transmitter*. The random variable F'_{ij} are assumed symmetric and i.i.d, i.e., $F'_{ij} = F'_{ji}$ and $F'_{ij} \sim F$. In this chapter, we only consider the Rayleigh fading case where F has an exponential distribution with cdf $G(x) = 1 - \exp\{-\mu x\}$ for $x \geq 0$, but other fading models could be considered. Let $\|x\|$ denote the norm of the vector $x \in \mathbb{R}^2$ and $l(\|x - y\|) = \|x - y\|^\alpha$ be the path loss between two locations $x \in \mathbb{R}^2$ and $y \in \mathbb{R}^2$ with pathloss exponent $\alpha > 2$. Then, the interference power that the j th receiver at location y experiences from the i th transmitter at location x is $F_{ij}/l(\|x - y\|)$.

2.2.2 Signal to Interference Ratio Model

The performance of a receiver is governed by its signal to interference plus noise ratio (SINR). Under the model given above, the SINR seen at the i -th receiver is

$$\text{SINR}_i = \frac{F_{ii}/l(r)}{I_{\Phi \setminus \{X_i\}} + W}, \quad (2.1)$$

where $I_{\Phi \setminus \{X_i\}} = \sum_{X_j \in \Phi \setminus \{X_i\}} E_j F_{ji}/l(\|X_i - X_j\|)$ is the aggregate interference power, or so-called shot noise, and W is the thermal noise. We shall focus on interference limited networks, when the impact of thermal noise is comparatively negligible. In this chapter we focus on such a regime and let $W = 0$. The reception model we consider is the so-called *outage reception model*, where a receiver can successfully decode a transmission if its received SINR exceeds a decoding threshold t , i.e., the i -th receiver gets $\log(1+t)$ bits per second (bps) per transmission if $\text{SINR}_i > t$ and zero otherwise⁴.

2.2.3 Carrier Sense Multiple Access Protocols

We consider a *slotted CSMA* network, where nodes compete with each other to access a shared medium. Carrier sensing is followed by data transmission at each slot. Each node contends with its ‘neighboring’ nodes using a (uniformly distributed on $[0, 1]$) timer value. The timer value is *independent* of everything else and each node transmits if it has the smallest timer value in its neighborhood and defers otherwise. CSMA provides a way to resolve contentions among nodes but does not take advantage of channel variations. In what follows, we introduce two distributed *opportunistic CSMA* protocols which take advantage of channel variations amongst transmitters

⁴Instead of outage model, one can consider SINR model, where the performance of a typical receiver is given as $\mathbb{E}^0[\log(1 + \text{SINR}_0)]$ bits per second where SINR_0 is the SINR of a typical receiver [10]. This is an appropriate model for wireless devices using adaptive modulation and coding technique. In this chapter, we consider the outage model for simplicity, but it can be easily extended to the adaptive modulation model.

and their receivers: opportunistic CSMA (O-CSMA) and Quantile-based CSMA (QT-CSMA).

Under O-CSMA, nodes whose channel gains are higher than a fixed threshold γ qualify to contend; we call this the *qualification process*. We assumed that channel feedback from each receiver is available to its associated transmitter each slot. Qualified nodes in turn, contend for transmission with their neighbors on that slot. Specifically, let $\Phi^\gamma = \{X_i \in \Phi \mid F_{ii} > \gamma\}$ denote the set of qualified nodes or *contenders*. Note that Φ^γ is a subset of Φ which is generated by independent marks with probability

$$p_\gamma = \mathbb{P}(F > \gamma), \quad (2.2)$$

so it is a homogeneous PPP with density $\lambda^\gamma \equiv \lambda p_\gamma$. Each contender $X_i \in \Phi^\gamma$ has a set of qualified nodes with which it contends. We say two transmitters X_i and X_j *contend* if the received interference they see from each other is larger than the carrier sensing threshold ν , i.e., if $F'_{ij}/l(\|X_i - X_j\|) > \nu$ and by symmetry $F'_{ji}/l(\|X_i - X_j\|) > \nu$. We call the set of contenders of a node its *neighborhood* and denote it by

$$\mathcal{N}_i^\gamma = \{X_j \in \Phi^\gamma : F'_{ji}/l(\|X_i - X_j\|) > \nu, j \neq i\}. \quad (2.3)$$

Contending nodes are not allowed to transmit simultaneously since they can potentially interfere with each other. To avoid collisions, every slot each node X_j in Φ^γ picks a random timer value T_j which is uniformly distributed on $[0, 1]$. At the start of each time slot node X_j starts its own timer which expires in T_j seconds. Each node senses the medium until its own timer expires. If no node (in its neighborhood) begins transmitting prior to that time, then, it starts transmitting, otherwise it defers. Under this mechanism, a node transmits only if the node's timer value is the minimum in its neighborhood, i.e., when T_i is equal to $\min_{j: X_j \in \mathcal{N}_i^\gamma \cup \{X_i\}} T_j$.

Note that the qualification process is a mechanism selecting nodes with high channel gains. Thus, all qualified nodes have channel gains larger than γ . The posterior

channel distribution after qualification is F conditioned on that $F > \gamma$, so given by a shifted exponential distribution

$$G_\gamma(x) \equiv \mathbb{P}(F < x \mid F > \gamma) = (1 - \exp\{-\mu(x - \gamma)\}) \mathbf{1}\{x \geq \gamma\}. \quad (2.4)$$

The qualification process not only increases the signal strength but also reduces the amount of interference, and therefore we can expect successful transmissions. However, the parameter γ should be chosen judiciously; otherwise there will either be too many transmitting nodes generating too much interference or too few transmitting nodes resulting in low spatial reuse. Neither case is desirable. Note that when $\gamma = 0$ this model corresponds to the standard CSMA one proposed in [11].

Under QT-CSMA one also has a qualification process with threshold γ . However, the active transmitters in a neighborhood are selected based on the *quantile of their current channel gain*; we refer to this as *quantile scheduling*. Specifically, we assume that channel quality F_{ii} is available to the transmitter X_i , and at each slot a qualified transmitter X_i computes its channel quantile $Q_i = G_\gamma(F_{ii})$ using its channel gain F_{ii} (conditioned on that $F_{ii} > \gamma$). This transforms the channel distribution to a uniform distribution on $[0, 1]$, which serves both as a relative indicator for channel quality and to determine the timer for collision avoidance. More recently under QT-CSMA X_i sets its timer value, say T_i , to $1 - Q_i$ and starts sensing the medium until its timer expires. If no transmitting node is detected prior T_i , then, the node accesses the medium, otherwise it defers. In other words, node X_i transmits only if it has the highest quantile in its neighborhood, i.e., when $Q_i = Q_i^{\max}$ where $Q_i^{\max} \equiv \max_{j: X_j \in \mathcal{N}_i^\gamma \cup \{X_i\}} Q_j$. Let $F_{i,\gamma}^{\max} = G_\gamma^{-1}(Q_i^{\max})$ be the channel fade of a transmitting node X_i or the channel fade given node X_i transmits, where $G_\gamma^{-1}(\cdot)$ is the inverse function of $G_\gamma(\cdot)$. Let $N_i^\gamma = |\mathcal{N}_i^\gamma|$ for simplicity; then $F_{i,\gamma}^{\max}$ is a $N_i^\gamma + 1$ st order statistic, i.e.,

$$F_{i,\gamma}^{\max} = \max \left[F_{1,\gamma}, F_{2,\gamma}, \dots, F_{N_i^\gamma+1,\gamma} \right], \quad (2.5)$$

whose distribution conditioned on $N_i^\gamma = n$ is given by

$$\mathbb{P}(F_{i,\gamma}^{\max} \leq x \mid N_i^\gamma = n) = (1 - \exp\{-\mu(x - \gamma)\})^{n+1} \mathbf{1}\{x \geq \gamma\}. \quad (2.6)$$

Note that QT-CSMA further exploits opportunism beyond the qualification process. Unlike O-CSMA, a QT-CSMA node transmits only when it has the best channel condition in its neighborhood, which should further improve its likelihood of successful transmission. One may surmise that QT-CSMA may work well even without qualification process since the quantile scheduling will fully take advantage of opportunistic gain from many nodes (so-called multi-user diversity). This will be explored later. For that purpose, we shall denote QT-CSMA with $\gamma = 0$ by QT₀-CSMA.

2.2.4 Notation

For a random variable I , let $\mathcal{L}_I(s) = \mathbb{E}[e^{-sI}]$ be the Laplace transform of I . Let $\|x\|$ be the magnitude of $x \in \mathbb{R}^2$. Given a countable set C , let $|C|$ be the cardinality of C . Let $\mathbf{1}\{\cdot\}$ denote the indicator function and let $B_l \equiv b(0, l)$ denote a ball centered at the origin with radius l . \mathbb{R}_+ denotes the set of non-negative real numbers. Let Φ be a stationary point process and \mathcal{Y} be a property of Φ . We will use below the reduced Palm probability \mathbb{P}^{l_0} of Φ . Intuitively, the probability that Φ satisfies the property \mathcal{Y} under \mathbb{P}^{l_0} is the conditional probability that $\Phi \setminus \{0\}$ satisfies property \mathcal{Y} given that Φ has a point at 0. This will be denoted as follows: $\mathbb{P}^0(\Phi \setminus \{0\} \in \mathcal{Y}) = \mathbb{P}^{0l}(\Phi \in \mathcal{Y})$. We define Φ^0 as a point process Φ given $0 \in \Phi$. \mathbb{E}^0 denotes Palm expectation, which is interpreted as the conditional expectation conditioned on a node at the origin [12, 102].

2.3 Performance Metrics

The two key performance metrics of interest in this chapter are spatial reuse and spatial fairness. The former measures how *efficiently* the frequency is reused or transmissions are packed by a given MAC protocol and the latter measures how *fairly* this is done across nodes in the network. We formally define these performance measures below.

Table 2.1: Summary of notations

X_i	i -th transmitter or its location in \mathbb{R}^2
Φ	Poisson point process denoting the set of transmitters $\{X_i\}_{i \geq 1}$.
λ	Density of nodes in Φ
F	Generic exponential random variable with mean $1/\mu$ denoting short term fading gain
$F_{ij}(= F_{ji})$	Short term fading gain between transmitter X_i and the receiver associated with X_j
$F'_{ij}(= F'_{ji})$	Short term fading gain between transmitter X_i and the transmitter X_j
γ	Qualification threshold
p_γ	Probability that a transmitter to qualify ($= P(F > \gamma)$)
Φ^γ	Set of qualified transmitters
$G_\gamma(\cdot)$	Cdf of random variable F_γ
Φ_M^γ	Set of active transmitters
$\Phi_M^{\gamma 0}$	Set of active transmitters Φ_M^γ given $0 \in \Phi_M^\gamma$
ν	Carrier sensing threshold
F_γ	Fading gain of O-CSMA
t	Decoding threshold
λ^γ	Density of qualified transmitters ($= \lambda p_\gamma$)
N_0^γ	Size of neighborhood of a typical node
$F_{0,\gamma}^{\max}(N_0^\gamma + 1)$	Fading gain of a typical QT-CSMA transmitter when the size of its neighborhood is N_0^γ
r	Distance between a transmitter and its associated receiver
$N_{s,0}^\gamma$	Size of neighborhood of typical node under the assumption $F'_{ij} = \mathbb{E}[F]$ in Section 2.6.1
$I_{\Phi_M^{\gamma 0} \setminus \{0\}}$	Aggregate interference power from transmitters in $\Phi_M^{\gamma 0} \setminus \{0\}$
$I_{\Phi_M^{\gamma 0} \setminus \{0\}}^{n,x}$	Aggregate interference power from transmitters in $\Phi_M^{\gamma 0} \setminus \{0\}$ conditioned on that the associated typical node has $N_0^\gamma = n$ contenders and it has channel gain $F_{0,\gamma}^{\max}(N_0^\gamma + 1) = x$
λ_{dens}	Asymptotic density of active transmitters
Φ_M^{csma}	Point process of active CSMA transmitters with density λ_{dens}
$I_{\Phi_M^{csma 0} \setminus \{0\}}$	Aggregate interference power from transmitters in $\Phi_M^{csma 0} \setminus \{0\}$

2.3.1 Spatial Reuse

As a measure of spatial reuse, we will use *the density of successful transmissions* which is defined as the mean number of nodes that successfully transmit per square meter. This is given by

$$d_{suc} = \lambda p_{tx} p_{suc}, \quad (2.7)$$

where λ denotes the density of transmitters, p_{tx} denotes the transmission probability of a typical transmitter, and p_{suc} denotes the transmission success probability. This metric not only measures the *level of spatial packing* through λp_{tx} but also the *quality of transmissions* through p_{suc} , which captures the interactions (though interference) among spatially distributed nodes.

Other relevant metrics, such as transmission capacity [113] given by $\log(1+t)\lambda p_{tx} p_{suc}$ or throughput density [10] given as $\mathbb{E}[\log(1 + \text{SINR})]\lambda p_{tx}$, could be used instead of (2.7), however we focus on (2.7) for simplicity.

2.3.2 Spatial Fairness

In an environment where nodes are randomly distributed in space, the nodes' locations (or topology) and protocol jointly affect the variability of interference seen at receivers, which will in turn result in spatial non-homogeneity in nodes' performance. Thus, it is worthwhile to *quantitatively* study the impact of such variability on fairness. In particular, we are interested in finding a *spatial* fairness index which captures a fairness of the long-term (*time-averaged*) performance across nodes in space. To that end, we define two types of spatial fairness indices.

The first captures the heterogeneity in performance due to nodes' locations. Recall that the performance of node, say X_i , is affected by the remaining nodes and their locations, i.e. $\Phi \setminus \{X_i\}$ and channel gains \mathbf{F}_i and \mathbf{F}'_i , where $\mathbf{F}'_i = (F'_{ij} : j \neq i)$. Let $f_i(\Phi, \mathbf{F}_i, \mathbf{F}'_i)$ be a finite value associated with $X_i \in \Phi$ denoting its performance. Then, $\mathbb{E}[f_i(\Phi, \mathbf{F}_i, \mathbf{F}'_i) \mid \Phi = \phi]$ denotes the time-averaged (or equivalently, the average

w.r.t. \mathbf{F}_i and \mathbf{F}'_i of the) performance for X_i given $\Phi = \phi$. To evaluate the fairness of $\mathbb{E}[f_i(\Phi, \mathbf{F}_i, \mathbf{F}'_i) | \Phi = \phi]$ across nodes $X_i \in \Phi = \phi$ in space we introduce Jain's fairness index [61], where

$$\text{FI} = \lim_{l \rightarrow \infty} \frac{\left(\sum_{X_i \in \phi \cap B_l} \mathbb{E}[f_i(\Phi, \mathbf{F}_i, \mathbf{F}'_i) | \Phi = \phi] \right)^2}{|\phi \cap B_l| \sum_{X_i \in \phi \cap B_l} (\mathbb{E}[f_i(\Phi, \mathbf{F}_i, \mathbf{F}'_i) | \Phi = \phi])^2}. \quad (2.8)$$

Given the spatial ergodicity of homogeneous PPPs, see [12], and simple algebra, it is easy to see that (2.8) becomes

$$\text{FI} = \frac{(\mathbb{E}^0 [\mathbb{E}[f_0(\Phi, \mathbf{F}_0, \mathbf{F}'_0) | \Phi]])^2}{\mathbb{E}^0[(\mathbb{E}[f_0(\Phi, \mathbf{F}_0, \mathbf{F}'_0) | \Phi])^2]}, \quad (2.9)$$

where \mathbf{F}_0 and \mathbf{F}'_0 denote the channel fading of a typical node at the origin and accordingly $\mathbb{E}[f_0(\Phi, \mathbf{F}_0, \mathbf{F}'_0) | \Phi]$ denotes the performance seen by the typical node centered at the origin.

The second fairness index captures the heterogeneity in performance across the sets of nodes with the same size of neighborhoods. We, let $\tilde{f}_i(N_i, \mathbf{F}_i, \mathbf{F}'_i)$ be a finite performance metric associated with X_i , where N_i is the number of neighbors of X_i . Then, $\mathbb{E}[\tilde{f}_i(N_i, \mathbf{F}_i, \mathbf{F}'_i) | N_i = n]$ denotes the time-averaged (or \mathbf{F}_i and \mathbf{F}'_i -averaged) value associated with X_i given X_i has a neighborhood of size $N_i = n$. The corresponding Jain's fairness index is given as

$$\tilde{\text{FI}} = \frac{\left(\mathbb{E}^0 \left[\mathbb{E} \left[\tilde{f}_0(N_0, \mathbf{F}_0, \mathbf{F}'_0) | N_0 \right] \right] \right)^2}{\mathbb{E}^0 \left[\left(\mathbb{E} \left[\tilde{f}_0(N_0, \mathbf{F}_0, \mathbf{F}'_0) | N_0 \right] \right)^2 \right]}. \quad (2.10)$$

Unlike (2.9), (2.10) does not capture a performance variability across nodes with the same number of contenders. However, (2.10) is a useful metric which is computable in many cases. Depending on the performance metric $f()$ of interest, we sometimes have $\text{FI} = \tilde{\text{FI}}$. In the sequel, we will focus on $\tilde{\text{FI}}$ as our measure of spatial fairness.

2.4 Transmission Performance Analysis

In this section, we derive expressions for the access and transmission success probabilities which in turn are used to compute the density of successful transmissions for our opportunistic scheduling schemes. We begin by restating some known results from [10, 11] modified to fit to our setting.

2.4.1 Previous Results

Proposition 1. (*Laplace Transform of Shot-Noise for Non-homogeneous Poisson field*) [11] Let $\Phi_h = \{X_i, F_i\}$ be an independently marked non-homogeneous PPP in \mathbb{R}^2 with spatial density $h(x)dx$. Then, the Laplace transform of the associated shot-noise interference $I_{\Phi_h}(r) = \sum_{X_i: (X_i, F_i) \in \Phi_h} F_i/l(\|X_i - r\|)$ at location $r \in \mathbb{R}^2$ is given by

$$\mathcal{L}_{I_{\Phi_h}(r)}(s) = \mathbb{E} [e^{-sI_{\Phi_h}(r)}] = \exp \left\{ - \int_{\mathbb{R}^2} \left(1 - \mathcal{L}_F \left(\frac{s}{l(\|x - r\|)} \right) \right) h(x) dx \right\}. \quad (2.11)$$

In particular, if F is an exponential random variable with rate μ , we have

$$\mathcal{L}_{I_{\Phi_h}(r)}(s) = \exp \left\{ - \int_{\mathbb{R}^2} \frac{h(x)}{1 + \frac{\mu}{s}l(\|x - r\|)} dx \right\}. \quad (2.12)$$

Proposition 2. (*Mean size of Neighborhood*) [11] The number of neighbors of a typical node is Poisson with mean

$$\bar{N}_0^\gamma = \mathbb{E} [N_0^\gamma] = \mathbb{E}^0 \left[\sum_{X_i \in \Phi^\gamma \setminus \{0\}} \mathbf{1} \{F_i > \nu l(\|X_i\|)\} \right] = \lambda^\gamma \int_{\mathbb{R}^2} \exp \{-\nu \mu l(\|x\|)\} dx = \frac{2\pi \lambda^\gamma \Gamma(2/\alpha)}{\alpha(\nu \mu)^{2/\alpha}}. \quad (2.13)$$

Proposition 3. (*Conditional Transmission Probability under CSMA protocol*) [11] For the O-CSMA model given in Section 4.2 with qualified transmitter density λ^γ , the probability that a qualified node $x_1 \in \mathbb{R}^2$ transmits given there is a transmitter $x_0 \in \mathbb{R}^2$ with $\|x_1 - x_0\| = \tau$ which transmits (i.e., wins its contention), i.e., $\mathbb{P}(E_1 =$

$1 \mid E_0 = 1, \{x_0, x_1\} \subset \Phi^\gamma, \|x_1 - x_0\| = \tau) \equiv h(\tau, \lambda^\gamma)$, is

$$h(\tau, \lambda^\gamma) = \frac{\frac{2}{b(\tau, \lambda^\gamma) - N_0^\gamma} \left(\frac{1 - e^{-\bar{N}_0^\gamma}}{N_0^\gamma} - \frac{1 - e^{-b(\tau, \lambda^\gamma)}}{b(\tau, \lambda^\gamma)} \right) (1 - e^{-\nu\mu(\tau)})}{\frac{1 - e^{-\bar{N}_0^\gamma}}{N_0^\gamma} - e^{-\nu\mu(\tau)} \left(\frac{1 - e^{-\bar{N}_0^\gamma}}{(\bar{N}_0^\gamma)^2} - \frac{e^{-\bar{N}_0^\gamma}}{N_0^\gamma} \right)}, \quad (2.14)$$

where

$$b(\tau, \lambda^\gamma) = 2\bar{N}_0^\gamma - \lambda^\gamma \int_0^\infty \int_0^{2\pi} e^{-\nu\mu(l(x) + l(\sqrt{\tau^2 + x^2 - 2\tau x \cos\theta}))} x d\theta dx. \quad (2.15)$$

Proposition 4. (Plancherel-Parseval Theorem) C3.3 of [19] If σ_1 and σ_2 are square integrable complex functions, i.e., $\int_{\mathbb{R}} |\sigma_i(x)|^2 dx < \infty$ for $i = 1, 2$, then

$$\int_{\mathbb{R}} \sigma_1(x) \sigma_2^*(x) dx = \int_{\mathbb{R}} \hat{\sigma}_1(s) \hat{\sigma}_2^*(s) ds, \quad (2.16)$$

where $\hat{\sigma}_i(s) = \int_{\mathbb{R}} \sigma_i(x) e^{-2j\pi s x} dx$ is the Fourier transform of σ_i and σ_i^* is the complex conjugate of σ_i .

2.4.2 O-CSMA

Access Probability of a Typical Transmitter The access probability is the probability that a typical node transmits. As described earlier, under O-CSMA, only nodes who qualify can contend, so the network after the qualification process is indeed equivalent to a network with node density λ^γ . The channel distribution function of a qualified node, say X_i is given by (2.4). Let $E_i = \mathbf{1}\{F_{ii} > \gamma, T_i < \min_{j: X_j \in \mathcal{N}_i^\gamma} T_j\}$ be the transmission indicator for $X_i \in \Phi$, i.e., that it qualifies and wins the contentions process in its neighborhood, and $\Phi_M^\gamma = \{X_i \in \Phi \mid E_i = 1\}$ be the set of active transmitters. We define the transmission probability of the typical node (at the origin) as

$$p_{tx}^{op}(\lambda, \gamma, \nu) = \mathbb{P}^0 \left(F_{00} > \gamma, T_0 < \min_{j: X_j \in \mathcal{N}_0^\gamma} T_j \right). \quad (2.17)$$

Note that the two events in (2.17) are independent. To compute the probability of the second event, we condition on T_0 , i.e.,

$$\mathbb{P}^0 \left(T_0 < \min_{j: X_j \in \mathcal{N}_0^\gamma} T_j \right) = \mathbb{E}^0 \left[\mathbb{P}^0 \left(T_0 < \min_{j: X_j \in \mathcal{N}_0^\gamma} T_j \mid T_0 \right) \right]. \quad (2.18)$$

The conditional probability within the above expectation is the probability that X_0 has no neighboring node whose timer value is less than T_0 for a given T_0 , i.e.,

$$\mathbb{P}^0 \left(\{X_j \in \Phi \setminus \{X_0\} \text{ s.t. } F_{jj} > \gamma, F'_{j0} > \nu l(\|X_j - X_0\|), j \neq 0, T_j < T_0\} = \emptyset \mid T_0 \right). \quad (2.19)$$

The density measure of such nodes at location $x \in \mathbb{R}^2$ with $F_{jj} = f_1$, $F'_{j0} = f_2$ and $T_j = t$ is

$$\Lambda(dt, df_1, df_2, dx) = \mathbf{1}\{t < T_0\} dt \mathbf{1}\{f_1 > \gamma\} G(df_1) \mathbf{1}\{f_2 > \nu l(\|x\|)\} G(df_2) \lambda dx.$$

Thus, the conditional void probability of such nodes, i.e., (2.19), corresponds to

$$\begin{aligned} \exp \left\{ - \int_{\mathbb{R}^2} \int_0^\infty \int_0^\infty \int_0^1 \Lambda(dm, df_1, df_2, dx) \right\} &= \exp \left\{ -M_0 p_\gamma \int_{\mathbb{R}^2} 1 - G(\nu l(\|x\|)) \lambda dx \right\} \\ &= \exp \left\{ -M_0 p_\gamma \bar{N}_0 \right\}. \end{aligned} \quad (2.20)$$

Substituting (2.20) into (2.18) gives

$$p_{tx}^{op}(\lambda, \gamma, \nu) = \frac{1 - \exp \left\{ -p_\gamma \bar{N}_0 \right\}}{\bar{N}_0}. \quad (2.21)$$

Note that the spatial mean number of contenders for a typical node under O-CSMA is given by $p_\gamma \bar{N}_0$ since individual nodes qualify with probability p_γ . The case with $\gamma = 0$ (or $p_\gamma = 1$) corresponds to the pure CSMA scheme without a qualification step.

Transmission Success Probability of a Typical Receiver Next, we compute the transmission success probability of a receiver associated with a typical active transmitter X_0 at the origin:

$$p_{suc}^{op}(\lambda, \gamma, \nu, t) = \mathbb{P}^0 \left(\frac{F_{00}/l(r)}{I_{\Phi_M^\gamma \setminus \{0\}}} > t \mid F_{00} > \gamma \right), \quad (2.22)$$

where

$$I_{\Phi_M^\gamma \setminus \{0\}} \equiv \sum_{X_j \in \Phi_M^\gamma \setminus \{0\}} F_{j0}/l(\|X_j - (0, r)\|) \quad (2.23)$$

is a shot noise interference. Note that the interference we consider is the shot noise from Matérn CSMA transmitters *seen by the receiver of a typical transmitter* (which is *different* from a shot noise seen at a random point), so, the shot noise in (2.23) should be understood as a conditional shot noise conditioned on that $0 \in \Phi_M^\gamma$. When we refer the shot noise outside $\mathbb{P}^0(\cdot)$, we will use $I_{\Phi_M^{\gamma_0}}$ instead of $I_{\Phi_M^\gamma}$, where $\Phi_M^{\gamma_0}$ (the Palm version of Φ_M^γ) is Φ_M^γ given $0 \in \Phi_M^\gamma$. Then, the shot noise of interest can be written as

$$I_{\Phi_M^{\gamma_0} \setminus \{0\}} \equiv \sum_{X_j \in \Phi_M^{\gamma_0} \setminus \{0\}} F_{j0}/l(\|X_j - (0, r)\|) \quad (2.24)$$

For notational simplicity let F_γ be a random variable with the distribution function (2.4) which is independent of F_{00} . Then, (2.22) can be rewritten as follows by conditioning on F_γ :

$$\mathbb{P}^0 \left(F_\gamma > tl(r)I_{\Phi_M^\gamma \setminus \{0\}} \right) = \mathbb{E} \left[\mathbb{P}^0 \left(F_\gamma > tl(r)I_{\Phi_M^\gamma \setminus \{0\}} \mid F_\gamma \right) \right]. \quad (2.25)$$

Note that it is hard to compute (2.25) since $\Phi_M^{\gamma_0} \setminus \{0\}$ is a point process induced by the qualification process followed by the CSMA protocol, which has dependency among node locations. It is called as a Matérn CSMA process [11]. Thus, following [11], we approximate the shot noise $I_{\Phi_M^{\gamma_0} \setminus \{0\}}$ with $I_{\Phi_h^{\gamma_0} \setminus \{0\}} = \sum_{X_j \in \Phi_h^{\gamma_0} \setminus \{0\}} F_{j0}/l(\|X_j - (0, r)\|)$ which is a shot noise seen at the receiver of X_0 in a non-homogeneous PPP Φ_h^γ with density $\lambda^\gamma h(\tau, \lambda^\gamma)$ for $\tau > 0$, where $\lambda^\gamma \equiv p_\gamma \lambda$ and $h(\tau, \lambda)$ is the conditional probability that a CSMA transmitter at distance τ from the origin be active conditioned on an active CSMA transmitter at the origin with the density of nodes being λ^γ , see (2.14). Since h is a function which converges to 0 as $\tau \rightarrow 0$, and converges to p_{tx}^{op} as $\tau \rightarrow \infty$, it captures well the modification of the interference due to the presence of the transmitter at the origin. The h for a certain parameter sets is shown in Fig. 2.9a. Then, we have

$$\mathbb{P}^0 \left(F_\gamma > tl(r)I_{\Phi_M^\gamma \setminus \{0\}} \right) \approx \mathbb{E} \left[\mathbb{P}^0 \left(F_\gamma > tl(r)I_{\Phi_h^\gamma \setminus \{0\}} \mid F_\gamma \right) \right]. \quad (2.26)$$

Let $\xi_h(x)$ be the probability density function of $I_{\Phi_h^{\gamma^0} \setminus \{0\}}$. Then, using an indicator function, we can rewrite right hand side of (2.26) as

$$\mathbb{E} \left[\int_{-\infty}^{\infty} \xi_h(x) \mathbf{1}\{0 < x < \frac{F_\gamma}{tl(r)}\} dx \right]. \quad (2.27)$$

Clearly $\mathbf{1}\{0 < x < \frac{F_\gamma}{tl(r)}\}$ is square integrable for $r > 0$ and $t > 0$, and $\xi_h(x)$ is square integrable⁵. We can apply Plancherel-Parseval Theorem in (2.16) to (2.27) followed by a change of variables to get

$$\int_{-\infty}^{\infty} \mathcal{L}_{I_{\Phi_h^{\gamma^0} \setminus \{0\}}} (2i\pi tl(r)s) \frac{\mathcal{L}_{F_\gamma}(-2i\pi s) - 1}{2\pi i s} ds. \quad (2.28)$$

Noting that $\mathcal{L}_{F_\gamma}(s) = \frac{\mu}{\mu+s} e^{-s\gamma}$, we get

$$p_{suc}^{op}(\lambda, \gamma, \nu, t) \approx \int_{-\infty}^{\infty} \mathcal{L}_{I_{\Phi_h^{\gamma^0} \setminus \{0\}}} (2i\pi l(r)ts) \frac{\frac{\mu}{\mu-2i\pi s} \exp\{2i\pi s\gamma\} - 1}{2i\pi s} ds. \quad (2.29)$$

The last step is to compute the Laplace transform $\mathcal{L}_{I_{\Phi_h^{\gamma^0} \setminus \{0\}}}(s)$ which is given as

$$\mathcal{L}_{I_{\Phi_h^{\gamma^0} \setminus \{0\}}}(s) = \exp \left\{ -\lambda^\gamma \int_0^\infty \int_0^{2\pi} \frac{h(\tau, \lambda^\gamma) \tau d\theta d\tau}{1 + \mu f(\tau, r, \theta)/s} \right\}, \quad (2.30)$$

where $f(\tau, r, \theta) = l(\sqrt{\tau^2 + r^2 - 2\tau r \cos \theta})$. Replacing (2.30) into (2.29) gives a numerically computable integral form for the outage probability.

2.4.3 QT-CSMA

Access Probability of a Typical Transmitter Computing the access probability of a typical QT-CSMA node is not much different from that of an O-CSMA node. Under QT-CSMA, a node can transmit if its timer expires first or equivalently it has the highest quantile in its neighborhood. Let E_i be the transmission indicator of node $X_i \in \Phi$, i.e., $E_i = \mathbf{1}\{F_{ii} > \gamma, Q_i > \max_{j: X_j \in \mathcal{N}_i^\gamma} Q_j\}$. Let $\Phi_M^\gamma = \{X_i \in \Phi \text{ s.t. } E_i = 1\}$

⁵Note that the pdf of Poisson shot noise interference from Poisson transmitters with finite density is square integrable, see [10]. The existence of a Poisson point process of which shot noise dominates $I_{\Phi_h^{\gamma^0} \setminus \{0\}}$ implies that the pdf of $I_{\Phi_h^{\gamma^0} \setminus \{0\}}$ is square integrable.

be a thinned version of Φ containing only active transmitters. Then, using a similar technique as above, the access probability of a typical node X_0 at the origin under QT-CSMA is computed as follows:

$$p_{tx}^{qt}(\lambda, \gamma, \nu) = \mathbb{E}^0 \left[\frac{p_\gamma}{N_0^\gamma + 1} \right] = \frac{1 - \exp\{-p_\gamma \bar{N}_0\}}{\bar{N}_0}. \quad (2.31)$$

Since all Q_i s in (2.31) are uniform random variables, the result is the same as (2.21).

Transmission Success Probability of a Typical Receiver Next we compute the transmission success probability of a receiver associated with a typical transmitter X_0 at the origin. To determine the success probability, we need to characterize the fading gain $F_{0,\gamma}^{\max}$ and the interference power that the receiver experiences. We shall explicitly denote the fact that $F_{0,\gamma}^{\max}$ depends on $N_0^\gamma + 1$ by writing $F_{0,\gamma}^{\max}(N_0^\gamma + 1)$ in what follows. The aggregate interference from concurrent active transmitters in $\Phi_M^{\gamma_0} \setminus \{0\}$ to the receiver of X_0 is given by $I_{\Phi_M^{\gamma_0} \setminus \{0\}}$ as (2.24). Then, the success probability of a typical QT-CSMA receiver is written as

$$p_{suc}^{qt}(\lambda, \gamma, \nu, t) = \mathbb{P}^0(F_{0,\gamma}^{\max}(N_0^\gamma + 1) > tl(r)I_{\Phi_M^{\gamma_0} \setminus \{0\}}). \quad (2.32)$$

Unlike the case in (2.25), the $F_{0,\gamma}^{\max}(N_0^\gamma + 1)$ is no longer independent of the Palm version of $I_{\Phi_M^{\gamma_0} \setminus \{0\}}$. To see this intuitively, consider two extreme cases. First, suppose $F_{0,\gamma}^{\max}(N_0^\gamma + 1)$ has a very small value, say ϵ , then, this implies the channel gains of X_0 's neighbors are concentrated within the small interval $[0, \epsilon]$; so, the neighbors of X_0 's neighbors are not likely to defer their transmissions, which in turn means X_0 's receiver would experience somewhat stronger interference. By contrast, if $F_{0,\gamma}^{\max}(N_0^\gamma + 1)$ has a large value, say ω , then, the fading gains of X_0 's neighbors would be distributed on $[0, \omega]$, which is more likely to cause their neighbors to defer. This on average makes the interference level seen at the receiver smaller than in the previous case.

That is, $I_{\Phi_M^{\gamma_0} \setminus \{0\}}$ depends on both N_0^γ and $F_{0,\gamma}^{\max}(N_0^\gamma + 1)$. By conditioning on N_0^γ and $F_{0,\gamma}^{\max}(N_0^\gamma + 1)$, (2.32) can be written as

$$\mathbb{E}^0 \left[\mathbb{P}^0 \left(F_{0,\gamma}^{\max}(N_0^\gamma + 1) > tl(r)I_{\Phi_M^{\gamma_0} \setminus \{0\}} \mid N_0^\gamma, F_{0,\gamma}^{\max}(N_0^\gamma + 1) \right) \right]. \quad (2.33)$$

As in (2.25), we approximate $I_{\Phi_M^{\gamma_0} \setminus \{0\}}$ for a given $N_0^\gamma = n$ and $F_{0,\gamma}^{\max}(N_0^\gamma + 1) = x$ by a non-homogeneous Poisson point process Φ_u^γ with density $\lambda^\gamma u(n, x, \tau, \lambda, \gamma)$, where $u(n, x, \tau, \lambda, \gamma)$ is the conditional probability that a node y_1 transmits conditioned on following facts: 1) y_0 transmits, i.e., $E_0 = 1$, 2) $N_0^\gamma = n$, 3) $F_{0,\gamma}^{\max}(N_0^\gamma + 1) = x$ or equivalently y_0 's timer value T_0 is given as $t_0 = 1 - G_\gamma(x)$, 4) both y_0 and y_1 belong to Φ^γ , and 5) y_1 is τ meter away from y_0 . This can be written as

$$u(n, x, \tau, \lambda, \gamma) = \mathbb{P}(E_1 = 1 \mid E_0 = 1, N_0^\gamma = n, F_{0,\gamma}^{\max}(N_0^\gamma + 1) = x, \{y_0, y_1\} \subset \Phi^\gamma, \|y_0 - y_1\| = \tau). \quad (2.34)$$

Using the fact that $1 - G_\gamma(x)$ is one-to-one mapping from $[\gamma, \infty]$ to $[0, 1]$, we can rewrite (2.34) as

$$u(n, x, \tau, \lambda, \gamma) = \mathbb{P}(E_1 = 1 \mid E_0 = 1, N_0^\gamma = n, T_0 = t_0, \{y_0, y_1\} \subset \Phi^\gamma, \|y_0 - y_1\| = \tau). \quad (2.35)$$

Note that the probability (2.35) is a function of n , t_0 , τ and λ^γ ; so it is convenient to use the function u' such that

$$u(n, x, \tau, \lambda, \gamma) = u'(n, 1 - G_\gamma(x), \tau, \lambda^\gamma).$$

It is shown in Appendix 2.9 that this function is given by

$$u'(n, t_0, \tau, \lambda) = \frac{\bar{N}_0 G(\nu l(\tau))}{n + (\bar{N}_0 - n) G(\nu l(\tau))} \left(\frac{(1 - e^{-t_0 \bar{N}_0 (1 - p_s)})}{\bar{N}_0 (1 - p_s)} + (1 - t_0) e^{-\bar{N}_0 (1 - p_s)} \sum_{k=0}^n \frac{k!}{\eta^{k+1}} \left(1 - e^{-\eta \sum_{j=0}^k \frac{\eta^j}{j!}} \right) \binom{n}{k} p_s^k (1 - p_s)^{n-k} \right), \quad (2.36)$$

with $p_s = p_s(\tau, \lambda) = 2 - \frac{b(\tau, \lambda)}{N_0}$, and $\eta = \bar{N}_0 (1 - p_s) (t_0 - 1)$.

Then, (2.33) can be approximated with

$$\mathbb{E}^0 \left[\mathbb{P}^0 \left(F_{0,\gamma}^{\max}(N_0^\gamma + 1) > tl(r) I_{\Phi_u^\gamma \setminus \{0\}} \mid N_0^\gamma, F_{0,\gamma}^{\max}(N_0^\gamma + 1) \right) \right]. \quad (2.37)$$

Let $\xi_u^{n,x}$ be the conditional pdf of $I_{\Phi_u^{\gamma_0} \setminus \{0\}}$ given $N_0^\gamma = n$ and $F_{0,\gamma}^{\max}(N_0^\gamma + 1) = x$. Then, (2.37) can be rewritten as

$$\mathbb{E}^0 \left[\int_{-\infty}^{\infty} \xi_u^{N_0^\gamma, F_{0,\gamma}^{\max}(N_0^\gamma+1)}(y) \mathbf{1} \left\{ 0 \leq y \leq \frac{F_{0,\gamma}^{\max}(N_0^\gamma+1)}{tl(r)} \right\} dy \right], \quad (2.38)$$

where $\mathbf{1} \left\{ 0 \leq y \leq \frac{F_{0,\gamma}^{\max}(N_0^\gamma+1)}{tl(r)} \right\}$ and $\xi_u^{n,x}$ are both square integrable, see [10]. Applying the Plancherel-Parseval Theorem in (2.16) and performing the change of variables gives

$$p_{suc}^{qt}(\lambda, \gamma, \nu, t) \approx \mathbb{E}^0 \left[\int_{-\infty}^{\infty} \mathcal{L}_{I_{\Phi_u^{\gamma} \setminus \{0\}}^{N_0^\gamma, F_{0,\gamma}^{\max}(N_0^\gamma+1)}}(2i\pi l(r)ts) \frac{\exp \{2i\pi s F_{0,\gamma}^{\max}(N_0^\gamma+1)\} - 1}{2i\pi s} ds \right]. \quad (2.39)$$

Note that the expectation in (2.39) is with respect to N_0^γ and $F_{0,\gamma}^{\max}(N_0^\gamma+1)$, and $I_{\Phi_u^{\gamma} \setminus \{0\}}^{n,x}$ is a random variable with cdf $\mathbb{P}^0(I_{\Phi_u^{\gamma} \setminus \{0\}} < z \mid N_0^\gamma = n, F_{0,\gamma}^{\max}(N_0^\gamma+1) = x)$. We have

$$\mathcal{L}_{I_{\Phi_u^{\gamma} \setminus \{0\}}^{n,x}}(s) = \exp \left\{ -\lambda^\gamma \int_0^\infty \int_0^{2\pi} \frac{u'(n, 1 - G_\gamma(x), \tau, \lambda^\gamma) \tau d\theta d\tau}{1 + \mu f(\tau, r, \theta)/s} \right\}. \quad (2.40)$$

Replacing (2.40) into (2.39) gives the numerically computable approximation of p_{suc}^{qt} .

2.5 Spatial Reuse

In this section, we compare the spatial reuse achieved by O-CSMA vs QT-CSMA in three different node density regimes. To better understand the results or the behavior of protocols as a function of λ , γ , and ν , we first study how transmission probability and success probability change as the functions of the parameters, and then we compare the performance of O-CSMA and QT-CSMA. A brief performance comparison between O-ALOHA and O-CSMA follows.

2.5.1 System Behavior in Function of System Parameters

Density of Active Transmitters λp_{tx} In Fig 2.2, we show the density of active transmitters λp_{tx} as a function λ . As λ increases, a higher number of active transmitters is achieved, which saturates to a value we will call the asymptotic density of active transmitters.

Definition 1. (Asymptotic density of active transmitters) For a given carrier sensing threshold ν , the asymptotic density of active transmitters $\lambda_{dens}(\nu)$ is defined as

$$\lambda_{dens}(\nu) \equiv \lim_{\lambda \rightarrow \infty} \lambda p_{tx}^{op}(\lambda, \gamma, \nu) = \lim_{\lambda \rightarrow \infty} \lambda p_{tx}^{qt}(\lambda, \gamma, \nu). \quad (2.41)$$

Note that $\lambda_{dens}(\nu)$ is not the function of γ , since numerator $\exp\{-p_\gamma \bar{N}_0\}$ in $p_{tx}^{op/qt}(\lambda, \gamma, \nu)$ vanishes as $\lambda \rightarrow \infty$, see (2.21) and (2.31). It is easy to show that $\lambda_{dens}(\nu) = 1/\hat{N}_0$, where $\hat{N}_0 = \bar{N}_0^\gamma / \lambda^\gamma = \mathbb{E}[\int_{\mathbb{R}^2} \mathbf{1}\{F' > \nu l(\|x\|\}) dx]$ is the *mean neighborhood size* of a typical transmitter. Note that since each active transmitter occupies the area of average size \hat{N}_0 , intuitively, we can have at most $\frac{1}{\hat{N}_0}$ active transmitters per unit space in the asymptotically dense network. Note that both O-CSMA and QT-CSMA have the same asymptotic density of transmitters $\lambda_{dens}(\nu)$ due to the transmitter selection process of the CSMA protocol.

As γ increases, the density of qualified transmitters, λp_γ , reduces, which accordingly decreases λp_{tx} , but the limiting value $\lambda_{dens}(\nu)$ is not affected. As ν increases, the mean occupied area gets smaller which allows a higher density of active transmitters, and accordingly $\lambda_{dens}(\nu)$ increases as a function of ν .

Success Probability of O-CSMA Fig. 2.3a shows the success probability $p_{suc}^{op}(\lambda, \gamma, \nu, t)$ as a function of λ for various γ and ν values. The general behavior of $p_{suc}^{op}(\lambda, \gamma, \nu, t)$ is as follows. As γ increases, the signal quality at receivers improves and at the same time the density of active transmitters goes down, which results in reduced interference at the receiver. Thus, increasing γ increases SINR at receivers, and thus increases success probability. If ν increases, the mean occupied area goes down resulting in a higher number of active transmitters, which accordingly generate a stronger aggregate interference. Thus both the received SINR and success probability are decreased. Regarding the behavior of $p_{suc}^{op}(\lambda, \gamma, \nu, t)$ as a function of λ , we have the following proposition.

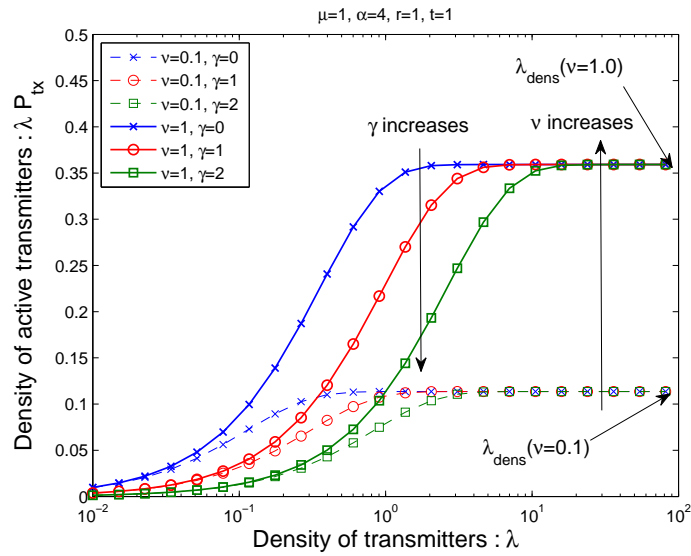


Figure 2.2: The density of active transmitters for O/QT-CSMA increases and saturates as λ increases due to the carrier sensing in CSMA protocol. Increasing the qualification threshold γ reduces the density of qualified transmitters without affecting the asymptotic density of active transmitters $\lambda_{dens}(\nu)$; so the effect is a shift of the curves to the right hand side. Increasing carrier sensing threshold ν increases $\lambda_{dens}(\nu)$ since it makes the mean size of a typical transmitter's neighborhood smaller.

Proposition 5. *If $\lambda \rightarrow \infty$ while $\nu, \gamma < \infty$ are fixed, we have that*

$$\lim_{\lambda \rightarrow \infty} p_{suc}^{op}(\lambda, \gamma, \nu, t) = \lim_{\lambda \rightarrow \infty} \mathbb{P}^0 \left(F_\gamma > tl(r) I_{\Phi_M^\gamma \setminus \{0\}} \right) < 1. \quad (2.42)$$

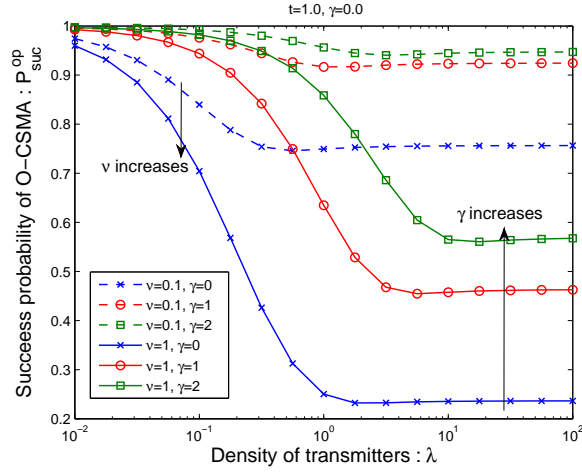
This is because F_γ is exponentially distributed with an infinite support and $I_{\Phi_M^{\gamma_0} \setminus \{0\}}$ converges in distribution to a random variable $I_{\Phi_M^{csma0} \setminus \{0\}} \equiv \sum_{X_i \in \Phi_M^{csma0} \setminus \{0\}} F_{i0} / l(|X_i|)$, where Φ_M^{csma0} is a Matérn CSMA process with a density $\lambda_{dens}(\nu)$ given an active transmitter at the origin, see Appendix 2.10. Since both random variables have infinite support in \mathbb{R}_+ , $\mathbb{P}^0 \left(F_\gamma > tl(r) I_{\Phi_M^\gamma \setminus \{0\}} \right)$ converges to a positive value between 0 and 1. It is not easy to find the limit since this would require characterizing $I_{\Phi_M^{csma0} \setminus \{0\}}$.

Success Probability of QT-CSMA Fig. 2.3b shows the success probability $p_{suc}^{qt}(\lambda, \gamma, \nu, t)$ as a function of λ for various γ and ν values. The general behavior of $p_{suc}^{qt}(\lambda, \gamma, \nu, t)$ is as follows. As γ increases, the interference seen at the receiver decreases due to the reduced density of active transmitters. However it is not clear how the received signal strength would change. Indeed increasing γ , should shift F_γ to the right hand side (improving the signal strength) but, at the same time, it decreases the size of neighborhood, thus reducing the opportunistic gain from picking the node with the best channel. Fig. 2.3b suggests that the positive effect is larger than the negative effect, i.e., as ν increases, $p_{suc}^{qt}(\lambda, \gamma, \nu, t)$ decreases due to the increased interference. One thing to note is that if the density λ becomes large enough, then, the success probability increases and eventually converges to 1 due to the increasing opportunistic gain; this is summarized in the following proposition.

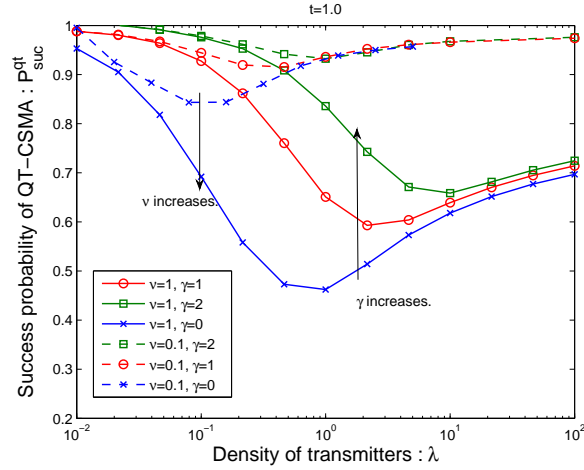
Proposition 6. *If $\lambda \rightarrow \infty$ while $\nu, \gamma < \infty$ are kept fixed, we have $p_{suc}^{qt}(\lambda, \gamma, \nu, t)$ converging to 1, i.e.,*

$$\lim_{\lambda \rightarrow \infty} p_{suc}^{qt}(\lambda, \gamma, \nu, t) = \lim_{\lambda \rightarrow \infty} \mathbb{P}^0 \left(F_{0,\gamma}^{\max}(N_0^\gamma + 1) > tl(r) I_{\Phi_M^\gamma \setminus \{0\}} \right) = 1. \quad (2.43)$$

This result can be intuitively understood as follows. As λ increases, N_0^γ and $F_{0,\gamma}^{\max}(N_0^\gamma + 1)$ increase (meaning $\lim_{\lambda \rightarrow \infty} \mathbb{P}(N_0^\gamma > x) = 1$ and $\lim_{\lambda \rightarrow \infty} \mathbb{P}(F_{0,\gamma}^{\max}(N_0^\gamma + 1) > x) = 1$)



(a) The success probability of O-CSMA decreases as λ increases, but converges to a value between 0 and 1 since interference $I_{\Phi_M^{\gamma^0} \setminus \{0\}}$ converges to $I_{\Phi_{CSMA0}^{\gamma^0} \setminus \{0\}}$ in distribution. If the qualification threshold γ increases, it increases F_γ so the success probability increases, and the limiting value $\lim_{\lambda \rightarrow \infty} p_{suc}^{op}(\lambda, \gamma, \nu, t)$ also increases. While, if carrier sensing range ν increases, it increases the density of active transmitters, which accordingly increases interference, which deteriorates the success probability.



(b) As λ increases, the success probability of QT-CSMA decreases at first, but bounces and converges to 1 due to the increasing opportunistic gain. As the qualification threshold γ increases, the success probability increases due to increased opportunistic gain. While, if carrier sensing range ν increases, the success probability decreases due to increased aggregate interference power.

Figure 2.3: The success probability versus the density of transmitters for various ν and γ .

for all fixed $x > 0$), and $I_{\Phi_M^{\gamma_0 \setminus \{0\}}}$ converges in distribution to a random variable $I_{\Phi_M^{csma0 \setminus \{0\}}}$ defined in Proposition 5. The success probability of O-CSMA and QT-CSMA are compared in the following proposition.

Proposition 7. *Under the same parameter set, the success probability of QT-CSMA is always larger than O-CSMA, i.e., $p_{suc}^{qt}(\lambda, \gamma, \nu, t) \geq p_{suc}^{op}(\lambda, \gamma, \nu, t)$, for a given λ, γ, ν , and t .*

This follows from a stochastic ordering relation : $F_\gamma^{\max} \geq^{st} F_\gamma$, see (2.5). Note that this implies that the density of successful transmissions of QT-CSMA is always higher than that of O-CSMA, i.e., $d_{suc}^{qt}(\lambda, \gamma, \nu, t) \geq d_{suc}^{op}(\lambda, \gamma, \nu, t)$ for a given parameter set λ, γ, ν and t .

Remark 2.5.1. The above observations suggest that the effects of adjusting γ and ν are similar in that both control the amount of interference in the network versus the opportunistic gain which are achieved. However, this does not imply that O-CSMA can optimize its performance by tweaking only one of them while fixing the other, but interestingly this seems to work for QT-CSMA. In the following sections, we will further explore this idea of reducing the number of parameters for QT-CSMA.

2.5.2 Performance Comparison of O-CSMA and QT-CSMA

We consider networks in three different density regimes : a network with an intermediate density, an asymptotically dense network, and an asymptotically sparse network. By asymptotically dense (sparse) networks, we mean networks whose node density λ keeps increasing to ∞ (decreasing to 0). Dense and sparse, networks are particularly interesting since the former gives maximum performance limits for O-CSMA and QT-CSMA networks under a given parameter set, and the latter allows us to evaluate the performance of an individual node because it is a regime where interactions with other nodes vanish. In addition to the importance of the two regimes, we have p_{suc}^{op} and p_{suc}^{qt} converging to 1 for an appropriately scaled or chosen γ in

these two regimes, which allows a simple analysis. While, in the intermediate density regime, p_{suc}^{op} and p_{suc}^{qt} are strictly less than 1, so we can only compare their performance through numerical computations.

Networks in an intermediate density regime We evaluate the performance of a network in an intermediate density regime for various γ and ν values. Note that it is no surprise to find that QT-CSMA always does better than O-CSMA under the same parameter set, see Proposition 7. Thus, we focus instead on the comparison between QT₀-CSMA (QT-CSMA with $\gamma = 0$) and O-CSMA.

Case $\nu = 1$: Fig.2.4a shows the density of successful transmissions for QT₀-CSMA and O-CSMA as a function of λ for various values of γ and for $\nu = 1$, $t = 1$, and $\mu = 1$. As λ gets larger, $d_{suc}^{op}(\gamma, \lambda)$ increases as a result of the increasing density of active transmitters; however they converge to fixed values since both the density of active transmitters and success probability converge. The differences among the asymptotic values of $p_{suc}^{op}(\gamma)$ s, see Fig. 2.3a, lead to the differences among $d_{suc}^{op}(\gamma)$ s. For large γ , p_{suc}^{op} is close to 1, so, as λ gets large, d_{suc}^{op} gets closer to λ_{dens} which is the maximum performance that O-CSMA can achieve. While, when λ is small, d_{suc}^{op} decreases as γ increases because the losses coming from the decreased density of active transmitters are not compensated by the gain from the increased quality of transmissions.

The performance of QT₀-CSMA is also shown. Interestingly, the performance of QT₀-CSMA seems to be better than O-CSMA for almost all γ values. This proves that quantile scheduling without qualification can fully take advantage of opportunistic gains for the given parameter set. The trends are similar when $\nu = 0.1$, which are not shown here.

Case $\nu = 5$: Fig. 2.4b shows three interesting phenomena. First, as λ increases, the density of successful transmissions of O-CSMA peaks and then decreases to converge to its limiting value. The peak happens since $\lambda p_{tx}^{op}(\lambda)$ converges earlier than

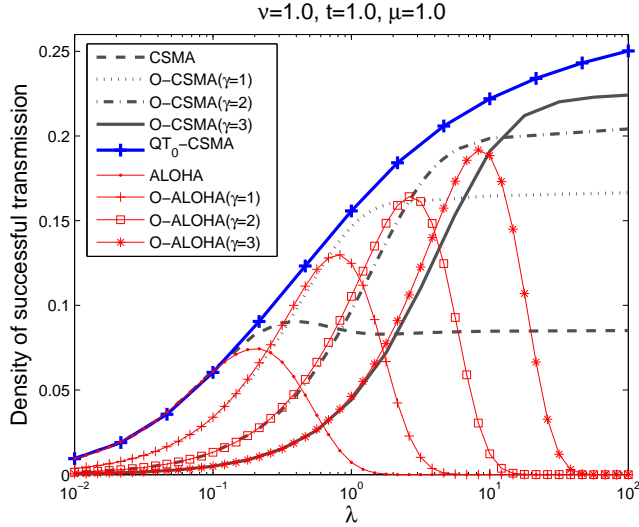
$p_{suc}^{op}(\lambda)$. Roughly speaking, if $d_{suc}^{op}(\lambda)$ hits its peak, $\lambda p_{tx}^{op}(\lambda)$ is very close to its limiting value and from that point it increases very slowly, while $p_{suc}^{op}(\lambda)$ keeps decreasing and converges at a larger λ value. Note that this phenomenon implies that the interference suppression from carrier sensing capability is not working well in a high density network. In other words, the carrier sensing threshold $\nu = 5$ is too large (or neighborhood of a node too narrowly defined) making the system less robust to changes in node density. The monotonic behavior shown in Fig. 2.4a seems to be more desirable since it is predictable for system designer/operators.

The second interesting phenomenon is that the density of successful transmissions for QT₀-CSMA is worse than that of O-CSMA when $\lambda \gtrsim 2 \times 10^{-2}$. This is again due to ν too large. If ν is too large, the size of neighborhood becomes too small for QT₀-CSMA to take advantage of opportunistic gains and the small neighborhood induces a dense packing which accordingly results in strong interference. Considering ν as a parameter controlling both interference and opportunistic gain, the smaller values are desirable.

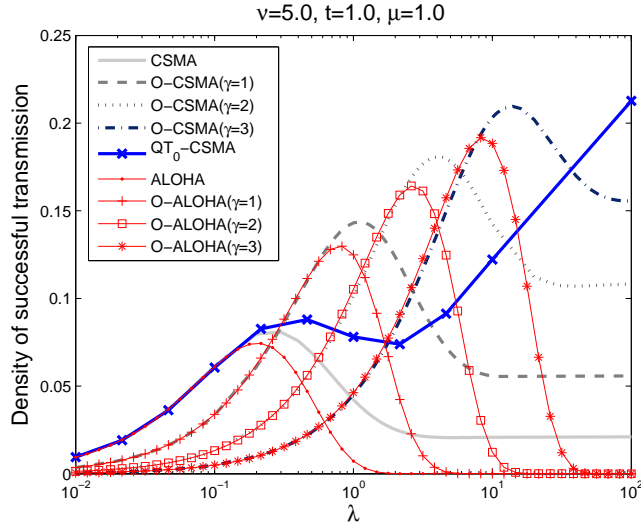
Third, the density of successful transmissions for QT₀-CSMA keeps increasing as λ increases. This happens because the size of neighborhood keeps increasing as λ increases. Indeed, the limiting value is even higher than the maximum value which O-CSMA can achieve. This will be further explored later when we consider a dense network.

Remark 2.5.2. The above results show that performance is highly dependent on the selected parameters. For O-CSMA, both ν and γ should be chosen appropriately. However, for QT₀-CSMA, only ν needs to be selected, which is a key advantage of using QT₀-CSMA. As shown above if ν is properly chosen, QT₀-CSMA provides a more robust⁶ performance than O-CSMA. Considering λ is usually an uncontrollable parameter, this kind of robust property is very desirable.

⁶By “robust” we mean QT₀-CSMA gives better performance than O-CSMA in all λ values.



(a) For $\nu = 1$, the density of successful transmissions of QT_0 -CSMA is uniformly higher than that of O-CSMA for all node densities $\lambda > 0$ and qualification thresholds $\gamma > 0$. Appropriately chosen ν (or neighborhood size) both increases opportunistic gain of QT_0 -CSMA and controls the amount of aggregate interference effectively even for large λ .



(b) If ν is set to too large (small neighborhood), the CSMA protocol allows too many active transmitters which generate too strong aggregate interference for increasing λ . Furthermore due to the small neighborhood size, QT_0 -CSMA cannot fully take advantage of opportunism. While O-CSMA can increase γ to select only nodes with high channel gains. This corresponds to the case where ν is inappropriately chosen for QT_0 -CSMA.

Figure 2.4: The density of successful transmissions in a network with intermediate density

Asymptotically Dense Networks The maximum achievable performance of O/QT-CSMA is obtained when $\lambda \rightarrow \infty$ since this is the regime where the space can be packed with a maximum number of active transmitters. To study this regime, we fix ν for both O-CSMA and QT-CSMA and study how the selection of γ affects the density of successful transmissions. Intuitively, for both O-CSMA and QT-CSMA to achieve high performance in dense networks, one should select γ to take advantage of nodes' high channel gains. Recall that increasing γ makes the received signal power stronger, which results in higher success probability, but at the same time it makes it harder for nodes to qualify. Thus, the question is how to scale γ as a function of λ .

In the sequel, we will show that γ should be increased no faster than as a logarithmic function of λ to achieve maximal performance, otherwise the network degenerates and behaves like a sparse network. We will show that a “*phase transition*” occurs for the density of successful transmissions depending on the scaling speed of γ . To that end, we consider following fact.

Proposition 8. *If both $\lambda \rightarrow \infty$ and $\gamma \rightarrow \infty$, then,*

$$\lim_{\lambda, \gamma \rightarrow \infty} p_{suc}^{op}(\lambda, \gamma, \nu, t) = \lim_{\lambda, \gamma \rightarrow \infty} p_{suc}^{qt}(\lambda, \gamma, \nu, t) = 1. \quad (2.44)$$

This is because, for O-CSMA, F_γ keeps increasing as γ increases (meaning that $\lim_{\gamma \rightarrow \infty} P(F_\gamma > x) = 1$ for any fixed $x > 0$) while $I_{\Phi_M^{\gamma_0} \setminus \{0\}}$ converges in distribution to a limiting random variable $I_{\Phi_M^{csmo} \setminus \{0\}}$, see Appendix 2.10. Similar argument can be made for QT-CSMA.

Following theorem provides our main result on the performance O-CSMA in the asymptotically dense regime.

Theorem 1. *For $\lambda \rightarrow \infty$ and fixed $\nu > 0$, the asymptotic density of successful transmissions is upper bounded by the asymptotic density of transmitters, i.e.,*

$$\lim_{\lambda \rightarrow \infty} d_{suc}^{op}(\lambda, \gamma, \nu, t) \leq \lambda_{dens}(\nu), \quad (2.45)$$

where equality holds when $\gamma(\lambda) = c \log(\lambda/\lambda_q)$ with constants $c < \frac{1}{\mu}$ and $\lambda_q > 0$.

Proof. We have a few cases to consider depending on the scaling of γ . First, if γ is a fixed constant, we have that

$$\lim_{\lambda \rightarrow \infty} \lambda p_{tx}^{op} = \lim_{\lambda \rightarrow \infty} \frac{1 - \exp\{-e^{-\mu\gamma} \lambda \hat{N}_0\}}{\hat{N}_0} = \lambda_{dens}(\nu) \quad (2.46)$$

and $0 < \lim_{\lambda \rightarrow \infty} p_{suc}^{op}(\lambda, \gamma, \nu, t) < 1$ by Proposition 5. Thus, we have $\lim_{\lambda \rightarrow \infty} d_{suc}^{op}(t, \gamma, \nu, \lambda) < \lambda_{dens}(\nu)$. While if $\gamma = c \log(\lambda/\lambda_q)$ for $c > 0$ and $\lambda_q > 0$, we have

$$\lim_{\lambda \rightarrow \infty} \lambda p_{tx}^{op} = \lim_{\lambda \rightarrow \infty} \frac{1 - \exp\{-\lambda^{1-\mu c} \lambda_q^{\mu c} \hat{N}_0\}}{\hat{N}_0} = \begin{cases} \lambda_{dens} & \text{if } c < \frac{1}{\mu} \\ \lambda_{dens}(1 - \exp\{-\lambda_q \hat{N}_0\}) & \text{if } c = \frac{1}{\mu} \\ 0 & \text{if } \frac{1}{\mu} < c, \end{cases} \quad (2.47)$$

and $\lim_{\lambda \rightarrow \infty} p_{suc}^{op}(\lambda, \gamma, \nu, t) = 1$ by Proposition 8. This completes the proof. \square

Theorem 1 says that $\gamma(\lambda)$ needs to be scaled no faster than as a logarithmic function of λ , specifically $\gamma(\lambda) = c \log(\lambda/\lambda_q)$, for an O-CSMA network to achieve its maximum asymptotic density of successful transmissions. In doing so, a logarithmic increase is the fastest, but increasing speed should not be too fast. Precisely, it should be slow enough to have a sufficient number of contending nodes so as to increase spatial reuse. More specifically, we see a sharp performance change or phase transition phenomenon depending on the value of speed parameter c as shown in (2.47), see Fig.2.5. The phase transition phenomenon can be explained by observing how the density of qualified transmitters

$$\lambda p_{\gamma(\lambda)} = \lambda e^{-\mu\gamma(\lambda)} = \lambda^{1-\mu c} \lambda_q^{\mu c} \quad (2.48)$$

behaves as a function c when $\lambda \rightarrow \infty$. Depending on the value of c we have following three cases.

- If $c < \frac{1}{\mu}$, then we have $\lim_{\lambda \rightarrow \infty} \lambda p_{\gamma(\lambda)} = \infty$, which implies there exists enough qualified contenders to achieve high spatial reuse.

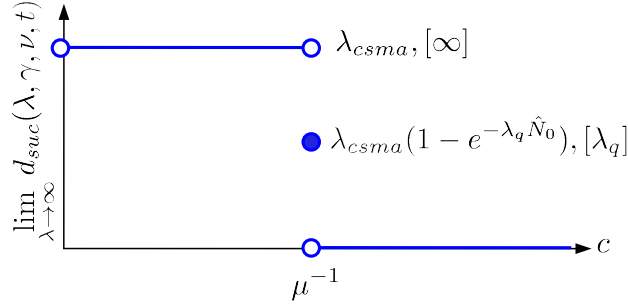


Figure 2.5: The asymptotic density of successful transmissions for O/QT-CSMA exhibits a phase transition phenomenon depending on the value of the scaling speed constant c when qualification threshold γ is selected as the logarithm function of node density λ : $\gamma = c \log(\lambda/\lambda_q)$ with $c > 0$ and $a > 0$. The quantities in the square bracket denote the associated density of qualified nodes $\lim_{\lambda \rightarrow \infty} \lambda p_{\gamma}(\lambda)$ which are always larger than their associated asymptotic density of successful transmissions.

- If $c = \frac{1}{\mu}$, then we have $\lim_{\lambda \rightarrow \infty} \lambda p_{\gamma}(\lambda) = \lambda_q$. The constant density implies that the space can not be fully reused due to a lack of qualified nodes to compete and fill the space.
- If $c > \frac{1}{\mu}$, then we have $\lim_{\lambda \rightarrow \infty} \lambda p_{\gamma}(\lambda) = 0$ because of γ increasing too fast compared to λ . This means that the density of qualified nodes decreases as λ increases.

Note that the gap between λ_{dens} and $\lambda_{dens}(1 - \exp\{-\lambda_q \hat{N}_0\})$ in (2.47) can be made arbitrarily small by selecting λ_q large.

The asymptotic performance of QT-CSMA can also be analyzed in a similar way using Propositions 8 and 6. Proposition 8 and Theorem 1 implies that if γ is scaled as a function of λ , QT-CSMA will experience the same phase transition phenomenon. While if γ is constant, QT-CSMA can achieve $\lambda_{dens}(\nu)$. From the above discussion, O-CSMA and QT-CSMA have the same *maximum* asymptotic performance provided γ is appropriately chosen. However, *for a given parameter set $(\lambda, \gamma, \nu, t)$, QT-CSMA is always better than or equal to O-CSMA.*

QT₀-CSMA's performance gain compared to O-CSMA is given in following corollary.

Corollary 1. *For a given $\nu > 0$, if γ scales like $\gamma(\lambda) = c \log(\lambda/\lambda_q)$ with $\lambda_q > 0$, then, the performance gain of QT₀-CSMA to O-CSMA is given by*

$$\lim_{\lambda \rightarrow \infty} \frac{d_{suc}^{qt}(\lambda, 0, \nu, t)}{d_{suc}^{op}(\lambda, \gamma, \nu, t)} = \lim_{\lambda \rightarrow 0} \frac{p_{tx}^{qt}}{p_{tx}^{op}} = \begin{cases} 1 & \text{if } c < \frac{1}{\mu} \\ \frac{1}{1 - e^{-\lambda_q \hat{N}_0}} & \text{if } c = \frac{1}{\mu} \\ \infty & \text{if } \frac{1}{\mu} < c. \end{cases} \quad (2.49)$$

Asymptotically Sparse Networks In this section, we consider asymptotically sparse networks, where $\lambda \rightarrow 0$. Note that the density of successful transmissions in this case goes to 0, but the comparison (performance ratio) is still meaningful since it is equivalent to comparing the performance of an individual transmitter-receiver pair experiencing no interference. For a fixed $\gamma > 0$, the O-CSMA and QT-CSMA have the same asymptotic performance: $\lim_{\lambda \rightarrow 0} \frac{d_{suc}^{qt}(\lambda, \gamma, \nu, t)}{d_{suc}^{op}(\lambda, \gamma, \nu, t)} = 1$ since $\lim_{\lambda \rightarrow 0} \frac{p_{suc}^{qt}(\lambda, \gamma, \nu, t)}{p_{suc}^{op}(\lambda, \gamma, \nu, t)} = 1$. Whereas QT₀-CSMA has an exponential gain (as a function of γ) versus O-CSMA. This is captured in the next result.

Theorem 2. *For $\lambda \rightarrow 0$ and $\nu > 0$, the asymptotic performance gain of QT₀-CSMA to O-CSMA with a fixed $\gamma \geq 0$ is given by $e^{\mu\gamma}$.*

Proof. Using $\lim_{\lambda \rightarrow 0} \frac{p_{suc}^{qt}(\lambda, 0, \nu, t)}{p_{suc}^{op}(\lambda, \gamma, \nu, t)} = 1$, it is straightforward to compute the gain. Applying L'Hopital's rule, we have

$$\lim_{\lambda \rightarrow 0} \frac{d_{suc}^{qt}(\lambda, 0, \nu, t)}{d_{suc}^{op}(\lambda, \gamma, \nu, t)} = \lim_{\lambda \rightarrow 0} \frac{p_{tx}^{qt}}{p_{tx}^{op}} = \lim_{\lambda \rightarrow 0} \frac{1 - \exp\{-\lambda \hat{N}_0\}}{1 - \exp\{-e^{-\mu\gamma} \lambda \hat{N}_0\}} = \lim_{\lambda \rightarrow 0} \frac{\exp\{-\lambda \hat{N}_0(1 - e^{-\mu\gamma})\}}{e^{-\mu\gamma}} = e^{\mu\gamma}. \quad (2.50)$$

This is an expected result since O-CSMA nodes qualify with probability $p_\gamma = e^{-\mu\gamma}$ and qualified nodes in the sparse network will transmit with almost no contention. This shows that in sparse networks O-CSMA should select $\gamma = 0$ to get the same performance as QT₀-CSMA. \square

Note that in the above two cases (asymptotically dense and sparse networks) it turned out that O-CSMA needs to adapt its γ value as a function of node density λ to maximize its performance. This is a big disadvantage for O-CSMA versus QT₀-CSMA since it is hard to estimate λ in practice.

2.5.3 Performance Comparison of O-CSMA and O-ALOHA

In this section, we compare the asymptotic performance of O-CSMA and O-ALOHA in [10,112] for which the density of successful transmissions is given by $d_{suc}^{oA} = \lambda p_{tx}^{oA} p_{suc}^{oA}$, where p_{tx}^{oA} is the transmission probability of each node and p_{suc}^{oA} is the success probability of a typical node. By selecting $p_{tx}^{oA} = p_\gamma$, we can make the density of active transmitters in O-ALOHA network be equal to the density of qualified transmitters in O-CSMA. We have following result for the performance of O-CSMA and O-ALOHA.

Theorem 3. *Under the above setting $p_{tx}^{oA} = p_\gamma$ and $\gamma = c \log(\lambda/\lambda_q)$ with $\lambda_q > 0$ and $c > 0$, we have following asymptotic performance ratio depending on the value of c :*

$$\lim_{\lambda \rightarrow \infty} \frac{d_{suc}^{op}}{d_{suc}^{oA}} = \lim_{\lambda \rightarrow \infty} \frac{\lambda p_{tx}^{op} p_{suc}^{op}}{\lambda p_\gamma p_{suc}^{oA}(\lambda, \gamma)} = \begin{cases} \infty & \text{if } c < \frac{1}{\mu} \\ \frac{\lambda_{dens}(\nu)(1-\exp\{-\lambda_q \hat{N}_0\})}{\lambda_q p_{suc}^{oA}(\lambda, \gamma)} & \text{if } c = \frac{1}{\mu} \\ 1 & \text{if } c > \frac{1}{\mu}. \end{cases} \quad (2.51)$$

where $p_{suc}^{oA}(\lambda, \gamma) = \int_{-\infty}^{\infty} \mathcal{L}_I(2i\pi l(r)ts) \frac{\mathcal{L}_{F_\gamma}(-2i\pi s) - 1}{2i\pi s} ds$

with $\mathcal{L}_I(s) = \exp\left\{-\lambda 2\pi \int_0^\infty \frac{\tau}{1 + \frac{\mu\tau^\alpha}{s}} d\tau\right\}$ and $\mathcal{L}_{F_\gamma}(s) = e^{-s\gamma} \frac{\mu}{\mu+s}$, see [Baccelli09]

Proof. Depending on the value of c , we have three cases. First, if $c < \frac{1}{\mu}$, the density of transmitters for O-ALOHA keeps increasing as $\lambda \rightarrow \infty$, which makes a typical receiver using O-ALOHA experience a success probability of 0 due to increasing interference which is unbounded. While d_{suc}^{op} converges to a non-zero value, so we have infinite gain in this case. Second, if $c = \frac{1}{\mu}$, the density of qualified transmitters for both O-CSMA and O-ALOHA converge to finite numbers, so the amount of interference is limited, accordingly this results in non-zero performance. Third, if $c > \frac{1}{\mu}$, the densities of

qualified transmitters in O-CSMA and transmitters in O-ALOHA decrease to 0 and both p_{suc}^{op} and $p_{suc}^{oA} \rightarrow 1$ as $\lambda \rightarrow \infty$. Applying L'Hopital's rule, we have ratio 1. \square

2.6 Spatial Fairness

2.6.1 Unfairness in CSMA Networks

In this section, we compare the spatial fairness performance of the O/QT-CSMA protocols. It has been reported that *non-slotted* CSMA networks are unfair [32, 111]. The two main reasons are the irregular topology of network and the combination of carrier sensing mechanism and binary exponential backoff which can cause starvation. There have been efforts towards improving fairness by tuning protocols, for example, adjusting carrier sensing range [33] or using node specific access intensity [108, 109, 111].

In *slotted* systems, unfairness partially disappears simply due to *slotting*. Indeed in a slotted system, all nodes' contention windows are reset every slot, which prevents starvation. Accordingly, fairness improves significantly. However, unfairness due to irregular topologies remains. We will show in this section that our opportunistic scheduling scheme can improve fairness.

2.6.2 Spatial Fairness for Access Frequency

We first evaluate spatial fairness in terms of the fraction of time that each node can access the medium. We will show how nodes' random locations impact this metric. We need following assumption.

Assumption 1. We assume that the contenders of node X_i is the set of nodes located in the disc $b(X_i, (\nu\mu)^{-\alpha})$ or equivalently $F'_{ij} = \frac{1}{\mu} = \mathbb{E}[F]$ with probability 1.

Under this assumption, the neighbors of a node is *not* affected by fading, so the size of a node's neighborhood stays fixed, e.g., might be based on the average channel gain. This might be a reasonable assumption in a system, e.g., where each node's

contending neighbors are dynamically maintained based on their average fading gains to the node. Note that F_{ij} is still a random variable. Let

$$N_{s,i}^\gamma = N_{s,i}^\gamma(\Phi) = |\{X_j \in \Phi : 1/\mu l(\|X_i - X_j\|) > \nu, i \neq j\}|$$

be a random variable denoting the number of X_i 's neighborhood under the static fading assumption⁷, it corresponds to the number of nodes inside a disk $b(X_i, (\nu\mu)^{-\frac{1}{\alpha}})$. This is a Poisson random variable with mean $\lambda\pi(\nu\mu)^{-\frac{2}{\alpha}}$. Recall that a node with n contenders accesses the channel with probability $\frac{p_\gamma}{n+1}$. This corresponds to the *fraction of time* the node accesses the channel. We will call this quantity the *access frequency* of the node to differentiate it from the access probability (e.g., p_{tx}^{op} or p_{tx}^{qt}) which is interpreted as the fraction of nodes transmitting in space in a typical slot. Note that since the access frequency depends only on $N_{s,i}^\gamma$, so we have $\mathbb{E}[f_i(\Phi, \mathbf{F}_i, \mathbf{F}'_i) | \Phi] = \mathbb{E}[\tilde{f}_i(N_{s,i}^\gamma, \mathbf{F}_i, \mathbf{F}'_i) | N_{s,i}^\gamma] = \frac{p_\gamma}{N_{s,i}^\gamma + 1}$. The corresponding spatial fairness index on access frequency across randomly distributed nodes is given as follows:

$$\tilde{\text{FI}}_{ac}(\bar{N}_{s,0}^\gamma) = \frac{\left(\mathbb{E}\left[\frac{p_\gamma}{N_{s,0}^\gamma + 1}\right]\right)^2}{\mathbb{E}\left[\left(\frac{p_\gamma}{N_{s,0}^\gamma + 1}\right)^2\right]} = \frac{e^{\bar{N}_{s,0}^\gamma} + e^{-\bar{N}_{s,0}^\gamma} - 2}{\bar{N}_{s,0}^\gamma (Ei(\bar{N}_{s,0}^\gamma) - \log \bar{N}_{s,0}^\gamma - \eta)}, \quad (2.52)$$

where $\bar{N}_{s,0}^\gamma = \mathbb{E}[N_{s,0}^\gamma]$, $Ei(x) = -\int_{-x}^{\infty} t^{-1} e^{-t} dt$ is an exponential integral function, and $\eta = 0.5772\dots$ is the Euler-Mascheroni constant.

Fig.2.6a shows the fairness index of access frequency for O/QT-CSMA versus $\bar{N}_{s,0}^\gamma(\nu)$. If $\bar{N}_{s,0}^\gamma$ is small, almost every contending node sends, in fact all transmitters have access frequency close to p_γ , so the fairness index is close to 1. If $\bar{N}_{s,0}^\gamma$ is relatively small, as $\bar{N}_{s,0}^\gamma$ (which is mean and the variability of the number of contenders) increases, the variability of access frequency, i.e., $\frac{p_\gamma}{N_{s,0}^\gamma + 1}$, across nodes increases resulting in a decrease in fairness. However, if $\bar{N}_{s,0}^\gamma$ is relatively large, the fairness

⁷Note the difference between $N_{s,i}^\gamma$ and N_i^γ , where the latter is the number of neighbors without the static fading assumption.

index eventually increases again since, in this regime, the variability of access frequency $\frac{p\gamma}{N_{s,0}^\gamma+1}$ decreases and converges to 0, which in turn increases fairness. Note that the fairness curve has its minimum value 0.73019... Specifically, the minimizer $n^* \equiv \arg \min_{n>0} \text{FI}_{ac}(n) \approx 2.9736657$ can be found by solving $\frac{d}{dn} \tilde{\text{FI}}_{ac}(n) = 0$. Based on this, we have following proposition.

Proposition 9. Under the Assumption 1, the spatial fairness for access frequency of slotted O/QT-CSMA is worst, roughly 0.73 when the mean number of contenders of a typical transmitter is roughly 3.

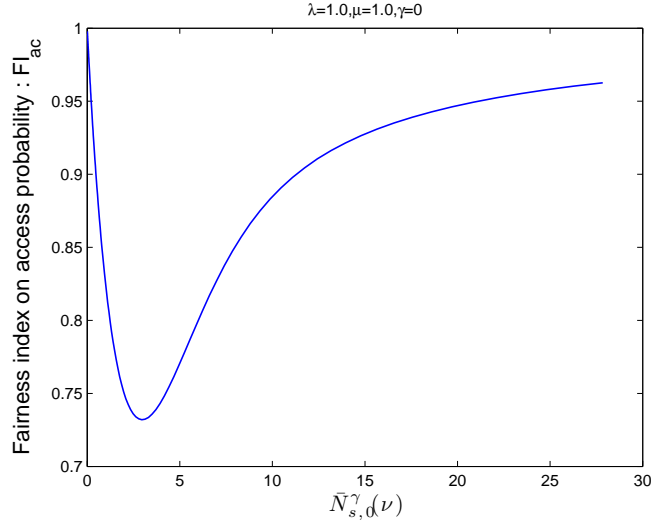
2.6.3 Spatial Fairness of the Frequency of Successful Transmissions

In this section, we consider the fairness of the frequency of successful transmissions. Specifically, we will show that opportunistic CSMA schemes can, to a certain extent, remove topological unfairness. We first define the spatial fairness of the frequency of successful transmissions.

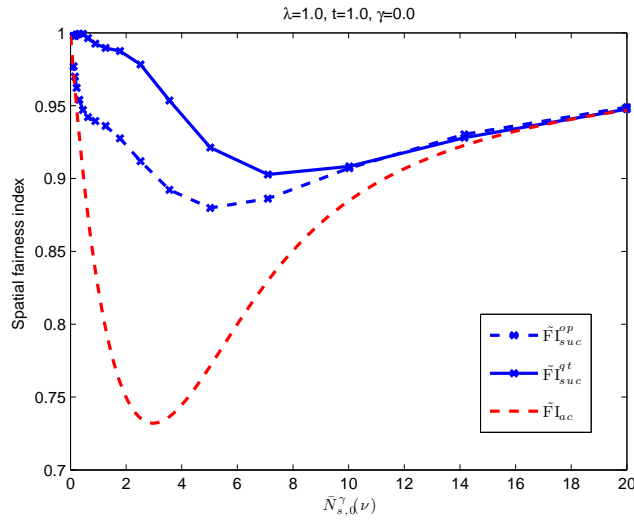
For O-CSMA, we define $\frac{p\gamma}{N_{s,0}^\gamma+1} \bar{p}_{suc}^{op}(\gamma, N_{s,0}^\gamma)$ as the frequency of successful transmission of a typical receiver with $N_{s,0}^\gamma$ neighbors, where $\frac{p\gamma}{N_{s,0}^\gamma+1}$ is the access frequency and $\bar{p}_{suc}^{op}(\gamma, N_{s,0}^\gamma)$ is the conditional success probability conditioned on that its associated transmitter has $N_{s,0}^\gamma$ contenders, which is given by

$$\begin{aligned} \bar{p}_{suc}^{op}(\gamma, N_{s,0}^\gamma = n) &= \mathbb{P}^0 \left(F_\gamma > t I_{\Phi_{M \setminus \{0\}}^\gamma} l(r) \mid N_{s,0}^\gamma = n \right) \\ &\approx \mathbb{E}^0 \left[\int_{-\infty}^{\infty} \mathcal{L}_{I_{\Phi_u^\gamma \setminus \{0\}}^{N_{s,0}^\gamma, F_\gamma}}(2i\pi l(r)ts) \frac{e^{2i\pi s F_\gamma} - 1}{2i\pi s} ds \mid N_{s,0}^\gamma = n \right], \end{aligned} \quad (2.53)$$

where $I_{\Phi_u^\gamma \setminus \{0\}}^{N_{s,0}^\gamma, F_\gamma}$ given $N_{s,0}^\gamma = n$ is the interference seen by a typical receiver conditioned on that it has n neighbors. Accordingly, the fairness index is given by



(a) When $\bar{N}_{s,0}^\gamma$ is relatively small, the fairness index on access frequency decreases as the mean number of contenders $\bar{N}_{s,0}^\gamma$ decreases, but when $\bar{N}_{s,0}^\gamma$ is relatively large it arises soon as $\bar{N}_{s,0}^\gamma$ increases. The fairness has minimum value ~ 0.73 when $\bar{N}_{s,0}^\gamma \approx 3$.



(b) The fairness index on the frequency of successful transmissions is higher than the fairness index on the access frequency. Note that both O-CSMA and QT-CSMA increase fairness significantly because nodes with larger neighborhood size has higher success probability, which compensates their low access frequency. The amount compensated by QT-CSMA is larger than that by O-CSMA due to quantile scheduling.

Figure 2.6: Fairness index of access frequency versus the mean number of contenders $\bar{N}_{s,0}^\gamma(\nu)$ under the Assumption 1.

$$\tilde{\text{FI}}_{suc}^{op}(\gamma, \bar{N}_{s,0}^\gamma) = \frac{\left(\mathbb{E}^0 \left[\frac{p_\gamma}{N_{s,0}^\gamma + 1} \bar{p}_{suc}^{op}(\gamma, N_{s,0}^\gamma) \right] \right)^2}{\mathbb{E}^0 \left[\left(\frac{p_\gamma}{N_{s,0}^\gamma + 1} \bar{p}_{suc}^{op}(\gamma, N_{s,0}^\gamma) \right)^2 \right]}. \quad (2.54)$$

For QT-CSMA, we take a similar approach. We define $\frac{p_\gamma}{N_{s,0}^\gamma + 1} \bar{p}_{suc}^{qt}(\gamma, N_{s,0}^\gamma)$ as the frequency of successful transmission of a typical receiver with $N_{s,0}^\gamma$ neighbors, where $\frac{p_\gamma}{N_{s,0}^\gamma + 1}$ is the access frequency and $\bar{p}_{suc}^{qt}(\gamma, N_{s,0}^\gamma)$ is the conditional success probability conditioned on that its associated transmitter has $N_{s,0}^\gamma$ contenders, which is given by

$$\begin{aligned} \bar{p}_{suc}^{qt}(\gamma, N_{s,0}^\gamma = n) &= \mathbb{P}^0 \left(F_{0,\gamma}^{\max}(N_{s,0}^\gamma + 1) > tI_{\Phi_{M \setminus \{0\}}^\gamma} l(r) \mid N_{s,0}^\gamma = n \right). \\ &\approx \mathbb{E}^0 \left[\int_{-\infty}^{\infty} \mathcal{L}_{I_{\Phi_u^\gamma \setminus \{0\}}^{N_{s,0}^\gamma, F_{0,\gamma}^{\max}(N_{s,0}^\gamma + 1)}}(2i\pi l(r)ts) \frac{e^{2i\pi s F_{0,\gamma}^{\max}(N_{s,0}^\gamma + 1)} - 1}{2i\pi s} ds \mid N_{s,0}^\gamma = n \right]. \end{aligned} \quad (2.55)$$

The fairness metric of interest in this section corresponds to the second type (2.10) only, and the corresponding fairness index on successful transmission is given by

$$\tilde{\text{FI}}_{suc}^{qt}(\gamma, \bar{N}_{s,0}^\gamma) = \frac{\left(\mathbb{E}^0 \left[\frac{p_\gamma}{N_{s,0}^\gamma + 1} \bar{p}_{suc}^{qt}(\gamma, N_{s,0}^\gamma) \right] \right)^2}{\mathbb{E}^0 \left[\left(\frac{p_\gamma}{N_{s,0}^\gamma + 1} \bar{p}_{suc}^{qt}(\gamma, N_{s,0}^\gamma) \right)^2 \right]}. \quad (2.56)$$

Using the expression of $\mathcal{L}_{I_{\Phi_u^\gamma \setminus \{0\}}^{N_{s,0}^\gamma, F_{0,\gamma}^{\max}(N_{s,0}^\gamma + 1)}}$ in (2.40) and $N_{s,0}^\gamma \sim \text{Poisson}(\bar{N}_{s,0}^\gamma)$, accordingly $\tilde{\text{FI}}_{suc}^{qt}$ can be numerically computed.

$\tilde{\text{FI}}_{suc}^{qt}$ and $\tilde{\text{FI}}_{suc}^{op}$ are plotted in Fig.2.6b for $\gamma = 0$. The figure shows that the fairness on the frequency of successful transmissions achieved by QT₀-CSMA is much improved versus that of O-CSMA. The gain is significant in the regime where $\bar{N}_{s,0}^\gamma$ is less than or equal to roughly 10. In this regime, QT₀-CSMA increases the success probability of receivers a lot. This reduces the performance differences among nodes caused by different access frequency (or topology) since nodes with a large number of neighbors who get low access frequency have higher success probability. In other words, the higher success probability compensates the low access frequency, which

decreases the variability in performance. In the regime where $\bar{N}_{s,0}^\gamma$ is large (or ν is small), the density of concurrent transmitters becomes small, which generates weak interference. Thus, most nodes succeed in their transmissions with high probability irrespective of the number of neighbors, so in this regime there is not much gained from opportunism increasing the success probability. Thus, QT₀-CSMA and O-CSMA have almost the same performance. As γ increases, fairness decreases and eventually converges to the fairness curve of O-CSMA where $\gamma \rightarrow \infty$ since there will be little difference between \bar{p}_{suc}^{qt} and \bar{p}_{suc}^{op} .

So far, it has been shown that opportunistic CSMA can improve fairness. However, with this results only, it is not clear how these protocols tradeoff the density of successful transmissions versus fairness. We consider this next.

2.6.4 Tradeoff between Spatial Fairness and Spatial Reuse

It has been noted that there exists a limited set of network topologies (e.g., line or circle networks) where both high fairness and “spatial reuse” or “throughput” can be both achieved [34, 109]. However, in the random networks we consider, there will be tradeoffs due to the randomness of node locations, contentions and protocols. To explore these we introduce the following notations.

Definition 2. (FD-pair) We call (a, b) an achievable FD-pair if a fairness index a and density of successful transmissions b can be achieved under a given protocol parameter choice.

Definition 3. (Dominance) For FD-pairs (a, b) and $(c, d) \in \mathbb{R}_+^2$, we say that the (a, b) *dominates* (c, d) if $a \geq c$ and $b \geq d$. We denote this relation with $(c, d) \preceq (a, b)$.

We consider the set of FD-pairs that are not dominated by any other pairs, i.e., the Pareto-frontier. For a given FD-pair (a, b) , we define the set of FD-pairs dominated by (a, b) as follows.

Definition 4. (Dominated set) For a FD-pair $(a, b) \in \mathbb{R}_+^2$, we call the set

$$\Lambda(a, b) = \{(x, y) \in \mathbb{R}_+^2 \text{ s.t. } (x, y) \preceq (a, b)\} \quad (2.57)$$

as the dominated set of the FD-pair (a, b) . Note that $(a, b) \in \Lambda(a, b)$.

In particular, we define the dominated set for O-CSMA, for a given t and λ , by

$$\Omega^{op}(\lambda, t) = \bigcup_{\gamma \geq 0, \nu \geq 0} \Lambda(\tilde{\text{FI}}_{suc}^{op}(\lambda, \gamma, \nu, t), d_{suc}^{op}(\lambda, \gamma, \nu, t)). \quad (2.58)$$

The dominated set for QT-CSMA is similarly defined. The dominated set QT₀-CSMA for a given t and λ is defined as

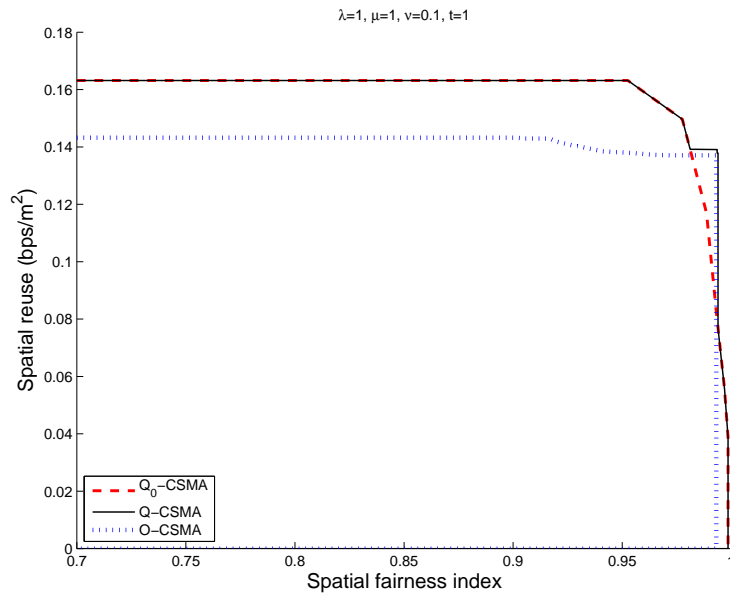
$$\Omega_0^{qt}(\lambda, t) = \bigcup_{\nu \geq 0} \Lambda(\tilde{\text{FI}}_{suc}^{qt}(\lambda, 0, \nu, t), d_{suc}^{qt}(\lambda, 0, \nu, t)). \quad (2.59)$$

Definition 5. (Pareto-Frontier) For a given set of FD-pairs, the subset of FD-pairs which are not dominated by any other FD-pairs is called as Pareto-frontier.

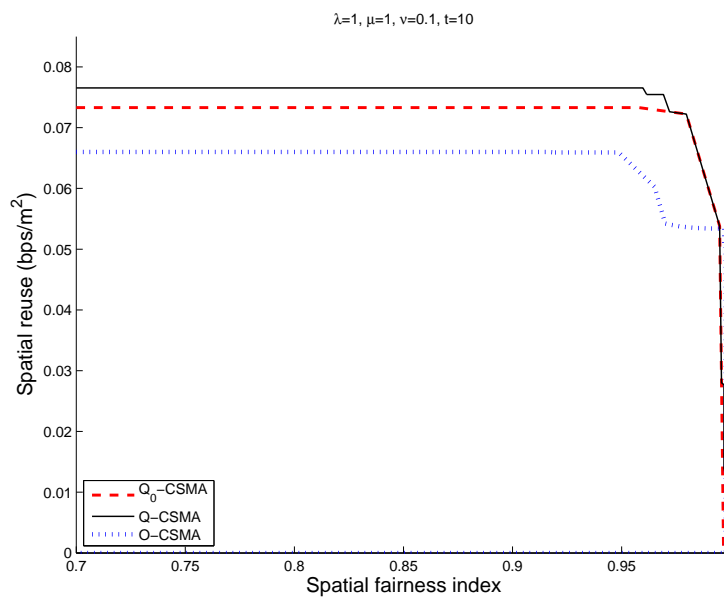
We plotted three Pareto-frontiers for O-CSMA, QT-CSMA, and QT₀-CSMA or their dominated sets $\Omega^{op}(\lambda, t)$, $\Omega^{qt}(\lambda, t)$ and $\Omega_0^{qt}(\lambda, t)$ for two decoding SIR $t = 1$ and $t = 10$ in Fig. 2.7a and 2.7b respectively. We note that the dominated set of QT-CSMA is not the super set of that of O-CSMA, and vice versa. However, the dominated set of QT-CSMA is larger than that of O-CSMA. The gain comes from the joint improvement of spatial reuse and fairness performance. One notable thing is that $\Omega_0^{qt}(\lambda, t)$ is very close to $\Omega^{qt}(\lambda, t)$, which shows again the effectiveness of quantile based approach in taking advantage of dynamic channel variations and multi-user diversity.

2.7 System implementation

In this section, we briefly describe a possible implementation of the O/QT-CSMA protocols. We will focus on the aspect of slot structure together with the operation of



(a) Case $t = 1$: low decoding SIR regime



(b) Case $t = 10$: high decoding SIR regime

Figure 2.7: Comparison of the dominated sets of O-CSMA, QT-CSMA and QT₀-CSMA.

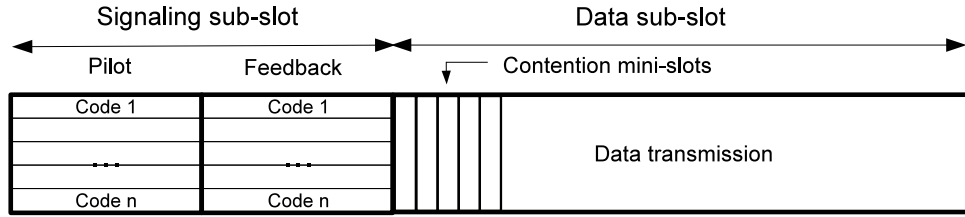


Figure 2.8: Slot structure for CDMA case.

protocols but not give full fledged detailed protocols - this is beyond the scope of this chapter. We will make several key assumptions in our development. First, we assume that nodes are perfectly synchronized with external and/or internal aids, e.g., each node might use pilot signals from GPS-synchronized cellular base stations and might run a distributed synchronization algorithm to further synchronize as done in [118]. For a discussion of the impact of imperfect sync, see [98]. Second, we assume that fading is symmetric and changing each slot. Third, the node density λ is assumed to be in a moderate range, i.e., not unrealistically dense.

In what follows, we describe a possible frame structure for transmissions. It is composed of two sub-slots : one for signaling and the other for data transmission, see Fig. 2.8.

2.7.1 Signaling sub-slot

In the signaling sub-slot, each transmitter sends a pilot signal to its associated receiver and the receiver feeds back the measured channel status between them. We consider the method suggested in [10], where the receiver estimates its channel status based on the received pilot power. However, the received pilot at the receiver may include both desired and undesired signals (interference) which makes the estimate inaccurate. To mitigate the impact of interference, we can assign each transmitter a CDMA code (CDMA approach) or a time slot (TDMA approach) for sending its pilot signal. However, since the number of codes or time slots are limited, two or more nodes can use the same resource, so the protocol should be designed to work in such a

way that two nodes using the same resource are sufficiently separated to mitigate the impact of interference, e.g., as done in [71, 89]. One can also use an OFDM approach like [118], where each node picks a single sub-carrier to send its pilot signal.

Once the receiver estimates, its channel status, it feeds back the estimate, say \hat{F}_{ii} . If the transmitter uses O-CSMA and $\hat{F}_{ii} > \gamma$, then it contends otherwise it defers. While, if it uses QT-CSMA and $\hat{F}_{ii} > \gamma$, then it updates its channel status statistics \hat{G}_γ (i.e. empirical cdf of \hat{F}_{ii}) and determines its current discretized version of quantile as $\frac{k}{w}$ if $\frac{k}{w} \leq \hat{G}_\gamma(\hat{F}_{ii}) < \frac{k+1}{w}$ for $k = 0, \dots, w-1$, where w is the maximum number of mini-slots (similar to the size of the contention window) used for contention.

2.7.2 Data sub-slot

In the data transmission sub-slot, qualified nodes contend and only winners transmit. In the contention phase composed of w mini-slots, each qualified node sets its timer value to a random value uniformly distributed in $\{1, 2, \dots, w\}$ if it is O-CSMA node, or sets it to k defined above if it is QT-CSMA node. All qualified nodes start to decrement their timer values by one every mini-slot. All nodes whose timer values reach 0 start transmitting from the mini-slot until the end of the data sub-slot. Other nodes which sense the transmissions prior to their timeout defer in the slot.

Since w is finite, a collision can occur if two or more nodes select the same mini-slot. The transmission probability (considering collision) with w mini-slots is computed as

$$p_{tx}^{col}(w) = p_\gamma \sum_{i=0} \left[\sum_{t=1}^w \frac{1}{w} \left(1 - \frac{t}{w}\right)^i \right] \frac{p_\gamma \bar{N}_0^i}{i!} e^{-p_\gamma \bar{N}_0} = \frac{p_\gamma (1 - \exp\{-p_\gamma \bar{N}_0\})}{w (\exp(p_\gamma \bar{N}_0/w) - 1)}. \quad (2.60)$$

Note that we can easily show $p_{tx}^{col}(w)$ converges as $w \rightarrow \infty$ to the transmission probabilities without collision given (2.21) and (2.31). Note that to see overall impact of collision, p_{suc} also needs to be recomputed considering collision. Studying the impact of collision is left to future work.

2.8 Conclusion

In this chapter, we considered the spatial reuse and fairness for wireless ad-hoc networks using two different channel-aware CSMA protocols. We used an analytical framework based on stochastic geometry to derive the transmission probability and success probability for a typical node, and from there two spatial performance metrics, the density of successful transmissions and spatial fairness index were computed.

We showed that QT-CSMA achieves higher spatial reuse and fairness than O-CSMA, and more interestingly the simple version of QT-CSMA with one *less* parameter can achieve uniformly better spatial reuse performance in a wide range of node densities for appropriately chosen carrier sense threshold. This implies that the joint interference and opportunistic gain control approach of QT-CSMA is good enough in achieving high spatial reuse.

It was also shown that the inherent unfairness arising from irregular topology in real world network can be removed to a large extent by using QT-CSMA. By characterizing the behavior of spatial reuse and fairness pair, we showed that although O-CSMA has one more parameter to adjust, its set of achievable pair was smaller than that of QT-CSMA. Surprisingly, the simple version of QT-CSMA (QT₀-CSMA) has almost the same set of achievable pairs as QT-CSMA.

Thus, we conclude that the joint carrier sense and quantile scheduling approach of QT-CSMA is not only an effective way in improving spatial reuse/fairness performance by compromising interference and transmitter density but also a practical low complexity approach with one less parameter and robustness.

2.9 Appendix : Derivation of $u'(n, t_0, \tau, \lambda)$

In this appendix, we derive u' for $n \in \{0, 1, 2, \dots\}$, $t_0 \in [0, 1)$, $\tau > 0$, and $\lambda > 0$, which is defined as

$$u'(n, t_0, \tau, \lambda) = \mathbb{P}(E_1 = 1 \mid E_0 = 1, N_0 = n, T_0 = t_0, \{y_0, y_1\} \subset \Phi, \|y_0 - y_1\| = \tau).$$

Let $\Phi = \{X_i\}$ be an homogeneous PPP with density λ . N_0 is the number of neighbors of y_0 and T_0 is the timer value of y_0 . In the sequel, we omit the conditioning events $\{y_0, y_1\} \subset \Phi$ and $\|y_0 - y_1\| = \tau$ for simplicity. By applying Bayes' rule, we have

$$\mathbb{P}(E_1 = 1 \mid E_0 = 1, N_0 = n, T_0 = t_0) = \frac{\mathbb{P}(E_1 = 1, E_0 = 1 \mid N_0 = n, T_0 = t_0)}{\mathbb{P}(E_0 = 1 \mid N_0 = n, T_0 = t_0)}. \quad (2.61)$$

The denominator is simply given by

$$\mathbb{P}(E_0 = 1 \mid N_0 = n, T_0 = t_0) = (1 - t_0)^n \quad (2.62)$$

since for y_0 to transmit, all its n neighbors should have timer values larger than t_0 independently. To compute the numerator, we condition on the event that y_0 and y_1 are neighbors, i.e., $\{y_1 \in \mathcal{N}_0\} = \{F'_{01} > \nu\ell(\|y_0 - y_1\|)\}$, then by the law of total probability we have

$$\begin{aligned} \mathbb{P}(E_1 = E_0 = 1 \mid N_0 = n, T_0 = t_0) &= \underbrace{\mathbb{P}(E_1 = E_0 = 1, y_1 \in \mathcal{N}_0 \mid N_0 = n, T_0 = t_0)}_{=0} \\ &+ \underbrace{\mathbb{P}(E_1 = E_0 = 1 \mid N_0 = n, T_0 = t_0, y_1 \notin \mathcal{N}_0)}_C \underbrace{\mathbb{P}(y_1 \notin \mathcal{N}_0 \mid N_0 = n, T_0 = t_0)}_D. \end{aligned} \quad (2.63)$$

If y_0 and y_1 can see each other, it is impossible for both to transmit at the same time, so the first term is equal to 0. We denote the second and third terms by C and D respectively.

2.9.1 Computing C

The term C is a conditional probability conditioned on that y_0 and y_1 do not see each other. However, they may share some neighbors; so to compute this term we

need to further condition on the event that some portion of y_0 's contenders are also seen by y_1 . Let $\mathcal{K} = \mathcal{N}_0 \cap \mathcal{N}_1$ be the set of shared neighbors between y_0 and y_1 and $K(\tau) \equiv |\mathcal{K}|$ be the number of them. Note that $K(\tau) \sim \text{Poisson}(\bar{K})$ where the mean $\bar{K}(\tau)$ is computed as

$$\begin{aligned} \bar{K}(\tau) &= \mathbb{E} \left[\sum_{X_i \in \Phi} \mathbf{1} \{F'_{i0} > \nu l(\|X_i - y_0\|)\} \mathbf{1} \{F'_{i1} > \nu l(\|X_i - y_1\|)\} \right] \\ &= \lambda \int_{\mathbf{R}^2} \mathbb{P}(F_{i0} > \nu l(\|x\|)) \mathbb{P}(F_{i1} > \nu l(\|x - y_1\|)) dx \\ &= \lambda \int_0^{2\pi} \int_0^\infty e^{-\mu\nu(l(r)+l(\sqrt{\tau^2+r^2-2\tau r \cos\theta}))} r dr d\theta. \end{aligned} \quad (2.64)$$

By conditioning on the number of shared neighbors, $K = K(\tau)$, we rewrite the C as

$$C = \sum_{k=0}^n \underbrace{\mathbb{P}(E_0 = E_1 = 1 \mid N_0 = n, T_0 = t_0, K = k, y_1 \notin \mathcal{N}_0)}_{\equiv A_k} \underbrace{\mathbb{P}(K = k \mid N_0 = n, T_0 = t_0, y_1 \notin \mathcal{N}_0)}_{\equiv B_k}. \quad (2.65)$$

We let the first and second terms in the summation be A_k and B_k , respectively.

Computing B_k B_k is the probability that two nodes y_0 and y_1 share k common contenders conditioned on that y_0 has n contenders. Since each contender of y_0 is independently seen by y_1 , the number of shared contenders K for a given N_0 is a Binomial random variable with parameters n and p_s , where p_s is the probability that one of y_0 's neighbors is seen by y_1 . Then, we have

$$\begin{aligned} B_k &= \mathbb{P}(K = k \mid N_0 = n, T_0 = t_0, y_1 \notin \mathcal{N}_0) \\ &\stackrel{a}{=} \mathbb{P}(K = k \mid N_0 = n, y_1 \notin \mathcal{N}_0) \\ &= \binom{n}{k} p_s^k (1 - p_s)^{n-k}, \end{aligned} \quad (2.66)$$

where in $\stackrel{a}{=}$, we used the fact that $\{T_0 = t_0\}$ is independent of $\{K = k\}$, and $p_s(\tau)$ is computed as

$$\begin{aligned}
p_s(\tau) &= \mathbb{P}(X \in \mathcal{N}_1 \mid X \in \mathcal{N}_0) \\
&= \frac{\mathbb{E}[\mathbb{P}(X \in \mathcal{N}_1, X \in \mathcal{N}_0 \mid X)]}{\mathbb{E}[\mathbb{P}(X \in \mathcal{N}_0 \mid X)]} \\
&= \frac{\lambda \int_{\mathbf{R}^2} \mathbb{P}(F'_0 > \nu l(\|x\|)) \mathbb{P}(F'_1 > \nu l(\|x - y_1\|)) dx}{\lambda \int_{\mathbf{R}^2} \mathbb{P}(F > \nu l(\|x\|)) dx} \\
&= \frac{\bar{K}(\tau)}{\bar{N}_0}. \tag{2.67}
\end{aligned}$$

Using (2.15), (2.67) can be rewritten as $p_s = p_s(\tau, \lambda) = 2 - \frac{b(\tau, \lambda)}{N_0}$.

Computing A_k A_k can be rewritten as

$$A_k = \mathbb{E}[\mathbb{P}(E_1 = E_0 = 1 \mid N_0 = n, T_0 = t_0, K = k, T_1, y_1 \notin \mathcal{N}_0)]$$

by conditioning on that the timer value of y_1 equal to t_1 , i.e., $\{T_1 = t_1\}$. Note that either all the shared neighbors in \mathcal{K} have timer values larger than t_1 , i.e., $\{T_j^c \geq t_1, \forall C_j \in \mathcal{K}\}$ where T_j^c is the timer value of contender $C_j \in \mathcal{K}$, or there exist one or more neighbors with timer value(s) smaller than t_1 , i.e., $\{\exists C_j \text{ s.t. } T_j^c < t_1\}$. Using the law of total probability, the probability inside the expectation can be written as follows:

$$\begin{aligned}
&\mathbb{P}(E_1 = E_0 = 1 \mid N_0 = n, T_0 = t_0, K = k, T_1 = t_1, y_1 \notin \mathcal{N}_0) \\
&= \underbrace{\mathbb{P}(E_1 = E_0 = 1 \mid N_0 = n, T_0 = t_0, K = k, T_1 = t_1, y_1 \notin \mathcal{N}_0, T_j^c \geq t_1 \forall C_j \in \mathcal{K})}_{\equiv A_{k1}} \tag{2.68}
\end{aligned}$$

$$\begin{aligned}
&\times \underbrace{\mathbb{P}(T_j^c \geq t_1 \forall C_j \in \mathcal{K} \mid N_0 = n, T_0 = t_0, K = k, T_1 = t_1, y_1 \notin \mathcal{N}_0)}_{\equiv A_{k2} = (1 - t_1)^k} \tag{2.69}
\end{aligned}$$

$$\begin{aligned}
&+ \underbrace{\mathbb{P}(E_1 = 1, E_0 = 1 \mid N_0 = n, T_0 = t_0, K = k, T_1 = t_1, y_1 \notin \mathcal{N}_0, \exists C_j \text{ s.t. } T_j^c < t_1)}_{\equiv A_{k3} = 0} \tag{2.70}
\end{aligned}$$

$$\times \mathbb{P}(\exists C_j \text{ s.t. } T_j^c < t_1 \mid N_0 = 1, T_0 = t_0, K = k, T_1 = t_1, y_1 \notin \mathcal{N}_0).$$

Let (2.68), (2.69), and (2.70) be A_{k1} , A_{k2} , and A_{k3} respectively. We have $A_{k3} = 0$ since if there exist any neighbor with timer value strictly smaller than t_1 , it prevents y_1 from transmitting, so E_1 can not be 1. A_{k2} is the probability that all shared neighbors in \mathcal{K} have timer values larger than t_1 , which is simply given as $A_{k2} = (1 - t_1)^k$ since each timer is independent and uniform in $[0, 1]$. Before we compute A_{k1} , we need to define several random variables.

- Let $N_1 \sim \text{Poisson}(\bar{N}_0)$ be a random variable denoting the number of contenders of y_1 .
- Let $N_{1x} \sim \text{Poisson}(\bar{N}_{1x})$ be a random variable denoting the number of contenders of y_1 which are not shared by y_0 . Note that $N_{1x} + K = N_1$ and $\bar{N}_{1x} = \bar{N}_0(1 - p_s)$.
- Let $N_{1x}^{<t_1} \sim \text{Poisson}(\bar{N}_{1x}^{<t_1})$ be a random variable denoting the number of contenders of y_1 which are not shared by y_0 and with timer values smaller than t_1 . Note that $\bar{N}_{1x}^{<t_1} = t_1 \bar{N}_{1x} = t_1 \bar{N}_0(1 - p_s)$.

To compute A_{k1} , we consider the following two sub-cases $t_1 \leq t_0$ and $t_0 < t_1$. If $t_1 \leq t_0$, then

- y_1 transmits (or $E_1 = 1$) only if it finds no additional neighbors who have timer values smaller than t_1 and are not seen by y_0 , i.e, if $N_{1x}^{<t_1} = 0$, and
- y_0 transmits (or $E_0 = 1$) only if all $T_j^c \sim \text{Uniform}[t_1, 1] \forall C_j \in \mathcal{K}$ is larger than t_0 , which happens with probability $\left(\frac{1-t_0}{1-t_1}\right)^k$ and remaining $n - k$ contenders have timer values larger than t_0 , which happens with probability $(1 - t_0)^{n-k}$.

Note that, as in the previous case, $\{E_0 = 1\}$ and $\{E_1 = 0\}$ are conditionally independent; so we have that

$$A_{k1} = e^{-\bar{N}_{1x}^{<t_1}} \frac{(1 - t_0)^n}{(1 - t_1)^k} \quad \text{if } t_0 \geq t_1. \quad (2.71)$$

In the other case where $t_0 < t_1$,

- y_0 transmits (or $E_0 = 1$) if $n - k$ neighbors have timer values larger than t_0 , which happens with probability $(1 - t_0)^{n-k}$, and
- y_1 transmits (or $E_1 = 1$) only when it finds no additional neighbors who have timer values smaller than t_1 and do not see y_0 , i.e., $N_{1x}^{<t_1} = 0$.

Note that, as in previous case, $\{E_0 = 1\}$ and $\{E_1 = 0\}$ are conditionally independent, so we have

$$A_{k1} = e^{-\bar{N}_{1x}^{<t_1}} (1 - t_0)^{n-k} \quad \text{if } t_0 < t_1. \quad (2.72)$$

A_{k1} in above two cases can be written as follows using indicator functions:

$$A_{k1} = e^{-t_1 \bar{N}_0(1-p_s)} \left(\frac{(1 - t_0)^n}{(1 - t_1)^k} \mathbf{1}\{t_1 \leq t_0\} + (1 - t_0)^{n-k} \mathbf{1}\{t_0 < t_1\} \right). \quad (2.73)$$

Un-conditioning with respect to the event $\{T_1 = t_1\}$ in $A_{k1}A_{k2}$ gives

$$\begin{aligned} A_k &= \int_0^1 e^{-t_1 \bar{N}_0(1-p_s)} \left((1 - t_0)^n \mathbf{1}\{t_1 \leq t_0\} + (1 - t_0)^{n-k} (1 - t_1)^k \mathbf{1}\{t_0 < t_1\} \right) dt_1 \\ &= (1 - t_0)^n \int_0^{t_0} e^{-t_1 \bar{N}_0(1-p_s)} dt_1 + (1 - t_0)^{n-k} \int_{t_0}^1 (1 - t_1)^k e^{-t_1 \bar{N}_0(1-p_s)} dt_1 \\ &\stackrel{a}{=} (1 - t_0)^n \left(\frac{1 - e^{-t_0 \bar{N}_0(1-p_s)}}{\bar{N}_0(1-p_s)} + \frac{(t_0 - 1)e^{-\bar{N}_0(1-p_s)} (\Gamma(k+1, \eta) - \Gamma(k+1))}{\eta^{k+1}} \right) \\ &\stackrel{b}{=} (1 - t_0)^n \left(\frac{1 - e^{-t_0 \bar{N}_0(1-p_s)}}{\bar{N}_0(1-p_s)} + \frac{(1 - t_0)e^{-\bar{N}_0(1-p_s)} k!}{\eta^{k+1}} \left(1 - e^{-\eta} \sum_{j=0}^k \frac{\eta^j}{j!} \right) \right), \end{aligned} \quad (2.74)$$

where in $\stackrel{a}{=}$, $\Gamma(a, x) = \int_x^\infty t^{a-1} e^{-t} dt$ is the incomplete gamma function with $\Gamma(a) \equiv \Gamma(a, 0)$ and $\eta = \bar{N}_0(1-p_s)(t_0 - 1)$, and in $\stackrel{b}{=}$ we used the fact that $\frac{\Gamma(k+1, \eta)}{\Gamma(k+1)} = \sum_{j=0}^k \frac{\eta^j}{j!} e^{-\eta}$. Replacing (2.74) and (2.66) in (2.65) gives

$$C = \mathbb{P}(E_1 = E_0 = 1 \mid N_0 = n, T_0 = t_0, y_1 \notin \mathcal{N}_0) = \sum_{k=0}^n A_k B_k. \quad (2.75)$$

2.9.2 Computing D

We now compute $D = \mathbb{P}(y_1 \notin \mathcal{N}_0 \mid N_0 = n, T_0 = t_0)$ in (2.63). Note that $\{N_0 = n\}$ and $\{y_1 \notin \mathcal{N}_0\}$ are not independent since it is likely that y_1 is the neighbor of y_0 if $N_0 = n$ is large, but $\{y_1 \notin \mathcal{N}_0\}$ and $\{T_0 = t_0\}$ are independent since being neighbors of a node does not depend on timer values. Thus, we have $D = \mathbb{P}(y_1 \notin \mathcal{N}_0 \mid N_0 = n)$. Applying Bayes' rule, we get

$$D = \frac{\mathbb{P}(y_1 \notin \mathcal{N}_0, N_0 = n)}{\mathbb{P}(N_0 = n)} = \frac{\mathbb{P}(N_0 = n \mid y_1 \notin \mathcal{N}_0)\mathbb{P}(y_1 \notin \mathcal{N}_0)}{\mathbb{P}(N_0 = n)}, \quad (2.76)$$

where we have

$$\mathbb{P}(N_0 = n \mid y_1 \notin \mathcal{N}_0) = \frac{\bar{N}_0^n}{n!} e^{-\bar{N}_0} \quad (2.77)$$

and

$$\mathbb{P}(y_1 \notin \mathcal{N}_0) = \mathbb{P}(F'_{10} < \nu l(\tau)) = G(\nu l(\tau)) \quad (2.78)$$

for numerator. To compute $\mathbb{P}(N_0 = n)$, the denominator⁸ in (2.76), we need to consider whether y_1 is seen by y_0 or not. Using the law of total probability, we have

$$\begin{aligned} \mathbb{P}(N_0 = n) &= \mathbb{P}(N_0 = n \mid y_1 \in \mathcal{N}_0)\mathbb{P}(y_1 \in \mathcal{N}_0) + \mathbb{P}(N_0 = n \mid y_1 \notin \mathcal{N}_0)\mathbb{P}(y_1 \notin \mathcal{N}_0) \\ &= \frac{\bar{N}_0^{n-1}}{(n-1)!} e^{-\bar{N}_0} (1 - G(\nu l(\tau))) + \frac{\bar{N}_0^n}{n!} e^{-\bar{N}_0} G(\nu l(\tau)) \\ &= \frac{\bar{N}_0^{n-1}}{(n-1)!} e^{-\bar{N}_0} \left(1 + \left(\frac{\bar{N}_0}{n} - 1 \right) G(\nu l(\tau)) \right). \end{aligned} \quad (2.79)$$

Note that as expected $\mathbb{P}(N_0 = n) \rightarrow \mathbb{P}(N_0 = n \mid y_1 \notin \mathcal{N}_0)$ as $\tau \rightarrow \infty$ (or $G(\tau) \rightarrow 1$), and $\mathbb{P}(N_0 = n) \rightarrow \mathbb{P}(N_0 = n \mid y_1 \in \mathcal{N}_0)$ as $\tau \rightarrow 0$ (or $G(\tau) \rightarrow 0$). Then, replacing (2.77), (2.78), and (2.79) in (2.76) gives the following for $n \geq 0$,

$$D = \frac{\bar{N}_0 G(\nu l(\tau))}{n + (\bar{N}_0 - n)G(\nu l(\tau))}. \quad (2.80)$$

Recall that D is the probability that y_1 is not the neighbor of y_0 given $N_0 = n$. Thus, $D \rightarrow 1 (D \rightarrow 0)$ as $\tau \rightarrow \infty (\tau \rightarrow 0)$ makes sense.

⁸Recall that $\mathbb{P}(N_0 = n)$ is indeed $\mathbb{P}(N_0 = n \mid \|y_0 - y_1\| = \tau)$.

2.9.3 Computing u'

Now, replacing term C in (2.75) and D in (2.80) to (2.63) gives

$$\mathbb{P}(E_1 = E_0 = 1 \mid N_0 = n, T_0 = t_0) = \frac{\bar{N}_0 G(\nu l(\tau))}{n + (\bar{N}_0 - n)G(\nu l(\tau))} \sum_{k=0}^n A_k B_k. \quad (2.81)$$

Finally, (2.61) is given as

$$\begin{aligned} u'(n, t_0, \tau, \lambda) = & \frac{\bar{N}_0 G(\nu l(\tau))}{n + (\bar{N}_0 - n)G(\nu l(\tau))} \left(\frac{1 - e^{-t_0 \bar{N}_0 (1-p_s)}}{\bar{N}_0 (1-p_s)} + \right. \\ & \left. + (1-t_0) e^{-\bar{N}_0 (1-p_s)} \sum_{k=0}^n \frac{k!}{\eta^{k+1}} \left(1 - e^{-\eta \sum_{j=0}^k \frac{\eta^j}{j!}} \right) \binom{n}{k} p_s^k (1-p_s)^{n-k} \right), \end{aligned} \quad (2.82)$$

where $p_s = p_s(\tau, \lambda) = 2 - \frac{b(\tau, \lambda)}{\bar{N}_0}$ and $\eta = \bar{N}_0 (1-p_s)(t_0 - 1)$.

2.9.4 Impact of n and t_0

Fig.2.9a gives plots for $u'(n, t_0, \tau, \lambda)$ for $t_0 = 0.5$, $\lambda = 1$ and for $n = 0, \dots, 20$. Observe how u' changes as the distance τ between y_0 and y_1 changes. As τ gets large, y_1 behaves like a typical node in space which is not affected by the existence of y_0 . The latter case is verified by the fact that all curves u' converge to the value $\frac{1-e^{-\bar{N}_0}}{\bar{N}_0}$ as $\tau \rightarrow \infty$, which is indeed the transmission probability of a typical CSMA node. As τ gets small, there is a strong correlation between y_1 and y_0 which are likely to be neighbors. The behavior of u' in this case depends on the value of n . In particular, if $n = 0$, u' increases as $\tau \rightarrow 0$; since y_1 will see no contenders as is the case for y_0 , while if $n > 0$, as $\tau \rightarrow 0$, y_1 will see one or more contenders as seen by y_0 , and it will be more likely that y_1 is a neighbor of y_0 . If y_1 is a neighbor of y_0 , then due to the condition $\{E_0 = 1\}$, y_1 must have a timer value larger than t_0 , so the conditional transmission probability u approaches 0. As n increases, y_1 is more likely to be preempted by y_0 and its neighbors, thus u' decreases.

Fig.2.9b shows the impact of y_0 's timer value, t_0 , on u' for $n = 5$. Note that the condition $\{E_0 = 1\}$ implies that n neighbors of y_0 have timer values between t_0 and

1. Thus, if t_0 gets large, y_1 will transmit with high probability since the neighbors of y_0 will have timer values larger than t_0 , which can be easily preempted by y_1 's timer. While if t_0 gets small, y_1 is more likely to be preempted by y_0 's neighbors, so u' decreases in this case.

2.10 Appendix : Convergence of $I_{\Phi_M^\gamma}$

Consider a Matérn CSMA process which is induced by a CSMA mechanism from a PPP with density λ . In this CSMA network, the density of active transmitters λp_{tx} converges to a value as $\lambda \rightarrow \infty$ due to the CSMA protocol. Accordingly, the amount of interference *seen at a typical receiver* also converges to a random variable, say $I_{\Phi_M^{csma}}$. The objective of this section is to prove that $I_{\Phi_M^{csma}}$ is almost surely finite, i.e., $\mathbb{P}(I_{\Phi_M^{csma}} < \infty) = 1$.

To that end, we first show that for a given monotonically increasing sequence of node densities $\lambda^{[1]} \leq \lambda^{[2]} \leq \lambda^{[3]} \leq \dots$ and associated *marked* PPPs $\Psi^{[1]}, \Psi^{[2]}, \Psi^{[3]}, \dots$ denoting transmitters, the sequence of aggregate interference seen by a typical receiver $I_{\Phi_M^{[1]}}, I_{\Phi_M^{[2]}}, I_{\Phi_M^{[3]}}, \dots$,⁹ stochastically and monotonically increases, i.e.,

$$I_{\Phi_M^{[1]}} \leq^{st} I_{\Phi_M^{[2]}} \leq^{st} I_{\Phi_M^{[3]}} \leq^{st} \dots \quad (2.83)$$

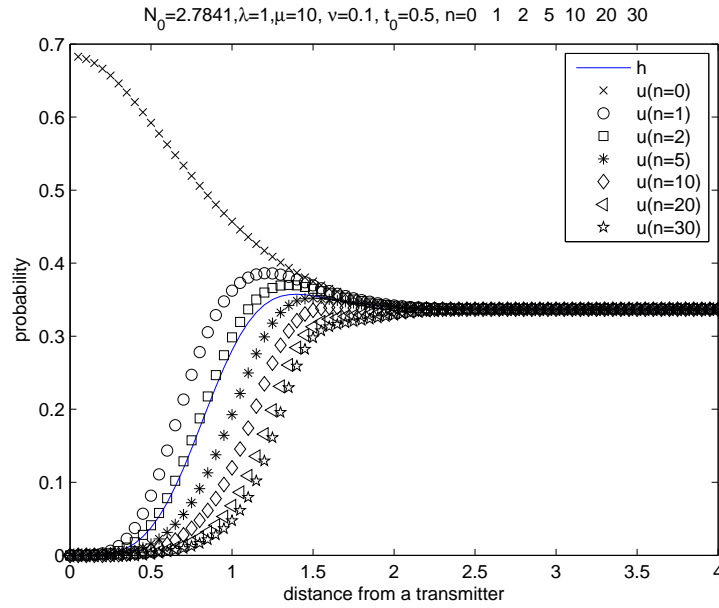
We will use coupling argument to show this. To that end, we will construct the copy $\Psi^{(n)}$ of each process $\Psi^{[n]}$ and couple them such that following strict inequalities hold with probability 1:

$$I_{\Phi_M^{(1)}} \leq I_{\Phi_M^{(2)}} \leq I_{\Phi_M^{(3)}} \leq \dots, \quad (2.84)$$

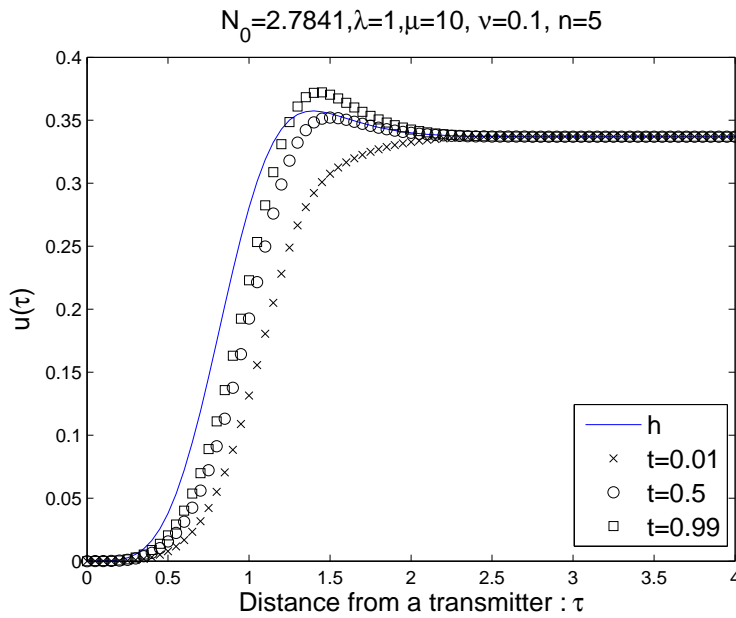
where $I_{\Phi_M^{(n)}}$ is the associated aggregate interference of $\Psi^{(n)}$ seen at a typical receiver for $n = 1, 2, \dots$ ¹⁰. Note that we use square bracket $[n]$ to denote n -th original process

⁹ $\Phi_M^{[i]}$ is a Matérn CSMA process associated with the original marked process $\Psi^{[i]}$. The relation is explained in detail later.

¹⁰ $\Phi_M^{(i)}$ is a Matérn CSMA process associated with the copied process $\Psi^{(i)}$.



(a) $h(\cdot)$ for various n values



(b) $h(\cdot)$ for various t values

Figure 2.9: $h(\cdot)$ is a function computed in (2.14). $u'(\cdot)$ is a function we computed above for $N_0 = n \geq 0$ and $t_0 \in [0, 1)$.

and curly bracket (n) to denote the copy of it. Clearly, (2.84) implies convergence of $I_{\Phi_M^{(n)}}$ to a random variable, say $I_{\Phi_M^{csma}}$ (possibly infinite). We will then use the results in [114] to show that $I_{\Phi_M^{csma}}$ is almost surely finite.

Constructing n -th network $\Psi^{(n)}$

We consider

$$\Psi^{(n)} = \left\{ \left(X_i^{(n)}, E_i^{(n)}, T_i^{(n)} \right) \right\} \quad (2.85)$$

given $(X_0^{(n)} = 0, E_0^{(n)} = 1, T_0^{(n)}, \mathbf{F}_0^{(n)}, \mathbf{F}'_0^{(n)}) \in \Psi^{(n)}$, with a node density $\lambda^{[n]}$, where $T_i^{(n)} \sim \text{Uniform}[0, 1]$ are marks corresponding timer values and

$$E_i^{(n)} = \mathbf{1}\{T_i^{(n)} < \min_{X_j^{(n)} \in \mathcal{N}_i^{(n)}} T_j^{(n)}\}$$

is the transmission indicator of node $X_i^{(n)}$. Let $\Phi^{(n)} = \{X_i^{(n)}\}$ and $\Phi_M^{(n)} = \{X_i^{(n)} \in \Phi^{(n)} \mid E_i^{(n)} = 1\}$. Then, the aggregate interference seen by the receiver of a transmitter X_0 is given as $I_{\Phi_M^{(n)}} = \sum_{X_j \in \Phi_M^{(n)} \setminus \{0\}} F_{ji}^{(n)} / l(\|X_j - (0, r)\|)$.

Constructing coupled timers

We scale the timer values $T_i^{(n)}$ for the n -th network such that it is uniformly distributed in $[0, \frac{\lambda^{[n]}}{\lambda^{[n+1]}}]$, i.e., let $T_{ci}^{(n)} = \frac{\lambda^{[n]}}{\lambda^{[n+1]}} T_i^{(n)}$. Let a PPP with compressed timer values as

$$\Psi_c^{(n)} = \left\{ \left(X_i^{(n)}, E_i^{(n)}, T_{ci}^{(n)} \right) \mid (X_i^{(n)}, E_i^{(n)}, T_i^{(n)}) \in \Psi^{(n)} \right\}. \quad (2.86)$$

Note that the timer value scaling maintains the order of timer values, so there is no change in E_i . Let $\Phi_c^{(n)} = \{X_i^{(n)}\}$ and $\Phi_{cM}^{(n)} = \{X_i^{(n)} \in \Phi_c^{(n)} \mid E_i^{(n)} = 1\}$, then, the aggregate interference from $\Phi_{cM}^{(n)}$ is the same as $I_{\Phi_M^{(n)}}$, i.e.,

$$I_{\Phi_{cM}^{(n)}} = I_{\Phi_M^{(n)}}. \quad (2.87)$$

Differential PPP

Consider an another marked PPP

$$\hat{\Psi}^{(n)} = \left\{ \left(\hat{X}_i^{(n)}, \hat{E}_i^{(n)}, \hat{T}_i^{(n)} \right) \right\} \quad (2.88)$$

with density $\hat{\lambda}^{[n]} = \lambda^{[n+1]} - \lambda^{[n]}$ for the given $\lambda^{[n+1]} \geq \lambda^{[n]}$ and $\hat{\Phi}^{(n)} = \{\hat{X}_i^{(n)}\}$ and $\hat{\Phi}_M^{(n)} = \{\hat{X}_i^{(n)} \in \hat{\Phi}^{(n)} \mid \hat{E}_i^{(n)} = 1\}$ ¹¹. By construction we will ensure that $\hat{\Psi}^{(n)}$ is independent of $\Psi^{(n)}$. We let the timer values $\hat{T}_i^{(n)}$ be uniformly distributed on $[\frac{\lambda^{[n]}}{\lambda^{[n+1]}}, 1]$ and have *nodes $\hat{X}_i^{(n)}$ to contend nodes with those in $\hat{\Psi}^{(n)}$ as well as in $\Psi^{(n)}$* . Let $\hat{F}_{ji}^{(n)}$ be the fading channel between $\hat{X}_j^{(n)} \in \hat{\Phi}^{(n)}$ and $\hat{X}_i^{(n)} \in \hat{\Phi}^{(n)}$ and $H_{ji}^{(n)}$ as the fading channel between a transmitter $X_j^{(n)} \in \Phi^{(n)}$ and a transmitter $\hat{X}_i^{(n)} \in \hat{\Phi}^{(n)}$. Then, we can define two different neighborhoods for $\hat{X}_i^{(n)}$: one in $\hat{\Phi}^{(n)}$ given as

$$\hat{\mathcal{N}}_i^{(n)} = \left\{ \hat{X}_j^{(n)} \in \hat{\Phi}^{(n)} \mid \hat{F}_{ji}^{(n)} > \nu l(\|\hat{X}_j^{(n)} - \hat{X}_i^{(n)}\|), j \neq i \right\} \quad (2.89)$$

and the other in $\Phi^{(n)}$ given as

$$\mathcal{M}_i^{(n)} = \left\{ X_j^{(n)} \in \Phi^{(n)} \mid H_{ji}^{(n)} > \nu l(\|X_j^{(n)} - \hat{X}_i^{(n)}\|) \right\}. \quad (2.90)$$

Using above definitions, we can define the transmission indicator as

$$\hat{E}_i^{(n)} = \mathbf{1} \left\{ \hat{T}_i^{(n)} < \min \left\{ \min_{\hat{X}_j^{(n)} \in \hat{\mathcal{N}}_i^{(n)}} \hat{T}_j^{(n)}, \min_{X_k^{(n)} \in \mathcal{M}_i^{(n)}} T_k^{(n)} \right\} \right\}. \quad (2.91)$$

Note that every node in $\hat{\Phi}^{(n)}$ which contends with at least one node in $\Phi^{(n)}$ defers its transmission since its timer value is always larger than $\frac{\lambda^{[n]}}{\lambda^{[n+1]}}$. Let

$$\Delta I_{\hat{\Phi}_M^{(n)}} = \sum_{\hat{X}_j^{(n)} \in \hat{\Phi}_M^{(n)}} H_{j0}^{(n)} / l(\|\hat{X}_j^{(n)} - (0, r)\|)$$

be the interference seen by the receiver of the transmitter X_0 in $\Phi_M^{(n)}$ from transmitters only in $\hat{\Phi}_M^{(n)}$, where $H_{j0}^{(n)}$ is the fading channel between a transmitter $\hat{X}_j^{(n)} \in \hat{\Phi}^{(n)}$ and the receiver of $X_0 \in \Phi^{(n)}$.

¹¹Note that we do *not* condition on $0 \in \hat{\Phi}_M^{(n)}$.

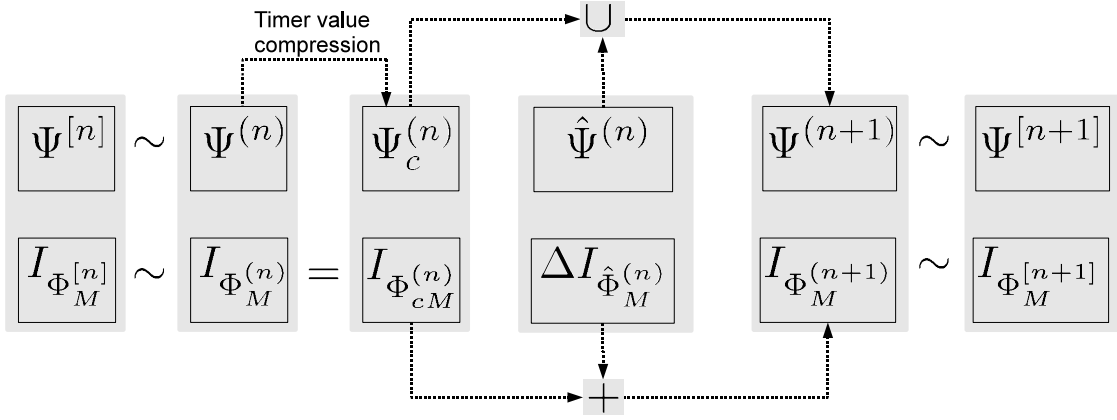


Figure 2.10: Constructing $\Psi^{(n+1)}$ from $\Psi^{(n)}$ and $\hat{\Psi}^{(n)}$.

Constructing $n + 1$ th network $\Psi^{(n+1)}$

Now, we construct $\Psi^{(n+1)}$ by the union of the the timer scaled point process and the differential point process:

$$\Psi^{(n+1)} = \Psi_c^{(n)} \cup \hat{\Psi}^{(n)}. \quad (2.92)$$

Note that $\Psi_c^{(n)}$ and $\Psi^{(n)}$ contribute $\frac{\lambda^{[n]}}{\lambda^{[n+1]}}$ and $1 - \frac{\lambda^{[n]}}{\lambda^{[n+1]}}$ fraction of nodes to $\Psi^{(n+1)}$ respectively. This makes a randomly chosen node in $\Psi^{(n+1)}$ has a timer value uniformly distributed on $[0,1]$. Thus, $\Psi^{(n+1)} = \{(X_i^{(n+1)}, E_i^{(n+1)}, T_i^{(n+1)})\}$ is indeed a marked PPP with density $\lambda^{[n+1]}$, where $T_i^{(n+1)}$ is uniformly distributed on $[0,1]$. Let $I_{\Phi_M}^{(n+1)}$ be the aggregate interference seen by a typical receiver, then, it is given as the sum of the interferences

$$I_{\Phi_M}^{(n+1)} = I_{\Phi_{cM}}^{(n)} + \Delta I_{\hat{\Phi}_M}^{(n)}, \quad (2.93)$$

since $I_{\Phi_{cM}}^{(n)}$ is independent of nodes in $\Psi^{(n)}$, which is the direct result of the timer value separation. Now clearly the two point processes $\Psi_c^{(n)}$ and $\Psi^{(n+1)}$ are coupled such that their aggregate interference satisfy :

$$I_{\Phi_{cM}}^{(n)} \leq I_{\Phi_M}^{(n+1)}. \quad (2.94)$$

Using (2.87), this can be rewritten as $I_{\Phi_M^{(n)}} \leq I_{\Phi_M^{(n+1)}}$, which implies the stochastic dominance relation $I_{\Phi_M^{(n)}} \leq^{st} I_{\Phi_M^{(n+1)}}$. Since $I_{\Phi_M^{(n)}} \sim I_{\Phi_M^{[n]}}$ and $I_{\Phi_M^{(n+1)}} \sim I_{\Phi_M^{[n+1]}}$, we have

$$I_{\Phi_M^{[n]}} \leq^{st} I_{\Phi_M^{[n+1]}}. \quad (2.95)$$

Fig.2.10 summarizes our coupling argument.

Convergence of $I_{\Phi_M^{[n]}}$

Since increasing random variables converge (possibly to ∞), $I_{\Phi_M^{(n)}}$ (or equivalently $I_{\Phi_M^{[n]}}$) converges to a random variable as $n \rightarrow \infty$. Let the converging value be denoted by $I_{\Phi_M^{csma}} \equiv \lim_{n \rightarrow \infty} I_{\Phi_M^{[n]}}$. We rewrite the results from [114] in our context as follows.

Proposition 10. (*Existence of shot noise*) [114] *For a given random variable I , if $\lim_{s \rightarrow 0} \mathbb{E}[e^{-sI}] = 1$, then, I has a well-behaved distribution or finite a.s..*

Note that Φ_M^{csma} is a Matérn CSMA process with density λ_{csma} , which is stationary and ergodic. Then, we can apply following results from [114].

Proposition 11. (*Necessary and sufficient conditions, Corollary 1.2 in [114]*). *The necessary and sufficient conditions for the existence of $I_{\Phi_M^{csma}}$ are*

$$\int_0^\infty \int_0^\delta xw(x; y) y dx dy < \infty, \text{ and} \quad (2.96)$$

$$\left| \int_0^\infty \int_0^\delta w(x; y) y dx dy \right| < \infty \quad (2.97)$$

for $\delta > 0$, where $w(x; y) = P(F > xy^\alpha) = \exp\{-\mu xy^\alpha\}$.

Using the fact that $x \leq \delta$ and $w(x; y) > 0$, it is sufficient to show (2.97) only, i.e., we have

$$\int_0^\infty \int_0^\delta xw(x;y)ydx dy \leq \delta \int_0^\infty \int_0^\delta w(x;y)ydx dy$$

$$= \frac{\delta}{\mu} \int_0^\infty y^{1-\alpha}(1 - \exp\{-\mu\delta y^\alpha\})dy \quad (2.98)$$

$$\stackrel{a}{=} -\frac{\delta^{2-\frac{2}{\alpha}}}{\alpha\mu^{2/\alpha}}\Gamma\left(\frac{2-\alpha}{\alpha}\right) < \infty. \quad (2.99)$$

In $\stackrel{a}{=}$, we used the results in 370p of [47], which holds for $\alpha > 2$. Using Theorem 2 of [114] and bounding technique, one can also show the existence of the *approximate* of $I_{\Phi_M^{csma}}$, which is a non-homogeneous Poisson shot noise.

Chapter 3

Understanding the Design Space of Cognitive Networks

3.1 Introduction

FCC and researchers have observed the scarcity and the underutilization of spectrum resources which suggests that a new model of spectrum usage is required, usually referred to as cognitive radio/network, see e.g., [8, 35, 83, 123]. The basic approach is to allow unlicensed or secondary devices to opportunistically access a spectrum allocated to licensed or primary devices. The focus of this chapter is on the transmission capacity of cognitive networks, in particular on characterizing the spatial or temporal spectrum opportunities for secondary devices and their interaction with primary devices. Specifically, we consider two scenarios, denoted $S1$ and $S2$, based on the transmit power level of PTxs and whether the PTxs transmit the same signal or not.

In Scenario 1 ($S1$), we model primary transmitters (PTx) corresponding to high-power broadcasting towers, e.g., a fixed or mobile TV broadcasting station, sending the same signal to multiple primary receivers (PRx). This is usually called a single frequency network (SFN). The coverage of a single PTx is relatively large, e.g., tens of kilometers, and receivers can successfully decode the signal if they belong to the coverage area of at least one transmit station. Signals from different stations are treated as delayed multi-path. Cognitive or secondary devices can transmit in regions where the primary signal is not detected.

In Scenario 2 ($S2$), we model PTxs' corresponding to low-power broadcasting stations having a small coverage area. Transmit power is assumed to be very small

compared to high power broadcasting. These PTxs can be private stations sending information to nearby primary receivers; for example, a microphone, a station broadcasting commentary on a current game in small stadium. In this scenario two nearby PTxs can interfere with each other, which was not possible in $S1$. We assume that each PRx is the receiver of its nearest PTx.

In both cases, PTxs are not aware of the existence of secondary devices and the same secondary network characteristics are assumed where secondary transmitters (STx) and receivers (SRx) are involved in ad-hoc or peer to peer low power transmissions.

Related work. In this chapter we explore the capacity of cognitive wireless networks from a spatial reuse perspective. A spatial model reflecting the physical characteristics such as signal attenuation, interference, geographical locations of nodes is considered.

These types of models have been used in evaluating the capacity of *networks* before. In particular, in [49] and numerous subsequent papers, see survey in [52], various spatial models have been introduced, where nodes are randomly distributed on a plane and signal attenuation is function of an attenuation factor and the distance between transmitter and receiver. In addition, [13], [113] and [112] explored the capacity of networks in terms of transmission capacity, which measures transmitted bits per second per meter square. Their models capture the subtle interactions between nodes in terms of outage, so they allow the computation of the exact capacity rather than the scaling behavior. However, most of this research focuses on capacity analysis for *homogeneous* networks.

Recently, these methodologies have been extended to evaluate the performance of multiple networks with different priorities in the context of cognitive networks; for example, [62, 120] focus on scaling laws but for “two networks with different access priority”. In their work, primary and secondary networks are found to have the same capacity scaling law $\Theta(\sqrt{n/\log n})$ and $\Theta(\sqrt{m/\log m})$ where n and m correspond to

the primary/ secondary receiver densities. [95] studied the impact of secondary node transmission power on the reliability of detection performance and the transmission opportunity for secondary nodes. However, this work considers only a single secondary node with randomly distributed multiple primary nodes. Overlaid spectrum sharing between two different networks was studied in [58], where the mobile ad-hoc devices are overlaid with uplink transmissions of an existing cellular network and the capacity trade-off between two networks was characterized. However, in this work, the secondary nodes do not have spatial detection or cognitive function. [110] studied cognitive networks with single primary and multiple secondary transmitters. A bound on the radius of the primary exclusive region, i.e., where the primary transmitter can communicate with its receivers under an outage constraint, was found based on various system parameters. [88] considered a carrier sensing based cognitive network where two types of nodes access medium with different access priority. Poisson approximation was used to deal with the inhomogeneous node distribution.

Contributions In this chapter, we model *both* primary and secondary devices as point processes, which allows us to capture the impact from both PTxs and STxs to both PRxs and SRxs. We also model the cognitive operation of secondary devices; as a result, the two processes are *dependent* on each other. Our model delivers rich insights on system performance and design tradeoffs in terms of coverage, node density, outage probability, and capacity. Our contributions can be summarized as follows.

- First, we provide a novel and mathematically tractable Boolean disk model for primary and secondary networks, which is simple yet captures the stochastic nature of the interaction between the two networks. The coverage reduction of PTxs and the impact of hidden PTxs on outage, node density and capacity of STxs are characterized.

- Second, we identify several important design parameters: detection radius (or detection SINR threshold), decoding SINR threshold and transmit power of STx, which affect the achievable capacity of the secondary network. It is shown that a conservatively selected detection radius can severely decrease the capacity of a secondary network and that the optimal decoding SINR of SRxs depends on the density of PTxs. We also show that a secondary network with a conservative detection radius can achieve higher capacity if the associated primary network has more bursty coverage. While an ideally chosen detection radius makes the achievable capacity of the secondary network be independent of the burstiness of primary network's coverage, it does introduce interference to PRxs. We provide *rules of thumb* on how to tune these design parameters to maximize the capacity of the cognitive network.
- Finally, we characterize the joint network capacity regions for the primary and secondary networks for two different broadcasting scenarios. In the high power broadcasting scenario $S1$, the joint network capacity region of the two networks is approximately bounded by a linear function. In contrast, in the low power broadcasting scenario $S2$, it turns out that the joint network capacity region of two networks is convex due to self interference of primary nodes.

Organization This chapter is organized as follows. In Section 3.2, our system model is described and in Section 3.3 and 3.4 outage probabilities of primary and secondary network are derived. We investigate the joint network capacity in Section 3.5 and the impact of system parameters on capacity in Section 3.6. Concluding remarks are given in Section 3.7.

3.2 System Model

3.2.1 Preliminary Definitions

We first define the notation that will be used throughout this chapter. $b(x, r)$ denote a ball centered at location $x \in \mathbf{R}^2$ with radius r . Let $\|x - y\|$ denote a distance between two points x and y in \mathbf{R}^2 and $|A|$ denote the area of set $A \subset \mathbf{R}^2$. For $x, y, z \in \mathbf{R}^2$ and $a, b, c \in \mathbf{R}$ we define following two set-related notations: $K(x, a, y, b) = b(y, b) \setminus b(x, a)$, and $H(x, a, y, b, z, c) = b(z, c) \setminus (b(x, a) \cup b(y, b))$. We denote the area of these sets with $k(x, a, y, b)$ and $h(x, a, y, b, z, c)$ respectively. To further simplify notation, with a slight abuse of notation let $K(d, a, b) = b(O, b) \setminus b((-d, 0), a)$ and $k(d, a, b) = |K(d, a, b)|$. For a random variable Q , let $\mathcal{L}_Q(s) \equiv \mathbb{E}[e^{-sQ}]$ denote the Laplace transform of the random variable Q .

3.2.2 Path loss and Interference Model

We assume a free space path loss model $d^{-\alpha}$ given an attenuation factor α and distance d between transmitter/interferer and receiver. When SINR is computed, only the dominant interferer is considered. If the dominant interferer is within the interference radius of the receiver, the receiver fails to receive; otherwise, the interferer is ignored. The interference radius is conservatively determined based on various factors such as interference power, signal power, noise and the receiver's decoding SINR. In our interference model, we do not take into account the additive nature of interference. Indeed this so called protocol interference model is widely used [49, 72, 74] and this model produces asymptotically tight estimates [112, 113].

3.2.3 Primary Network Model

The primary network consists of a set of PTx-PRx pairs. We model only the locations of PTxs which for simplicity are assumed to follow a homogeneous Poisson point process (HPPP) $\Pi_p = \{X_i\}$ in \mathbf{R}^2 with intensity λ_p . We use X_i to denote both the i -th PTx and its location in \mathbf{R}^2 . PTxs transmit with the same transmission

power ρ_p and realize a rate $b_p = \log(1 + \beta_p)$ bps where β_p is the SINR threshold to decode PTx's signal. In $S1$, a PRx Y can decode the signal from PTxs if it is within PTxs' coverage area, $B(\Pi_p, d_p) \equiv \cup_{X_i \in \Pi_p} b(X_i, d_p)$ and, at the same time, is not interfered by a STx; here d_p denotes the target coverage radius of PTxs. A PRx Y can be interfered by STxs if one or more active STxs exist within its interference region $b(Y, r_{sp})$, where r_{sp} is STx's interference radius of a PRx w.r.t to a STx. In $S2$, the model is similar except that a PRx can also be interfered by other PTxs if they are within the interference radius r_{pp} of the PRx.

3.2.4 Secondary Network Model

The secondary network consists of a set of STx-SRx pairs. The STxs are modeled by HPPP $\Pi_s = \{Z_i\}$ with intensity λ_s . We assume that all the STxs sense the medium at the same time and only STxs which detect the absence of PTxs attempt to transmit in Aloha fashion. This again represents a strong simplification. So, it is possible that a SRx is interfered by one or more other active STxs, causing an outage. Indeed, this model can be viewed as a snapshot of active secondary nodes at a typical time slot. Note that not all the STxs are allowed to transmit since some of them are blocked out by PTxs and accordingly inactive. We assume that a STx uses a simple *signal energy detection* scheme to detect whether there are PTxs within its detection radius r_d . A SRx W is interfered by PTxs if one or more PTx exist within $b(W, r_{ps})$, where r_{ps} is the interference radius of a SRx w.r.t a PTx. For a given primary process Π_p , we model the active STxs by a point process $\Pi_s^a = \Pi_s^a(\Pi_p) = \{Z_i \in \Pi_s | Z_i \notin B(\Pi_p, r_d)\}$ with intensity $\lambda_s^a(z, \Pi_p) = \lambda_s \mathbf{1}\{z \notin B(\Pi_p, r_d)\}$ at $z \in \mathbf{R}^2$. Note that Π_s^a is a stationary doubly stochastic or Cox process with a random intensity measure [102]. Also note that for a given π_p , a realization of Π_p , this process of active STx corresponds to a thinned process, where the thinning is spatially correlated depending on the π_p . Thus, the resulting process is a non-HPPP. We assume that a STx transmits to a SRx which is located a fixed distance d_s away with transmission power ρ_s . Like PTx,

a STx transmits $b_s = \log(1 + \beta_s)$ bps, where β_s is the SNR threshold to decode STx's signal. The STx's signal can interfere with both PRxs and un-intended SRxs; that is, STx Z_i in $b(Y, r_{sp})$ can interfere PRx Y and STx Z in $b(W, r_{ss})$ can interfere with SRx W , where r_{sp} and r_{ss} are the interference radii of a PRx and a SRx w.r.t. a STx respectively.

3.2.5 System Model Parameters

In this section, we discuss the system parameter selection. We shall assume that β_p , β_s , and the tolerable interference I_p are specified as part of the system design. I_p corresponds to the amount of interference that PRxs can tolerate at the edge of PTxs' coverage and can be understood as a performance margin to overcome uncertainty in noise and interference. Given these parameters, the following system parameters can be determined. We first determine PTx's maximum coverage radius d_p from PRx's successful reception condition, i.e, if a PRx receives successfully, then its received SINR, assuming noise η and maximum tolerable interference I_p at the coverage edge, should be larger than the decoding SINR threshold, which gives following:

$$d_p \equiv \sup \left\{ d > 0 \mid \frac{\rho_p d^{-\alpha}}{\eta + I_p} > \beta_p \right\} = \left(\frac{\rho_p}{(\eta + I_p)\beta_p} \right)^{\frac{1}{\alpha}}.$$

Second, we determine PRx's interference radius with respect to a PTx r_{pp} . In $S1$, $r_{pp} = 0$ since all PTxs transmit the same signal. In $S2$, for successful decoding, the SINR of a PRx a distance d ($< d_p$) away from its nearest PTx should be larger than the decoding threshold. Considering the interference from the nearest dominant PTx only, we have

$$r_{pp}(d) \equiv \inf \left\{ r > 0 \mid \frac{\rho_p d^{-\alpha}}{\eta + \rho_p r^{-\alpha}} > \beta_p \right\} = \rho_p^{\frac{1}{\alpha}} \left(\frac{\rho_p}{d^\alpha \beta_p} - \eta \right)^{-\frac{1}{\alpha}}.$$

Third, the SINR at the above receiver should be larger than β_p even when interference from STx is considered: $\frac{\rho_p d^{-\alpha}}{\eta + \rho_s r^{-\alpha}} > \beta_p$, this allows us to define a PRx's interference

radius with respect to a STx as

$$r_{sp}(d) \equiv \inf \left\{ r > 0 \mid \frac{\rho_p d^{-\alpha}}{\eta + \rho_s r^{-\alpha}} > \beta_p \right\} = \rho_s^{\frac{1}{\alpha}} \left(\frac{\rho_p}{d^\alpha \beta_p} - \eta \right)^{-\frac{1}{\alpha}}.$$

Note that $r_{pp}(d)$ and $r_{sp}(d)$ are both functions of d . As a PRx gets closer to its nearest PTx, r_{pp} and r_{sp} get smaller and the PRx become increasingly robust to interference. However, a PRx near the coverage edge is more vulnerable to interference. Fourth, for a SRx to decode a STx signal, the received SINR at the SRx should be larger than the decoding threshold β_s : $\frac{\rho_s d_s^{-\alpha}}{I + \eta} > \beta_s$, from which we define SRx's maximum tolerable amount of interference

$$I_s \equiv \sup \left\{ I > 0 \mid \frac{\rho_s d_s^{-\alpha}}{I + \eta} > \beta_s \right\} = \frac{\rho_s d_s^{-\alpha}}{\beta_s} - \eta. \quad (3.1)$$

Fifth, for a SRx to decode a STx signal, the amount of interference from its nearest PTx should be less than the maximum tolerable interference: $\rho_p r^{-\alpha} < I_s$. This leads us to determine a SRx's interference radius with respect to a PTx as

$$r_{ps} \equiv \inf \left\{ r > 0 \mid \rho_p r^{-\alpha} < I_s \right\} = \left(\frac{\rho_p}{I_s} \right)^{\frac{1}{\alpha}}. \quad (3.2)$$

Finally, for a SRx to decode a STx's signal, the amount of interference from the nearest interfering STx should be less than the tolerable interference: $\rho_s r^{-\alpha} < I_s$. Thus, SRx's interfering radius with respect to a STx is given as

$$r_{ss} \equiv \inf \left\{ r > 0 \mid \rho_s r^{-\alpha} < I_s \right\} = \left(\frac{\rho_s}{I_s} \right)^{\frac{1}{\alpha}}. \quad (3.3)$$

Note that I_s , r_{ps} , and r_{ss} above have been selected conservatively.

3.2.6 Parameter Sets for Scenarios

Here, we consider two sets of parameters for two different scenarios. The following parameters are common to both scenarios: $\alpha = 3$, $N_o = -174\text{dBm}$, $\eta = N_o \times 20 \times 10^6$, $\rho_s = 1\text{mW}$, $\beta_s = 20$, $I_s = 5 \times 10^{-8}$ and $d_s = 10\text{m}$. For $S1$, we use $\rho_p = 100\text{W}$, $\beta_p = 10$,

$I_p = 5\eta$, $d_p = 27560\text{m}$, $r_{pp} = 0$, $r_{ps} = 1259\text{m}$, and $r_{ss} = 27\text{m}$. For $S2$, we use $\rho_p = 1\text{W}$, $\beta_p = 20$, $I_p = \rho_s \times 20^{-\alpha}$, $d_p = 73.7\text{m}$, and $r_{ps} = 271\text{m}$. Note that I_p is selected such that $r_{sp} = 20$.

3.3 Performance of Primary Network

3.3.1 Outage Probability of Primary Receiver

In this section, we consider two outage probabilities for a PRx Y ; first, the conditional outage probability when the PRx Y is a distance d from its nearest PTx, which shows how the outage probability changes as d increases; second, the outage probability of a randomly located PRx. Let $P_{o,1}(d)$ denote the outage probability of a PRx a distance d away from its nearest PTx. Note that the following results cover both $S1$ and $S2$ with r_{pp} defined accordingly.

Theorem 4. (*Conditional Outage Probability of a PRx at d from its nearest PTx*)
For given λ_p , λ_s and d_p , a PRx Y 's outage probability given d away from its nearest PTx X_i is

$$P_{o,1}(d) = 1 - \mathbf{1}_{\{d < d_p\}} e^{-\lambda_p \pi (d_{pp}^2 - d^2)} \mathcal{L}_{L(d, \Pi_p^{(2)})}(\lambda_s)$$

where $L(d, \Pi) = \int_{K(X_i, r_d, Y, r_{ps})} \mathbf{1}_{\{z \notin B(\Pi, r_d)\}} dz$, $d_{pp} = \max\{d, r_{pp}\}$, and $\Pi_p^{(2)} = \{\Pi_p \cap \overline{b(Y, d_{pp})}\} \cup \{X_i\}$.

Proof. We define following for notational simplicity:

$$\begin{aligned} K_1 &\equiv K(X_i, r_d, Y, r_{ps}) \\ A &= \{Y \text{ not interfered by PTx}\} = \{\Pi_p \cap b(Y, d_{pp}) = \emptyset\} \\ B &\equiv \{Y \text{ not interfered by STx}\} = \{\Pi_s^a \cap b(Y, r_{sp}) = \emptyset\} \\ C &= \{\|X_i - Y\| = d\}, \end{aligned}$$

Suppose a PRx Y is located at the origin and its nearest PTx X_i is at $(-d, 0)$. Then, as shown in Fig.3.1a, for $d < d_p$ the shaded region is a PTx-free area since

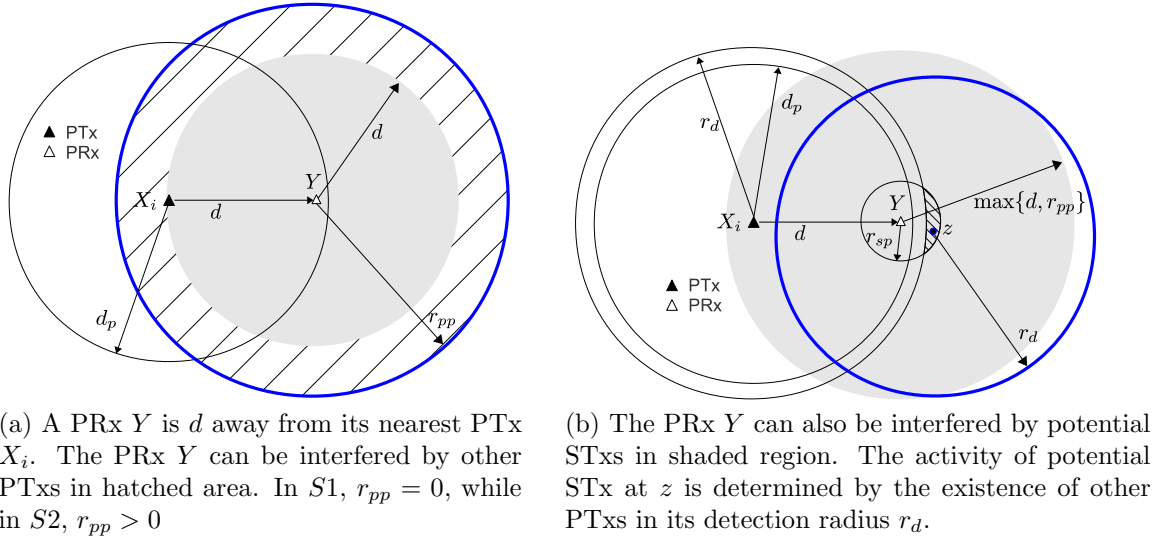


Figure 3.1: A primary transmitter and an associated receiver

the PTx X_i is the nearest one to the PRx Y . The PRx Y can be interfered with by potential PTxs in its interference area $b(Y, r_{pp})$ or by potential STxs in $b(Y, r_{sp})$. But, due to condition C , potential PTxs can exist only at $b(Y, r_{pp}) \setminus b(Y, d)$ as shown in Fig.3.1a. Also, as shown in Fig.3.1b, not all potential STxs in $b(Y, r_{sp})$ are active since $b(X_i, r_d)$ is cleared out by the X_i , so there is no active STxs in $b(Y, r_{sp}) \cap b(X_i, r_d)$. Uncleared potential STxs in the K_1 hatched area, can give harmful interference to Y . The activity of each potential STx, e.g., z in K_1 is affected by the existence of surrounding PTx in $b(z, r_d)$. Then, the conditional outage probability conditioned on the event $\{\|X_i - Y\| = d\}$ or equivalently C is given by

$$\begin{aligned}
 P_{o,1}(d) &= P(Y \text{ fails to receive} | \|X_i - Y\| = d) \\
 &= 1 - P(Y \text{ receives} | C) \\
 &= 1 - P(AB | C) \\
 &= 1 - P(A | C) P(B | AC).
 \end{aligned}$$

$P(A | C)$ and $P(B | AC)$ can be computed as follows:

$$\begin{aligned}
 P(A | C) &= P(\Pi_p \cap b(Y, d_{pp}) = \phi | \Pi_p \cap b(Y, d) = \phi) \\
 &= \exp \left\{ -\lambda_p \pi (d_{pp}^2 - d^2) \right\},
 \end{aligned}$$

$$\begin{aligned}
P(B|AC) &= P(B|A) \\
&\stackrel{a}{=} \mathbb{E}[P(B|A, \Pi_p) | A] \\
&= \mathbb{E}[P(\Pi_s^a \cap b(Y, r_{sp} = \phi|A, \Pi_p)) | A] \\
&= \mathbb{E}\left[\exp\left\{-\int_{K_1} \lambda_s^a(z, \Pi_p) dz\right\} | A\right] \\
&= \mathbb{E}[\exp\{-\lambda_s L(d, \Pi_p)\} | A] \\
&\stackrel{b}{=} \mathbb{E}[\exp\{-\lambda_s L(d, \Pi_p^{(2)})\}].
\end{aligned} \tag{3.4}$$

In equality $\stackrel{a}{=}$, \mathbb{E} denotes conditional expectation w.r.t Π_p . In equality $\stackrel{b}{=}$, we used the fact that Π_p conditioned on A is the same as $\Pi_p^{(2)}$. If $d_p \leq d$, we assume Y is out of coverage, so $P_{o,1}(d) = 1$. \square

The outage of randomly located PRx is given as follows.

Fact 1. (*Outage Probability of Randomly located PRx*) Let a random variable D be the distance between Y and its nearest PTx X_i . Its cumulative distribution function is known to be $F_D(x) = 1 - \exp\{-\lambda_p \pi x^2\}$. Then, the outage probability of a randomly located node is given by

$$\begin{aligned}
P_{o,1}^R(\lambda_p, \lambda_s) &= \mathbb{E}_D[P_{o,1}(D)] \\
&= \int_0^\infty P_{o,1}(d) dF_D(x) \\
&= \int_0^{d_p} P_{o,1}(x) dF_D(x) + \int_{d_p}^\infty dF_D(x) \\
&= \int_0^{d_p} P_{o,1}(x) dF_D(x) + \exp\{-\lambda_p \pi d_p^2\}.
\end{aligned}$$

And, the upper bound $P_{o,1}^{R,u}$ and lower bound $P_{o,1}^{R,l}$ are found by plugging $P_{o,1}^u$ and $P_{o,1}^l$ respectively.

Geometrically, the random variable $L(d, \Pi_p^{(2)})$ above denotes the area of the part of the set $b(Y, r_{ps}) \setminus b(X_i, r_d)$ which is not covered by the Boolean process $B(\Pi_p^{(2)}, r_d)$.

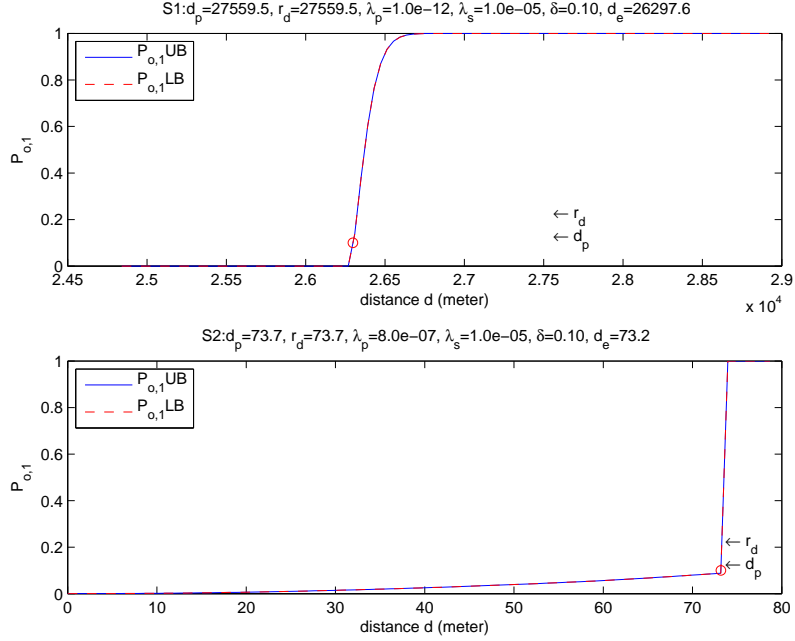


Figure 3.2: The impact from harmful interference from STxs and PTxs when r_d is set to d_p are shown. In $S1$ (upper figure), PRx around the edge of coverage experience increased $P_{o,1}$ due to interference from STxs. In $S2$ (down figure), not only STxs but also other PTxs give interference to PRxs. So $P_{o,1}$ starts to increase even when PRx is very close to its nearest PTx.

The Laplace transform of $L(d, \Pi_p^{(2)})$ is not easily computable. So, we compute upper and lower bounds. They are omitted from this proposal to keep it short.

Before we compute the quantities, we introduce a technique to bound the transform for such non-negative random variables.

Lemma 1. (*Bounding non-negative random variable*) *If M is a random variable with support $[0, p]$ and mean $\mathbb{E}[M]$. Then, for any convex function ϕ , $\mathbb{E}[\phi(M)] \leq \phi(0) - \frac{\mathbb{E}[M]}{p}(\phi(0) - \phi(p))$.*

Proof is given in Appendix 3.8.

Corollary 1. *For $d < d_p$, lower and upper bounds on PRx's conditional outage*

probability are given by:

$$P_{o,1}^l(d) = 1 - e^{-\lambda_p \pi (d_{pp}^2 - d^2)} \left(1 - \frac{l}{l_m} (1 - e^{-\lambda_s l_m}) \right),$$

$$P_{o,1}^u(d) = 1 - e^{-\lambda_p \pi (d_{pp}^2 - d^2)} e^{-\lambda_s l},$$

where $l = \mathbb{E} \left[L \left(d, \Pi_p^{(2)} \right) \right]$ and $l_m = k(d, r_d, r_{sp})$.

Proof. The lower bound is found by applying Lemma 1, and upper bound is found by applying Jensen's inequality. \square

Note that l can be computed numerically:

$$l = \int_{K_1} P(z \notin \Pi_p^{(2)}) dz = \int_{K_1} \exp \{ -\lambda_p k(\|z\|, d_{pp}, r_d) \} dz$$

We define the covering probability given as follows.

Definition 6. (Covering Probability) We define the covering probability as $P_{c,1}(\lambda_p, \lambda_s) \equiv 1 - P_{o,1}^R(\lambda_p, \lambda_s)$ where $P_{o,1}^R(\lambda_p, \lambda_s) = \mathbb{E}[P_{o,1}(D)] = \int_0^{d_p} P_{o,1}(x) dF_D(x) + \exp \{ -\lambda_p \pi d_p^2 \}$.

This covering probability is a metric showing the fraction of area covered by PTxs for given λ_p . So, the higher it is for fixed λ_p , the more efficiently the spectrum is used. Note that the increase of the number of interferers can decrease the covering probability or coverage. So, it will be used later to define the capacity of the primary network in Section 3.5. Note that it is straightforward to find the lower and upper bounds on $P_{o,1}^R$ and thus on $P_{c,1}$ using Corollary 1.

Fig.3.2 shows $P_{o,1}(d)$ as a function of distance d for $S1$ and $S2$ when $r_d = d_p$. Outage probabilities increase for $d < d_p$ due to the interference from STxs. To protect PRxs, we need to make STxs conservative in their transmission. We can do this by increasing the detection radius of STx r_d to ensure all STx transmitters are far enough from PRxs. This suppresses the amount of interference from STxs to PRxs. Recall that

a PRx Y at coverage edge $d = d_p$ can be interfered by STx in $b(Y, r_{sp}(d_p))$. So, by selecting r_d such that

$$r_d \geq d_p + r_{sp}(d_p), \quad (3.5)$$

we can conservatively protect PRxs.

3.4 Performance of Secondary Network

3.4.1 Outage Probability of a Typical Secondary Receiver

In this section, we consider the outage probability $P_{o,2}$ of a typical SRx denoted here by W . This is a conditional probability conditioned on the existence of an active STx Z_i transmitting to the SRx W as shown in Fig. 3.3. Note that Z_i is not necessarily the nearest STx to W . This is the worst case outage probability since we fix $\|W - Z_i\|$ to d_s . For the STx Z_i to be active, there should be no PTxs within STx's detection area; so, we condition on the event $\Pi_p \cap b(Z_i, r_d) = \emptyset$, and $\|W - Z_i\| = d_s$. Note that STx Z_i 's detecting the absence of PTxs does not guarantee the successful reception at the SRx W since STx Z_i 's detection area may or may not be the super set of SRx W 's interference area $b(W, r_{ps})$. So, a potentially harmful PTx can be located there. The interference from other STxs to the SRx W can also cause an outage at the SRx W . The following results captures the impact of the both PTxs and STxs, on the outage of a typical SRx W .

Theorem 5. (*SRx's Conditional Outage Probability*) For given λ_p and λ_s , the outage probability of a SRx W a distance d_s away from its STx Z_i is given by

$$P_{o,2}(\lambda_p, \lambda_s) = 1 - e^{-\lambda_p |b(W, r_{ps}) \setminus b(Z_i, r_d)|} \mathcal{L}_{Q(r_{ss}, \Pi_p^{(3)})}(\lambda_s),$$

where $Q(r, \Pi) \equiv \int_{b(O, r)} \mathbf{1}_{\{z \notin B(\Pi, r_d)\}} dz$, and $\Pi_p^{(3)} = \Pi_p \cap \overline{b(Z_i, r_d) \cup b(W, r_{ps})}$.

Proof. To evaluate the outage of a SRx W which is associated with a typical active STx Z_i we condition on the a typical active STx Z_i and associated SRx W a distance

d_s from Z_i . See Fig.3.3. For notational simplicity, we define the following three events:

$$\begin{aligned}
D &\equiv \{W \text{ not interfered by STx}\} = \{\Pi_s^a \cap b(W, r_{ss}) = \emptyset\} \\
E &\equiv \{W \text{ not interfered by PTx}\} = \{\Pi_p \cap b(W, r_{ps}) = \emptyset\} \\
F &\equiv \{Z_i \text{ does not detect any PTx in } b(Z_i, r_d)\} \\
&= \{\Pi_p \cap b(Z_i, r_d) = \emptyset\}.
\end{aligned} \tag{3.6}$$

Then, $P_{o,2}$ is given as follows:

$$\begin{aligned}
P_{o,2} &= P(W \text{ fails to receive} | Z_i \text{ transmits, } \|Z_i - W\| = d_s) \\
&\stackrel{a}{=} 1 - P(W \text{ receives} | F) \\
&= 1 - P(DE|F) \\
&= 1 - P(E|F) P(D|EF),
\end{aligned} \tag{3.7}$$

where from a we omitted conditioning on $\{\|Z_i - W\| = d_s\}$ for notational simplicity.

We can compute closed form expressions for $P(E|F)$ and $P(D|EF)$ as follows:

$$\begin{aligned}
P(E|F) &= P(\Pi_p \cap b(W, r_{ps}) = \emptyset | \Pi_p \cap b(Z_i, r_d) = \emptyset) \\
&= \exp\{-\lambda_p k(d_s, r_d, r_{ps})\}.
\end{aligned}$$

$$\begin{aligned}
P(D|EF) &= \mathbb{E}[P(D|EF\Pi_p) | EF] \\
&= \mathbb{E}\left[\exp\left\{-\int_{b(W, r_{ss})} \lambda_s^a(z, \Pi_p) dz\right\} | EF\right] \\
&= \mathbb{E}\left[\exp\left\{-\int_{b(W, r_{ss})} \lambda_s \mathbf{1}\{z \notin B(\Pi_p, r_d)\} dz\right\} | EF\right] \\
&= \mathbb{E}\left[\exp\{-\lambda_s Q(r_{ss}, \Pi_p^{(3)})\}\right],
\end{aligned}$$

where $Q(r, \Pi) \equiv \int_{b(W, r)} \mathbf{1}\{z \notin B(\Pi, r_d)\} dz$, and $\Pi_p^{(3)} = \Pi_p \cap \overline{b(Z_i, r_d) \cup b(W, r_{ps})}$. \square

Corollary 2. (*Upper and Lower Bound of SRx's Conditional Outage Probability*) For given λ_p and λ_s , the upper and lower bound of a SRx's outage probability are given as follows.

$$P_{o,2}^u(\lambda_p, \lambda_s) = 1 - e^{-\lambda_p k(d_s, r_d, r_{ps})} e^{-\lambda_s q},$$

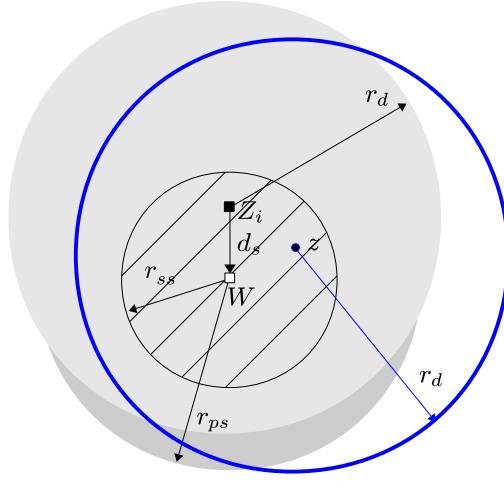


Figure 3.3: Conditioned on that there is no PTxs in $b(Z_i, r_d) \cup b(W, r_{ps})$, the outage of a SRx W can be caused by potential STxs in the hatched region $b(W, r_{ss})$. Whether a potential STxs, e.g., at location $z \in b(W, r_{ss})$, can give harmful interference to W depends on the potential PTxs in $b(z, r_d) \setminus (b(Z_i, r_d) \cup b(W, r_{ps}))$.

$$P_{o,2}^l(\lambda_p, \lambda_s) = 1 - e^{-\lambda_p k(d_s, r_d, r_{ps})} \left(1 - \frac{q}{q_m} (1 - e^{-\lambda_s q_m}) \right)$$

where $q = \mathbb{E} \left[Q \left(r_{ss}, \Pi_p^{(3)} \right) \right]$ and $q_m = \pi r_{ss}^2$.

Proof. The lower bound is found by applying Jensen's inequality. And, the upper bound is found using Lemma 1. \square

The q is computed numerically based on:

$$\begin{aligned} q &= \mathbb{E} \left[\int_{b(W, r_{ss})} \mathbf{1} \{ z \notin B(\Pi_p^{(3)}, r_d) \} dz \right] \\ &= \int_{b(W, r_{ss})} P(z \notin B(\Pi_p^{(3)}, r_d)) dz \\ &= \int_{b(W, r_{ss})} P(\Pi_p \cap b(z, r_d) \setminus (b(Z_i, r_d) \cup b(W, r_{ps})) = \phi) dz \\ &= \int_{b(W, r_{ss})} P(\Pi_p \cap H(Z_i, r_d, W, r_{ps}, z, r_d) = \phi) dz \\ &= \int_{b(W, r_{ss})} \exp \{ -\lambda_p h(Z_i, r_d, W, r_{ps}, z, r_d) \} dz. \end{aligned}$$

Geometrically, q is the size of mean interference area where potential harmful STxs can be located. Intuitively, a smaller q allows a larger number of concurrent STxs.

3.4.2 Impact of Primary Network : Outage Wall

Fig. 3.4 shows the outage performance as a function of λ_s for different values of λ_p . In this setting, the outage increases not only as λ_p increases but also as λ_s increases. This exhibits the impact of interference on SRx from PTxs and STxs. Setting $\lambda_s = 0$ gives a lower bound on $P_{o,2}(\lambda_p, 0)$, which we call *outage wall*:

$$P_{o,2}^w(\lambda_p, d_s) = 1 - \exp \{-\lambda_p |b(W, r_{ps}) \setminus b(Z_i, r_d)|\},$$

i.e., we can not do any better than this for STx. Note that for a given $\lambda_p > 0$, an outage lower than this can not be achieved even when $\lambda_s = 0$, unless $|b(W, r_{ps}) \setminus b(Z_i, r_d)| = 0$. Recall that $|b(W, r_{ps}) \setminus b(Z_i, r_d)|$ corresponds to the area, dark shaded region in Fig.3.3, where undetectable and potentially harmful PTxs can be located. If we set r_d such that

$$r_d \geq d_s + r_{ps} \tag{3.8}$$

then, PTx-free area $b(Z_i, r_d)$ will eventually cover the SRx W 's interference area $b(W, r_{ps})$, which results in $|b(W, r_{ps}) \setminus b(Z_i, r_d)| = 0$. That is, no hidden PTxs exist any more. If the secondary network is to have an outage performance requirement, it should be larger than the $P_{o,2}^w(\lambda_p, d_s)$ otherwise the requirement will not be met.

3.4.3 Transmission Density

In this section we consider the transmission density of the secondary network. This is of particular interest since it tells us how much we can exploit the spatial(or temporal) spectrum holes. The density will be found without any outage requirement on SRx. Bit per transmission times the transmission density with an outage requirement will later be defined as *transmission capacity* in Section 3.5. Below we give the definition of the transmission density followed by its upper and lower bounds.

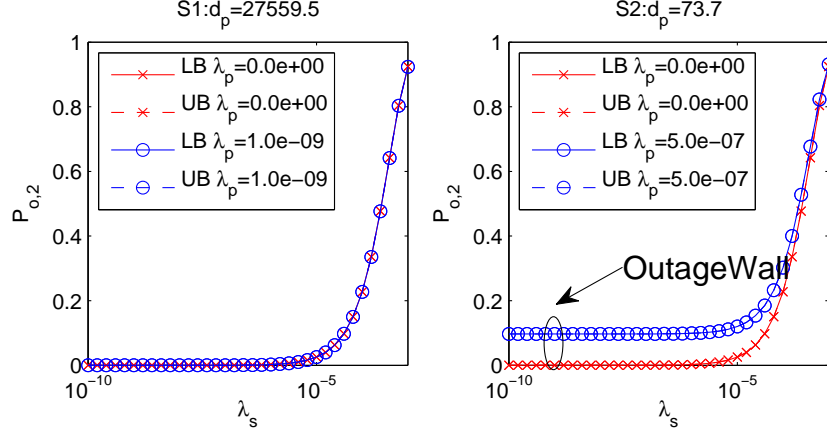


Figure 3.4: $P_{o,2}(\lambda_p, \lambda_s)$ were shown for $S1$ and $S2$. If any hidden PTx exists ($|b(W, r_{ps}) \setminus b(Z_i, r_d)| > 0$), then $P_{o,2}(\lambda_p, \lambda_s)$ can not be lowered than its outage wall $P_{o,2}^w(\lambda_p, d_s)$ even if $\lambda_s \rightarrow 0$. In legends, UB and LB mean upper and lower bound respectively.

Definition 7. (Transmission density of Secondary Network) For given λ_p , λ_s and transmission probability of STx P_{tx} , (i.e., the probability that a STx be active) the transmission density of secondary network is the number of successful transmission per unit area between secondary STx and SRx pairs, which is given as

$$T_s(\lambda_p, \lambda_s) = \lambda_s P_{tx} (1 - P_{o,2}(\lambda_p, \lambda_s)). \quad (3.9)$$

Corollary 3. Upper and lower bounds on secondary network's throughput $T_s(\lambda_p, \lambda_s)$ are found as follows:

$$T_s^l = \lambda_s \exp\{-\lambda_p c_1\} \exp\{-\lambda_s q\}, \quad (3.10)$$

$$T_s^u = \lambda_s \exp\{-\lambda_p c_1\} \left(1 - \frac{q}{q_m} (1 - \exp\{-\lambda_s q_m\})\right), \quad (3.11)$$

where $c_1 = \pi r_d^2 + k(d_s, r_d, r_{ps})$, and $q = \mathbb{E}\left[Q\left(r_{ss}, \Pi_p^{(3)}\right)\right]$.

Proof. P_{tx} is given as $e^{-\pi r_d^2}$ and T_s^l and T_s^u are found by replacing $P_{o,2}$ in (3.9) with $P_{o,2}^u$ and $P_{o,2}^l$ respectively. \square

Fig. 3.5 shows T_s as a function of λ_s for various values of λ_p . These curves are indeed similar to those of pure Aloha. When STxs are sparse, density increase is larger than

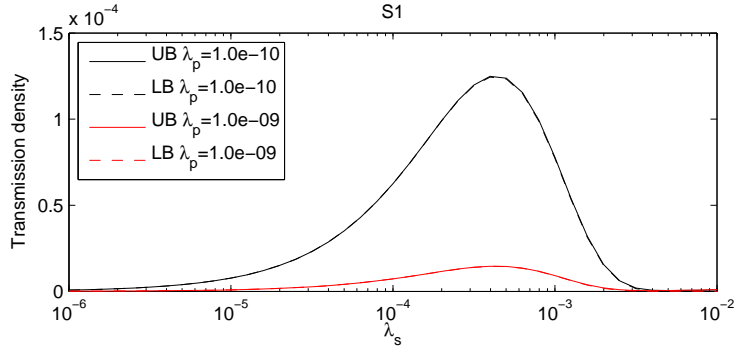


Figure 3.5: Transmission density of secondary network T_s is maximized at λ_s^* and exponentially decreases as λ_p increases.

the outage increase. However, after the curve hits a peak at a certain density, called as an optimal contention density, it drops since outage increase dominates density increase. The optimal contention density which maximizes T_s is considered below. One insight we get from (3.10) and (3.11) is the impact from primary network. The PTxs with density λ_p scales down the T_s as factors of $\exp\{-\lambda_p \pi r_d^2\} \exp\{-\lambda_p k(d_s, r_d, r_{ps})\}$ i.e., two factors: transmission opportunities and hidden PTxs exponentially reduce the successful transmission of secondary network. PTxs also have an impact through the $q(\lambda_p)$ term, but the exponential term dominates. We find throughput maximizing contention density in following theorem.

Theorem 6. (Optimal contention density of STx) For given λ_p , the lower and upper bounds of optimal contention density, $\lambda_s^{*l}(\lambda_p) = \arg \max_{\lambda_s > 0} T_s^l(\lambda_p, \lambda_s)$ and $\lambda_s^{*u}(\lambda_p) = \arg \max_{\lambda_s > 0} T_s^u(\lambda_p, \lambda_s)$ are given as follows:

$$\lambda_s^{*l} = \frac{1}{q}, \text{ and } \lambda_s^{*u} = \frac{1}{q_m} \left(1 - W_0 \left(\left(1 - \frac{q_m}{q} \right) e \right) \right),$$

where W_0 is the W_0 -branch of Lambert W function.

Proof. Differentiating w.r.t λ_s and equating zero, $dT_2^l(\lambda_s)/d\lambda_s = 0$, gives λ_s^{*l} . To find λ_s^{*u} , let $u = \exp\{-\lambda_p c_1\}$ and $v = 1 - \frac{q}{q_m}$. Then, we have $T_2^u(\lambda_s) = uv\lambda_s + u(1-v)\lambda_s \exp\{-\lambda_s q_m\}$. $dT_2^u(\lambda_s)/d\lambda_s = 0$ gives $we^w = \frac{ve}{v-1}$ by letting $w = 1 - \lambda_s q_m$.

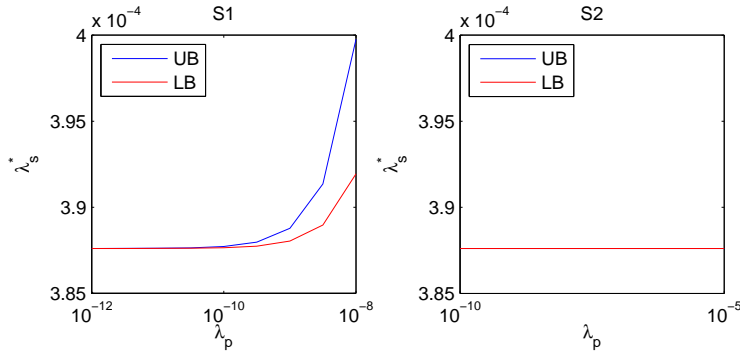


Figure 3.6: Optimal contention density λ_s^* is not sensitive to λ_p in the regime of interest

Then, we have $w = W_0\left(\frac{ve}{v-1}\right)$. Note that in the regime of interest, we have $\frac{ve}{v-1} > -\frac{1}{e}$, which guarantees w is real in $[-1, \infty)$. Then, we have $\lambda_s^{u*}(\lambda_p) = \frac{1}{\pi r_{ss}^2} \left(1 - W_0\left(\frac{ve}{v-1}\right)\right)$. This completes proof. \square

Fig.3.6 shows the optimal contention density as a function of λ_p for $S1$ and $S2$. In $S1$, $\lambda_s^*(\lambda_p)$ is not sensitive to λ_p and very close to $1/q_m$ in the regime of interest ($\lambda_p < 10^{-9}$) and it eventually increases as λ_p increases. In $S2$, λ_s^* is constant $1/q_m$. This is because in $S2$, we have $r_{ps} \geq r_{ss} + r_d$, so $b(z, r_d) \setminus (b(Z_i, r_d) \cup b(W, r_{ps})) = \emptyset$, see Fig.3.3. This means that there do not exist any surrounding PTxs that can suppress the activity of harmful STxs in $b(W, r_{ss})$. So, in $S2$ we always have $q = q_m$. We have two implications from this. Firstly, the operation of the secondary network, from transmission perspective, is relatively unaffected by the primary network. That is, once an area where secondary network can operate is identified, the operation of the secondary network is similar to that where a secondary network operates alone. This fact is again confirmed by the outage probability. Replacing the optimal contention density in $P_{o,2}^u(\lambda_p, \lambda_s)$ gives an upper bound on the outage probability under maximum throughput as follows:

$$P_{o,2}^u(\lambda_p, \lambda_s^{l*}) = 1 - \exp\left\{-\left(1 + \lambda_p k(d_s, r_d, r_{ps})\right)\right\}.$$

Note that in this operating regime, we have $P_{o,2}^u(\lambda_p, \lambda_s^{l*}) \simeq 1 - \frac{1}{e}$ due to $1 + \lambda_p k(d_s, r_d, r_{ps}) \approx 1$. Recall that $1 - \frac{1}{e} \simeq 0.63$ is the outage probability of Aloha

in a homogeneous network at its maximum throughput. Secondly, we have $\lambda_s^{*l} \geq \frac{1}{q_m}$ for $\lambda_p > 0$, where $\frac{1}{q_m} \approx \frac{1}{\pi d_s^2 \beta_s^{2/\alpha}}$ corresponds to the maximum contention density of a homogeneous Poisson network in [13]. This means a maximum spatial density of successful transmission is achieved at higher or equal density than that of a homogeneous network. This is because some of the potentially harmful STxs are suppressed by PTxs and accordingly the conditional outage probability decreases, which eventually pushes λ_s^* to increase. This is a somewhat surprising result since PTxs are helpful in decreasing $P_{o,2}$ and increasing λ_s^* .

3.5 Capacity and Joint Network Capacity Region

In this section, we characterize the joint capacity of the primary and secondary networks. The joint network capacity region is of interest since it characterizes all the possible operating regimes. Specifically it is of interest to understand how much capacity the secondary network can achieve for a given primary network capacity.

3.5.1 Outage Requirement for Secondary Network (ϵ -constraint)

To this end, we first impose an outage constraint on secondary network transmission, called the ϵ -constraint. To support a certain level of QoS, we require the outage be kept low. We will of course find that the capacity region changes as a function of the outage constraint ϵ . We first update the result on the contention density taking into account the ϵ -constraint.

Fact 2. (*Maximum Contention Density under ϵ -constraint*) Under an outage constraint ϵ for $P_{o,2}(\lambda_p, \lambda_s)$, the lower and upper bound of the contention density λ_s^ϵ is given as follows by letting $\bar{\epsilon} = P_{o,2}^u(\lambda_p, \lambda_s^{\epsilon,l})$ and $\epsilon = P_{o,2}^l(\lambda_p, \lambda_s^{\epsilon,u})$ with $\bar{\epsilon} = 1 - \epsilon$, $k_2 = |b(W, r_{ps}) \setminus b(Z_i, r_d)|$

$$\lambda_s^{\epsilon,l} = \left[-\frac{k_2}{q} \lambda_p + \frac{1}{q} \log \frac{1}{1 - \epsilon} \right]^+ \quad (3.12)$$

$$\lambda_s^{\epsilon,u} = \left[-\frac{1}{q_m} \log \left(1 - \frac{q_m}{q} (1 - \bar{\epsilon} \exp \{ \lambda_p k_2 \}) \right) \right]^+.$$

where $q = \mathbb{E} \left[Q \left(r_{ss}, \Pi_p^{(3)} \right) \right] = \int_{b(W, r_{ss})} \exp \{ -\lambda_p h (Z_i, r_d, W, r_{ps}, z, r_d) \} dz$ which can be computed numerically.

Fig.3.7 shows the maximum contention density λ_s^ϵ as a function of λ_p for two different cases $\epsilon = 0.1$ and 0.3 when $k(d_s, r_d, r_{ps}) \neq 0$. Note that $\lambda_s^\epsilon(0) = \frac{1}{q_m} \log \frac{1}{1-\epsilon}$ corresponds to the result found in homogeneous Poisson network [113]. Again, note that $\frac{1}{k_2} \log \frac{1}{1-\epsilon}$ satisfying $\lambda_s^\epsilon \left(\frac{1}{k_2} \log \frac{1}{1-\epsilon} \right) = 0$ is the maximum λ_p allowed under ϵ -constraint. In other words, if $\lambda_p > \frac{1}{k_2} \log \frac{1}{1-\epsilon}$, then, ϵ -constraint is not satisfied even when $\lambda_s = 0$. Actually, this result is tied to outage wall result in Section 3.4.2 and obtainable by letting $\epsilon > P_{o,2}^w(\lambda_p)$; i.e., a valid outage constraint should be larger than outage wall. One interesting fact is that $\lambda_s^{\epsilon,l}$ looks linear in λ_p but actually *not* since q decreases as λ_p increases. And, note that k_2 the area where the hidden PTxs can exist increases, the slope $|k_2/q|$ increases and which means $\lambda_s^{\epsilon,l}$ becomes more sensitive to λ_p . While if $k_2 = 0$ (as in $S1$), then λ_s^ϵ is not much affected by λ_p . Finally, note that for large ϵ it is possible that $\lambda_s^* < \lambda_s^\epsilon$, so the *optimal contention density under ϵ -constraint* is given as $\min\{\lambda_s^*, \lambda_s^\epsilon\}$.

3.5.2 Capacity of Primary and Secondary Network

The capacity of the primary network is related to the fraction of covered area (through the covering probability in Definition 6) and the amount of information broadcasted from these stations, which is defined as follows.

Definition 8. (Capacity of Primary Network) For given λ_p and λ_s^ϵ . The capacity of the primary network C_1 is defined as

$$C_1(\lambda_p, \lambda_s^\epsilon) = \mathbb{E} [N_1(\lambda_p, \lambda_s^\epsilon)] = b_p P_{c,1}(\lambda_p, \lambda_s^\epsilon).$$

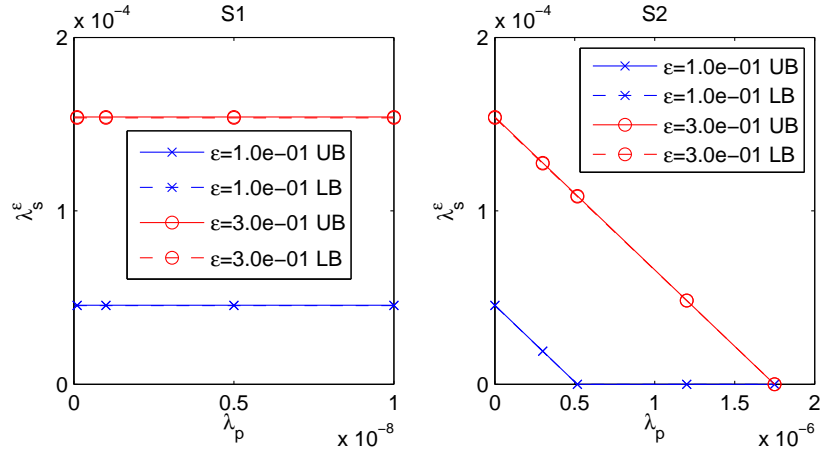


Figure 3.7: Contention density of secondary node under ϵ -constraint (Left: $S1$ with $k_2 = 0$, Right: $S2$ with $k_2 > 0$) were shown. In $S2$ as λ_p increases, the number of hidden PTxs increases, which eventually suppresses λ_s^ϵ .

Fact 3. (Lower bound and upper bounds of C_1) The lower and upper bounds of $C_1(\lambda_p, \lambda_s^\epsilon)$ are given as $C_1^l(\lambda_p, \lambda_s^\epsilon) = b_p P_{c,1}^l(\lambda_p, \lambda_s^{\epsilon,u})$ and $C_1^u(\lambda_p, \lambda_s^\epsilon) = b_p P_{c,1}^u(\lambda_p, \lambda_s^{\epsilon,l})$ respectively.

In a similar manner, we can define the capacity for secondary network. It can be understood as the achievable throughput given an outage constraint ϵ .

Definition 9. The capacity of secondary network under ϵ -constraint are defined as follows:

$$C_{2,\epsilon}(\lambda_p, \lambda_s^\epsilon) = b_s \lambda_s^\epsilon P_{tx}(1 - \epsilon) = b_s \lambda_s^\epsilon (1 - \epsilon) \exp\{-\lambda_p \pi r_d^2\},$$

where P_{tx} is the transmission probability of a typical STx.

Fact 4. The lower and upper bound of $C_{2,\epsilon}(\lambda_p, \lambda_s^\epsilon)$ are given as $C_{2,\epsilon}^l(\lambda_p, \lambda_s^\epsilon) = b \lambda_s^{\epsilon,l} (1 - \epsilon) \exp\{-\lambda_p \pi r_d^2\}$ and $C_{2,\epsilon}^u(\lambda_p, \lambda_s^\epsilon) = b_s \lambda_s^{\epsilon,u} (1 - \epsilon) \exp\{-\lambda_p \pi r_d^2\}$ respectively.

Note that if $|b(W, r_{ps}) \setminus b(Z_i, r_d)| = 0$ for a fixed C_1 , the C_2 increases as ϵ increases until it is maximized at $\epsilon = 1 - \frac{1}{e}$ and will start to decrease as ϵ increases over $1 - \frac{1}{e}$.

3.5.3 Joint Network Capacity Region

Based on the definitions of C_1 and C_2 , we now define the joint network capacity region \mathbb{C}_ϵ , which is the set of achievable operating points (C_1, C_2) subject to outage constraint.

Definition 10. The joint network capacity region is defined as

$$\mathbb{C}_\epsilon = \{(x, y) \in \mathbf{R}_+^2 \mid \exists \lambda_p \geq 0 \text{ s.t. } x = C_1(\lambda_p), y \leq C_{2,\epsilon}(\lambda_p)\}.$$

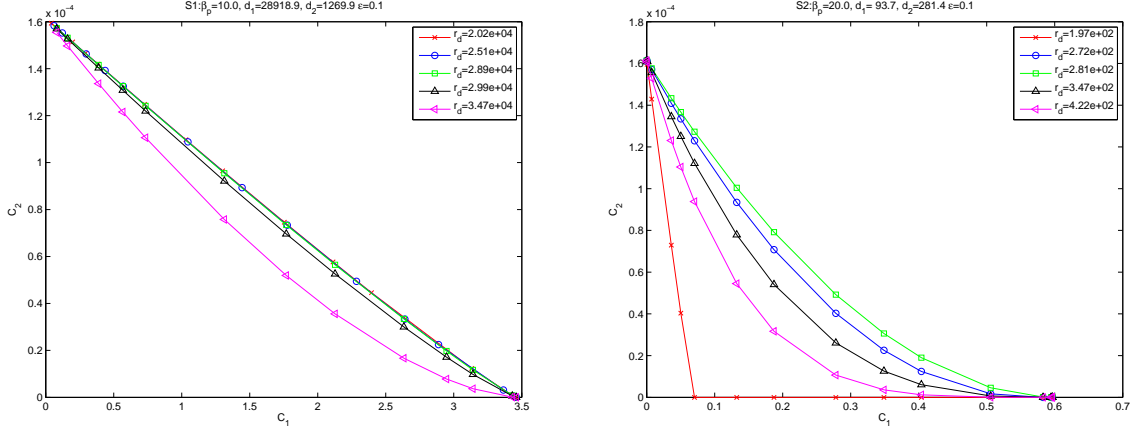
3.6 Impact of System Parameters

3.6.1 Impact of Detection Radius and Optimization

We consider the case where we need to determine r_d . Let $d_1 = d_p + r_{sp}(d_p)$ and $d_2 = d_s + r_{ps}$ and suppose that the target decoding SINR of the two networks are given as β_p and β_s . Then, $C_2^{\epsilon,l}$ below is a function of r_d :

$$C_2^{\epsilon,l}(r_d) = \log(1 + \beta_s) \lambda_s^{\epsilon,l}(r_d) (1 - \epsilon) \exp\{-\lambda_p \pi r_d^2\}.$$

Recall that $\lambda_s^{\epsilon,l}$ in (3.12) has $k_2 \equiv |b(W, r_{ps}) \setminus b(Z_i, r_d)|$ term, which is a function of r_d . Suppose $r_d < d_2$. Then, increasing r_d makes $k_2 \rightarrow 0$, which consequently reduces harmful interference from hidden PTxs and the outage probability. So, increasing $r_d (< d_2)$ increases $\lambda_s^{\epsilon,l}$. Note that q is also a decreasing function of r_d but hardly changes. Once if $r_d \geq d_2$, then, we have $k_2 = 0$ and $\lambda_s^{\epsilon,l}$ increases very slowly and looks constant. We observe that if $r_d < d_2$ increasing $\lambda_s^{\epsilon,l}$ dominates decreasing $\exp\{-\lambda_p \pi r_d^2\}$, which makes $C_2^{\epsilon,l}$ increasing. While if $r_d \geq d_2$ the latter dominates and $C_2^{\epsilon,l}$ starts to decrease. So, from the perspective of reducing the impact from hidden PTxs, $r_d = d_s + r_{ps}$ is a near optimal choice so as to maximize capacity. But along with maximizing $C_2^{\epsilon,l}$ it is also necessary to protect primary receivers (note that this maximizes C_1). So, r_d should be chosen as follows.



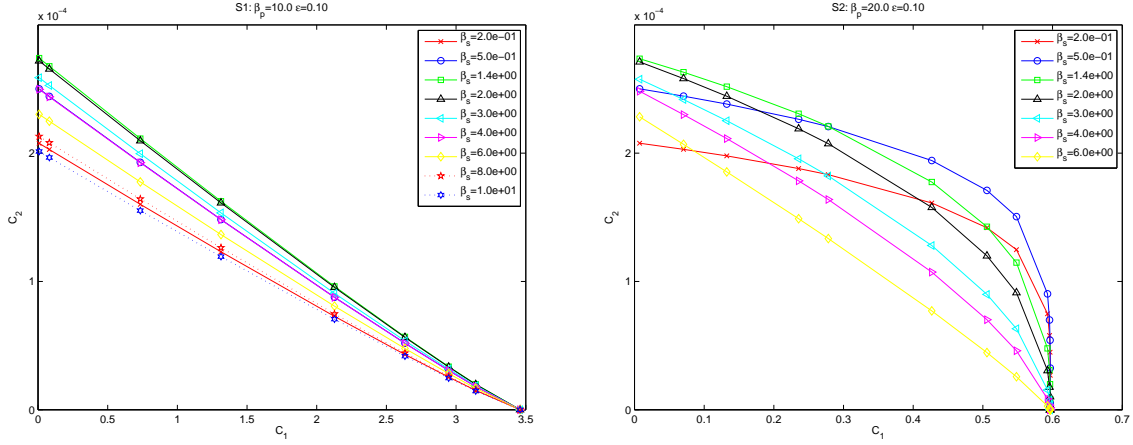
(a) Joint network capacity region for scenario $S1$ where $d_2 < d_1$ was shown for various r_d values. Increasing r_d over $d_1 \approx 2.02 \times 10^4$ decreases $C_2^{\epsilon,l}$ since too large r_d decreases transmission opportunity of STxs.

(b) Joint network capacity region for scenario $S2$ where $d_1 < d_2$ was shown for various r_d values. $C_2^{\epsilon,l}$ is maximized at $r_d = d_2 \approx 2.81 \times 10^2$. If $r_d < d_2$, we have hidden PTx and this forces $C_2^{\epsilon,l}$ hit to zero as λ_p increases.

Figure 3.8: Joint network capacity region as a function of r_d .

Rule of Thumb 1. (RT1) For given $d_1 = d_p + r_{sp}(d_p)$ and $d_2 = d_s + r_{ps}$, choose the the detection radius of STxs as $r_d = \max\{d_1, d_2\}$. It is the sub-optimal choice for maximizing secondary capacity.

Increasing r_d further is not helpful to increasing capacity since it exponentially reduces transmission opportunities. Fig.3.8a shows the change in the joint network capacity region for $S1$ for various values of r_d when $d_1 = 2.02 \times 10^4 > d_2$. Since $d_2 < d_1$ in $S1$, $C_2^{\epsilon,l}$ decreases as r_d increases due to decreasing transmission opportunity. Fig.3.8b shows the joint network capacity region for $S2$. In this case choosing $r_d = d_2$ achieves near maximum $C_2^{\epsilon,l}$ since we have $d_1 < d_2$. Note that C_1 in $S2$ can not reach its limit point $b_p = \log(1 + \beta_p) = 4.39$ due to the self interference from PTx to PRx, while in $S1$, it achieves its limit. Also as exhibited, in Fig.3.8b if λ_p is too large for a case $r_d < d_2$, it forces $C_2^{\epsilon,l}$ to get a zero capacity due to its zero contention density. Recall that if $r_d < d_2$, then the hidden PTx still exist and increasing λ_p eventually forces λ_s^ϵ



(a) Joint network capacity region for scenario S1 was shown for various β_s values. $C_2^{\epsilon,l}$ is maximized at $\beta_s = \beta_s^*(0)$ for broad ranges of λ_p . The limiting capacity of C_1 corresponds to $\log_2(1 + \beta_p) = 3.46$. Note that as λ_p increases, C_1 increases and $C_2^{\epsilon,l}$ decreases.

(b) Joint network capacity region for scenario S2 was shown for various β_s values. In S2, β_s^* maximizing $C_2^{\epsilon,l}$ depends on λ_p . The limiting capacity of C_1 shrinks from $\log_2(1 + \beta_p) = 4.39$ to 0.6 due to increased self interference. The ultimate joint network capacity region shown as dotted line.

Figure 3.9: Joint network capacity region as a function of β_s .

to zero.

3.6.2 Impact of Decoding SNR and Optimization

Consider the case where we need to determine β_s given all other parameters except r_d which is a function of β_s by RT1. The transmission capacity of secondary network depends on several terms which increase (\nearrow) and decrease (\searrow) with β_s as follows:

$$C_2^{\epsilon,l}(\beta_s) = c_2 \underbrace{\log(1 + \beta_s)}_{\nearrow} \underbrace{(1/q(\beta_s))}_{\searrow} \underbrace{\exp\{-\lambda_p \pi r_d(\beta_s)^2\}}_{\searrow} \quad (3.13)$$

for some constant $c_2 > 0$. Note that as β_s increases $r_{ss} \approx d_s \beta_s^{1/\alpha}$ increases, and accordingly $q(\beta_s)$ also increases. Also as β_s increases, r_{ps} increases, which eventually increases r_d since r_d is assumed to be selected according to the RT1. This exhibits the tradeoff between the three terms in (3.13). *Increasing the transmission*

rate (or increasing β_s) makes the SRx more sensitive to interference and accordingly under a fixed ϵ allows fewer concurrent transmitters (decreasing node density) and may discourage transmission attempts (decreasing transmission opportunity). Since $C_2^{\epsilon,l}(\beta_s)$ is a product of both increasing and decreasing terms there exists a unique maximum point β_s^* maximizing $C_2^{\epsilon,l}$, which is a function of λ_p . For $\lambda_p = 0$, we can analytically find β_s^* after ignoring noise term. Setting $dC_2^{\epsilon,l}/d\beta_s = 0$ gives $\beta_s^*(0) = \exp\left\{W_0\left(-\frac{\alpha}{2e^{\alpha/2}}\right) + \frac{\alpha}{2}\right\} - 1$ for $\alpha > 2$. For $\lambda_p > 0$, $\beta_s^*(\lambda_p)$ can be found numerically.

Suppose that a minimum required data rate (or equivalently decoding SINR) for secondary node's applications is specified as a design requirement, denote it by β_s^m . Then, from the above discussion, it follows that there exists an optimal decoding SINR $\beta_s^*(\lambda_p)$. This suggests following.

Rule of Thumb 2. (RT2) For a given λ_p and an application-required decoding SINR β_s^m , the operating decoding SINR chosen as $\beta_s^o = \max\{\beta_s^*(\lambda_p), \beta_s^m\}$ maximizes the secondary capacity while satisfying the application requirement.

Replacing $\beta_s^*(\lambda_p)$ in RT2 with $\beta_s^*(0)$ makes the rule of thumb easy to use but gives sub-optimal performance. Figs. 3.9a and 3.9b show the changes in the joint network capacity region under various β_s for $S1$ and $S2$. In $S1$, $C_2^{\epsilon,l}$ is maximized at $\beta_s^* = 1.4$ at almost all λ_p values, accordingly, β_s^* maximizes joint network capacity region. By contrast in $S2$, as λ_p increases β_s^* decreases, so $\beta_s^*(0)$ is sub-optimal. Note that β_s only affects the performance of secondary devices so only $C_2^{\epsilon,l}$ is affected. Note that the joint network capacity region of $S1$ is roughly bounded by linear boundary, this is because we have $d_p \approx r_d$, then $P_{c,1} \approx e^{-\lambda_p \pi r_d^2}$ and from the definition of C_1 and $C_2^{\epsilon,l}$, it is straightforward to show the linear relationship. In $S2$, we have self interference in the primary network, so the limiting capacity of $C1$ can not reach to

$b_p = \log_2(1 + \beta_p) = 4.39$, which makes the joint network capacity region as convex.

3.6.3 Impact of Coverage's Burstiness on Secondary Capacity

In this section, we show how the burstiness of a primary network's coverage affects the capacity of an associated secondary network¹. For that end, we define the notion of burstiness for Boolean process and make assumptions for simple analysis.

We adopt the definition of burstiness introduced in [14]. For two given primary networks A and B with the same fixed coverage c , we say that the Network A has a more bursty coverage than the Network B if the Network A has a larger coverage radius than that of the Network B. Fig. 3.10 shows the realizations of two primary networks' coverage with the same coverage area, where the union of bright gray discs is the coverage of PTxs and the union of dark gray regions around it is the guard band to protect PRxs from STxs. The thickness of the band is given as $\kappa r_{sp}(d_p)$ for given $r_{sp}(d_p)$ and $\kappa \geq 0$ is a measure of the conservativeness of detection radius. If $\kappa = 0$, there is no guard band, otherwise the guard band is chosen conservatively.

We make the following assumptions.

(A1) *Let the detection radius of STxs be determined as $r_d = \max\{d_p + \kappa r_{sp}(d_p), d_s + r_{ps}\}$ for some $\kappa \geq 0$ according to (RT1).*

(A2) *Assume that ϵ -contention density λ_s^ϵ is a constant with respect to d_p and ρ_s , though it changes slowly as a function of them.*

(A3) *Assume the primary networks of interest have the fixed coverage fraction $0 < c < 1$, i.e., $P(O \in B(\Pi_p, d_p)) = c$ which gives a following condition: $1 - \exp\{-\lambda_p \pi d_p^2\} = c$.*

We need the assumption (A2) to make the optimization process simple. Note that $C_2^{\epsilon, l}$ is proportional to both λ_s^ϵ and P_{tx} , where both terms are the functions of d_p . However, we maximize P_{tx} only over d_p since λ_s^ϵ varies slowly over d_p . With the above settings, we have following observations.

¹This section along with Section 3.6.4 applies to only S1.

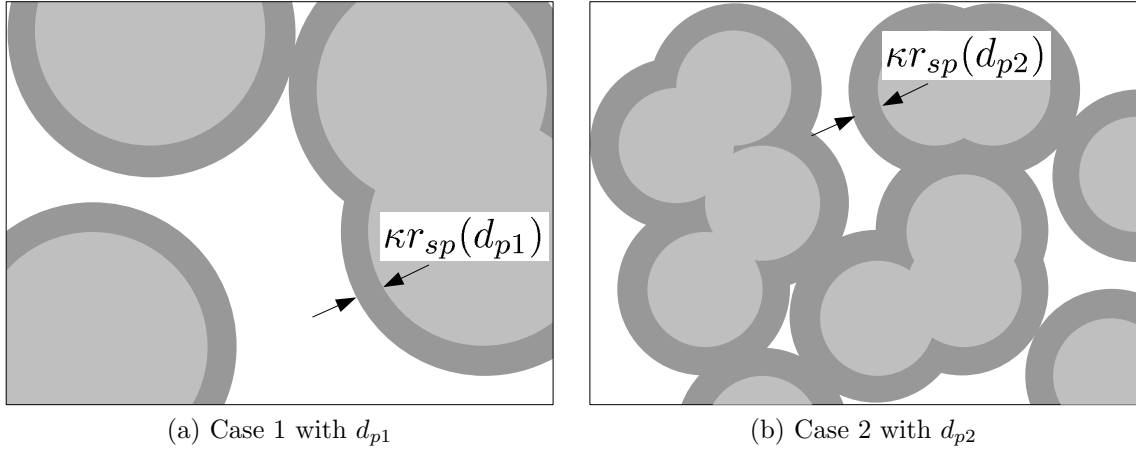
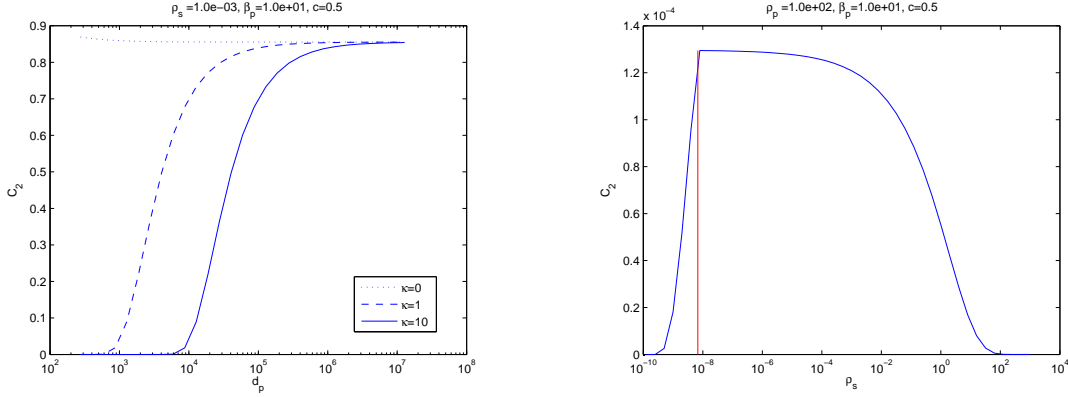


Figure 3.10: Two realizations of primary network with the same coverage but different coverage radii were shown. Coverage and guard region were shown as bright and dark gray region respectively. Note that the thickness of guard band is the same, i.e., $\kappa r_{sp}(d_{p1}) = \kappa r_{sp}(d_{p1})$.

Proposition 12. *Under the assumptions, if $r_d = d_p$ (or $\kappa = 0$), then the capacity of the secondary network is not affected by the burstiness of the primary network's coverage (or d_p). If $r_d > d_p$ (or $\kappa > 0$), then the capacity of the secondary network decreases as the primary network's coverage gets less bursty. The capacity decrease depends on the conservativeness of detection radius κ .*

Note that $\kappa = 0$ implies there is no conservativeness in detection radius and no guard bands, then it is straightforward to see that $C_2^{\epsilon,l}$ is a constant since λ_s^ϵ and P_{tx} are constants by (A2) and (A3) respectively. However, if $\kappa > 0$, the conservativeness of the detection radius affects $C_2^{\epsilon,l}$. Intuitively, this happens because the area consumed by the guard band increases as the primary network becomes less bursty (or smaller d_p), which results in a smaller transmission probability. That is, $P_{tx} = \exp\{-\lambda_p \pi r_d^2\} = (1 - c)^\gamma$ with $\gamma = 1 + \frac{\kappa r_{sp}(d_p)}{d_p}$ decreases as d_p decreases. If d_p approaches to 0, then all the non-covered region is used for guard band purpose and there is no room for secondary nodes to operate, leading to zero capacity ($C_2^{\epsilon,l} = 0$).

Fig. 3.11a shows the relation between burstiness and capacity under various con-



(a) For a fixed coverage ($c = 0.5$), a primary network with more bursty coverage and less conservative detection radius allows higher secondary capacity C_2 .

(b) There exist an optimal ρ_s^* which maximizes $C_2^{\epsilon,l}$. ρ_s^* can be approximated by $\hat{\rho}_s^*$ maximizing transmission probability of STxs. Vertical line denotes $\hat{\rho}_s^*$.

Figure 3.11: Impact of burstness of coverage and STx's transmit power on C_2

servativeness. It is clearly shown that in general more bursty network has higher $C_2^{\epsilon,l}$ and less conservative detection radius admits higher capacity $C_2^{\epsilon,l}$. Note that $\kappa = 0$ case has almost flat capacity $C_2^{\epsilon,l}$, which makes the assumption (A2) valid.

3.6.4 Impact of Transmit Power of STxs and Optimization

In this section, we show the existence of an optimal transmit power for secondary nodes which maximizes the secondary capacity. An approximation of the optimal transmit power is provided.

We keep the above assumptions (A1) and (A2) with $\kappa = 1$ and make an additional assumption as follows.

(A4) Assume that it is required by system design requirements that secondary nodes' tolerable interference level should be at least I_s^{\min} , which consequently determines the minimum required transmit power $\rho_s^{\min} = \inf \left\{ \rho_s > 0 \mid \frac{\rho_s d_s^{-\alpha}}{\eta + I_s^{\min}} > \beta_s \right\} = \beta_s d_s^\alpha (\eta + I_s^{\min})$.²

²Note that ρ_s , d_s , and I_s have dependency among them. In previous sections, I_s^{\min} was the function of given ρ_s and d_s . While in this section we fix I_s and d_s , which gives ρ_s^{\min} .

λ_s^ϵ is again a constant due to (A2) and thus we optimize $P_{tx}(\rho_s)$ over ρ_s to maximize $C_2^{\epsilon,l}$. Note that $r_d = \max\{d_1, d_2\}$ chosen by (A1) is a function of ρ_s . Specifically, $d_1(\rho_s) = d_p + r_{sp}(d_p, \rho_s)$ is a monotonically increasing function of ρ_s , while $d_2(\rho_s) = d_s + r_{ps}(\rho_s)$ is a monotonically decreasing function of ρ_s . Thus, there exist an optimal ρ_s minimizing $r_d(\rho_s)$. Note that minimizing detection radius r_d maximizes the transmission probability P_{tx} , and accordingly maximizes $C_2^{\epsilon,l}$. Let ρ_s^* be the optimal transmit power, then $d_p + r_{sp}(d_p, \rho_s^*) = d_s + r_{ps}(\rho_s^*)$ holds. Since it is hard to find a closed form expression for ρ_s^* , we find an approximation $\hat{\rho}_s^*$ using the fact that $d_p + r_{sp}(d_p, \rho_s^*) \approx d_p$. With the approximation, solving $r_{ps}(\rho_s^*) \approx d_p - d_s$ gives $\rho_s^* \approx \beta_s d_s^\alpha \left(\eta + \frac{\rho_p}{(d_p - d_s)^\alpha} \right)$. Then considering the minimum required transmit power, we have an approximated value of ρ_s^* given as follows.

Rule of Thumb 3. (RT3) For a given secondary system design requirements β_s , d_s and ρ_s^{\min} , choose the transmit power of secondary node as

$$\hat{\rho}_s^* = \max \left\{ \rho_s^{\min}, \beta_s d_s^\alpha \left(\eta + \frac{\rho_p}{(d_p - d_s)^\alpha} \right) \right\}. \quad (3.14)$$

It is a sub-optimal choice for maximizing the secondary capacity.

Fig.3.11b shows $C_2^{\epsilon,l}$ as a function of ρ_s , which is maximized at $\rho_s = \rho_s^*$. The red vertical line denotes the approximation $\hat{\rho}_s^*$, which is quite close to the optimal value. If $\rho_s^* < \rho_s$, increasing transmit power ρ_s increases detection radius $r_d = d_p + r_{sp}(d_p, \rho_s)$ and makes it more conservative, which accordingly results in a capacity loss. While if $\rho_s < \rho_s^*$, decreasing transmit power ρ_s increases detection radius $r_d = d_s + r_{ps}(\rho_s)$ since decreasing transmit power ρ_s makes SRx more vulnerable to the interference from PTxs, similarly which causes the loss of secondary capacity.

3.7 Concluding Remarks

We have explored the interdependency between the primary and secondary networks with different access priorities to single frequency band in terms of the outage probability and joint network capacity region. The model suggests that the detection radius(or detection sensitivity) of cognitive device needs to be determined carefully not only to protect primary receivers but also to minimize the impact from hidden primary transmitters. Along with this, we have shown that there exists an optimal decoding SINR and transmit power of cognitive devices that maximizes the capacity of cognitive network. Furthermore we show that primary networks with bursty coverage admit higher secondary capacity. We note that these parameters (except primary transmit power) are easily adjustable without requiring complex algorithms or hardware modification.

3.8 Appendix : Proof of Lemma 1

Before the proof we first introduce a useful concept called increasing convex ordering between two random variables.

Definition 11. (Increasing Convex Ordering on two random variables) We say that X is less than Y in *increasing convex order*, denoted $X \leq^{icx} Y$ ³, if $\mathbb{E}[\phi(X)] \leq \mathbb{E}[\phi(Y)]$ for all increasing and convex functions $\phi : \mathbf{R} \rightarrow \mathbf{R}$ such that expectations are defined, or if $\mathbb{E}[(X - t)^+] \leq \mathbb{E}[(Y - t)^+]$ for all $t \geq 0$.

Proposition 13. *If X and Y are non-negative random variables such that $\mathbb{E}[X] = \mathbb{E}[Y]$ then $X \leq^{icx} Y$, if and only if $\mathbb{E}[\phi(X)] \leq \mathbb{E}[\phi(Y)]$ for all ϕ convex for which the expectations are defined.*

Now we proof the Lemma 1.

Proof. We will construct a Bernoulli random variable N such that $P(N = 0) = 1 - \frac{\mathbb{E}[M]}{p}$ and $P(N = p) = \frac{\mathbb{E}[M]}{p}$ and show that $\mathbb{E}[(M - t)^+] \leq \mathbb{E}[(N - t)^+]$ or equivalently $\int_t^\infty \bar{F}_M(x)dx \leq \int_t^\infty \bar{F}_N(x)dx$ holds for all $t \geq 0$, where $\bar{F}_M(x)$ and $\bar{F}_N(x)$ denote the complementary cumulative distribution function. Note that $\bar{F}_M(x) = \mathbb{E}[M]/p$ for $0 \leq x < p$. Let $\alpha = \inf \{x | \bar{F}_M(x) \leq m/p\}$, and recalling that \bar{F}_M is non-increasing, it follows that for any x such that $x \geq \alpha$ we have $\bar{F}_M(x) \leq \bar{F}_N(x) = m/p$ whence for any $t \geq \alpha$, $\int_t^\infty \bar{F}_M(x)dx \leq \int_t^\infty \bar{F}_N(x)dx$. Now consider x such that $0 \leq x < \alpha$, in this case we have that $\bar{F}_M(x) \geq \bar{F}_N(x) = m/p$ so if $0 \leq t < \alpha$ we have that

$$\int_t^\infty \bar{F}_M(x)dx = \int_0^\infty \bar{F}_M(x)dx - \int_0^t \bar{F}_M(x)dx \quad (3.15)$$

$$= m - \int_0^t \bar{F}_M(x)dx \quad (3.16)$$

$$\leq m - \int_0^t \bar{F}_N(x)dx \quad (3.17)$$

$$= \int_t^\infty \bar{F}_N(x)dx, \quad (3.18)$$

³Note that \leq^{icx} was denoted as \leq_v in [96] and \leq_c in [101].

where we have used the fact that $\int_0^\infty \bar{F}_M(x)dx = \int_0^\infty \bar{F}_N(x)dx = m$. Then which implies $M \leq^{icx} N$. We have $\mathbb{E}[M] = \mathbb{E}[N]$ and $\mathbb{E}[\phi(N)] = \phi(0) - \frac{\mathbb{E}[N]}{p}(\phi(0) - \phi(p))$. The result follows by Proposition 13. \square

Chapter 4

Heterogeneous Environments and RF-Environment Awareness

4.1 Introduction

Detecting underutilized spectrum or white space, while protecting licensed receivers, is a challenging task. The fundamental difficulty in detecting white space is *uncertainty* in the environment e.g., noise, shadowing, fading, licensed receivers' locations, limited detection capability of wireless devices, etc. Perhaps the simplest solution to this problem, explained in more detail later, is to apply a threshold to the measured licensed transmitter's signal energy. To avoid interference to primary receivers, one can make the cognitive radios very sensitive by reducing their signal energy detection threshold. However, this results in a large exclusion region around each primary transmitter, inside which no cognitive devices are allowed to transmit [110]. The performance of this simple method is particularly poor when the secondary devices must contend with uncertainty and heterogeneity, e.g., inside/outside, environments. Circumventing this problem requires a fundamentally different approach. Indeed the uncertainty can be significantly reduced if cognitive devices have more detailed information on their operating environment. We shall refer to such cognitive devices as RF-environment aware.

In this chapter, we will study the interplay between the transmission capacities of primary and secondary nodes, under different levels of RF-environment awareness. Our aim is to quantify the capacity and understand the impact of various system parameters. In particular three white space detection methods for secondary nodes are considered and gains are evaluated in terms of the joint network capacity region.

Related Work. There have been numerous efforts towards optimizing parameter selection in such networks, e.g., transmission power [57, 95] or primary exclusion zone (equivalently, the signal energy detection threshold¹). The analysis and insights of [81, 110], are limited due to remaining uncertainties, e.g., noise, interference, shadowing [103]. To reduce uncertainty, [9, 50, 73, 124] have suggested the use of additional information, which is either obtained on fly or preloaded on cognitive devices. In these work, cognitive devices can access or have some form of database with information on the environment, for instance but not limited to, the geographical information and availability of spectrum usage opportunities (or the strength of primary signal) at various locations, the characteristics of primary devices, usage pattern of licensed bands, statistics of channel availability, and spectrum sharing policy. The most effective approach, among these, may be letting the cognitive devices know the exact locations of primary receivers to be protected. As long as they are safe from interference, cognitive devices can operate freely. The work of [115] shows an approach to detect passive receivers like televisions by detecting the leakage power of the passive receivers' oscillators. They suggested the use of sensors detecting the leakage power and sending weak beacon like signals indicating their existence to nearby cognitive devices.

Other techniques have been proposed to help cognitive devices reduce the chances of mis-detection and false alarm causing poor utilization of white space. Still, the key question is how to *quantify* the relative benefits of these techniques. The work in [53] attempts to compare the data base access approach in [124] versus the pure signal energy detection approach in [110] but their model is limited to a *single* primary transmitter and receiver pair. In a similar setting, [55] explores the impact of imperfect additional information on the performance of cognitive radio systems. They

¹In [37], FCC requires the detection threshold low enough to detect even weak TV signal as low as -114dBm. In this chapter, we study the performance of cognitive networks under various detection thresholds (or detection radii). This permits us to evaluate how this parameter impacts network capacity.

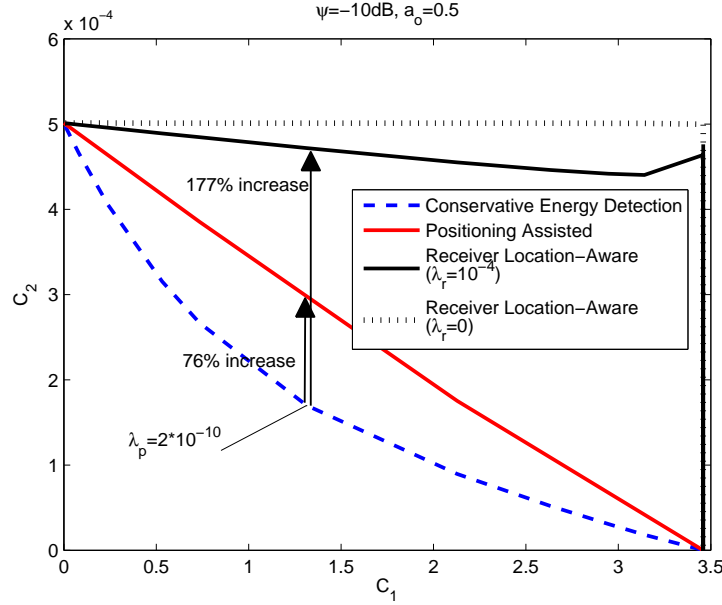


Figure 4.1: The joint network capacity region of primary (C_1) and secondary capacity (C_2) was shown under 10dB of penetration loss for three different white space detection techniques. 50% of STxs are indoor and remaining 50% are outdoor. λ_r denotes the density of primary receivers. When the density of primary transmitter is $\lambda_p = 2 \times 10^{-10}$, the gain of positioning-assisted technique to signal energy detection technique is 76%, and that of receiver location-aware technique is 177%.

showed via simulations the tradeoff between the resolution of radio environment information and performance of cognitive radios. We summarize the key contributions of this chapter as follows.

Contributions. We summarize the key contributions of this chapter as follows.

First, we build a stochastic model based on the model in Chapter 3 that captures the inter-dependency between two networks with multiple primary and secondary nodes with different access priorities. The model is rich enough to capture the impact of heterogeneous indoor or outdoor environment on secondary nodes' white space detection techniques. The outage probabilities and joint network capacity region for primary and secondary nodes are derived. Second, we *quantify* the relative gains of three different levels of RF-environment awareness and study the impact of indoor

shadowing on their associated joint network capacity region. We show that capacity trade-offs between primary and secondary networks depend on white space detection technique, resulting in joint network capacity regions which range from complement convex to linear to (almost) convex, see e.g., Fig.4.1. Not surprisingly the signal energy detection approach's network capacity region is the smallest, but, perhaps surprisingly, secondary network's capacity exhibits a non-monotonic behavior in the attenuation associated with indoor shadowing. By contrast when secondary nodes use positioning assisted and receiver location-aware techniques substantial gains in capacity can be realized, and their capacity increases *monotonically* as indoor shadowing increases. A final key observation quantified in this chapter is how the capacity gain of knowing primary receivers locations versus simply knowing the position of primary transmitters, varies with the density of primary receivers. This suggests that when a system has a high density of primary receivers, such detailed information may not be worthwhile, i.e., simpler cognitive mechanisms may suffice.

Organization This chapter is organized as follows. In Section 4.2, we provide a detailed description of our model, white space detection techniques, and definitions of the relevant system parameters. In Section 4.3, evaluation methodology is explained with overview of results. In Sections 4.4 to 4.6, the outage probabilities of primary and secondary receivers under three different sensing techniques are computed. These outage probabilities are used to find the maximum contention densities of STxs under an outage constraint in Section 4.7. In Section 4.8, we define the capacity of primary and secondary networks and combine them to compute a joint network capacity region. Section 4.9 concludes this chapter.

4.2 System Model

The model considered in this chapter is similar to that of Chapter 3 with some additional elements. To that end, we summarize the entire model once again.

4.2.1 Indoor Shadowing, Pathloss, and Interference Model

Indoor Shadowing In order to understand the impact of complex heterogenous environments on cognitive network capacity we shall model a network where indoor and outdoor nodes coexist. Signals propagating from the inside to the outside, and vice versa, see, for simplicity, a *fixed* attenuation ψ , where $0 \leq \psi \leq 1$, due to building walls. We refer to this as a indoor shadowing level. In practice such losses are highly dependent on a building's construction materials - measurements suggest variations from -40dB to 0dB [84].

Pathloss Propagation in the environment is captured using a simple free space pathloss model. That is, if both the transmitter and receiver are outdoors, or both within the same building, then, the attenuation factor is $d^{-\alpha}$, where d is the distance from the transmitter to the receiver, and α is the pathloss attenuation factor. If one of them is outdoors while the other indoors, then the signal is attenuated by an additional factor ψ associated with the traversing building walls. If the transmitter and receiver are indoor but in different buildings, then, a further additional factor of ψ is introduced, giving a total attenuation of $\psi^2 d^{-\alpha}$. Such a model could be made richer by considering different path loss attenuations in indoors and outdoors as well as variable indoor shadowing, yet as we will see in the sequel, analysis is already quite complex, and perhaps to first order it suffices towards understanding the role of heterogeneity in the network environment.

Interference Model Throughout this chapter, the signal to interference plus noise ratio (SINR) at a receiver, is computed based only on the dominant interferer, i.e., that which contributes the most interference, and a fixed SINR decoding threshold. Thus an outage corresponds to having at least one interfering node within a given disc of a fixed radius centered at the receiver. The *interference radius* of a receiver depends on various parameters including the ambient noise power, interferer's transmit power,

receiver's received signal power and the decoding threshold. This will be discussed in more detail in Section 4.2.5.

4.2.2 Primary Network

We shall assume the locations of active primary transmitters (PTx) follow a Poisson point process (PPP) $\Pi_p = \{X_j\}$ with intensity λ_p on \mathbf{R}^2 . Here X_j denotes both j -th PTx as well as its location. A PTx X_j uses a transmit power ρ_p and covers a region $b(X_j, d_p)$, where $b(x, r)$ denotes a disc centered at x with radius r and d_p is the coverage radius of a PTx. A primary receiver (PRx) located within the PTxs' coverage area $B(\Pi_p, d_p) \equiv \cup_{X_j \in \Pi_p} b(X_j, d_p)$, is assumed to successfully receive the primary signal as long as it does not see secondary interferers. We let β_p denote the decoding SINR for PTx's signal and $b_p = \log(1 + \beta_p)$ be the transmission rate of PTxs. The locations Π_r of PRxs are assumed to follow a homogenous PPP conditioned on the coverage area of the PTxs, thus this is a stationary doubly stochastic process (or Cox process) with a random intensity measure given by $\lambda_r \mathbf{1}\{z \in B(\Pi_p, d_p)\}$ at location $z \in \mathbf{R}^2$, where $\mathbf{1}\{\}$ denotes the indicator function, see [102]. A PRx Y is interfered by STxs if there is at least one secondary transmitter (STx) in $b(Y, r_{sp})$, where r_{sp} is the interference radius of a PRx with respect to a STx, determined in Section 4.2.5. We assume that all PTxs and PRxs are outdoors². This is a worst case scenario since indoor PRxs, if any, are better protected from interference. We refer to (Π_p, Π_r) as the primary network.

²In real world, some PRxs are indoors. However, we only consider outdoor PRxs in this chapter since assuming some portion of PRxs are indoors has almost no impact on our results. This is because the operations or parameters of secondary nodes are determined based on/considering only the performance of outdoor PRxs that are in worse condition than indoor PRxs in terms of robustness to interference.

4.2.3 Secondary Network

The locations of STxs are also modeled as a PPP Π_s on \mathbf{R}^2 but with intensity λ_s . The locations of indoor secondary transmitters (iSTx) Π_{si} are obtained by independent thinning of Π_s with probability a_i . The remaining STxs Π_{so} correspond to outdoor secondary transmitters (oSTx). Thus Π_{si} and Π_{so} are PPP with intensities $\lambda_{si} \equiv a_i \lambda_s$ and $\lambda_{so} \equiv a_o \lambda_s$ respectively, where $a_o = 1 - a_i$.

We assume STxs use a cognitive function to detect white space and then contend with each other using a simple ALOHA protocol, as done in [13, 112, 113]. STxs transmit at power ρ_s . Not all STxs in Π_{si} and Π_{so} are active, so we will introduce additional processes to denote active STxs. These are once again Cox processes with non homogenous intensity given the locations of the primary network $\{\Pi_p, \Pi_r\}$. Specifically, the intensity of active iSTxs at location z given $\{\Pi_p, \Pi_r\}$ is given by

$$a_i \lambda_s \mathbf{1} \{ \text{iSTx at } z \text{ is active under } \{ \Pi_p, \Pi_r \} \}$$

where the indicator function depends on a the white space detection technique being considered. Techniques, for determining the transmission opportunities for STxs, will be explained the next section. We assume each STx has an associated secondary receiver (SRx) randomly located at a fixed distance d_s and both are either indoor or outdoors.³ Note that SRxs can be interfered by unintended STxs or PTxs. More specifically, an outage may occur at oSRx W_o if there are one or more oSTxs within $b(W_o, r_{ss}^{oo})$; or if, there are one or more iSTxs in $b(W_o, r_{ss}^{io})$, where r_{ss}^{oo} and r_{ss}^{io} are the interference radii of a oSRx with respect to oSTxs and iSTxs respectively. In general $r_{ss}^{oo} \geq r_{ss}^{io}$ since iSTx will offer less interference to oSRx due to penetration loss ψ . Similarly an iSRx W_i can be interfered by either oSTxs in $b(W_i, r_{ss}^{oi})$ or iSTxs in $b(W_i, r_{ss}^{ii})$, where r_{ss}^{oi} and r_{ss}^{ii} are the interference radii of a iSRx with respect to a oSTx and iSTx respectively. Generally $r_{ss}^{oi} \geq r_{ss}^{ii}$ holds since iSTx gives less

³By assuming fixed distance d_s between STx and SRx, we do worst case analysis.

interference to iSRx due to the strong penetration loss ψ^2 . An oSRx W_o is interfered by PTxs if there exist any PTx in $b(W_o, r_{ps})$, where r_{ps} is the interference radius of oSRx with respect to a PTx. Similarly, a iSRx W_i can be interfered by PTxs if there exist any PTx in $b(W_i, r_{ps}^i)$, where r_{ps}^i is the interference radius of a iSRx with respect to a PTx. We assume that STxs transmit with rate $b_s = \log(1 + \beta_s)$ where β_s is the decoding SINR threshold for STx's signal. The various parameters introduced here will be specified in Section 4.2.5.

4.2.4 White Space Detection

Three different methods are considered for detecting transmission opportunities for secondary nodes. They are neither the worst nor the best, but rather represent the spectrum of possible approaches exploiting different levels of RF-environment awareness that STxs could have of the surrounding environment. Note that in [37,38] FCC requires cognitive devices to have either signal energy detection scheme or geo-location/data base access scheme that corresponds to the first and second methods in our work. Cognitive devices relying only on the signal energy detection method can be allowed to be used but should pass FCC's much more rigorous test.

Signal Energy Detection Based Cognitive Devices. Signal energy detection is a simple technique which relies on measuring the PTxs' signal energy at a STx's location. If it is below a predetermined detection threshold, the STx infers that there is no PTx in its detection – again modeled as a disc centered at the STx and a given detection radius. Increasing the threshold makes the STx only sensitive to PTxs which are close by, i.e., the detection radius is a strictly decreasing function of the threshold. Decreasing the threshold makes the detector more sensitive, and accordingly the STx will behave conservatively. Although this approach appears reasonable it has a serious weakness. A STx which is indoors will see an attenuated signal from outdoor PTxs, and may conclude there are no nearby PTxs, and transmit within coverage area of PTxs possibly producing harmful interference to PRxs. To preclude from this

happening, the detection threshold needs to be set very conservatively. This point will be discussed further in Section 4.4.1 where we will quantify the impact of iSTxs on PRx's outage probability. In the sequel we let E-STx(E-SRx) denote STx(SRx) using the signal energy detection method. When we need to be more specific on node's location, i.e., indoor or outdoor, we use E-iSTx(E-iSRx) and E-oSTx(E-oSRx) for an indoor and an outdoor E-STx(E-SRx) node respectively.

Positioning-assisted Cognitive Devices. A STx using positioning-assisted detection is aware of the actual locations of nearby PTxs. We assume that either the device has preloaded map in its memory or it can access remote database. The device periodically samples its current location using its built-in positioning module and checks if it is safe to transmit or not. We assume that when STxs are outdoors they use Global Positioning System(GPS) technology and when they are indoors they use indoor positioning technology [76] or infer its location information based on previous history of location information. Two similar ideas were discussed in [9, 50]. A cognitive device using this approach knows the coverage area of PTxs, and so does not have the drawback of mis-detecting PTxs discussed for the previous method. It allows both indoor and outdoor STxs to correctly detect the presence of PTxs or equivalently the regions where STxs are not allowed to transmit. In fact, this approach is equivalent to a technique letting a cognitive device know whether it is indoors or outdoors. The device using the information can adaptively adjust its signal energy detection threshold so as to protect primary receivers and to maximize its transmission opportunity. We shall use a similar naming convention, where G-STx(G-SRx), G-iSTx(G-iSRx) and G-oSTx(G-oSRx) denote a positioning-assisted STx(SRx), a positioning-assisted indoor STx(SRxs), and a positioning-assisted outdoor STx(SRx) respectively.

Receiver Location-Aware Cognitive Devices. Lastly suppose cognitive devices can detect the locations of both PTxs and PRxs. Whether this is implementable depends on the nature of PRxs. If the PRxs are passive it may not be easy to detect them. However, even in this case, it may not be totally impossible if one can detect

the leakage power of receiver's oscillator, see [115]. [4] shows that this kind of detecting scheme is implementable and have been used in the UK to find people watching TV without buying licenses. If PRxs can send a signal (beacon) to indicate their existence to nearby STxs, then, it is of course much easier to detect and protect them. Alternatively the location of PRxs to be protected could be registered in a database accessible by STxs. We shall thus suppose STxs are able to detect the presence of PRxs within a certain radius. This affords cognitive devices the highest degree of RF-environment awareness. STxs can now transmit within the coverage of PTxs⁴ as long as they do not give harmful interference to PRxs (or equivalently there are no PRxs close to them).

We again adopt a naming convention, where L-STx(L-SRx), L-iSTx(L-iSRx) and L-oSTx(L-oSRx) denote a receiver location-aware STx(SRx), a receiver location-aware indoor STx(SRx), and a receiver location-aware outdoor STx(SRx) respectively.

4.2.5 System Model Parameters

Below we derive many of the above mentioned model parameters, from those specified as a part of system design and requirements, e.g., ρ_p , ρ_s , β_p and β_s . We let i_p denote the maximum tolerable interference at the edge of PTx's coverage area. i_p is a design parameter that corresponds to a performance margin which makes receivers robust to a certain amount of interference, so we assume this value is given and fixed. This, and the successful reception condition for PRx, determine the coverage range d_p of a PTx. That is, under maximum interference, the received SINR of a PRx at distance d where $d < d_p$ from its nearest PTx should be larger than the decoding

⁴According to the current rule by FCC, cognitive devices are not allowed to operate inside the coverage of primary transmitter. But, in this chapter, by allowing it we study how much capacity improvement we can expect if we can overcome the current limitation.

SINR threshold β_p , which defines the coverage range of a PTx as

$$d_p \equiv \sup \left\{ d > 0 \mid \frac{\rho_p d^{-\alpha}}{\eta + i_p} > \beta_p \right\} = \left(\frac{\rho_p}{(\eta + i_p)\beta_p} \right)^{\frac{1}{\alpha}},$$

where η denotes the noise power. By considering i_p in computing d_p , we do a worst case analysis.

Next we determine the smallest allowable distance $r_{sp}(d)$ between an oSTx and a PRx, given the latter is a distance d from its nearest PTx. Ensuring successful reception means that:

$$r_{sp}(d) \equiv \inf \left\{ r > 0 \mid \frac{\rho_p d^{-\alpha}}{\eta + \rho_s r^{-\alpha}} > \beta_p \right\} = \rho_s^{\frac{1}{\alpha}} \left(\frac{\rho_p}{d^\alpha \beta_p} - \eta \right)^{-\frac{1}{\alpha}}. \quad (4.1)$$

We will call $r_{sp}(d)$ the *PRx's interference radius with respect to an oSTx*. The *PRx's interference radius with respect to an iSTx* is similarly given by

$$r_{sp}^i(d) \equiv \inf \left\{ r > 0 \mid \frac{\rho_p d^{-\alpha}}{\eta + \psi \rho_s r^{-\alpha}} > \beta_p \right\} = \psi^{\frac{1}{\alpha}} r_{sp}(d).$$

Note that $r_{sp}(d)$ and $r_{sp}^i(d)$ are strictly increasing functions of d . Indeed, as the PRx gets further away from its nearest PTx, the PRx is increasingly vulnerable to interference, and so the above radii increase. In the sequel we will occasionally omit the dependency of r_{sp} and r_{sp}^i on d .

Next we determine the maximum tolerable interference of a SRx i_s . A SRx a distance d_s away from its STx can decode the signal from the STx, if the received SINR is larger than β_s ; this gives the following requirement

$$i_s \equiv \sup \left\{ i > 0 \mid \frac{\rho_s d_s^{-\alpha}}{\eta + i} > \beta_s \right\} = \frac{\rho_s d_s^{-\alpha}}{\beta_s} - \eta. \quad (4.2)$$

In turn an *oSRx's interference radius w.r.t. a PTx*, r_{ps} can be determined by ensuring the interference from its nearest PTx does not exceed i_s , i.e.,

$$r_{ps} \equiv \inf \left\{ r > 0 \mid \rho_p r^{-\alpha} + \eta \leq i_s \right\} = \left(\frac{\rho_p}{i_s - \eta} \right)^{\frac{1}{\alpha}}. \quad (4.3)$$

Similarly, the *iSRx's interference radius w.r.t. a PTx* r_{ps}^i follows by including the additional indoor shadowing level ψ that the indoor SRx would see:

$$r_{ps}^i \equiv \inf \{r > 0 | \psi \rho_p r^{-\alpha} + \eta \leq i_s\} = \psi^{\frac{1}{\alpha}} r_{ps}. \quad (4.4)$$

There are four different types of SRx's interference radii related to STxs. The *oSRx's interference radius w.r.t. an oSTx* r_{ss}^{oo} is computed as follows. For an oSRx to receive its oSTx's signal without outage, the noise plus interference from its nearest interfering oSTx to the oSRx should not exceed the tolerable interference $\rho_s r^{-\alpha} + \eta \leq i_s$, giving

$$r_{ss}^{oo} \equiv \inf \{r > 0 | \rho_s r^{-\alpha} + \eta \leq i_s\} = \left(\frac{\rho_s}{i_s - \eta} \right)^{\frac{1}{\alpha}}.$$

The *oSRx's interference radius w.r.t. an iSTx* r_{ss}^{io} is determined by the interference condition $\psi \rho_s r^{-\alpha} + \eta \leq i_s$, which gives

$$r_{ss}^{io} \equiv \inf \{r > 0 | \psi \rho_s r^{-\alpha} + \eta \leq i_s\} = \psi^{\frac{1}{\alpha}} r_{ss}^{oo}.$$

The *iSRx's interference radius w.r.t. an oSTx* r_{ss}^{oi} is determined by the interference condition $\psi \rho_s r^{-\alpha} + \eta \leq i_s$, giving

$$r_{ss}^{oi} \equiv \inf \{r > 0 | \psi \rho_s r^{-\alpha} + \eta < i_s\} = \psi^{\frac{1}{\alpha}} r_{ss}^{oo}.$$

The *iSRx's interference radius w.r.t. an iSTx* in a different building r_{ss}^{ii} is determined by the interference condition $\psi^2 \rho_s r^{-\alpha} + \eta \leq i_s$, giving

$$r_{ss}^{ii} \equiv \inf \{r > 0 | \psi^2 \rho_s r^{-\alpha} + \eta \leq i_s\} = \psi^{\frac{2}{\alpha}} r_{ss}^{oo}.$$

A STx using *signal energy detection*, E-STx, ensures there are no PTxs close by, i.e., within its *detection radius* r_d , so as to indirectly protect PRxs. The baseline detection radius used for E-oSTx is defined as

$$r_d \equiv \max \{d_p + r_{sp}(d_p), d_s + r_{ps}\}. \quad (4.5)$$

The first term in the maximum ensures that the STx is far enough so as to not harm PRx which is at the edge, i.e., a distance d_p , from its associated PTx. Thus STx's can send only if they are outside the PTxs' coverage area plus an additional guard zone. The second term corresponds to minimum distance a SRx must be from a PTx, r_{ps} plus the SRx's fixed distance d_s from its associated STx. If the secondary network includes indoor STx then protecting PRxs requires increasing the detection radius to $r_d^E \equiv \psi^{-\frac{1}{\alpha}} r_d$. We discuss this in more detail in the sequel along with modeling of detection radii for the two other white space detection methods to be considered.

4.2.6 Preliminary Definitions

In this section, we define some further notations used throughout this chapter. Let $|\mathcal{A}|$ denote the area of a set $\mathcal{A} \subset \mathbf{R}^2$. Let $\|x - y\|$ denote the distance between x and y in \mathbf{R}^2 . We define a set $K(x, r_x; y, r_y) \equiv b(y, r_y) \setminus b(x, r_x)$ in \mathbf{R}^2 . Let $\mathcal{L}_{\{Q\}}(\lambda_s) \equiv \mathbb{E} [e^{-\lambda_s Q}]$ be the Laplace transform of a random variable Q . For simplicity we let $q_m^{oo} = \pi (r_{ss}^{oo})^2$, $q_m^{io} = \pi (r_{ss}^{io})^2$, $q_m^{oi} = \pi (r_{ss}^{oi})^2$, $q_m^{ii} = \pi (r_{ss}^{ii})^2$, $q_m^o = a_i q_m^{io} + a_o q_m^{oo}$ and $q_m^i = a_i q_m^{ii} + a_o q_m^{io}$. For a given $x \in \mathbf{R}^2$ and PPP Π , $x \notin B(\Pi, r)$ and $\Pi \cap b(x, r) = \emptyset$ will denote the same event.

4.2.7 Parameter Set

Throughout this chapter, we use the following representative parameters to compute the system model parameters defined in Section 4.2.5: $\alpha = 3$, $\eta = N_o \times 20 \times 10^6$, $i_p = 5\eta$, $\rho_p = 100\text{W}$, $\rho_s = 1\text{mW}$, $\beta_p = 10$, $\beta_s = 1.4$, where $N_o = -174\text{dBm}$ is an noise power spectral density. Some of the resulting computed system parameters are as follows: $d_p = 27560\text{m}$, $i_s = 7.14 \times 10^{-7}$, $d_s = 10\text{m}$, $r_{ps} = 519\text{m}$, and $r_{ss}^{oo} = 11.18\text{m}$. See [3, 16, 81] for some realistic parameter values. and [65] for parameter selection.

ρ_p	Transmit power of PTx
ρ_s	Transmit power of STx
β_p	Decoding SINR of PRx
β_s	Decoding SINR of SRx
d_p	Coverage range radius of PTx
i_p	Maximum tolerable interference of PRx at the edge of PTx coverage
i_s	Max tolerable interference of a SRx at distance d_s from its STx
r_d^E	Detection radius of E-oSTx
r_d^L	Detection radius of L-oSTx
r_{ps}	Interference radius of oSRx w.r.t. PTx
r_{ps}^i	Interference radius of iSRx w.r.t. PTx
r_{ss}^{oo}	Interference radius of oSRx w.r.t. oSTx
r_{ss}^{io}	Interference radius of oSRx w.r.t. iSTx
r_{ss}^{oi}	Interference radius of iSRx w.r.t. oSTx
r_{ss}^{ii}	Interference radius of iSRx w.r.t. iSTx
r_d	Detection radius (baseline)
$r_{sp}(d)$	Interference radius of a PRx w.r.t. to oSTx
$r_{sp}^i(d)$	Interference radius of a PRx w.r.t. to iSTx
r_d^{Ei}	Detection radius of E-iSTx
r_d^{Li}	Detection radius of L-iSTx
α	Pathloss attenuation factor
a_i	Fraction of indoor STxs
a_o	Fraction of outdoor STxs ($= 1 - a_i$)
λ_s	Density of STxs
ψ	Indoor shadowing level
λ_p	Density of PTxs
η	Noise power

Table 4.1: Summary of Parameters

4.2.8 Weaknesses of Model

Our model has several weaknesses. First, our channel model accounts for pathloss attenuation and indoor/outdoor shadowing factor only. Fading is not considered. Second, our interference model does not account for the additive nature of interference. Indeed as mentioned earlier, we assume that outages are caused solely by the dominant interferer. This choice is driven mathematical simplicity, yet for spatially distributed nodes, this has been proven as a fairly good model [49,72,74]. Moreover, it turns out that outage probability computed with this simple disk model corresponds to the lower bound of outage computed considering shot noise interference, and it has been shown that the lower bound is asymptotically tight, see [112,113]. Third, the location of primary transmitters is modeled as PPP. Clearly this is not likely to be true in practice for any type of designed infrastructure. Still this provides a simple caricature of the spatial variability one might see in such deployments. Finally, we assume STxs transmit in Aloha fashion, this again is assumed for tractability, following [13,56,112,113]. Some of our results could perhaps be extended to account for clustering in PTxs and/or STxs, yet via a non-homogenous point process but from now it seems reasonable to focus on understanding the homogenous case.

4.3 Computing joint Network capacity Region Roadmap and Overview of Results

4.3.1 Computing a Joint Network Capacity Region Roadmap

Our goal is to compare the *joint network capacity region*

$$\Lambda = \{(C_1, C_2) | (C_1, C_2) \text{ are achievable}\},$$

i.e., the set of achievable primary and secondary capacity pairs (C_1, C_2) , under the three white space detection techniques. The notion of joint network capacity region studied in this chapter is *different* from the classical one in information theory [28] in at least three ways. First, a primary network's *broadcast coverage capacity* C_1 is

defined as the average number of bits that can be successfully received by potential receivers per second per square meter per Hertz. Since the primary network operates in the broadcast mode this is simply proportional to transmission rate b_p times the fraction of covered area. The covered area depends on the density of primary transmitters λ_p and potentially also on secondary nodes' behavior if it fails to protect the primary network. Second, the secondary network's *transmission capacity* C_2 is the average number of successfully transmitted bits per second per square meter per Hertz subject to an ϵ -outage constraint summed over indoor and outdoor transmissions. This is similar to the notion introduced in [13, 113], except that in a cognitive network context, the secondary nodes' transmission capacity depends on the density of primary nodes, fractions of indoor/outdoor secondary nodes, the environment, e.g., path loss and indoor shadowing as well as the white space detection technique being used. Third, a pair (C_1, C_2) is "achievable" if there exists a density of primary and secondary nodes such that the average spatial capacity of both the primary and secondary network is (C_1, C_2) . Note that C_1 and C_2 correspond to averages computed over an ensemble of Poisson distributed primary and secondary nodes under our system models. The mathematical definition of the joint network capacity region will be given in Section 4.8.

The computation of the joint network capacity region involves three steps. First determining the outage probabilities for primary and secondary (indoor/outdoor) nodes. This is carried out for each white space detection technique in Sections 4.4–4.6. Second, for a fixed intensity of primaries nodes λ_p determining the optimal intensity of secondary transmissions λ_s^ϵ which meets the outage constraint ϵ , see Section 4.7. Third, computing the joint network capacity region by varying the possible intensity of primary nodes see in Section 4.8. Prior to doing so, we discuss some of the key obtained results.

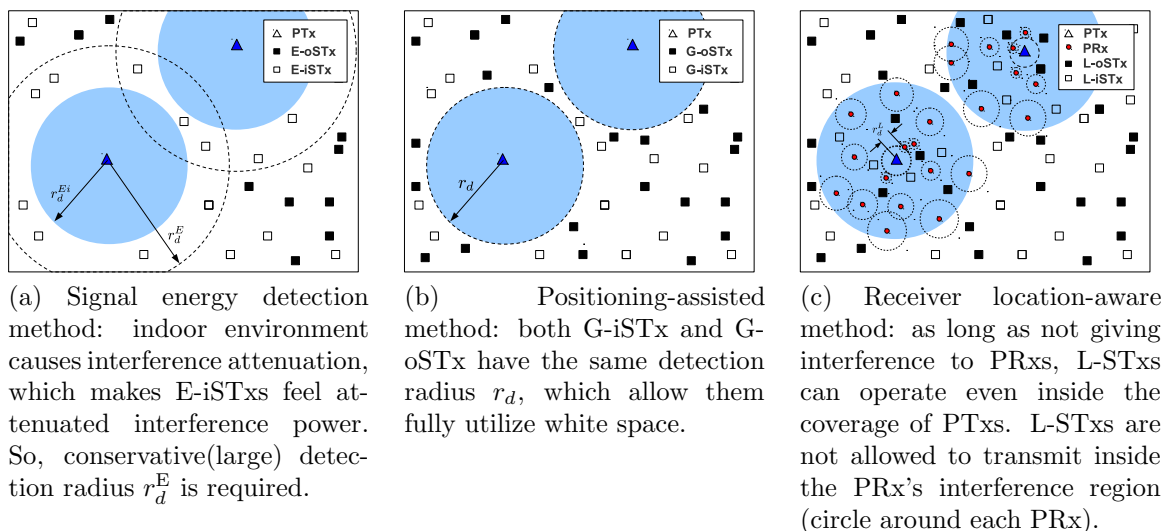


Figure 4.2: A typical realization of primary and secondary networks under three white space detection methods is shown. Shaded region denotes the coverage of PTxs with radius d_p .

4.3.2 Overview of Results

Fig.4.1 exhibits representative joint network capacity regions for the cognitive network under the three white space detection mechanisms considered, while Fig.4.2 exhibits the geometry underlying these results. As expected the capacity is enhanced when secondary nodes have a higher degree of RF-environment awareness.

In the signal energy sensing scenario the detection radius must be set conservatively because indoor STx can not properly infer the location of PTxs and thus protect PRxs. As shown in Fig.4.2a E-oSTx nodes can only operate if they are outside this larger radius r_d^E , while because of the indoor shadowing E-iSTx can operate outside the ('correct') radius r_d . As exhibited in Fig.4.1 the joint network capacity region for this scenario is surprisingly complement convex. Note it is tempting to think time sharing would convexify the network capacity region, yet this does not make sense in the scenario of interest, i.e., where a pre-installed broadcasting network's licensed spectrum is being opportunistically used by an ad hoc cognitive network.

The positioning-assisted white space detection technique solves this problem since all G-STxs are made directly aware of the coverage area of PTxs. Fig.4.2b shows a typical realization of the two networks, where both G-iSTxs and G-oSTx can operate outside coverage area of PTxs. The joint network capacity region is shown to be roughly linear in this case, see Fig.4.1.

Last, if STxs are aware of primary receivers' locations one obtains substantial capacity improvements. Indeed, depending on the locations of PRxs, L-STxs can opportunistically transmit *within* the coverage area of PTxs, so the capacity gains now depend on the density of primary receivers, see Fig.4.1. Fig.4.2c, exhibits the geometry underlying this scenario. The small discs around each PRx denote its interference region w.r.t. a L-oSTx⁵. To protect PRxs no L-oSTx should reside in such discs. The radii of these discs are defined in (4.1) as $r_{sp}(d)$ which is strictly increasing function of distance d to its nearest PTx. Perhaps counterintuitively, L-STxs located closer to PTxs are more likely to transmit than L-STxs far from them. Also surprisingly, it turns out that this phenomenon is helpful in increasing secondary capacity when λ_p is high, this can be seen in Fig.4.1, where the receiver location aware capacity region for $\lambda_r = 10^{-4}$ exhibits a non monotonic behavior on the right hand side.

4.4 Performance of Signal Energy Detection Technique

In this section, we evaluate the outage probability of a PRx and E-oSRx. We will first show that if an indoor STx chose its detection radius r_d (or equivalently detection threshold) naively, this can negatively impact PRxs. For notational simplicity, let Π'_{so} and Π'_{si} be Cox processes denoting active (or transmitting) E-oSTxs and E-iSTxs with intensities $a_o\lambda_s\mathbf{1}\{z \notin B(\Pi_p, r_d)\}$ and $a_i\lambda_s\mathbf{1}\{z \notin B(\Pi_p, r_d^i)\}$ at $z \in \mathbf{R}^2$ respectively and, where $r_d^i \equiv \psi^{\frac{1}{\alpha}}r_d$.

⁵We can also draw its interference region w.r.t. a L-iSTx, but it is omitted for simplicity.

4.4.1 Outage Probability of Primary Receivers

Suppose we set the detection threshold, say I_d , of E-STxs such that $\rho_p r^{-\alpha} > I_d$ for $r < r_d$. Then, E-oSTxs would detect any PTxs within r_d and would not interfere PRxs that are at the edge of the PTxs' coverage area. However, E-iSTx can only detect PTxs within r_d^i , which potentially makes them mis-detect PTxs between r_d^i and r_d . To show the negative impact of this parameter choice, we shall compute the outage probability of a PRx as a function of distance d to its nearest PTx.

Theorem 7. (*Conditional Outage Probability of PRx with E-STxs*) For given λ_p , λ_s , and d_p , a PRx Y 's outage probability given it is a distance d away from its nearest PTx X is given by

$$P_{out}^p(d, \lambda_s) = 1 - \mathbf{1}\{d < d_p\} \mathcal{L}_{\{a_o L_1(d, \Pi_p^{(2)}) + a_i L_2(d, \Pi_p^{(2)})\}}(\lambda_s), \quad (4.6)$$

where $\Pi_p^{(2)} = \{\Pi_p \cap \overline{b(Y, d)}\} \cup \{X\}$,

$$L_1(d, \Pi) = \int_{K(X, r_d; Y, r_{sp})} \mathbf{1}\{z \notin B(\Pi, r_d)\} dz, \text{ and } L_2(d, \Pi) = \int_{K(X, r_d^i; Y, r_{sp}^i)} \mathbf{1}\{z \notin B(\Pi, r_d^i)\} dz.$$

Proof is given in Appendix 4.10. Note that geometrically $L_1(d, \Pi_p^{(2)}) = \int_{K(X, r_d; Y, r_{sp})} \mathbf{1}\{z \notin B(\Pi^{(2)}, r_d)\} dz$ is an area of $K(X, r_d; Y, r_{sp})$ which is not covered by the Boolean process $B(\Pi^{(2)}, r_d)$ and a similar interpretation applies to $L_2(d, \Pi_p^{(2)})$. $L_1(d, \Pi_p^{(2)})$ can be viewed as a random variable with finite support since it depends on the random process $\Pi_p^{(2)}$. Note that this area measures the amount of potential interferers. Thus, a larger area implies that the PRx Y is more likely to be interfered with. To compute the above Laplace transform $\mathcal{L}_{\{a_o L_1(d, \Pi_p^{(2)}) + a_i L_2(d, \Pi_p^{(2)})\}}(\lambda_s)$, we need to know the distributions of two random variables $L_1(d, \Pi_p^{(2)})$ and $L_2(d, \Pi_p^{(2)})$, but these are difficult to compute. So, we will compute upper and lower bounds on these quantities. The following corollary gives lower and upper bounds on $P_{out}^p(d)$ obtained using Lemma 1, while the upper bound is obtained using Jensen's inequality.

Corollary 2. For $d < d_p$, upper and lower bounds of a PRx's conditional outage

probability are given by:

$$P_{out}^{p,u}(d, \lambda_s) = 1 - \exp\{-\lambda_s(a_o l_1 + a_i l_2)\}, \text{ and}$$

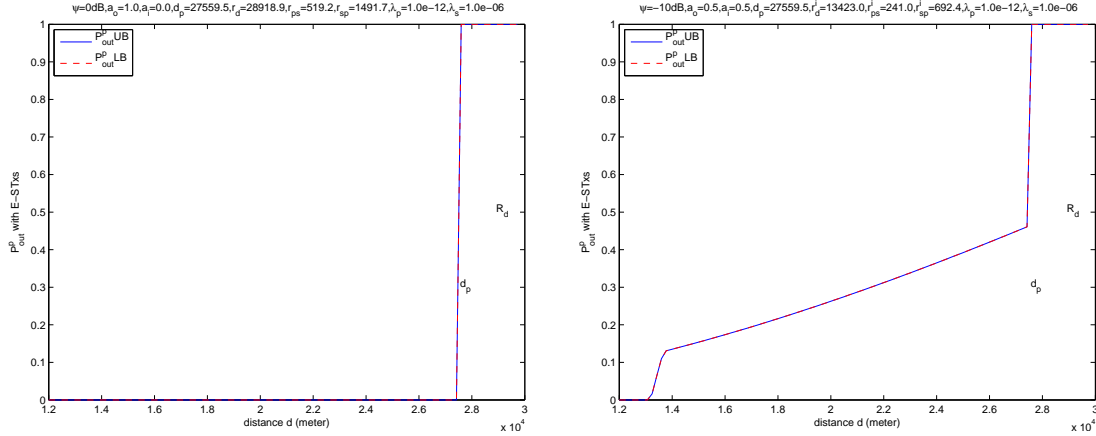
$$P_{out}^{p,l}(d, \lambda_s) = \frac{a_o l_1 + a_i l_2}{a_o l_{1m} + a_i l_{2m}} (1 - e^{-\lambda_s(a_o l_{1m} + a_i l_{2m})}),$$

where $l_1 = \mathbb{E}[L_1(d, \Pi_p^{(2)})]$, $l_2 = \mathbb{E}[L_2(d, \Pi_p^{(2)})]$, $l_{1m} = |K(X, r_d; Y, r_{sp})|$ and $l_{2m} = |K(X, r_d^i; Y, r_{sp}^i)|$.

In the sequel, we omit proofs of remaining corollaries giving such bounds since all of them can be proved using the same machinery. Note that $l_1 = \mathbb{E}[L_1(d, \Pi_p^{(2)})]$ and $l_2 = \mathbb{E}[L_2(d, \Pi_p^{(2)})]$ can be computed through numerical integration as follows:

$$\begin{aligned} l_1 &= \int_{K(X, r_d; Y, r_{sp})} P(z \notin B(\Pi_p^{(2)}, r_d)) dz \\ &= \int_{K(X, r_d; Y, r_{sp})} \exp\{-\lambda_p |K(X, d; z, r_d)|\} dz, \\ l_2 &= \int_{K(X, r_d; Y, r_{sp}^i)} P(z \notin B(\Pi_p^{(2)}, r_d^i)) dz \\ &= \int_{K(X, r_d; Y, r_{sp}^i)} \exp\{-\lambda_p |K(X, d; z, r_d^i)|\} dz. \end{aligned}$$

Fig.4.3a shows the outage probability of a PRx as a function of d to its nearest PTx when $a_o = 1$, i.e., when there are no E-iSTx. One PTx at the origin is considered. In this case, we have a coverage $d_p = 27559\text{m}$, and the detection radius r_d is set to $d_p + r_{sp}(d_p)$ after considering guard band of width $r_{sp}(d_p)$. As expected, the outage probability is zero for $d < d_p$ and non-zero otherwise. However if there exist indoor nodes (i.e., $a_i > 0$) with $\psi = -10\text{dB}$, we have a significant increase in the outage probability as shown in Fig.4.3b. Since $r_d^i < r_d$, the attenuated signal from the PTx makes E-iSTxs between r_d^i and r_d mis-detect the PTx and allows them to transmit even inside the coverage area of the PTx. This becomes increasingly severe if ψ gets stronger (or smaller). These two figures clearly show how poorly selected detection radii of STxs can give harmful interference to PRxs. To prevent this, one has to set



(a) If there is no indoor nodes (i.e., $\psi = 0$), setting $r_d = d_p + r_{sp}(d_p)$ is enough to protect PRxs from STxs' interference. Note that PRx's outage is zero for $d < d_p$. (b) If there exist 50% of indoor nodes ($a_i = 0.5$) with $\psi = -10\text{dB}$, they mis-detect the existence of nearby PTx and start transmitting even when they are inside the coverage i.e., when $d < d_p$. It causes severe increase of PRx's outage probability.

Figure 4.3: Impact of STxs' interference to outage probability of PRx at distance d to its nearest PTx

the detection threshold *conservatively* so that all the E-iSTxs at $d < d_p$ detect the PTx. We reconsider the outage probability calculation under a more conservative detection radius choice in next section.

4.4.2 Outage Probability for Primary Receiver with STxs using a Conservative Detection Threshold

In order to properly protect PRxs in the coverage area of PTxs, we shall make all STxs use the detection radius $r_d^E \equiv \psi^{-\frac{1}{\alpha}} r_d$, where r_d is the desired minimum detection radius defined in (4.5). Note that E-oSTxs using r_d^E can detect all PTxs in their detection radius r_d^E , but E-iSTxs using r_d^E only detect PTxs in an effective detection radius of $\psi^{\frac{1}{\alpha}} r_d^E = r_d$ since E-iSTxs are indoor and see attenuated PTx power. They see the PTxs' appear further away than their actual locations. So,

considering this effect, E-STxs must use a conservative detection radius r_d^E .

Accordingly, let Π_{so}^E and Π_{si}^E be Cox processes denoting active E-oSTxs and E-iSTxs that would arise given these new detection radii with intensities $a_o\lambda_s\mathbf{1}\{z \notin B(\Pi_p, r_d^E)\}$ and $a_i\lambda_s\mathbf{1}\{z \notin B(\Pi_p, r_d^{Ei})\}$ at $z \in \mathbf{R}^2$ respectively. Note that E-STxs no longer transmit inside the coverage area of the PTxs due to this new detection threshold. However, as a side effect this will make E-oSTx less likely to be active since they need to detect a larger PTx free area to be active. We update Theorem 7 and Corollary 2 by replacing r_d with r_d^E and r_d^i with $r_d^{Ei} \equiv \psi^{\frac{1}{\alpha}}r_d^E$, to obtain Theorem 8 and Corollary 3 respectively.

Theorem 8. (*Outage Probability of PRx with E-STxs with conservative detection radius*) For a PRx Y at a distance d from its nearest PTx, we have an outage probability

$$P_{out}^{pE}(d, \lambda_s) = 1 - \mathbf{1}\{d < d_p\} \mathcal{L}_{\{a_o L_3(d, \Pi_p^{(2)}) + a_i L_4(d, \Pi_p^{(2)})\}}(\lambda_s)$$

where $L_3(d, \Pi) = \int_{K(X, r_d^E; Y, r_{sp})} \mathbf{1}\{z \notin B(\Pi, r_d^E)\} dz$, and $L_4(d, \Pi) = \int_{K(X, r_d^{Ei}; Y, r_{sp}^i)} \mathbf{1}\{z \notin B(\Pi, r_d^{Ei})\} dz$.

This outage probability can be upper and lower bounded as follows.

Corollary 3. For $d < d_p$, upper and lower bounds on a PRx's conditional outage probability are given by:

$$P_{out}^{pE,u}(d, \lambda_s) = 1 - \exp\{-\lambda_s(a_o l_3 + a_i l_4)\} \quad \text{and} \\ P_{out}^{pE,l}(d, \lambda_s) = \frac{a_o l_3 + a_i l_4}{a_o l_{3m} + a_i l_{4m}} (1 - e^{-\lambda_s(a_o l_{3m} + a_i l_{4m})}),$$

where $l_3 = \mathbb{E}[L_3(d, \Pi_p^{(2)})]$, $l_4 = \mathbb{E}[L_4(d, \Pi_p^{(2)})]$, $l_{3m} = |K(X, r_d^E; Y, r_{sp})|$ and $l_{4m} = |K(X, r_d^{Ei}; Y, r_{sp}^i)|$.

Again l_3 and l_4 can be computed numerically, see Appendix 4.14. The outage probability of a PRx with E-STxs having conservative detection radius r_d^E is the same

as that in Fig.4.3a. Due to the increased detection radius, now PRxs are free from interference from E-STxs.

Next we compute the fraction of area of \mathbf{R}^2 where potential PRxs can successfully receive PTxs' transmission $P_c^E(\lambda_p) = 1 - \mathbb{E}[P_{out}^{pE}(D, \lambda_s)]$. Note that primary network's broadcasting coverage capacity is directly proportional to this quantity. We take the expectation of $P_{out}^{pE}(D, \lambda_s)$ w.r.t. the random variable D denoting the distance of a PRx⁶ to its nearest PTx; it can be shown to have a distribution function $F_D(x) = 1 - \exp\{-\lambda_p\pi x^2\}$. So, we have

$$\begin{aligned} \mathbb{E}[P_{out}^{pE}(D, \lambda_s)] &= \int_0^{d_p} P_{o,1}(d, \lambda_s^{\epsilon E}) dF_D(x) + \int_{d_p}^{\infty} dF_D(x) \\ &= \int_0^{d_p} P_{out}^{pE}(d, \lambda_s) dF_D(x) + e^{-\lambda_p\pi d_p^2}. \end{aligned}$$

4.4.3 Outage Probability of Outdoor Secondary Receiver

In this section, we consider the outage probability P_{out}^{soE} of a typical E-oSRx denoted here by W_o . This is a conditional outage probability conditioned on the existence of an active E-oSTx Z_o transmitting to an E-oSRx W_o as shown in Fig.4.4. Note that Z_o is not necessarily the nearest E-oSTx to the W_o . This can be viewed as a worst case analysis since we fix $\|W_o - Z_o\|$ to be d_s . For the E-oSTx Z_o to be active, there should be no PTxs within the E-oSTx's detection area; so, we condition on the event $Z_o \notin B(\Pi_p, r_d^E)$ and $\|W_o - Z_o\| = d_s$. Note that interference from other E-STxs can cause an outage at the the E-oSRx W_o . In the following therefore, we capture the impact from PTxs, E-oSTxs, and E-iSTxs on the outage of a typical E-oSRx W_o .

Theorem 9. (*Conditional Outage Probability of E-oSRx*): For given λ_p and λ_s , the conditional outage probability of a E-oSRx whose associated transmitter E-oSTx is a

⁶As discussed in Section 4.3.1, here PRx Y do not necessarily belong to Π_r .

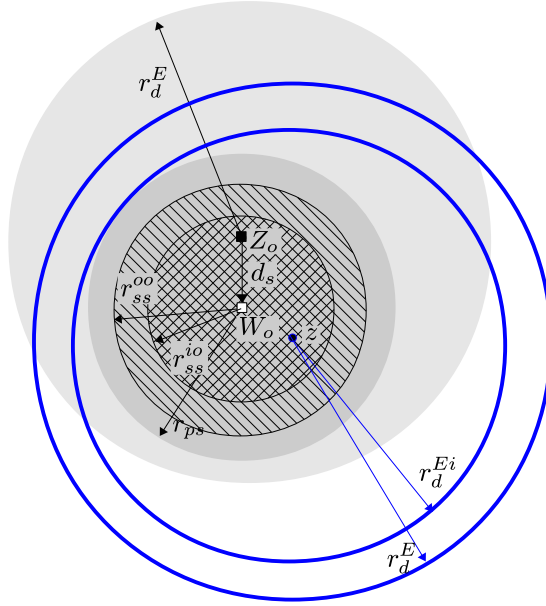


Figure 4.4: Conditioned that there are no PTxs in $b(Z_o, r_d^E) (\supset b(W_o, r_{ps}))$, an E-oSRx W_o can be interfered by potential E-oSTxs in $b(W_o, r_{ss}^{oo})$ or potential E-iSTxs in $b(W_o, r_{ss}^{io})$. Their activities are determined by surrounding PTxs in $b(z, r_d^E)$ for E-oSTxs and $b(z, r_d^{Ei})$ for E-iSTxs.

distance d_s away is given by

$$P_{out}^{soE}(\lambda_s) = 1 - \mathcal{L}_{\{a_o Q(r_{ss}^{oo}, \Pi_p^{(3)}, r_d^E) + a_i Q(r_{ss}^{io}, \Pi_p^{(3)}, r_d^{Ei})\}}(\lambda_s),$$

where $\Pi_p^{(3)} = \Pi_p \cap \overline{b(Z_o, r_d^E) \cup b(W_o, r_{ps})}$ and $Q(r, \Pi, t) \equiv \int_{b(W_o, r)} \mathbf{1}\{z \notin B(\Pi, t)\} dz$.

Proof is given in Appendix 4.11. We can again provide upper and lower bounds on P_{out}^{soE} which can be computed numerically, see Appendix 4.14, as follows.

Corollary 4. For given λ_p and λ_s , the upper and lower bounds of a E-oSRx's outage probability whose active associated E-oSTx is a distance d_s away are given as follows:

$$P_{out}^{soE,u}(\lambda_s) = 1 - \exp\{-\lambda_s q_E^o\} \quad \text{and}$$

$$P_{out}^{soE,l}(\lambda_s) = \frac{q_E^o}{q_m^o} (1 - \exp\{-\lambda_s q_m^o\}),$$

where $q_E^{oo} = \mathbb{E}_p[Q(r_{ss}^{oo}, \Pi_p^{(3)}, r_d^E)]$, $q_E^{io} = \mathbb{E}_p[Q(r_{ss}^{io}, \Pi_p^{(3)}, r_d^{Ei})]$, $q_E^o = a_o q_E^{oo} + a_i q_E^{io}$, and q_m^o is defined in Section 4.2.6.

Similarly, it is straightforward to compute $P_{out}^{siE}(\lambda_s)$ the outage probability of a typical E-iSRx. We omit it due to space limitations.

Fig.4.5 shows $P_{out}^{soE}(\lambda_s)$ and $P_{out}^{siE}(\lambda_s)$ the outage probabilities of a typical E-oSRx and E-iSRx respectively. They were evaluated under $\psi = -10\text{dB}$. As λ_s increases, both E-oSRxs and E-iSRxs are getting more interference from neighboring E-oSTxs and E-iSTxs, which accordingly increase the outage probabilities. Note that E-iSRxs get less interference, due to indoor shadowing, than E-oSRxs, so they see better (lower) outage probability.

Remark 4.4.1. We note that E-iSTx's having smaller outage probability than that of E-oSTx is phenomenon that occurs even under other white space detection techniques in Section 4.5 and 4.6 as long as $\psi < 1$. This lessens our burden on computing outage probabilities since we only care about the worst case outage probability. In fact, the maximum contention density of STxs under an outage constraint, which is computed in Section 4.7, is driven by the worst case outage probability. So, in the sequel, we will focus only on the outage probability for a typical outdoor nodes.

4.5 Performance of Positioning-assisted Technique

In this section, we evaluate the outage probabilities of a PRx, G-oSRx and G-iSTx. We assume a G-STx can access its exact location relative to PTxs using a geographic positioning module and determine whether to transmit or not. A G-STx can only transmit if it is outside of PTxs' coverage area. This is equivalent to G-STxs that are able to detect PTxs within a range r_d . We define following two processes Π_{so}^G and Π_{si}^G , denoting active G-oSTxs and G-iSTxs with densities $a_o\lambda_s\mathbf{1}\{z \notin B(\Pi_p, r_d)\}$ and $a_i\lambda_s\mathbf{1}\{z \notin B(\Pi_p, r_d)\}$ at $z \in \mathbf{R}^2$ respectively. The machinery used to find outage probabilities is similar to that used earlier for the densities of these two processes.

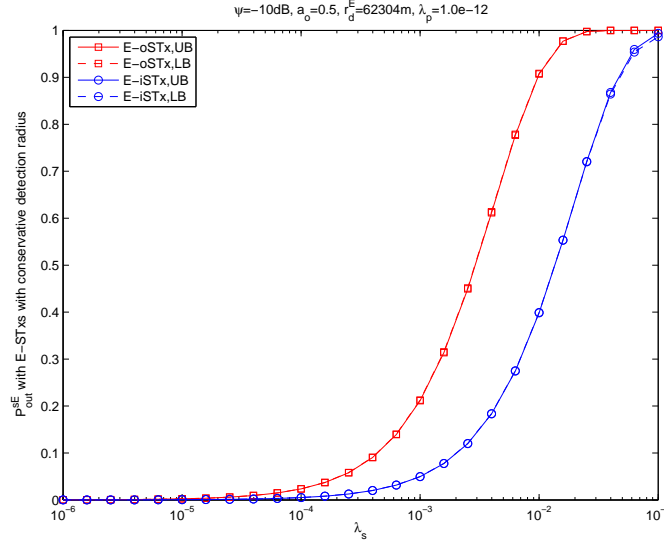


Figure 4.5: The outage probability of a typical E-oSTx and E-iSTx are shown. The gap between outage probability of E-oSTx and that of E-iSTx comes from the attenuated interference from outside to E-iSTxs.

4.5.1 Outage Probability of Primary Receiver

Since G-STxs are at least a distance r_d away from PRxs, they can not give harmful interference to PRxs. Thus, we have a simple result for the outage probability of a PRx.

Fact 5. *The outage probability of PRx with G-STxs is given as $P_{out}^{pG}(d) = 1 - \mathbf{1}\{d < d_p\}$ where d is the distance to its nearest PTx, and the fraction of \mathbf{R}^2 where potential PRxs can successfully receive PTxs' signal is given by $P_c^G(\lambda_p) = 1 - \mathbb{E}[P_{out}^{pG}(D)] = 1 - \exp\{-\lambda_p \pi d_p^2\}$.*

4.5.2 Outage Probability of Outdoor Secondary Receiver

In this section, we compute the outage probability P_{out}^{soG} of a typical G-oSRx W_o . This is a conditional outage probability conditioned on the existence of an active G-oSTx Z_o transmitting to the G-oSRx W_o . Note that Z_o is not necessarily the nearest G-oSTx to the W_o . This is the worst case outage probability since we fix $\|W_o - Z_o\|$

to d_s . For the G-oSTx Z_o to be active, there should be no PTxs within the G-oSTx's detection area; so, we condition on the event $Z_o \notin B(\Pi_p, r_d)$ and $\|W_o - Z_o\| = d_s$. Interference from other G-oSTxs and G-iSTxs to the G-oSRx W_o can cause the outage. The following theorem captures the impact of both PTxs, G-oSTxs, and G-iSTxs, on the outage of a typical G-oSRx W_o ; a proof is given in the Appendix 4.12.

Theorem 10. *(Conditional Outage Probability of G-oSRx) For a given λ_p and λ_s , the conditional outage probability of a G-oSRx at a distance d_s from its active associated G-oSTx is given by*

$$P_{out}^{soG}(\lambda_s) = 1 - \mathcal{L}_{\{a_o Q(r_{ss}^{oo}, \Pi_p^{(4)}, r_d) + a_i Q(r_{ss}^{io}, \Pi_p^{(4)}, r_d)\}}(\lambda_s),$$

where $\Pi_p^{(4)} = \Pi_p \cap \overline{b(Z_o, r_d) \cup b(W_o, r_{ps})}$ and $Q(r, \Pi, t) \equiv \int_{b(W_o, r)} \mathbf{1}\{z \notin B(\Pi, t)\} dz$.

Corollary 5. *For given λ_p and λ_s , the upper and lower bounds of a G-oSRx's outage probability are given as follows:*

$$P_{out}^{soG,u}(\lambda_s) = 1 - \exp\{-\lambda_s q_G^o\}, \quad \text{and}$$

$$P_{out}^{soG,l}(\lambda_s) = \frac{q_G^o}{q_m^o} (1 - \exp\{-\lambda_s q_m^o\})$$

where $q_G^{oo} = \mathbb{E}_p[Q(r_{ss}^{oo}, \Pi_p^{(4)}, r_d)]$, $q_G^{io} = \mathbb{E}_p[Q(r_{ss}^{io}, \Pi_p^{(4)}, r_d)]$ and $q_G^o = a_o q_G^{oo} + a_i q_G^{io}$.

The value of q_G^{oo} and q_G^{io} can be computed numerically, see Appendix 4.14. We omit the computation of P_{out}^{siG} the outage probability of a typical G-iSRx.

4.6 Performance of Receiver Location-Aware Technique

In this section, we consider the outage probabilities of a PRx and L-oSRx. Since L-STxs can detect the exact location of PRxs, they are allowed to transmit even if they lie within the coverage area of PTxs as long as neighboring PRxs are not harmed. We will set the detection radius for L-oSTx to $r_d^L = d_s + r_{ps}$, which accordingly determines the effective detection radius of L-iSTx as $r_d^{Li} = \psi^{\frac{1}{\alpha}} r_d^L$. Note that this

choice will ensure that L-STx protect its L-SRxs from hidden PTxs. Note that we have $r_d^L \ll r_d^E$, i.e., since we can detect and protect nearby PRxs directly r_d^L does not need to be as large as before.

4.6.1 Outage Probability of Primary Receiver

Since L-STxs do not give any harmful interference to PRxs, the outage probability of a PRx is given as follows:

Fact 6. *The outage probability of a PRx with L-STxs is given as $P_{out}^{pL}(d) = 1 - \mathbf{1}\{d \leq d_p\}$. And the fraction of \mathbf{R}^2 where potential PRxs can successfully receive STxs' signal is given as $P_c^L(\lambda_p) = 1 - \mathbb{E}[P_{out}^{pL}(D)] = 1 - \exp\{-\lambda_p \pi d_p^2\}$.*

4.6.2 Outage Probability of Secondary Receiver

In this section, we consider the outage probability of L-SRxs. As before, we focus on the outage probability of L-oSRx P_{out}^{sol} since it is higher than that of L-iSRxs. Note that L-oSTxs are allowed to transmit inside the coverage area of PTx, which makes P_{out}^{sol} for nodes inside the coverage area different than that of those which are outside. If an active L-oSRx is located within the coverage area of PTxs, then it is likely to have fewer potential interferers than an L-oSRx that is outside the coverage area. Indeed PRxs inside the coverage will suppress the activity of potential interferers L-STxs. By contrast there are no PRxs outside the coverage area, so L-oSRxs in this region are likely to see more interferers. To make this formal, we first define two subsets \mathcal{C}_o and \mathcal{N}_o of \mathbf{R} distinguishing two regions for L-oSRxs in terms of its distance to its nearest PTx d . If $d \in \mathcal{C}_o \equiv [r_{ps} + d_s, s_o)$, the L-oSRx is inside the PTx's coverage, while if $d \in \mathcal{N}_o \equiv [s_o, \infty)$, then it is outside. We have \mathcal{C}_o exclude $(0, r_{ps} + d_s)$ because if $d \in (0, r_{ps} + d_s)$, then the L-SRx will see an outage because it is too close to the PTx, i.e., this region is not of interest. The value s_o is a conservatively selected boundary for

the coverage area which is similar to d_p but smaller than d_p .⁷ In the sequel, when we compute the outage probability of a L-oSRx at distance d to its nearest PTx, we will suppose that if $d \in \mathcal{N}_i$ its associated L-oSTx and its potential secondary interferers see no surrounding PRxs ($\lambda_r = 0$) that they can interfere with, while if $d \in \mathcal{C}_o$, then the L-oSTx and its potential secondary interferers will see a non-zero uniform density of PRxs ($\lambda_r > 0$) they can interfere with. Note that introducing two sets \mathcal{N}_o and \mathcal{C}_o is a simplification since at the vicinity of d_p , there is a region where the density of PRx is non-uniform. By treating this intermediate region as outside of coverage, we simplify our computation. Also note that this is a conservative approximation since the computed outage probability under this assumption is higher than actual outage probability. Further details on the selection of s_o are explained in [66]. Using a similar argument for L-iSTx we can decide $\mathcal{C}_i = [r_{ps}^i + d_s, s_i)$, and $\mathcal{N}_i = [s_i, \infty)$, where s_i is the unique solution of $s_i + r_{ss}^{oi} + r_{sp}^i(d_p) = d_p$. Above observation is summarized as following fact.

Fact 7. *Let $P_{out}^{sol}(d)$ be the conditional outage probability of a L-oSRx at a distance d to its nearest PTx. Then, we have $P_{out}^{sol}(x) \leq P_{out}^{sol}(y)$ for any $x \in \mathcal{C}_o$ and $y \in \mathcal{N}_o$.*

This implies that fewer contending L-oSTxs are allowed outside of PTx's coverage area than inside. Since our focus is on the worst case, we only compute the outage probability of L-oSTxs in \mathcal{N}_o .

Before computing the outage probability, we let $\Pi_{s_o}^L$ and $\Pi_{s_i}^L$ denote Cox processes modeling L-oSTxs and L-iSTxs with densities

$$a_o \mathbf{1} \{T_o(z, \Pi_r)\} \mathbf{1} \{z \notin B(\Pi_p, r_d^L)\} \quad \text{and} \quad a_i \mathbf{1} \{T_i(z, \Pi_r)\} \mathbf{1} \{z \notin B(\Pi_p, r_d^{Li})\}$$

at $z \in \mathbf{R}^2$ respectively, where $T_o(z, \Pi_r)$ is an event defined as

$$T_o(z, \Pi_r) \equiv \left\{ \begin{array}{l} \text{L-oSTx at } z \text{ does not detect PRxs in } \Pi_r \\ \text{that it could potentially interfere with} \end{array} \right\}.$$

⁷Specifically, s_o is the unique solution of $s_o + r_{ss}^{oo} + r_{sp}(d_p) = d_p$, see [66] for further detail.

Note that $\mathbf{1}\{T_o(z, \Pi_r)\}$ is a random variable which is a function of $z \in \mathbf{R}^2$ and Π_r . If the distance between z and its nearest PTx belongs to \mathcal{N}_o , we have $\mathbf{1}\{T_o(z, \Pi_r)\} = 1$ with probability 1. Also the event $T_i(z, \Pi_r)$ can be defined in similar way and we have $\mathbf{1}\{T_i(z, \Pi_r)\} = 1$ for z whose distance to its nearest PTx belongs to \mathcal{N}_i . Then, the outage probability of a L-oSRx distance $d \in \mathcal{N}_o$ away from its nearest PTx is given in the following theorem, which is proven in the Appendix 4.13.

Theorem 11. *(Conditional Outage Probability of L-oSRx) For given λ_p and λ_s , the outage probability of a L-oSRx a distance $d \in \mathcal{N}_o$ away from its nearest PTx is given as follows:*

$$P_{out}^{soL}(d, \lambda_s) = 1 - \mathcal{L}_{\{a_o Q(r_{ss}^{oo}, \Pi_p^{(5)}, r_d^L) + a_i Q(r_{ss}^{io}, \Pi_p^{(5)}, r_d^{Li})\}}(\lambda_s)$$

where $\Pi_p^{(5)} = \Pi_p \cap \overline{b(Z_o, r_d^L) \cup b(W_o, s_o)}$, and $Q(r, \Pi, t) \equiv \int_{b(W_o, r)} \mathbf{1}\{z \notin B(\Pi, t)\} dz$.

We provide the upper and lower bounds of $P_{out}^{soL}(d)$.

Corollary 6. *For given λ_p and λ_s , upper and lower bounds on the outage probability of a L-oSRx a distance $d \in \mathcal{N}_o$ away from its nearest PTx are given as*

$$P_{out}^{soL,u}(d, \lambda_s) = 1 - \exp\{-\lambda_s q_L^o\} \quad \text{and} \quad (4.7)$$

$$P_{out}^{soL,l}(d, \lambda_s) = \frac{q_L^o}{q_m^o} (1 - \exp\{-\lambda_s q_m^o\}), \quad (4.8)$$

where $q_L^o = a_o q_L^{oo} + a_i q_L^{io}$, $q_L^{oo} = \mathbb{E}[Q(r_{ss}^{oo}, \Pi_p^{(5)}, r_d^L)]$ and $q_L^{io} = \mathbb{E}[Q(r_{ss}^{io}, \Pi_p^{(5)}, r_d^{Li})]$.

q_L^{oo} and q_L^{io} can be computed numerically, see Appendix 4.14.

Fact 8. *Note that for $d \in \mathcal{N}_o$, we have $q_L^{oo} = q_m^{oo}$, and $q_L^{io} = q_m^{io}$, since q_m^{oo} and q_m^{io} are constants, consequently the upper and lower bounds of P_{out}^{soL} are not affected by d as P_{out}^{soE} and P_{out}^{soG} aren't.*

Using a similar approach, we can also compute the outage probability of L-iSRx $P_{out}^{siL}(d)$.

4.7 Maximum Contention Density for Secondary Nodes given ϵ -outage constraint

In this section, we will find the maximum contention densities of STxs for each white space detection technique under an ϵ -outage constraint where $0 < \epsilon < 1$ and $\bar{\epsilon} = 1 - \epsilon$. This density maximizes the number of concurrent active STxs while keeping the outage probability of SRxs below ϵ for a given λ_p and a_o . In the process, we will take the minimum of the outdoor and indoor contention densities, because we need to satisfy the outage constraint for both indoor and outdoor nodes.

4.7.1 Density for E-STx

Given outage probabilities $P_{out}^{soE}(\lambda_s)$ and $P_{out}^{siE}(\lambda_s)$ obtained for E-oSRx and E-iSRx respectively, the maximum contention density for E-SRx which guarantees $P_{out}^{soE}(\lambda_s) \leq \epsilon$ and $P_{out}^{siE}(\lambda_s) \leq \epsilon$ is defined as $\lambda_s^{\epsilon E} \equiv \min \{ \lambda_{so}^{\epsilon E}, \lambda_{si}^{\epsilon E} \}$, where we have $\lambda_{so}^{\epsilon E} \equiv \max \{ \lambda_s | P_{out}^{soE}(\lambda_s) \leq \epsilon \}$ and $\lambda_{si}^{\epsilon E} \equiv \max \{ \lambda_s | P_{out}^{siE}(\lambda_s) \leq \epsilon \}$. We note that since interference is attenuated indoor, we can show $\lambda_{so}^{\epsilon E} \leq \lambda_{si}^{\epsilon E}$, and accordingly we have $\lambda_s^{\epsilon E} = \lambda_{so}^{\epsilon E}$. Upper and lower bounds on $\lambda_{so}^{\epsilon E}$ are given as follows:

$$\begin{aligned} \lambda_{so}^{\epsilon E, u} &\equiv \max \left\{ \lambda_s | P_{out}^{soE, l}(\lambda_s) \leq \epsilon \right\} = -\frac{1}{q_m^o} \log \left(1 - \frac{q_m^o}{q_E^o} \epsilon \right), \\ \lambda_{so}^{\epsilon E, l} &\equiv \max \left\{ \lambda_s | P_{out}^{soE, u}(\lambda_s) \leq \epsilon \right\} = -\frac{\log \bar{\epsilon}}{q_E^o}. \end{aligned}$$

Note that $\lambda_s^{\epsilon E}$ is a function of λ_p .

4.7.2 Density for G-STx

For the given outage probabilities $P_{out}^{soG}(\lambda_s)$ and $P_{out}^{siG}(\lambda_s)$ obtained for G-oSRx and G-iSRx respectively, the maximum contention density for G-STxs which guarantees $P_{out}^{soG}(\lambda_s) \leq \epsilon$ and $P_{out}^{siG}(\lambda_s) \leq \epsilon$ is given by $\lambda_s^{\epsilon G} \equiv \min \{ \lambda_{so}^{\epsilon G}, \lambda_{si}^{\epsilon G} \}$ where $\lambda_{so}^{\epsilon G} \equiv \max \{ \lambda_s | P_{out}^{soG}(\lambda_s) \leq \epsilon \}$ and $\lambda_{si}^{\epsilon G} \equiv \max \{ \lambda_s | P_{out}^{siG}(\lambda_s) \leq \epsilon \}$. Analogously with the previous case, we can show that $\lambda_{so}^{\epsilon G} \leq \lambda_{si}^{\epsilon G}$, and accordingly we have $\lambda_s^{\epsilon G} = \lambda_{so}^{\epsilon G}$.

Upper and lower bounds of $\lambda_{so}^{\epsilon G}$ are given by

$$\begin{aligned}\lambda_{so}^{\epsilon G,u} &\equiv \max \left\{ \lambda_s | P_{out}^{soG,l}(\lambda_s) \leq \epsilon \right\} = -\frac{1}{q_m^o} \log \left(1 - \frac{q_m^o}{q_G^o} \epsilon \right), \\ \lambda_{so}^{\epsilon G,l} &\equiv \max \left\{ \lambda_s | P_{out}^{soG,u}(\lambda_s) \leq \epsilon \right\} = -\frac{\log \bar{\epsilon}}{q_G^o}.\end{aligned}$$

Note that $\lambda_s^{\epsilon G}$ is a function of λ_p .

4.7.3 Density for L-STx

Note that in Section 4.6, we found the outage probability for a L-oSRx as a function of its distance d from its closest PTx, so the corresponding contention density will be also a function of d . For the outage probabilities $P_{out}^{soL}(\lambda_s)$ and $P_{out}^{siL}(\lambda_s)$ obtained for L-oSRx and L-iSRx respectively, the maximum contention density $\lambda_s^{\epsilon L}$ is defined as $\lambda_s^{\epsilon L} \equiv \min \left\{ \min_{d \in \mathcal{C}_o \cup \mathcal{N}_o} \lambda_{so}^{\epsilon L}(d), \min_{d \in \mathcal{C}_i \cup \mathcal{N}_i} \lambda_{si}^{\epsilon L}(d) \right\}$, where $\lambda_{so}^{\epsilon L}(d) \equiv \max \left\{ \lambda_s | P_{out}^{soL}(d, \lambda_s) \leq \epsilon \right\}$ and $\lambda_{si}^{\epsilon L}(d) \equiv \max \left\{ \lambda_s | P_{out}^{siL}(d, \lambda_s) \leq \epsilon \right\}$. Fact 7 implies that $\lambda_{so}^{\epsilon L}(x) \geq \lambda_{so}^{\epsilon L}(y)$ for $x \in \mathcal{C}_o$ and $y \in \mathcal{N}_o$, and $\lambda_{si}^{\epsilon L}(x) \geq \lambda_{si}^{\epsilon L}(y)$ for $x \in \mathcal{C}_i$ and $y \in \mathcal{N}_i$. It follows once again that $\lambda_{so}^{\epsilon L}(d) \leq \lambda_{si}^{\epsilon L}(d)$. By Fact 8, it turns out that $\lambda_s^{\epsilon L} = \lambda_{so}^{\epsilon L}$ is not a function of d . Upper and lower bounds of $\lambda_{so}^{\epsilon L}$ are defined as

$$\begin{aligned}\lambda_{so}^{\epsilon L,u} &\equiv \max \left\{ \lambda_s | P_{out}^{soL,l}(\lambda_s) \leq \epsilon \right\} = -\frac{1}{q_m^o} \log \left(1 - \frac{q_m^o}{q_L^o} \epsilon \right), \\ \lambda_{so}^{\epsilon L,l} &\equiv \max \left\{ \lambda_s | P_{out}^{soL,u}(\lambda_s) \leq \epsilon \right\} = -\frac{\log \bar{\epsilon}}{q_L^o}.\end{aligned}$$

Note that $\lambda_s^{\epsilon L}$ is a function of λ_p .

4.8 Joint Network Capacity Region

In this section, we define and compute the capacity of primary and secondary networks using the outage probability and contention densities computed in the previous sections. This will enable us to compute the joint network capacity region exhibiting trade-offs between the two networks.

4.8.1 Broadcast Coverage Capacity of Primary Network

The capacity of the primary network coexisting with E-STxs is defined as the mean number of bits that can be successfully received by potential PRxs per second per meter square per Hertz. It is given as b_p times the fraction of effectively covered area by PTxs in (4.7) as follows:

$$C_1^E(\lambda_p, \psi) = b_p P_c^E(\lambda_p, \lambda_s^{\epsilon E}, \psi).$$

Similarly, the capacity of primary network with G-STxs and L-STxs can be computed using P_c^G and P_c^L , they are denoted C_1^G and C_1^L respectively.

4.8.2 Transmission Capacity of Secondary Network

The notion of capacity for secondary network, which we adopt from [13, 113], is the transmission capacity measuring the average number of successfully transmitted bits per square meter per Hertz.

Transmission Capacity of Secondary Network with E-STxs For given λ_p and a_o , the capacity of a secondary network with E-STxs is defined as the sum of outdoor and indoor transmission capacities C_2^{Eo} and C_2^{Ei} :

$$\begin{aligned} C_2^E(\lambda_p, \psi, a_o) &= C_2^{Eo} + C_2^{Ei} \\ &= b_s a_o \lambda_s^{\epsilon E} P_{tx}^{Eo} \bar{\epsilon} + b_s a_i \lambda_s^{\epsilon E} P_{tx}^{Ei} \bar{\epsilon}, \end{aligned}$$

where $P_{tx}^{Eo} = \exp\{-\lambda_p \pi (r_d^E)^2\}$ and $P_{tx}^{Ei} = \exp\{-\lambda_p \pi (r_d^{Ei})^2\}$ are the transmission probabilities of a typical E-oSTx and E-iSTx respectively. Recall that for an E-oSTx (E-iSTx) to transmit it should detect the absence of PTxs in its corresponding detection region. A larger detection radius is good to protect PRxs and its intended SRx but reduces exponentially its transmission opportunity. Note that $\lambda_s^{\epsilon E}$ is also a function of λ_p .

Transmission Capacity of Secondary Network with G-STxs For a given λ_p and a_o , the capacity of a secondary network with G-STxs is defined as the sum of outdoor and indoor transmission capacities C_2^{Go} and C_2^{Gi} respectively:

$$\begin{aligned} C_2^G(\lambda_p, \psi, a_o) &= C_2^{Go} + C_2^{Gi} \\ &= b_s a_o \lambda_s^{\epsilon G} P_{tx}^{Go} \bar{\epsilon} + b_s a_i \lambda_s^{\epsilon G} P_{tx}^{Gi} \bar{\epsilon}, \end{aligned}$$

where $P_{tx}^{Go} = \exp\{-\lambda_p \pi r_d^2\}$ and $P_{tx}^{Gi} = \exp\{-\lambda_p \pi r_d^2\}$ are the transmission probabilities of G-oSTx and G-iSTx respectively. Note that $\lambda_s^{\epsilon G}$ is a function of λ_p .

Transmission Capacity of Secondary Network with L-STxs For a given λ_p , λ_r , and a_o , the capacity of a secondary network with L-STxs is defined as the expected value of the sum of two transmission capacities:

$$C_2^L(\lambda_p, \lambda_r, \psi, a_o) = C_2^L = \mathbb{E}[C_2^{Lo}(D) + C_2^{Li}(D)],$$

where $C_2^{Lo}(D) \equiv b_s a_o \lambda_s^{\epsilon L} P_{tx}^{Lo}(D) \bar{\epsilon}$ and $C_2^{Li}(D) \equiv b_s a_i \lambda_s^{\epsilon L} P_{tx}^{Li}(D) \bar{\epsilon}$ are the conditional capacities of a L-oSRx and a L-iSRx when they are located at distance D from its nearest PTx. Note that $\lambda_s^{\epsilon L}$ is not a function of D . The expected value can be computed as follows:

$$\begin{aligned} \mathbb{E}[C_2^{Lo}(D)] &= \sum_{\mathcal{A} \in \{\mathcal{C}_o, \mathcal{N}_o\}} \mathbb{E}[C_2^{Lo}(D) | D \in \mathcal{A}] P(D \in \mathcal{A}) \\ &= b_s a_o \lambda_s^{\epsilon L} \bar{\epsilon} \sum_{\mathcal{A} \in \{\mathcal{C}_o, \mathcal{N}_o\}} \mathbb{E}[P_{tx}^{Lo}(D) | D \in \mathcal{A}] P(D \in \mathcal{A}) \\ &= b_s a_o \lambda_s^{\epsilon L} \bar{\epsilon} (P_{tx}^{Loc} P(D \in \mathcal{C}_o) + P_{tx}^{Lon} P(D \in \mathcal{N}_o)), \end{aligned}$$

Similarly, we have

$$\mathbb{E}[C_2^{Li}(D)] = b_s a_i \lambda_s^{\epsilon L} \bar{\epsilon} (P_{tx}^{Lic} P(D \in \mathcal{C}_i) + P_{tx}^{Lin} P(D \in \mathcal{N}_i)),$$

where, P_{tx}^{Loc} , P_{tx}^{Lon} , P_{tx}^{Lic} and P_{tx}^{Lin} are conditional transmission probabilities of L-oSTx when $d \in \mathcal{C}_o$ and $d \in \mathcal{N}_o$ and that of L-iSTx when $d \in \mathcal{C}_i$ and $d \in \mathcal{N}_i$ respectively. They are computed as $P_{tx}^{Loc} = \mathbb{E}[\exp\{-\lambda_r \pi r_{sp}^2(D)\} | D \in \mathcal{C}_o]$, and $P_{tx}^{Lic} =$

$\mathbb{E}[\exp\{-\lambda_r \pi (r_{sp}^i(D))^2\} | D \in \mathcal{C}_i]$ and $P_{tx}^{Lon} = P_{tx}^{Lin} = 1$. These can be numerically computed since distribution of D is known. And, it is straightforward to find $P(D \in \mathcal{C}_o)$, $P(D \in \mathcal{N}_o)$, $P(D \in \mathcal{C}_i)$ and $P(D \in \mathcal{N}_i)$.

4.8.3 Joint Network Capacity Region

We define the joint network capacity region when secondary nodes using simple signal energy detection method as the set of achievable capacities for the primary and secondary networks, which is given as

$$\Lambda^E(\psi, a_o) \equiv \{ (x, y) \in \mathbf{R}^2 | \exists \lambda_p \geq 0, \text{ s.t.} \\ x = C_1^E(\lambda_p, \psi, a_o), 0 \leq y \leq C_2^E(\lambda_p, \psi, a_o) \}.$$

The joint network capacity regions for positioning-assisted and receiver location-aware techniques are denoted as $\Lambda^G(\psi, a_o)$ and $\Lambda^L(\lambda_r, \psi, a_o)$ respectively, that are similarly defined. Note that we have lower and upper bounds on the contention density rather than an exact value, so we get the lower (inner) and upper (outer) bounds on the capacity and joint network capacity region by replacing $\lambda_s^{\epsilon E}$ with $\lambda_s^{\epsilon E, u}$ or $\lambda_s^{\epsilon E, l}$. This also applies to other cases. In Figs.7-9, we only draw the lower bounds of joint network capacity regions since upper bounds are almost on top of associated lower bounds. In all cases $\epsilon = 0.1$ was used.

Impact of indoor shadowing (signal energy detection technique) Let us consider the impact of indoor shadowing on the joint network capacity region of two networks under the signal energy detection method. Fig.4.6a shows the joint network capacity regions under various values of indoor shadowing ψ . We make following interesting observations. If the primary network is sparse, in the regime with relatively low C_1 , as the shadowing level increases (i.e., ψ decreases), the capacity C_2 increases, further increases of ψ eventually decrease C_2 , that is $C_2(\lambda_p, \psi)$ has its maximum value at some ψ^* which is the function of C_1 . While if the primary network is dense, there

is not much change in capacity. This can be explained in following ways. As the level of indoor shadowing increases, the E-oSRxs receive less interference from E-STxs, which decreases the outage probability of E-oSRx and eventually leads to an higher contention density. It contributes to capacity as a *gain*. But simultaneously we also have a *loss*, which comes from the decreasing transmission probability caused by over-conservatively increasing detection radius. It discourages the transmission attempts of E-oSTxs and have a negative impact on capacity. The capacity increases if the increase of contention density dominates the decrease of transmission probability. And, the capacity decreases otherwise. Consider increasing shadowing level, then, the point that the loss dominates the gain comes late as the primary network gets sparse since the more sparse the primary network is, the more E-oSTxs it can accommodate. So, capacity C_2 in sparse network has its maximum at a certain ψ value. While, in dense network, both the gain and loss are comparable and are balanced so there is not much change in capacity.

Impact of indoor shadowing (positioning-assisted technique) We consider the impact of indoor shadowing on the joint network capacity region under positioning method, see Fig.4.6b. In this case, the joint network capacity region strictly increases as shadowing level increases. This is explained as follows. Recall that the detection performance of the positioning assisted method is not affected by indoor shadowing, so they can correctly detect the existence of PTxs within their detection radius r_d . Thus, there is no loss in transmission probability. However, the level of interference from other nodes is affected by the indoor shadowing level ψ . It turns out that there is only *gain* without *loss* as compared to signal energy detection case. In fact, as the shadowing level increases, G-oSRxs get less interference from G-iSRxs due to strong attenuation, which eventually allows a higher maximum contention density. Thus, we have only *gain*, which results in a strict increase of C_2 with ψ for all C_1 . The actual *gain of indoor shadowing* depends on the level of indoor shadowing, e.g. when

$\psi = -10\text{dB}$, the gain (compared to $\psi = 0\text{dB}$ case) is approximately 66% and when $\psi = -20\text{dB}$, the gain is roughly 200%. If $\psi \rightarrow -\infty\text{dB}$, then, the G-SRxs are free from interference from G-iSRxs and their performance is constrained by their self interference from G-oSTxs to G-oSRxs.

Impact of indoor shadowing (receiver location-aware technique) Fig.4.7a shows the joint network capacity region of the receiver location-aware method under $\lambda_r = 10^{-4}m^{-2}$. Due to the receiver detection function, more L-STxs can be active (even inside the coverage). This significantly increases the joint network capacity region. The same argument on decreased interference and resulting increased maximum density applies here. One interesting observation is that there exists a regime where both primary and secondary capacity increases together. This happens when the density of PTxs is very high. In this case L-STxs are more likely to succeed in their transmissions, since L-STxs close to PTxs require smaller region to be PRx free. Recall that those PRxs close to PTxs are receiving strong signals from PTxs, so it is hard for L-STxs to harm them. This allows a larger number of L-STxs be active close to PTxs than at the edge of the PTxs' coverage area. Fig.4.2c depicts this situation.

Note, however, that a further increase in λ_p forces C_2 to 0. This happens because once λ_p is large enough the entire \mathbf{R}^2 plane is covered by $B(\Pi_p, d_p)$ and C_1 reaches its limit 3.5. Further increases in λ_p increase the region $B(\Pi_p, r_d^{Li}) = \cup_{X \in \Pi_p} b(X, r_d^{Li})$ where no L-STxs are allowed to transmit. Note that $r_d^{Li} \ll d_p$ and STxs can potentially interfere with PRxs if they are located inside $B(\Pi_p, r_d^{Li})$. This reduces white space available to L-STxs, and accordingly C_2 eventually reaches 0. The *gain of shadowing* depends on the level of indoor shadowing, e.g. when $\psi = -10\text{dB}$ gain (compared to $\psi = 0\text{dB}$ case) is approximately 66% and when $\psi = -20\text{dB}$, the gain is roughly 200%. As $\psi \rightarrow -\infty\text{dB}$, interference from indoor devices to outdoor devices decreases, and the secondary capacity is limited by the self interference of L-oSTxs. The joint network capacity region is also affected by the density of primary receiver

λ_r as shown in Fig.4.7b . If $\lambda_r = 0$, then, the activity of L-STxs are hardly affected except the extreme case when $C_1 \sim 3.5$. As λ_r increases, L-STxs lose their transmission opportunities and accordingly secondary capacity decreases. If λ_r is very high, e.g, more than 10^{-2} , then, almost no L-STxs are allowed to transmit inside PTxs' coverage area. The joint network capacity region of this case is equivalent to that of the positioning-assisted technique. Thus, the capacity trade-off is almost linear.

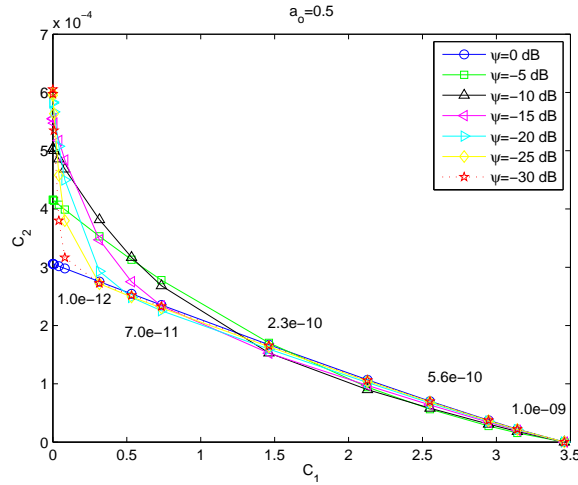
Impact of the Fraction of Indoor Nodes The fraction of indoor nodes $a_i = 1 - a_o$ has a direct impact on capacity. Let us consider how the joint network capacity region changes as a function of a_o . Fig.4.8a-4.8b show the joint network capacity region for two extreme situations, where $a_o = 1$ and $a_o = 0$ respectively. The case where $a_o = 0.5$ was shown in Fig.4.1. The indoor shadowing level ψ is fixed to -10 dB. The shapes of network capacity regions for $a_o = 1$ and $a_o = 0.5$ are similar to each other but the network capacity region for $a_o = 0$ is larger than that for $a_o = 1$. In Fig.4.8a, we have E-oSTxs using a very conservative detection radius, which makes them inefficiently utilize white space⁸. As the portion of indoor nodes a_i increases (or a_o decreases), iSTxs make less interference and oSTxs' outage probability decreases, which eventually allows a higher maximum contention density. C_2 increases and accordingly joint network capacity region is extended. At the other extreme with no outdoor nodes ($a_o = 0$), we have the same joint network capacity region for signal energy detection technique and positioning-assisted technique since there no longer are E-oSTxs which use white spectrum inefficiently. Note that the overall network capacity region is again significantly increased as compared to the case where $a_o = 1$. When $a_o = 0.5$, as shown in Fig.4.1, the gain of positioning-assisted technique to signal energy detection technique is 76% and that of receiver location-aware technique is

⁸Note that if an operator knows that there is no L-iSTxs at all, then they don't need to use conservative detection radii. Case $a_o = 1$ should be understood as the case where we have extremely small number of E-iSTxs while most are E-oSTxs. Their detection radii are set conservatively considering the E-iSTxs.

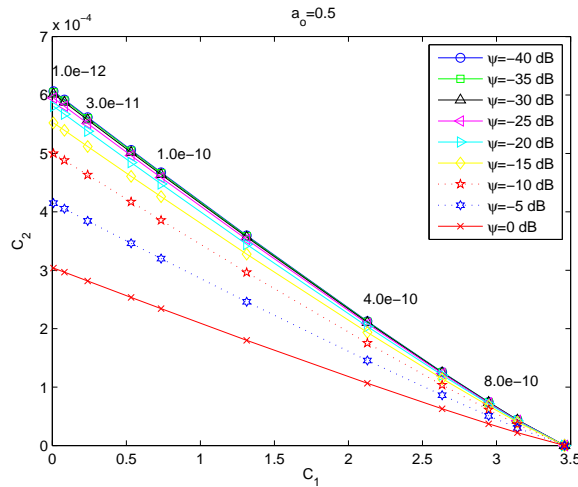
177% when $\lambda_p = 2 \times 10^{-10} m^{-2}$. This gain can be increased further in denser primary networks. From the above two observations, we conclude that indoor shadowing, which is a source of uncertainty from signal energy detection point of view, can increase the capacity of cognitive networks. If cognitive devices can access some knowledge on their environment or additional information they can best utilize the shadowing to improve network capacity.

4.9 Conclusion

In this chapter, we have *quantified* the gain of three different white space detection techniques with varying degrees of RF-environment awareness under an indoor shadowing environment. Using a simple stochastic geometric model where primary and secondary nodes were modeled as Poisson point processes, we derived the joint network capacity region of two networks. It turned out that when ad hoc cognitive networks used the signal energy detection method, indoor shadowing was a source of uncertainty that could either increase or decrease the capacity of networks. However, if secondary devices had a little bit of knowledge of the environment (shadowing), then, the shadowing became the source of “hidden” capacity, i.e., they were able to achieve a significantly higher capacity in a shadowing environment. We noted that the receiver location-aware white space detection technique was by far the most promising way of detecting and filling spatial white space, while positioning-assisted technique, which still results in a large improvement over signal energy detection scheme, was inferior than receiver location-aware technique. Our results showed that enabling cognitive devices to be aware of the locations of the PRxs will lead to significant performance gains depending on the density of PRx’s.

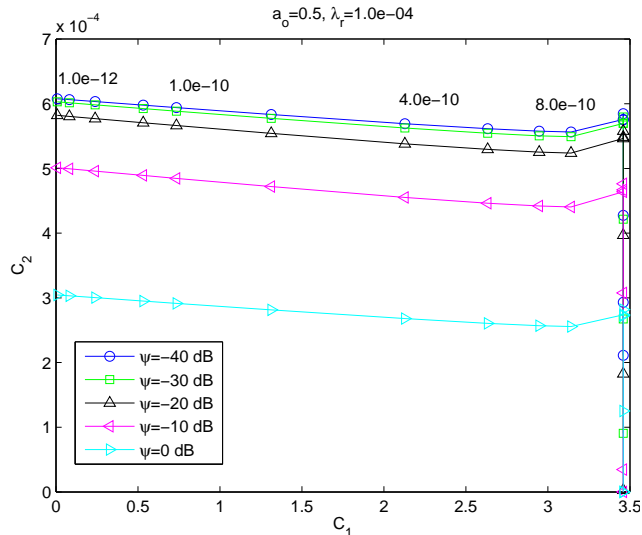


(a) joint network capacity regions under the signal energy detection method were shown for various values of indoor shadowing level ψ . If $\psi = 0$ dB, then the we have roughly linear tradeoff. As the shadowing level increases (as ψ decreases), network capacity region increases but after a certain point, it decreases.

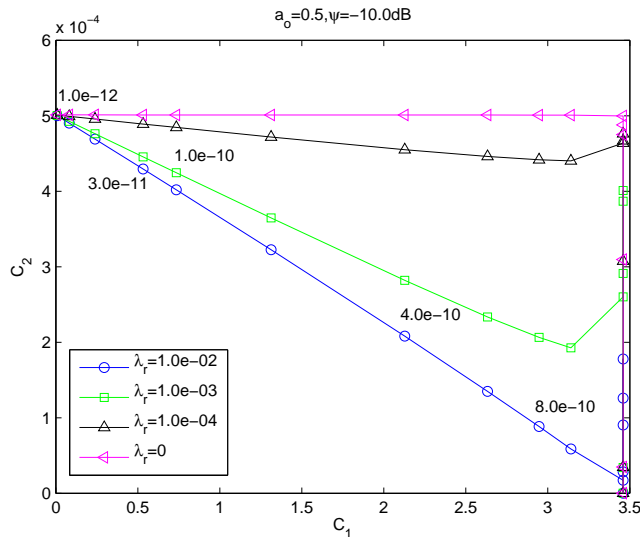


(b) Joint network capacity regions under the positioning-assisted method were shown for various values of indoor shadowing level ψ . The network capacity region increases strictly in ψ for all C_1 as the shadowing level increases.

Figure 4.6: Joint network capacity regions of signal energy detection method (left) and positioning-assisted method (right) under various indoor shadowing level ψ with fixed $a_o = 0.5$. The numbers above/below markers in graphs denote the density of PTxs λ_p at the collection of markers with the similar C_1 values.

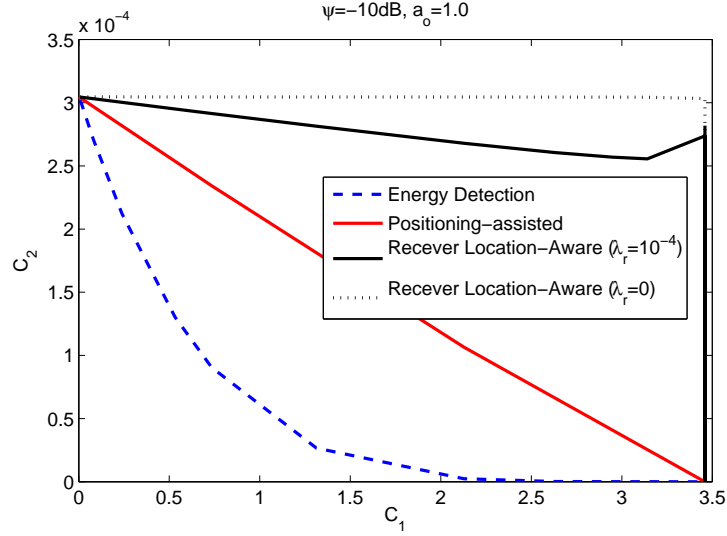


(a) Joint network capacity regions under the receiver location-aware method were shown for various values of indoor shadowing level ψ and $\lambda_r = 10^{-4}$. Increasing indoor shadowing increases the joint network capacity region. For fixed ψ , the shape of joint network capacity region depends on the density of PRxs (see right figure).

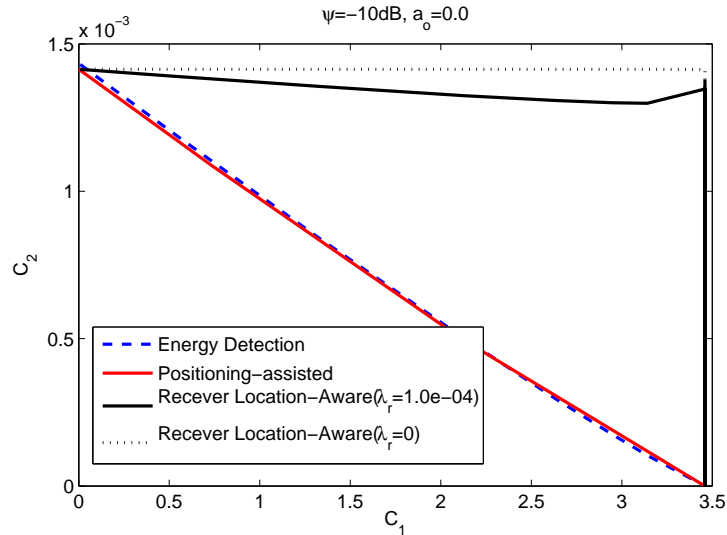


(b) The joint network capacity regions of receiver location-aware technique were shown for various values of primary receiver density λ_r . The joint network capacity region is maximized when $\lambda_r = 0$ and shrinks as λ_r increases.

Figure 4.7: Joint network capacity regions under receiver location-aware technique. The numbers above markers in graphs denotes the density of PTxs λ_p at the collection of markers with the similar C_1 values.



(a) Joint network capacity region when all cognitive devices are outdoor devices ($a_o = 1$). The joint network capacity regions are smaller than $a_o = 0.5$ case in Fig.4.1.



(b) Joint network capacity region when all cognitive devices are indoor devices ($a_o = 0$). The joint network capacity regions are larger than $a_o = 0.5$ case in Fig.4.1.

Figure 4.8: Joint network capacity region under various a_o with $\psi = -10\text{dB}$. Case $a_o = 0.5$ is shown in Fig.4.1.

4.10 Appendix : Proof of Theorem 7

Proof. We define following for notational simplicity:

$$\begin{aligned}
K_1 &\equiv K(X, r_d; Y, r_{sp}(d)) \quad \text{and} \quad K_2 \equiv K(X, r_d^i; Y, r_{sp}^i(d)), \\
A &\equiv \{Y \text{ not interfered by active E-STxs}\} \\
&= \{Y \notin B(\Pi_{so}^D, r_{sp}), Y \notin B(\Pi_{si}^D, r_{sp}^i)\} \\
B &\equiv \{\|X - Y\| = d\}.
\end{aligned}$$

Suppose that a PRx Y is located a distance $d \leq d_p$ from its nearest PTx X as shown in Fig.4.9a. Conditioning on this event means that there are no PTx within $b(Y, d)$; this is exhibited as a shaded disc in Fig. 4.9a. The PRx Y can be interfered by potential E-oSTxs in K_1 and E-iSTxs in K_2 . Note, however, that not all E-STxs in K_1 and K_2 are active since to be active they require a PTx free area around them. For example, in Fig.4.9a, an E-oSTx z requires the region $b(z, r_d)$ be PTx free. Similarly, an E-iSTx z requires the region $b(z, r_d^i)$ be PTx free. So, the conditional outage probability given the event B is given by $P_{out}^p(d) = P(Y \text{ fails to rcv} | B) = 1 - P(A|B)$, where $P(A|B)$ is computed as follows:

$$\begin{aligned}
P(A|B) &\stackrel{a}{=} \mathbb{E}[P(A|B, \Pi_p) | B] \\
&\stackrel{b}{=} \mathbb{E}[P(Y \notin B(\Pi_{so}^D, r_{sp}) | B, \Pi_p) P(Y \notin B(\Pi_{si}^D, r_{sp}^i) | B, \Pi_p) | B] \\
&\stackrel{c}{=} \mathbb{E}\left[\exp\left\{-\int_{K_1} a_o \lambda_s \mathbf{1}\{z \notin B(\Pi_p^{(2)}, r_d)\} dz\right\} \times \right. \\
&\quad \left. \exp\left\{-\int_{K_2} a_i \lambda_s \mathbf{1}\{z \notin B(\Pi_p^{(2)}, r_d^i)\} dz\right\} \middle| B\right] \\
&\stackrel{d}{=} \mathbb{E}\left[\exp\left\{-\lambda_s (a_o L_1(d, \Pi_p^{(2)}) + a_i L_2(d, \Pi_p^{(2)}))\right\}\right]
\end{aligned}$$

In $\stackrel{a}{=}$, we conditioned on Π_p , since event A depends on Π_p (note that Π_{so}^D and Π_{si}^D are processes depending on Π_p). In $\stackrel{b}{=}$, we used the fact that the events $\{Y \notin B(\Pi_{so}^D, r_{sp})\} = \{\Pi_{so}^D \cap b(Y, r_{sp}) = \emptyset\}$ and $\{Y \notin B(\Pi_{si}^D, r_{sp}^i)\} = \{\Pi_{si}^D \cap b(Y, r_{sp}^i) = \emptyset\}$ are conditionally independent given Π_p . In other words, for given primary transmitters' locations,

the locations of active indoor nodes and outdoor nodes are independent. In $\stackrel{c}{=}$, the two outage probabilities are given as the void probabilities of random areas which should not be covered by PTx process $\Pi_p^{(2)}$ out of K_1 and K_2 respectively. For simplicity we define $\Pi_p^{(2)}$ as Π_p conditioned on B . In $\stackrel{d}{=}$, the expectation \mathbb{E} is w.r.t. to a new conditioned random process $\Pi_p^{(2)}$, so we remove conditioning. If $d > d_p$, the PRx is out of PTx coverage area, so $P_{out}^p(d) = 0$. \square

4.11 Appendix : Proof of Theorem 9

Proof. Suppose that an E-oSTx Z_o detects the absence of PTxs in its detection range $b(Z_o, r_d^E)$ as shown in Fig.4.4. Consider Z_o 's intended receiver E-oSRx W_o which is a distance d_s from Z_o . Then, the conditional outage probability P_{out}^{soE} is given as

$$P(W_o \text{ fails to rcv} | Z_o \text{ txmits, } \|Z_o - W_o\| = d_s). \quad (4.9)$$

For notational simplicity we define following three events:

$$\begin{aligned} D &\equiv \{W_o \text{ not interfered by active STxs}\} = \{W_o \notin B(\Pi_{so}^E, r_{ss}^{oo}), W_o \notin B(\Pi_{si}^E, r_{ss}^{io})\}, \\ E &\equiv \{W_o \text{ not interfered by PTx}\} = \{W_o \notin B(\Pi_p, r_{ps})\}, \text{ and} \\ F &\equiv \{Z_o \text{ not detect PTx in } b(Z_o, r_d^E)\} = \{Z_o \notin B(\Pi_p, r_d^E)\}. \end{aligned}$$

Then, P_{out}^{soE} can be written as $P_{out}^{soE} \stackrel{a}{=} 1 - P(W_o \text{ rcvs} | F) = 1 - P(D|EF)P(E|F)$ where in $\stackrel{a}{=}$, we omitted conditioning on $\{\|Z_o - W_o\| = d_s\}$ for notational simplicity. $P(E|F)$ and $P(D|EF)$ can be computed as follows:

$$\begin{aligned} P(E|F) &= P(W_o \notin B(\Pi_p, r_{ps}) | Z_o \notin B(\Pi_p, r_d^E)) \\ &= \exp\{-\lambda_p |K(Z_o, r_d^E, W_o, r_{ps})|\} = 1. \end{aligned} \quad (4.10)$$

Note that for a given parameter set or a scenario of interest, we have

$|K(Z_o, r_d^E, W_o, r_{ps})| = 0$ since detection radius r_d^E is much larger than the interference radius r_{ps} , which results in $P(E|F) = 1$ in (4.10). Recall that $r_d^E \geq r_{ps} + d_s$ guarantees

the absence of hidden PTxs and therefore there is no negative impact from such PTxs. Thus we have that

$$\begin{aligned}
P(D|EF) &\stackrel{a}{=} \mathbb{E} \left[P(W_o \notin B(\Pi_{so}^E, r_{ss}^{oo}), W_o \notin B(\Pi_{si}^E, r_{ss}^{io}) | EF \Pi_p) | EF \right] \\
&\stackrel{b}{=} \mathbb{E} \left[P(W_o \notin B(\Pi_{so}^E, r_{ss}^{oo}) | EF, \Pi_p) P(W_o \notin B(\Pi_{si}^E, r_{ss}^{io}) | EF, \Pi_p) | EF \right] \\
&\stackrel{c}{=} \mathbb{E} \left[\exp \left\{ - \int_{b(W_o, r_{ss}^{oo})} \lambda_{so} \mathbf{1} \{z \notin B(\Pi_p^{(3)}, r_d^E)\} dz \right\} \times \right. \\
&\quad \left. \exp \left\{ - \int_{b(W_o, r_{ss}^{io})} \lambda_{si} \mathbf{1} \{z \notin B(\Pi_p^{(3)}, r_d^{Ei})\} dz \right\} \middle| EF \right] \\
&\stackrel{d}{=} \mathbb{E} \left[\exp \left\{ -\lambda_s (a_o Q(r_{ss}^{oo}, \Pi_p^{(3)}, r_d^E) + a_i Q(r_{ss}^{io}, \Pi_p^{(3)}, r_d^{Ei})) \right\} \right].
\end{aligned}$$

In the above equality $\stackrel{a}{=}$, we used conditional expectation \mathbb{E} given the event EF . In $\stackrel{b}{=}$, we used the fact that the two events are conditionally independent given Π_p and in $\stackrel{c}{=}$, the probability that W_o does not covered by the Boolean process $B(\Pi_{so}^E, r_{ss}^{oo})$ is given as the void probability of the area $b(W_o, r_{ss}^{oo})$. Since the density of process Π_{so}^E depends on the location z , the density should be integrated over $b(W_o, r_{ss}^{oo})$. The second probability is also computed in the same fashion. Futhermore we used the fact that Π_p conditioned on EF is the same as $\Pi_p^{(3)}$. In $\stackrel{d}{=}$, \mathbb{E} is taken w.r.t. the new random process $\Pi_p^{(3)}$. This completes the proof. \square

4.12 Appendix : Proof of Theorem 10

Proof. Suppose that a G-oSTx Z_o detects the absence of PTxs in its detection radius $b(Z_o, r_d)$ as shown in Fig.4.10. Consider Z_o 's intended receiver G-oSRx W_o which is a distance d_s from Z_o . Then, the conditional outage probability P_{out}^{soG} is given by

$$P(W_o \text{ fails to rcv} | Z_o \text{ txmits, } \|Z_o - W_o\| = d_s). \quad (4.11)$$

For notational simplicity we define the following three events:

$$\begin{aligned}
D &\equiv \{W_o \text{ is not interfered by any G-STx}\} \\
&= \{W_o \notin B(\Pi_{so}^G, r_{ss}^{oo}), W_o \notin B(\Pi_{si}^G, r_{ss}^{io})\}, \\
E &\equiv \{W_o \text{ is not interfered by any PTx}\} = \{W_o \notin B(\Pi_p, r_{ps})\}, \text{ and} \\
F &\equiv \{Z_o \text{ does not detect any PTx in } b(Z_o, r_d)\} = \{Z_o \notin B(\Pi_p, r_d)\}.
\end{aligned}$$

The probability of outage P_{out}^{soG} can be written as $P_{out}^{soG} \stackrel{a}{=} 1 - P(W_o \text{ rcvs}|F) = 1 - P(D|EF)P(E|F)$, where the equality $\stackrel{a}{=}$ follows by omitting conditioning on $\{\|Z_o - W_o\| = d_s\}$ for notational simplicity. $P(E|F)$ and $P(D|EF)$ are computed as follows:

$$\begin{aligned}
P(E|F) &= P(W_o \notin B(\Pi_p, r_{ps}) | Z_o \notin B(\Pi_p, r_d)) \\
&= \exp\{-\lambda_p |K(Z_o, r_d, W_o, r_{ps})|\} = 1.
\end{aligned} \tag{4.12}$$

$$\begin{aligned}
P(D|EF) &\stackrel{a}{=} \mathbb{E} [P(W_o \notin B(\Pi_{so}^G, r_{ss}^{oo}), W_o \notin B(\Pi_{si}^G, r_{ss}^{io}) | EF \Pi_p) | EF] \\
&\stackrel{b}{=} \mathbb{E} [P(W_o \notin B(\Pi_{so}^G, r_{ss}^{oo}) | EF \Pi_p) P(W_o \notin B(\Pi_{si}^G, r_{ss}^{io}) | EF \Pi_p) | EF] \\
&\stackrel{c}{=} \mathbb{E} \left[\exp \left\{ - \int_{b(W_o, r_{ss}^{oo})} \lambda_{so} \mathbf{1}\{z \notin B(\Pi_p^{(4)}, r_d)\} dz \right\} \times \right. \\
&\quad \left. \exp \left\{ - \int_{b(W_o, r_{ss}^{io})} \lambda_{si} \mathbf{1}\{z \notin B(\Pi_p^{(4)}, r_d)\} dz \right\} \middle| EF \right] \\
&= \mathbb{E} \left[\exp \left\{ -\lambda_s (a_o Q(r_{ss}^{oo}, \Pi_p^{(4)}, r_d) + a_i Q(r_{ss}^{io}, \Pi_p^{(4)}, r_d)) \right\} \right]
\end{aligned}$$

In the above equality $\stackrel{a}{=}$, \mathbb{E} is a conditional expectation conditioned on EF . In $\stackrel{b}{=}$, two events are conditionally independent given Π_p and in $\stackrel{c}{=}$, Π_p conditioned on EF is the same as $\Pi_p^{(4)}$. \square

4.13 Appendix : Proof of Theorem 11

Proof. We condition on that an L-oSRx W_o located a distance $d \geq s_o$ from its nearest PTx as shown in Fig.4.11. This ensures that there is no PTx in a shaded

disc $b(W_o, s_o)$. Note that our scenario (parameter selection) guarantees $b(W_o, s_o) \supset b(Z_o, r_d^L)$. An associated L-oSTx Z_o is located a distance d_s from the L-oSRx W_o . Then, the conditional outage probability $P_{out}^{soL}(d)$ is given by

$$P(W_o \text{ fails to rcv} | Z_o \text{ txmits, } \|Z_o - W_o\| = d_s, d \geq s_o). \quad (4.13)$$

For notational simplicity we define the following events.

$$\begin{aligned} D &\equiv \{W_o \text{ is not interfered by any L-STx}\} \\ &= \{W_o \notin B(\Pi_{so}^L, r_{ss}^{oo}), W_o \notin B(\Pi_{si}^L, r_{ss}^{io})\}, \\ E &\equiv \{W_o \text{ is not interfered by any PTx}\} = \{W_o \notin B(\Pi_p, r_{ps})\}, \\ F &\equiv \{Z_o \text{ does not detect any PTx in } b(Z_o, r_d^L)\} = \{Z_o \notin B(\Pi_p, r_d^L)\}, \\ G &\equiv \{d \geq s_o\} = \{W_o \notin B(\Pi_p, s_o)\}. \end{aligned}$$

Then, the outage probability is given by

$$\begin{aligned} P_{out}^{soL}(d) &= 1 - P(W_o \text{ rcvs} | FG) \\ &= 1 - P(DE | FG) \\ &= 1 - P(D | EFG) P(E | FG), \end{aligned}$$

where $P(E | FG)$ and $P(D | EFG)$ can be computed as follows:

$$P(E | FG) = \exp\{-\lambda_p \pi |b(W_o, r_{ps}) \setminus \{b(Z_o, r_d^L) \cup b(W_o, s_o)\}|\} = 1,$$

$$\begin{aligned} P(D | EFG) &= \mathbb{E}[P(W_o \notin B(\Pi_{so}^L, r_{ss}^{oo}), W_o \notin B(\Pi_{si}^L, r_{ss}^{io}) | EFG \Pi_p) | EFG] \\ &\stackrel{a}{=} \mathbb{E}[P(W_o \notin B(\Pi_{so}^L, r_{ss}^{oo}) | EFG \Pi_p) P(W_o \notin B(\Pi_{si}^L, r_{ss}^{io}) | EFG \Pi_p) | EFG] \\ &\stackrel{b}{=} \mathbb{E}[\exp\left\{-\int_{b(W_o, r_{ss}^{oo})} a_o \lambda_s \mathbf{1}\{T_o(z, \Pi_r)\} \mathbf{1}\{z \notin B(\Pi_p^{(5)}, r_d^L)\} dz\right\} \times \\ &\quad \exp\left\{-\int_{b(W_o, r_{ss}^{io})} a_i \lambda_s \mathbf{1}\{T_i(z, \Pi_r)\} \mathbf{1}\{z \notin B(\Pi_p^{(5)}, r_d^{Li})\} dz\right\} | EFG] \\ &\stackrel{c}{=} \mathbb{E}\left[\exp\{-\lambda_{so} Q(r_{ss}^{oo}, \Pi_p^{(5)}, r_d^L)\} \exp\{-\lambda_{si} Q(r_{ss}^{io}, \Pi_p^{(5)}, r_d^{Li})\} \Big| EFG\right] \\ &\stackrel{d}{=} \mathbb{E}[\exp\{-\lambda_s (a_o Q(r_{ss}^{oo}, \Pi_p^{(5)}, r_d^L) + a_i Q(r_{ss}^{io}, \Pi_p^{(5)}, r_d^{Li}))\}] \end{aligned}$$

In $\stackrel{a}{=}$, we use the fact that two events are conditionally independent. In $\stackrel{b}{=}$, we introduce Π_p conditioned on $EF\bar{G}$ which is denoted as $\Pi_p^{(5)}$. In $\stackrel{c}{=}$, we use the fact that $\mathbf{1}\{T_o(z, \cdot, \Pi_r)\} = \mathbf{1}\{T_i(z, \cdot, \Pi_r)\} = 1$ since W_o is in outside of PTx's converge. In $\stackrel{d}{=}$, \mathbb{E} is w.r.t. a new random process $\Pi_p^{(5)}$. This completes the proof. \square

4.14 Appendix : Numerically computed quantities

$$\begin{aligned}
l_1 &= \int_{K(X, r_d; Y, r_{sp})} P(z \notin B(\Pi_p^{(2)}, r_d)) dz = \int_{K(X, r_d; Y, r_{sp})} \exp\{-\lambda_p |K(X, d; z, r_d)|\} dz \\
l_2 &= \int_{K(X, r_d^i; Y, r_{sp}^i)} P(z \notin B(\Pi_p^{(2)}, r_d^i)) dz = \int_{K(X, r_d^i; Y, r_{sp}^i)} \exp\{-\lambda_p |K(X, d; z, r_d^i)|\} dz \\
l_3 &= \int_{K(X, r_d^E; Y, r_{sp})} P(z \notin B(\Pi_p^{(2)}, r_d^E)) dz = \int_{K(X, r_d^E; Y, r_{sp})} \exp\{-\lambda_p |K(X, d; z, r_d^E)|\} dz \\
l_4 &= \int_{K(X, r_d^{Ei}; Y, r_{sp}^i)} P(z \notin B(\Pi_p^{(2)}, r_d^{Ei})) dz = \int_{K(X, r_d^{Ei}; Y, r_{sp}^i)} \exp\{-\lambda_p |K(X, d; z, r_d^{Ei})|\} dz \\
q_E^{oo} &= \int_{b(W_o, r_{ss}^{oo})} P(z \notin B(\Pi_p^{(3)}, r_d^E)) dz = \int_{b(W_o, r_{ss}^{oo})} \exp\{-\lambda_p |K(Z_o, r_d^E; z, r_d^E)|\} dz \\
q_E^{io} &= \int_{b(W_o, r_{ss}^{io})} P(z \notin B(\Pi_p^{(3)}, r_d^{Ei})) dz = \int_{b(W_o, r_{ss}^{io})} \exp\{-\lambda_p |K(Z_o, r_d^E; z, r_d^{Ei})|\} dz \\
q_G^{oo} &= \int_{b(W_o, r_{ss}^{oo})} P(z \notin B(\Pi_p^{(4)}, r_d)) dz = \int_{b(W_o, r_{ss}^{oo})} \exp\{-\lambda_p |K(Z_o, r_d; z, r_d)|\} dz \\
q_G^{io} &= \int_{b(W_o, r_{ss}^{io})} P(z \notin B(\Pi_p^{(4)}, r_d)) dz = \int_{b(W_o, r_{ss}^{io})} \exp\{-\lambda_p |K(Z_o, r_d; z, r_d)|\} dz \\
q_L^{oo} &= \int_{b(W_o, r_{ss}^{oo})} P(z \notin B(\Pi_p^{(5)}, r_d^L)) dz = \int_{b(W_o, r_{ss}^{oo})} \exp\{-\lambda_p |K(W_o, s_o; z, r_d^L)|\} dz = q_m^{oo} \\
q_L^{io} &= \int_{b(W_o, r_{ss}^{io})} P(z \notin B(\Pi_p^{(5)}, r_d^{Li})) dz = \int_{b(W_o, r_{ss}^{io})} \exp\{-\lambda_p |K(W_o, s_o; z, r_d^{Li})|\} dz = q_m^{io}
\end{aligned}$$

4.15 Appendix : Computing Outage Probability of L-oSRx Potential Interfering area (PIA)

The main difficulty in calculating the outage of a L-oSRx arises when we need to determine if a L-oSTx can transmit when it is inside the coverage of a PTx. For a L-oSTx to transmit, it should check the absence of potential PRxs within its surroundings. To do this, we need to know the exact area or the set in \mathbf{R}^2 in which the presence of PRxs is problematic. We will call this set as the potential interfering area of a outdoor secondary transmitter. The difficulty is that the PIA not a disc. Recall that in Section 4.2.5 we defined numerous *interference radii* for *receivers*. In this context a fixed radius was enough to determine the potential locations of harmful transmitters (recall PTxs transmit with same power). But, the PIA for L-oSTxs, as is seen from the transmitter's point of view, depends on the surrounding receivers' SINR, and their SINR depends on their geographic distance to their closest PTx. We can specify the PIA of a L-oSTx at location z by $\mathcal{I}_z^o = \mathcal{I}_z^o(\Pi_p) \equiv \{x \in \mathbf{R}^2 \mid \|z - x\| \leq r_{sp}(\|x - \delta_x(\Pi_p)\|)\}$, where $\delta_x(\Pi_p) = \arg \min_{X \in \Pi_p} \|X - x\|$ is the closest point in Π_p to x . Note that the inequality $\|z - x\| \leq r_{sp}(\|x - \delta_x(\Pi_p)\|)$ corresponds to the condition that a PRx at x is interfered by a L-oSTx at z . So, the PIA \mathcal{I}_z^o denotes the set of potential locations of PRxs that L-oSTx at z can interfere with. Note that using the definition we can write $T_o(z, \Pi_r) = \{\mathcal{I}_z^o \cap \Pi_r = \emptyset\}$.

Approximating the size of PIA

The PIA $\mathcal{I}_{Z_o}^o$ for a L-oSTx Z_o is not a disc due to non-symmetric SINR of PRxs around the L-oSTx Z_o , but it is similar to disc. In Fig.4.12 we have a typical PIA, where shaded area denotes the PIA of L-oSTx Z_o at the origin and a PTx X is located at $(-20000,0)$. In this figure, one can find the radius of inner disc $\mathcal{I}_{Z_o}^{ol}$ and outer disc $\mathcal{I}_{Z_o}^{ou}$ sharing the same center with the PIA $\mathcal{I}_{Z_o}^o$ such that $\mathcal{I}_{Z_o}^{ol} \subset \mathcal{I}_{Z_o}^o \subset \mathcal{I}_{Z_o}^{ou}$ holds. Note that the $\mathcal{I}_{Z_o}^{ol}$ touches with the PIA $\mathcal{I}_{Z_o}^o$ at a the leftmost point of the PIA $\mathcal{I}_{Z_o}^o$ and the $\mathcal{I}_{Z_o}^{ou}$ touches with the PIA $\mathcal{I}_{Z_o}^o$ at b the rightmost point of the PIA $\mathcal{I}_{Z_o}^o$. These two

discs will be used to compute the approximate of the area of the PIA of Z_o .

The radius of the inner disc $\mathcal{I}_{Z_o}^{ol}$ is found using the fact that the distance from the PTx X to the L-oSTx Z_o is equal to the sum of the distance from the PTx X to the a and the distance from the a to the L-oSTx Z_o . Since a PRx at a 's closest PTx is the PTx X , its interference radius is given as $r_{sp}(\|a - X\|)$. That is, we have

$$\|Z_o - X\| = \|a - X\| + r_{sp}(\|a - X\|). \quad (4.14)$$

Using (4.1) and (4.14) after ignoring noise term, we get $\|a - X\| = \frac{\|Z_o - X\|}{1+\gamma}$, where $\gamma = \left(\frac{\rho_s \beta_p}{\rho_p}\right)^{\frac{1}{\alpha}}$, which gives the radius of the inner disc $\mathcal{I}_{Z_o}^{ol}$ as $\|a - Z_o\| = r_{sp}\left(\frac{\|Z_o - X\|}{1+\gamma}\right)$.

Similarly, the radius of the outer disc $\mathcal{I}_{Z_o}^{ou}$ is found using the fact that the distance from the PTx X to the b is equal to the sum of the distance from the PTx X to the L-oSTx Z_o and the distance from the L-oSTx Z_o to the b . Since a PRx at b 's closest PTx is the PTx X , its interference radius is given as $r_{sp}(\|b - X\|)$. That is, we have

$$\|b - X\| = \|Z_o - X\| + r_{sp}(\|b - X\|). \quad (4.15)$$

Again, using (4.1) and (4.15) after ignoring noise term, we get $\|b - X\| = \frac{\|Z_o - X\|}{1-\gamma}$, which eventually gives the radius of outer disc $\mathcal{I}_{Z_o}^{ou}$ as $\|b - Z_o\| = r_{sp}\left(\frac{\|Z_o - X\|}{1-\gamma}\right)$.

Edge Effect : Non-uniform Receiver Density

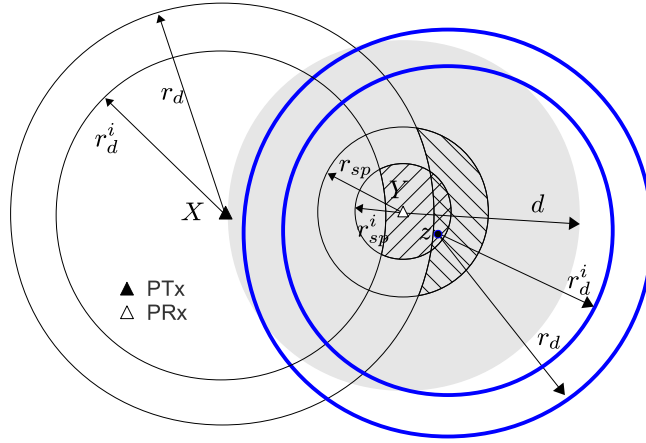
In the sequel we will compute the outage probability of a L-SRx W_o conditioned on its being a distance d from the nearest PTx X . We take this approach since r_{sp} is not a constant. We have following four cases illustrated in Fig.4.13. Case 1 is where $d < r_{ps}$ in which case the L-oSRx W_o is interfered by X with probability 1. So, this is not the case of interest. Case 2 is where $r_{ps} < d < s_o$ in which case s_o is the unique solution of $s_o + r_{ss}^{oo} + r_{sp}(d_p) = d_p$, then, $\lambda_r(z)$ is non-zero constant for all possible STx locations that need to be considered, i.e., for all $z \in \cup_{x \in b(W_o, r_{ss}^{oo})} \mathcal{I}_x^o$. Case 3 is where $s_o < d < s'_o$, where s'_o is the unique solution of $d_p + r_{sp}(d_p) + r_{ss}^{oo} = s'_o$, then, $\lambda_r(z)$ is non-uniform

in $\cup_{x \in b(W_o, r_{ss}^o)} \mathcal{I}_x^o$ since there is no PRx outside the coverage of PTxs. Finally, Case 4 is when $s'_o < d$ and we have constant $\lambda_r(z) = 0$ for all z considered. Note that for Case 2 and 3, P_{out}^{soL} , the outage probability of W_o , depends on the location of its associated L-oSTx Z_o , due to again $r_{sp}(\cdot)$ dependence on distance. But, in Case 4 $\lambda_r = 0$ makes P_{out}^{soL} independent of Z_o 's location. By the edge effect phenomenon we refer to the non-uniform receiver density around at the edge of coverage. This makes computation complicated, so as a conservative approximation, we merge Case 3 and 4 by also letting $\lambda_r(z) = 0$ in Case 3. This is indeed conservative in the sense that it increases P_{out}^{soL} since removing potential receivers encourages neighboring L-STxs to be active, which eventually acts as harmful interference to L-oSRx W_o of interest. We let $\mathcal{C}_o = [r_{ps} + d_s, s_o)$ and $\mathcal{N}_o = [s_o, \infty)$. These two sets correspond to the *conservatively* chosen sets denoting the inside and outside coverage of PTx where potential STxs can be located. Then, there are no hidden PTxs, which is guaranteed by our choice of r_d^L . We have following observation.

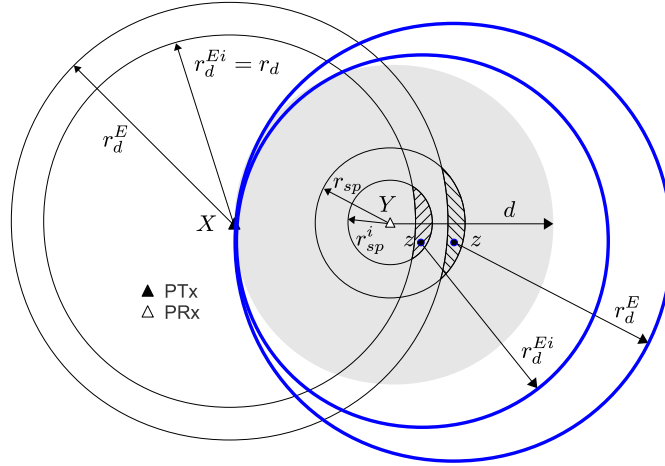
Fact 9. *Let $P_{out}^{soL}(d)$ and $P_{out}^{siL}(d)$ be the conditional outage probability of an L-oSRx and L-iSRx at distance d to their nearest PTxs respectively. Then, we have $P_{out}^{soL}(x) \leq P_{out}^{soL}(y)$ and $P_{out}^{siL}(x) \leq P_{out}^{siL}(y)$ for any $x \in \mathcal{C}_o$ and $y \in \mathcal{N}_o$.*

Intuitively, this is explained by the fact that for $y \in \mathcal{N}_o$ there are more potential active L-STxs giving harmful interference to L-oSRx W_o than the case where $x \in \mathcal{C}_o$ since the absence of PRxs encourages L-STxs to be active. That is, we have that $\mathbf{1}\{T_o(x, \Pi_r)\} \leq^{st} \mathbf{1}\{T_o(y, \Pi_r)\}$ for Π_r , and any $x \in \mathcal{C}_o$ and $y \in \mathcal{N}_o$, where \leq^{st} denotes a stochastic dominance relation. Same argument applies in the indoor case.

Remark 4.15.1. For a L-iSRx W_i and associated L-iSTx Z_i , we can make a similar argument. Then, we have $\mathcal{I}_z^i = \mathcal{I}_z^i(\Pi_p) \equiv \{x \in \mathbf{R}^2 \mid \|z - x\| \leq r_{sp}^i(\|x - \delta_x(\Pi_p)\|)\}$, $T_i(z, \Pi_r) = \{\mathcal{I}_z^i \cap \Pi_r = \emptyset\}$, $\mathcal{C}_i = [r_{ps}^i + d_s, s_i)$, $\mathcal{N}_i = [s_i, \infty)$, where s_i is the unique solution of $s_i + r_{ss}^{oi} + r_{sp}^i(d_p) = d_p$.



(a) By conditioning PRx Y at distance d to its nearest PTx X , we have no PTx in shaded region $b(Y, d)$. A PRx Y can be interfered by potential E-oSTxs in hatched region $\mathcal{K}_1 = b(Y, r_{sp}) \setminus b(X, r_d)$ or E-iSTxs in hatched region $\mathcal{K}_2 = b(Y, r_{sp}^i) \setminus b(X, r_d^i)$. The activity of potentially harmful E-iSTxs and E-oSTxs are affected by surrounding PTxs, e.g., E-oSTx z is active only when there is no PTxs in $b(z, r_d)$.



(b) By conditioning PRx Y at distance d to its nearest PTx X , we have no PTx in shaded region $b(Y, d)$. A PRx Y can be interfered by potential E-oSTxs in hatched region $\mathcal{K}_3 = b(Y, r_{sp}) \setminus b(X, r_d^E)$ or E-iSTxs in hatched region $\mathcal{K}_2 = b(Y, r_{sp}^i) \setminus b(X, r_d^{Ei})$. The activity of potential E-iSTxs and E-oSTxs are affected by surrounding PTxs, e.g., E-oSTx z is active only when there is no PTxs in $b(z, r_d^E)$.

Figure 4.9: PTx X and PRx Y were shown with E-STxs using signal energy detection method. Left figure corresponds to the case with detection radius considering only outdoor devices in Section 4.4.1 and right figure corresponds to the case with conservative detection radius in Section 4.5.2.

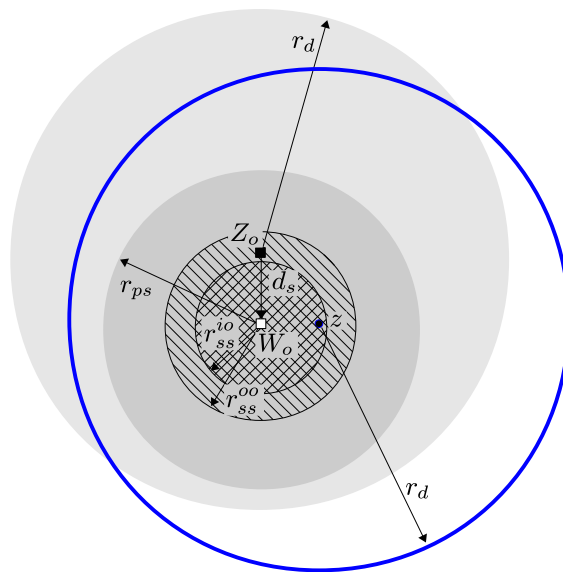


Figure 4.10: Conditioned that there are no PTxs in $b(Z_o, r_d) (\supset b(W_o, r_{ps}))$, a G-oSRx W_o can be interfered by potential G-oSTx in $b(W_o, r_{ss}^{oo})$ or G-iSTxs in $b(W_o, r_{ss}^{io})$. Their activities are determined by surrounding PTxs in $b(z, r_d)$ for both G-oSTxs and G-iSTxs.

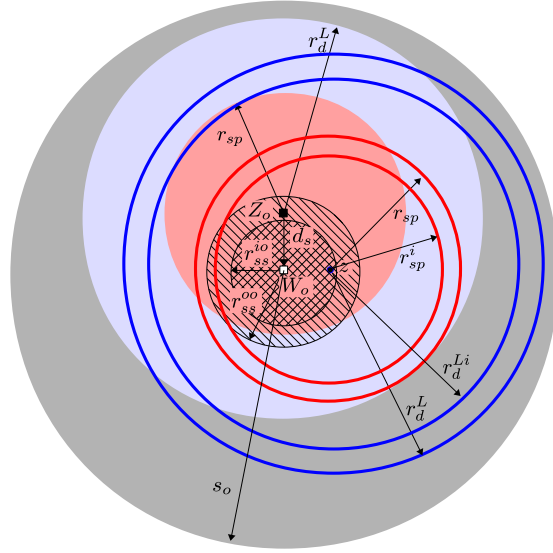


Figure 4.11: Conditioned that there are no PTxs in $b(W_o, s_o) (\supset b(Z_o, r_d^L))$, a L-oSRx W_o can be interfered by potential L-oSTx in $b(W_o, r_{ss}^{oo})$ or L-iSTxs in $b(W_o, r_{ss}^{io})$. Their activities are determined by surrounding PTxs, e.g., PTxs in $b(z, r_d^L)$ for a L-oSTx at z and PTxs in $b(z, r_d^{Li})$ for a L-iSTx at z . But, no PRxs outside of coverage and $r_{ss}^{oo} + r_d^L < s_o$ in our scenario guarantee that all harmful L-STxs are active.

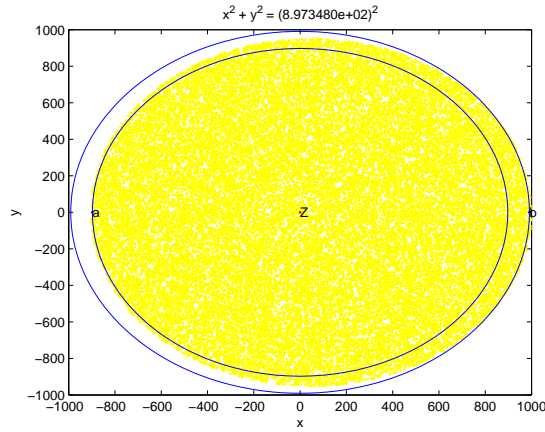


Figure 4.12: A PTx X is located at $(-20000, 0)$ and L-oSTx Z_o is located in the the origin. The PIA of the L-oSTx Z_o is drawn as shaded region. The inner and outer discs given as $\mathcal{I}_{Z_o}^{ol} = b(O, r_{sp}(\|X - a\|))$ and $\mathcal{I}_{Z_o}^{ou} = b(O, r_{sp}(\|X - b\|))$ respectively can be used to compute an approximated area of the PIA. The leftmost and rightmost point of the PIA are denoted as a and b in the figure.

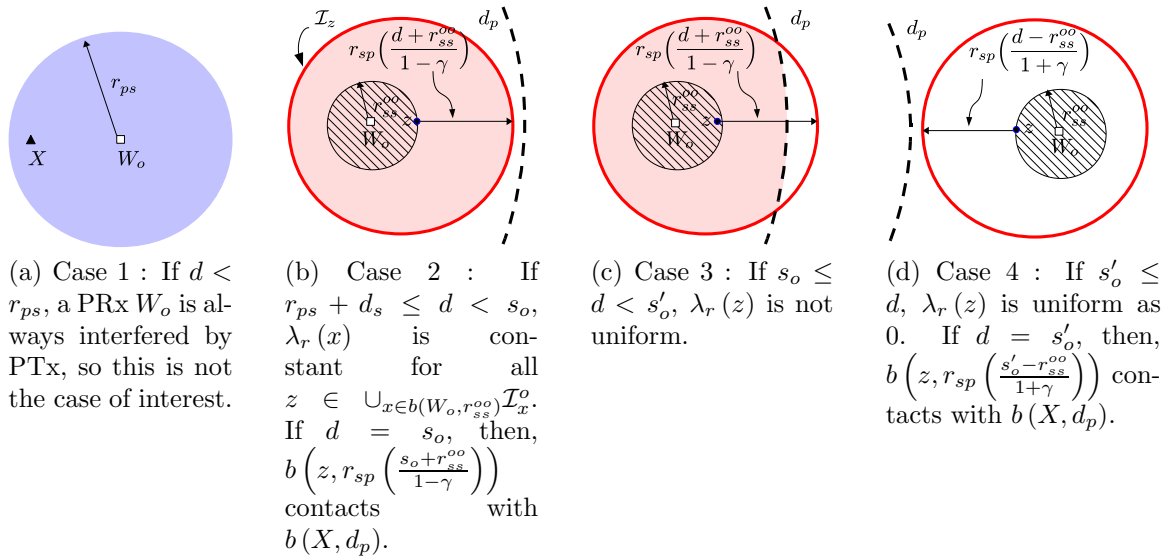


Figure 4.13: The PTx coverage $b(X, d_p)$ is partially shown as an dotted arc and hatched circle $b(W_o, r_{ss}^{oo})$ denotes a region where potentially harmful L-oSTxs to L-oSRx W_o can be located. For a L-oSTx $z \in b(W_o, r_{ss}^{oo})$, a PIA \mathcal{I}_z^o is drawn with solid thick line. Shaded region denotes a region where $\lambda_r(x) > 0$. In a non-shaded region inside \mathcal{I}_z , we have $\lambda_r(x) = 0$. There are four cases to consider depending the value of d . Case 3 can be merged with Case 4 by assuming $\lambda_r(z) = 0$ in Case 3. Figures were drawn for a L-oSRx only. For a L-iSRx r_{ps} , r_{sp} , r_{ss}^{oo} , and s_o should be replaced with r_{ps}^i , r_{sp}^i , r_{ss}^{oi} and s_i . respectively.

Chapter 5

Conclusion and Future Work

5.1 Conclusion

In this dissertation we considered ad hoc wireless networks where nodes share the same spectrum to communicate with neighboring nodes. In such networks, the broadcast nature of the wireless medium induces interactions among nodes; strongly interactions among close-by nodes through contention and weak ones among far away nodes through interference. The interactions make their performance spatially correlated, and this makes it hard to analyze the overall system performance. In our work, we used models borrowed from spatial point process theory to capture the subtle spatial dependencies among nodes and the resulting network performance.

More specifically in Chapter 2, we considered an ad-hoc network where nodes share a given spectrum resource. We propose two channel-aware CSMA protocols, namely O-CSMA and Q-CSMA, and evaluated their spatial reuse and fairness characteristics. We showed that Q_0 -CSMA, which relies only on quantile-based scheduling, was a more robust solution to extract opportunistic gain from channel variations. The robustness comes from the combination of multi-user diversity and the coupling between channel gain and timer values. This MAC has little additional complexity, and thus is a more attractive choice from an engineering perspective than O-CSMA. Although, the performance of two protocols was evaluated assuming collision-free timers and full channel-status feedback, we expect that the performance gains from the opportunistic operation will be significant relative to the loss due to the overheads required for such operation.

In Chapter 3, we considered spectrum sharing between nodes in two different networks: that is, primary (licensed) and secondary (unlicensed or cognitive) nodes coexist on a shared spectrum band. We showed how the spatial reuse of primary and secondary network depends on system design parameters such as transmit power, signal energy detection threshold (or physical carrier sensing threshold), and decoding SINR threshold. We showed that we can significantly increase the spatial reuse of the secondary network simply by optimizing the design parameters, suggesting some practical engineering rules of thumb.

In Chapter 4, we considered cognitive networks in heterogenous environments with added uncertainties. Three different white space detection techniques with different degrees of RF-environment awareness were evaluated in terms of the achievable joint network capacity region. Our focus was on quantifying the impact of additional information such as the geographical locations of transmitters or the existence of primary receivers, which can reduce the uncertainties in the environment and thus improve the spatial reuse of cognitive networks. Among the detection techniques we considered, the geo-positioning-assisted detection technique is getting more attention as a practical approach since a recent rule change by FCC on white space detection requirements; cognitive devices incorporating geo-location/database access techniques do not need to perform signal energy detection. However, we found that further improvements can be achieved by taking advantage of an “idling” area which is covered by primary transmitters but *not* used by primary receivers; our work shows that a receiver-location-aware technique can substantially improve the spatial reuse. These results provide insights to policy makers as well as system designers on how to build rules and systems to better utilize shared spectrum.

5.2 Future Work

Collision and feedback in an ad-hoc network. In Chapter 2, we considered CSMA protocols without collisions during contention resolution and errors in chan-

nel status feedback. However, most practical distributed MAC protocols experience collisions due to the limited resolution of timer values and signal propagation delay. Thus, it is worthwhile to explore the impact of collisions on the performance of ad-hoc networks, and tradeoff between performance and the required overhead. Perhaps, more critically, we assumed that channel quality information is always available to transmitters from their associated receivers. However, such feedback is often unreliable and incurs an overhead in practice. In particular, in an ad-hoc network when the locations of nodes (or network topology) are not controllable, the reliability or overhead depend(s) heavily on the locations/density of neighboring nodes and the amount of interference generated from neighboring nodes. Thus, it would be of interest to study the impact of channel feedback with errors on spatial reuse.

Spectrum sharing from a temporal reuse perspective. In Chapters 3 and 4, we considered the performance of cognitive networks from a spatial reuse perspective. As future work, it would be worthwhile to consider cognitive networks from a temporal reuse perspective. For example, in a scenario where two service providers make contracts with a (physical) network provider, one can build a resource sharing mechanism which divides the network's resources amongst them. The sharing mechanism will depend on the type of shared link (downlink or uplink), the service requirements, and the contracts. In such a setting, it would be interesting to explore how the sharing requirements should be structured and how such contracts affect the network's performance.

Bibliography

- [1] Draft Supplement to STANDARD FOR Telecommunications and Information Exchange Between Systems - LAN/MAN Specific Requirements - Part 11: Wireless Medium Access Control (MAC) and Physical Layer (PHY) Specifications: Medium Access Control (MAC) Enhancements for Quality of Service (QoS). *IEEE Std 802.11e/D3.0*, May 2002.
- [2] Achievable Transmission Capacity of Secondary System in Cognitive Radio Networks. *IEEE Inter. Conf. on Communication (ICC)*, May 2010.
- [3] Bluetooth Specification. Available at <http://www.bluetooth.com>.
- [4] TV Detection, Available at <http://www.tvlicensing.biz/detection/>.
- [5] IEEE 802.22. Working Group on Wireless Regional Area Networks. <http://www.ieee802.org/22>.
- [6] N. Abramson. The Aloha System - Another Alternative For Computer Communication. *Proc. AFIPS*, pages 295–298, 1970.
- [7] S. Adireddy and L. Tong. Exploting Decentralized Channel State Information for Random Access. *IEEE Trans. Infomation Theory*, 51(2):537–562, Feb 2005.
- [8] I. F. Akyildiz, W. Lee, M. C. Vuran, and S. Mohanty. NeXt Generation/Dynamic Spectrum Access/Cognitive Radio Wireless Networks: A Survey. *Elsevier Computer Network*, 50:2127–2159, Sep 2006.
- [9] A. B. H. Alaya-Feki, B. Sayrac, S. B. Jemaa, and E. Moulines. Interference Cartography for Hierarchical Dynamic Spectrum Access. *Proc. IEEE DySpan*, pages 1–5, Oct 2008.

- [10] F. Baccelli and B. Blaszczyszyn. Stochastic Analysis of Spatial and Opportunistic Aloha. *IEEE Jour. Select. Areas in Comm.*, 27(7):1105–1119, Sep 2009.
- [11] F. Baccelli and B. Blaszczyszyn. *Stochastic Geometry and Wireless Networks*, volume II. NOW Publisher, 2009.
- [12] F. Baccelli and B. Blaszczyszyn. *Stochastic Geometry and Wireless Networks*, volume I. NOW Publisher, 2009.
- [13] F. Baccelli, B. Blaszczyszyn, and P. Muhlethaler. An ALOHA Protocol for Multihop Mobile Wireless Networks. *IEEE Trans. Infomation Theory*, 52:421–436, Feb 2006.
- [14] S. J. Baek and G. de Veciana. Spatial Model for Energy Burden Balancing and Data Fusion in Sensor Networks Detecting Bursty Events. *IEEE Trans. Infomation Theory*, 53(10):3615–3628, Oct 2007.
- [15] P. Bahl, R. Chandra, and J Dunagan. SSCH: Slotted Seeded Channel Hopping for Capacity Improvement in IEEE 802.11 Ad-Hoc Wireless Networks. *Proc. ACM Mobicom*, Sep 2004.
- [16] P. Bahl, R. Chandra, T. Moscibroda, R. Murty, and M. Welsh. White Space Networking with Wi-Fi like Connectivity. *ACM SIGCOMM*, 39, Oct 2009.
- [17] T. Bonald. A Score-based Opportunistic Scheduler for Fading Radio Channels. *Proc. of European Wireless*, 2004.
- [18] R. Boorstyn, A. Kershenbaum, B. Maglaris, and V. Sahin. Throughput Analysis in Multihop CSMA Packet Radio Networks. *IEEE Trans. on Comm.*, 35(3):267–274, 1987.
- [19] P. Brémaud. *Mathematical Principles of Signal Processing*. Springer, 2002.

- [20] T. X. Brown. An Analysis of Unlicensed Device Operation in Licensed Broadcast Service bands. *Proc. IEEE DySpan*, pages 11 – 29, Nov 2005.
- [21] Marcelo M. Carvalho and J. J. Garcia-Luna-Aceves. A Scalable Model for Channel Access Protocols in Multihop Ad Hoc Networks. In *Proceedings of the 10th Annual International Conference on Mobile Computing and Networking, MobiCom '04*, pages 330–344, New York, NY, USA, 2004. ACM.
- [22] M. R. Chari, F. L., A. Mantravadi, R. Krishnamoorthi, R. Vijayan, G. K. Walker, and R. Chanhok. FLO Physical layer : An Overview. *IEEE Trans. Broadcasting*, 53(1):145–160, March 2007.
- [23] G. Chen and D. Kotz. A Survey of Context-Aware Mobile Computing Research. *Dartmouth Computer Science Technical Report TR2000-381*, 2000.
- [24] H. Chhaya and S. Gupta. Performance Modeling of Asynchronous Data Transfer Methods of IEEE 802.11 MAC Protocol. *Wireless Networks*, 3:217–234, 1997.
- [25] J. Choi and S. Bahk. Channel Aware MAC Scheme based on CSMA/CA. *IEEE VTC*, pages 1559–1563, May 2004.
- [26] T. C. Clancy. Achievable Capacity Under the Interference Temperature Model. *Proc. IEEE INFOCOM*, pages 794 – 802, 2007.
- [27] C. Cordeiro, K. Challapali, D. Birru, and N. Sai Shankar. IEEE 802.22: the First Worldwide Wireless Standard based on Cognitive Radios. *Proc. IEEE DySpan*, pages 328–337, 2005.
- [28] T. M. Cover and J. A. Thomas. *Elements of Information Theory*. WILEY, 2 edition, 2006.

- [29] T. Cui, L. Chen, and T. Ho. Energy Efficient Opportunistic Network Coding for Wireless Networks. *Proc. IEEE INFOCOM*, 2008.
- [30] Q. Dong, J. Wu, W. Hu, and J. Crowcroft. Practical Network Coding in Wireless Networks. *Proc. ACM Mobicom*, 2007.
- [31] J. M. Durante. Building Penetration Loss at 900 MHz. *Proc. IEEE Veh. Technol. Conf.*, 24:81–87, Dec 1973.
- [32] M. Durvy, O. Dousse, and P. Thiran. On The Fairness of Large CSMA Networks. *IEEE Jour. Select. Areas in Comm.*, 27:1093–1104, September 2009.
- [33] M. Durvy, O. Dousse, and P. Thiran. Self-Organization Properties of CSMA/CA Systems and Their Consequences on Fairness. *IEEE Trans. Information Theory*, 55:931–943, March 2009.
- [34] M. Durvy and P. Thiran. A Packing Approach to Compare Slotted and Non-slotted Medium Access Control. *IEEE INFOCOM*, pages 1–12, Apr 2006.
- [35] FCC. Spectrum Policy Task Force. *Rep. ET Docket no. 02-135*, November 2002.
- [36] FCC. Notice of Inquiry and Notice of Proposed Rulemaking. (ET Docket 03-237), 2003.
- [37] FCC. FCC Adopts Rules for Unlicensed Use of Television White Spaces. Nov 2008, Available at http://hraunfoss.fcc.gov/edocs_public/attachmatch/FCC-08-260A1.pdf.
- [38] FCC. FCC-10-174A1 : Second Memorandum Opinion and Order. Sep 2010.
- [39] S. Foss, T. Konstantopoulos, and S. Zachary. The Principle of a Single Big Jump: Discrete and Continuous Time Modulated Random Walks with Heavy-Tailed Increments. *Journal of Theoretical Probability*, 20(3):581–612, Sep 2007.

- [40] M. Franceschetti, O. Dousse, N. C. Tse, and P. Thiran. Closing The Gap in the Capacity of Wireless Networks via Percolation Theory. *IEEE Trans. Infomation Theory*, 53:1009–1018, 2007.
- [41] R. K. Ganti, J. G. Andrews, and M. Haenggi. High-SIR Transmission Capacity of Wireless Networks with General Fading and Node Distribution. *submitted to IEEE Trans. Infomation Theory*.
- [42] M. Garetto, T. Salonidis, and E. W. Knightly. Modeling Per-flow Throughput and Capturing Starvation in CSMA Multi-hop Wireless Networks. *IEEE INFOCOM*, 2006.
- [43] A. Ghasemi and E.S. Sousa. Collaborative Spectrum Sensing for Opportunistic Access in Fading Environments. *Proc. IEEE DySpan*, pages 131 – 136, 2005.
- [44] A. Ghasemi and E.S. Sousa. Spectrum Sensing in Cognitive Radio Networks: Requirements, Challenges and Design Trade-off. *IEEE Communications Magazine*, 46(4):32–39, Apr 2008.
- [45] R. Giacomelli, R. K. Ganti, and M. Haenggi. Outage Probability of General Ad Hoc Networks in the High-Reliability Regime. *submitted to IEEE/ACM Trans. Networking*.
- [46] I. Gitman. On The Capacity of Slotted ALOHA Networks and Some Design Problems. *IEEE Trans. Comm.*, 23(3):305–317, Mar 1975.
- [47] I.S. Gradshteyn and I.M. Ryzhik. *Tables of Integrals, Series, and Products*. Academic Press, Inc, 7 edition, 2007.
- [48] M. Grossglauser and D. N. C. Tse. Mobility Increase The Capacity of Ad Hoc Wireless Network. *IEEE Trans. Infomation Theory*, 10:477–486, 2002.

- [49] P. Gupta and P.R. Kumar. Capacity of Wireless Networks. *IEEE Trans. Information Theory*, 46:388–404, Mar 2000.
- [50] D. Gurney, G. Buchwald, L. Ecklund, S. Kuffner, and J. Grosspietsch. Geolocation Database Techniques for Incumbent Protection in the TV White Space. *Proc. IEEE DySpan*, 2008.
- [51] M. Haenggi, J. G. Andrews, F. Baccelli, O. Dousse, and M. Franceschetti. Stochastic Geometry and Random Graphs for the Analysis and Design of Wireless Networks. *IEEE Jour. Select. Areas in Comm.*, 27:1029–1046, Sep 2009.
- [52] B. Han and G. Simon. Capacity Of Wireless Ad Hoc Networks, A Survey. *Technical Report, available at <http://public.enst-bretagne.fr/~bhan/publications/capacity-survey.pdf>*, 2007.
- [53] M. F. Hanif, M. S., P. J. Smith, and P. A. Dmochowski. Interference and Deployment Issues for Cognitive Radio Systems in Shadowing Environments. *Proc. IEEE Int. Conf. on Comm. (ICC)*, 2009.
- [54] M. F. Hanif and P. J. Smith. On the Statistics of Cognitive Radio Capacity in Shadowing and Fast Fading Environments. *IEEE Trans. Wireless Comm.*, 9(2):844–852, Feb 2010.
- [55] M. F. Hanif, P. J. Smith, and M. Shafi. Performance of Cognitive Radio Systems with Imperfect Radio Environment Map Information. *Proc. Australian communication theory workshop, Sydney*, pages 61–66, Feb 2009.
- [56] A. Hasan and J. G. Andrews. The Guard Zone in Wireless Ad Hoc Networks. *IEEE Trans. Wireless Comm.*, 6(3):897–906, March 2007.
- [57] N. Hoven and A. Sahai. Power Scaling for Cognitive Radio. *WirelessCom Symposium on Emerging Networks*, 1:250–255, Jun 2005.

- [58] K. Huang, V. K. N. Lau, and Y. Chen. Spectrum Sharing Between Cellular and Mobile Ad Hoc Networks: Transmission-Capacity Trade-Off. *IEEE Jour. Select. Areas in Comm.*, 2009.
- [59] C. Hwang and J.M. Cioffi. Using Opportunistic CSMA/CA to Achieve Multi-User Diversity in Wireless LAN. *IEEE Globcom*, pages 4952 – 4956, Nov 2007.
- [60] S. A. Jafar and S. Srinivasa. Capacity Limits of Cognitive Radio With Distributed and Dynamic Spectral Activity. *IEEE Jour. Select. Areas in Comm.*, 25(3):529–537, April 2007.
- [61] R. K. Jain, D. M. Chiu, and W. R. Hawe. A Quantitative Measure Of Fairness And Discrimination For Resource Allocation In Shared Computer Systems. *DEC Research Report TR-301*, Sep 1984.
- [62] S. Jeon, N. Devroye, M. Vu, S. Chung, and V. Tarokh. Cognitive Networks Achieve Throughput Scaling of a Homogeneous Network. *submitted to IEEE Trans. Infomation Theory*, 2008.
- [63] A. Jovičić and P. Viswanath. Cognitive Radio: An Information- Theoretic Perspective. *IEEE Trans. Infomation Theory*, 55(9):3945–3958, Sep 2009.
- [64] A. Jovičić, P. Viswanath, and S. R. Kulkarni. Upper Bound to Transport Capacity of Wireless Networks. *IEEE Trans. Infomation Theory*, 50(11):2555–2565, Nov 2004.
- [65] Y. Kim and G. de Veciana. Understanding the Design Space for Cognitive Networks. *Sixth Workshop on Spatial Stochastic Models for Wireless Networks (SpaSWiN)*, June 2010.
- [66] Y. Kim and G. de Veciana. Joint Network Capacity Region of Cognitive Networks Heterogeneous Environments and RF-environment Awareness. *Technical*

Report, 2010

Available at <http://sites.google.com/site/yuchulkim>.

- [67] Y. Kim and G. de Veciana. Understanding The Design Space for Cognitive Networks. *Technical Report*, 2010
Available at <http://sites.google.com/site/yuchulkim>.
- [68] Y. Kim and G. de Veciana. Joint Network Capacity Region of Cognitive Networks Heterogeneous Environments and RF-Environment Awareness. *IEEE Jour. Select. Areas in Comm.*, 29(2), Feb 2011.
- [69] Y. Kim and G. de Veciana. Spatial Reuse and Fairness of Mobile Ad Hoc Networks with Channel-Aware CSMA Protocols. *Technical Report*, 2011
Available at <http://sites.google.com/site/yuchulkim>.
- [70] J.F.C Kingman. *Poisson Processes*. Clarendon Press, Oxford, 1993.
- [71] B. Ko and D. Rubenstein. Distributed Self-stabilizing Placement of Replicated Resources in Emerging Networks. *IEEE/ACM Trans. Netw.*, 13:476–487, June 2005.
- [72] U. Kozat and L. Tassiulas. Throughput Capacity of Random Ad Hoc Networks with Infrastructure Support. In *MobiCom '03: Proceedings of the 9th annual international conference on Mobile computing and networking*, pages 55–65, New York, NY, USA, 2003. ACM.
- [73] W. Krenik and A. Batra. Cognitive Radio Techniques for Wide Area Networks. *Design Automation Conference*, Jun 2005.
- [74] S. R. Kulkarni and P. Viswanath. A Deterministic Approach to Throughput Scaling in Wireless Networks. *IEEE Trans. Information Theory*, 50(6):1041–1049, Jun 2004.

- [75] B. Liu, P. Thiran, and D. Towsley. Capacity of a Wireless Ad Hoc Network with Infrastructure. In *MobiHoc '07: Proceedings of the 8th ACM international symposium on Mobile ad hoc networking and computing*, pages 239–246, New York, NY, USA, 2007. ACM.
- [76] H. Liu, H. Darabi, P. Banerjee, and J. Liu. Survey of Wireless Indoor Positioning Techniques and Systems. *IEEE Transactions on Systems, Man, and Cybernetics, Part C: Applications and Reviews*, 37:1067 – 1080, Nov 2007.
- [77] S. B. Lowen and M.C. Teich. Power-law Shot Noise. *IEEE Trans. Information Theory*, 36:1302–1318, Nov 1990.
- [78] S. Mubaraq M., R. Tandra, and A. Sahai. The Case for Wideband Sensing. *Proc. of Allerton Conf. on Comm. Control and Comp.*, 2008.
- [79] A. W. Marshall and I. Olkin. *Inequalities: Theory of Majorization and Its Applications*. Academic Press, Inc, 1979.
- [80] M. A. McHenry. NSF Spectrum Occupancy Measurements Project Summary. *Shared spectrum co*, Aug 2005.
- [81] M. A. McHenry, K. Steadman, and M. Lofquist. Determination of Detection Thresholds to Allow Safe Operation of Television Band "White Space" Devices. *Proc. IEEE DySpan*, pages 1–12, Oct 2008.
- [82] K. Medepalli and F. A. Tobagi. Towards Performance Modeling of IEEE 802.11 based Wireless Networks: A Unified Framework and its Applications. *IEEE INFOCOM*, 2006.
- [83] J Mitola, III and G Maguire, Jr. Cognitive Radio: Making Software Radios More Personal. *IEEE Personal Communication*, 6:13–18, Aug 1999.

- [84] D. Molkdar. Review on Radio Propagation into and within Buildings. *Microwaves, Antennas and Propagation, IEE Proceedings*, 138:61–73, Feb 1991.
- [85] Alfred Muller and Dietrich Stoyan. *Comparison Method for Stochastic Models and Risks*. John Wiley & Sons, Ltd, 2002.
- [86] T. Nandagopal, T. Kim, X. Gao, and V. Bharghavan. Achieving MAC Layer Fairness in Wireless Packet Networks. *Proc. ACM Mobicom*, 2000.
- [87] H. Q. Nguyen, F. Baccelli, and D. Kofman. A Stochastic Geometry Analysis of Dense IEEE 802.11 Networks. *IEEE INFOCOM*, page 1199, May 2007.
- [88] T. V. Nguyen and F. Baccelli. A Probabilistic Model of Carrier Sensing based Cognitive Radio. *DySpan*, 2010.
- [89] J. Ni, R. Srikant, and X. Wu. Coloring Spatial Point Processes With Application to Peer Discovery in Large Wireless Networks. *IEEE Trans. Net.*, 2010.
- [90] D. Park, H. Kwon, and B. Lee. Wireless Packet Scheduling Based on the Cumulative Distribution Function of User Transmission Rates. *IEEE Trans. Comm.*, 53:1919 – 1929, Nov 2005.
- [91] S. Patil and G. de Veciana. Managing Resources and Quality of Service in Wireless Systems Exploiting Opportunism. *IEEE/ACM Transactions on Networking*, 15(5):1046–1058, Oct 2007.
- [92] S. Patil and G. de Veciana. Measurement-Based Opportunistic Scheduling for Heterogenous Wireless Systems. *IEEE Transactions on Communications*, 57(9):2745–2753, Sep 2009.
- [93] S. J. Patsiokas, B. K. Johnson, and J. L. Dailing. Propagation of Radio Signals Inside Buildings at 150, 45A0N D 850 MHz. *Proc. IEEE Veh. Technol. Conf.*, 36:66 – 71, May 1986.

- [94] X. Qin and R. A. Berry. Distributed Approaches for Exploiting Multiuser Diversity in Wireless Networks. *IEEE Trans. Information Theory*, 52(2):392–413, Feb 2006.
- [95] W. Ren, Q. Zhao, and A. Swami. Power Control in Cognitive Radio Networks: How to Cross a Multi-Lane Highway. *IEEE Jour. Select. Areas in Comm.*, 27(7):1283–1296, Sep 2009.
- [96] S. M. Ross. *Stochastic Processes*. John Wiley & Sons, Inc, 1983.
- [97] B. Schilit, N. Adams, and R. Want. Context-Aware Computing Applications. *Proc. IEEE Workshop on Mobile Computing Sys. and App.*, pages 85–90, Dec 1994.
- [98] J. Shi, E. Aryafar, T. Salonidis, and E. W. Knightly. Synchronized CSMA Contention: Model, Implementation and Evaluation. *IEEE INFOCOM*, April 2009.
- [99] J. So and N. Vaidya. Multi-Channel MAC for Ad Hoc Networks: Handling Multi-Channel Hidden Terminals using a Single Transceiver. *Proc. ACM MobiHoc*, May 2004.
- [100] S. Srinivasa and S. A. Jafar. How Much Spectrum Sharing is Optimal in Cognitive Radio Networks? *IEEE Trans. Wireless Comm.*, 7(10):4010–4018, Oct. 2008.
- [101] D. Stoyan. *Comparison Methods For Queues and Other Stochastic Models*. John Wiley & Sons, 1983.
- [102] D. Stoyan, W. S. Kendall, and J. Mecke. *Stochastic Geometry and its Applications*. John Wiley & Sons, Ltd, 1995.

- [103] R. Tandra and A. Sahai. SNR Walls for Signal Detection. *IEEE Selected Topics in Signal Processing*, 2:4–17, Feb 2008.
- [104] F. A. Tobagi. Analysis of a Two-Hop Centralized Packet Radio Network - Part I : Slotted ALOHA. *IEEE Trans. Comm.*, 28(2):196–207, Feb 1980.
- [105] F. A. Tobagi. Analysis of a Two-Hop Centralized Packet Radio Network - Part II : Carrier Sense Multiple Access. *IEEE Trans. Comm.*, 28(2):208–216, Feb 1980.
- [106] F. A. Tobagi. Modeling and Performance Analysis of Multihop Packet Radio Networks. *Proc. IEEE*, 75(1):135–155, 1987.
- [107] D. Tse and P. Viswanath. *Fundamentals of Wireless Communication*. Cambridge University Press, 2005.
- [108] P. M. van de Ven, S. C. Borst, D. Denteneer, A. J.E.M. Janssen, and J. S.H. van Leeuwen. Equalizing Throughputs in Random-Access Networks. *SIGMETRICS Perform. Eval. Rev.*, 38:39–41, Oct 2010.
- [109] P.M. van de Ven, J.S.H. van Leeuwen, D. Denteneer, and A.J.E.M. Janssen. Spatial Fairness in Linear Random-Access Networks. *Performance Evaluation*, 2010.
- [110] M. Vu, N. Devroye, and V. Tarokh. On the Primary Exclusive Region of Cognitive Networks. *IEEE Trans. Wireless Comm.*, 8:3380–3385, Jul 2009.
- [111] Xin Wang and K. Kar. Throughput Modeling and Fairness Issues in CSMA/CA Based Ad-Hoc Networks. *IEEE INFOCOM*, 1:23–34, Mar 2005.
- [112] S. P. Weber, J. G. Andrews, and N. Jindal. The Effect of Fading, Channel Inversion, and Threshold Scheduling on Ad Hoc Networks. *IEEE Trans. Information Theory*, 53:4127–4149, Nov 2007.

- [113] S. P. Weber, X. Yang, J. G. Andrews, and G. de Veciana. Transmission Capacity of Wireless Ad Hoc Networks With Outage constraints. *IEEE Trans. Information Theory*, 51:4091–4102, Dec 2005.
- [114] M. Westcott. *On the Existence of a Generalized Shot-Noise Process*. Studies in Probabilities and Statistics. Papers in Honor of Edwin J.G. Pitman. Amsterdam, The Netherlands: North-Holland, 1976.
- [115] B. Wild and K. Ramchandran. Detecting Primary Receivers for Cognitive Radio Applications. *Proc. IEEE DySpan*, pages 124–130, 2005.
- [116] M. Win, P. C. Pinto, and L. A. Shepp. A Mathematical Theory of Network Interference and Its Applications. *Proc. IEEE*, 97(2):205–230, Feb 2009.
- [117] L. Wu and P. Varshney. Performance Analysis of CSMA and BTMA Protocols in Multihop Networks (I) - Single Channel Case. *Info. Sci. Elsevier*, 120:159–177, 1999.
- [118] X. Wu, S. Tavildar, S. Shakkottai, T. Richardson, J. Li, R. Laroia, and A. Jovicic. FlashLinQ: A Synchronous Distributed Scheduler for Peer-to-Peer Ad-hoc Networks. *Proc. of Allerton Conf. on Comm. Control and Comp.*, 2010.
- [119] Y. Wu, P. A. Chou, and S. Y. Kung. Information Exchange in Wireless Networks With Network Coding And Physical-Layer Broadcast. *Conference on Information Sciences and Systems (CISS)*, 2005.
- [120] C. Yin, L. Gao, and S. Cui. Scaling Laws of Overlaid Wireless Networks: A Cognitive Radio Network vs. A Primary Network. *submitted to IEEE/ACM Trans. Networking.*, 2008.
- [121] C. Yin, L. Gao, T. Liu, and S. Cui. Transmission Capacities for Overlaid Wireless Ad Hoc Networks with Outage Constraints. *IEEE Inter. Conf. on Communication (ICC)*, Jun 2009.

- [122] A. Zemplianov and G. de Veciana. Capacity of Ad Hoc Wireless Networks With Infrastructure Support. *IEEE Jour. Select. Areas in Comm.*, 23:657–667, March 2005.
- [123] Q. Zhao and B. M. Sadler. A Survey of Dynamic Spectrum Access. *IEEE Signal Processing Magazine*, 24(3):79–89, May 2007.
- [124] Y. Zhao, L. Morales, J. Gaeddert, K. Bae, J. Um, and J. H. Reed. Applying Radio Environment Maps to Cognitive Wireless Regional Area Networks. *Proc. IEEE DySpan*, pages 115–118, Apr 2007.

Vita

Yuchul Kim received his B.S. and M.S. degree in Electrical Engineering from Korea University in 2000 and Korea Advanced Institute of Science and Technology in 2003, respectively. He subsequently joined to Global Standard Research team in Samsung Electronics and worked as a standard engineer for 3GPP2 cdma2000 standardization. After three and half years, he entered graduate school at The University of Texas at Austin. In 2007, he started working under the supervision of Prof. Gustavo de Veciana and became the member of Wireless Networking and Communications Group. He interned at Qualcomm, San Diego from May to December 2008.

Permanent address: 3475 Lake Austin D
Austin, Texas 78703

This dissertation was typeset with L^AT_EX[†] by the author.

[†]L^AT_EX is a document preparation system developed by Leslie Lamport as a special version of Donald Knuth's T_EX Program.